MODELING AND SIMULATIONS OF EQUILIBRIUM OF ENVIRONMENTALLY SENSITIVE HYDROGELS

LUO RONGMO

NATIONAL UNIVERSITY OF SINGAPORE

2008

MODELING AND SIMULATIONS OF EQUILIBRIUM OF ENVIRONMENTALLY SENSITIVE HYDROGELS

LUO RONGMO

(*B.Eng & M.Eng, Zhejiang University, P.R. China*)

A THESIS SUBMITTED

FOR THE DEGREE OF DOCTOR OF PHILOSOPHY

DEPARTMENT OF MECHANICAL ENGINEERING

NATIONAL UNIVERSITY OF SINGAPORE

2008

Acknowledgement

My first thanks go to my parents, brother, and wife. My parents provide extremely hard-won opportunities that I have been privileged to choose from. My elder brother Wenmo guides and warms me as a lighthouse in my growth. My wife Yawen continuously supports me and stands in a line with me.

I would like to express my sincere gratitude to my supervisors Professor K. Y. Lam and Professor Hua Li. Special appreciation goes to Professor Lam for his sagacious guidance and support, much of which came at times when I needed it the most. I want to sincerely thank Professor Li for his academic parenting during my Ph.D. study. I have benefited so much from his training and impeccable standards on research, while giving constant encouragement.

In stressful four years, I have talked to many people in order to seek advice. On the technical side, I would like to thank Professor G. R. Liu of Department of Mechanical Engineering, Professor Somsak Swaddiwudhipong of Department of Civil Engineering, and Professor Karl Erik Birgersson of Department of Chemical and Biomolecular Engineering, NUS.

My colleagues in IHPC and friends in NUS made my stay in Singapore pleasurable. I have had so much fun with my office mates and friends, Yew Yong Kin, Chen Jun, Wang Zijie, Zou Xu, Zhang Guiyong, ChengYuan, Zhang Yingyan, Yiao Jianxin and Wang Sugui. Great thanks go to Bernard Kee for his friendship and many helps to my study and life. Many thanks also go to my tennis partners Dr. Yap, Dr. Gong, Mr. Ho, Gary…. Thanks to fellows, whom I cannot possibly list, for being helpful and cheerful friends.

This research was supported by the financial support from the Agency for Science, Technology and Research (A*STAR) of Singapore.

Table of Contents

Summary

Environmental-sensitive hydrogels are increasingly attracting the attention of researchers all over the world due to their remarkable behaviors of the volume phase transition, which causes swelling, shrinking and/or bending deformation. The hydrogel is responsive to small changes of the local environmental conditions. However, most studies have so far been experimental-based. The objective of this thesis is thus to develop multiphysics models with the capability of predicting the material properties and behavior of hydrogels responding to three kinds of environmental stimuli, namely the externally applied electric field, the pH-electric coupled stimuli and the blood glucose concentration of the surrounding solution.

In general, the mobile ions diffuse between the surrounding solution and the porous hydrogel when a stimulus is applied to the environmental-sensitive hydrogel. The diffusive ion concentrations then redistribute in both the solution and hydrogel. As a result, an osmotic pressure is generated due to the concentration difference over the interface between the solution and hydrogel, which drives the swelling or shrinking deformation of the hydrogel. The deformation of the hydrogel will give rise to the redistribution of the diffusive ion concentration and fixed charge group density, which causes a new difference in diffusive concentrations. The recurrent kinetics continues until the hydrogel reaches an equilibrium state.

Based on the mechanism mentioned above, this thesis presents a theoretical

framework for the analysis of the equilibrium behavior of the environmental-sensitive hydrogels. More specifically, it considers the chemo-electro-mechanical multi-energy coupled effects on the performance of the stimulus-responsive hydrogels to the blood glucose concentration, the pH-electric coupled stimuli and the externally applied electric voltage, respectively. They are presented by developing three mathematical models for those environmental-sensitive hydrogels, termed the Multi-Effect-Coupling Glucose-Stimulus (MECglu) model, the Multi-Effect-Coupling pH-Electric-Stimulus (MECpHe) model, and the refined Multi-Effect-Coupling Electric-Stimulus (rMECe) model, respectively.

The models are examined by comparing the simulation results with experimental data published in open literature, and substantial agreements are achieved. It is thus confirmed that the three models, MECglu, MECpHe and rMECe models, are able to efficiently simulate the response of the environmental-sensitive hydrogels to the change of the blood glucose concentration, the coupled pH-electric stimuli and the externally applied electric voltage, respectively. Furthermore, systematical simulations are conducted here for discussion of the influences of many environmental conditions and physical parameters on the equilibrium behaviors of the environmental-sensitive hydrogels. They include the enzyme concentration and the initial fixed charge density within the hydrogel, the solution oxygen concentration, the solution pH, the ionic strength and ionic valence of surrounding solution, the Young's modulus and the initial geometry of the hydrogel. In order to elucidate the complicated swelling mechanism, the studies are also carried out using the developed models for discussion of the effects

of these parameters on the distributions of the diffusive ionic concentrations and electric potential in both the hydrogel and the surrounding solution, on the distribution of the fixed charge density within the hydrogel, and on the degree of equilibrium swelling, the displacement and bending deformation of the environmentally sensitive hydrogels. Based on the simulations and discussions, several significant conclusions are drawn. They provide useful guideline for further understanding of material properties and responsive performance of the stimulus-responsive hydrogels to environmental change. The three models developed in this thesis can also be employed to optimize design of smart hydrogel based biomedical devices.

Nomenclature

c_f	fixed charge density
c_k	ionic concentration of species k
c_{m0}^s	total ionizable groups per unit solid volume
D_k	diffusion coefficient of the spicies k
E_0	Young's modulus
$\boldsymbol{E}$	strain tensor of solid matrix
$\boldsymbol{F}$	deformation gradient tensor
F	Faraday's constant
f_{ij}	frictional drag coefficients between the inter-diffusing i and j components
ΔG	Gibbs free energy
$\boldsymbol{I}$	identity tensor
I	ionic strength
$\boldsymbol{J}_k$	flux of the species k
K_a	dissociation constant
n	number of mole
p	pressure
$p_{osmotic}$	osmotic pressure
$\boldsymbol{P}$	first Piola-Kirchhoff stress tensor
R	universal gas constant
r	chemical reaction ratio
$\boldsymbol{S}$	second Piola-Kirchhoff stress tensor
T	absolute temperature (K)
V_e	electric voltage

V_i	volume of phase
z_f	valence number of fixed charge group
z_k	valence numbers of ionic species *k*
v_k	velocity of the component *k*
α	volume fraction of phase
β	order of polynomial
ε	relative dielectric constant
ε_0	dielectric constant
ϕ	volume fraction
γ	chemical activity coefficient
υ	Poisson's ratio
π	osmotic pressure
λ , μ	Lame constants
μ^k	chemical potential of component *k*
μ_0^k	chemical potential of component *k* at the reference configuration

AMPS	2-acrylamido-2-methylpropane sulfonic acid)
DEA	*N*,*N*-Diethylaniline
DEAAm	*N*,*N*-diethylacrylamide
DEAEM	diethylaminoethyl methacrylate
DMAAm	*N*,*N*-dimethylacrylamide)
DMAEMA	*N,N*-dimethylaminoethyl methacrylate
EDMA	ethyleneglycol dimethacrylate
HEMA	hydroxyethyl methacrylate
HPMA	*N*-(2-hydroxypropyl)methacrylamide
IDDM	insulin-dependent diabetes mellitus

IMPC	ionic polymer-metal composite
LCST	lower critical solution temperature
LPIM	local point interpolation method
MAAc	methacrylic acid
MBAAm	*N*,*N*'-methylenebis(acrylamide)
MLPG	meshless Petrov-Galerkin method
NIPAAm	*N*-isopropylacrylamide
PAA	poly(acrylic acid)
PBA	phenylboronic acid
PEG	poly(ethylene glycol)]
PIM	point interpolation method
PVA	polyvinyl acetate/alcohol
PVC	poly(vinyl chloride)
PVP	poly(*N*-vinyl-2-pyrrolidone)
RKPM	reproducing kernel particle method
SPH	smooth particle hydrodynamics
VBC	vinylbenzyl chloride

List of Figures

List of Tables

Chapter 1
Introduction

1.1 A Brief Background of Smart Hydrogels

Hydrogels are the hydrophilic polymers with the three-dimensional crosslinked macromolecular networks, and capable of imbibing large amount of water or biological fluid while maintaining their structure. In general, the hydrogels consist of three phases: the polymeric matrix solid phase, the interstitial fluid phase, and the ionic phase including the mobile ions and the fixed charged groups attached onto the polymeric chains. The solid matrix is crosslinked by homopolymers or copolymers with chemical or physical methods, such as tie-points, junctions, entanglements and crystallites (Stauffer and Peppas, 1992; Hickey and Peppas, 1995; Peppas and Mongia, 1997; Kizilay and Okey, 2003), and provides the structure and physical integrity of hydrogels which ensure them exhibiting a thermodynamic compatibility with water and allow them to swell in aqueous media (Flory and Rehner, 1943; Flory, 1953).

According to the nature of the pendant groups attached onto the crosslinked polymeric networks, the hydrogels are classified into neutral or ionic ones (Peppas et al., 2000). The ionic hydrogels are ionizable and then called polyelectrolyte hydrogels. The ionic groups in the polyelectrolyte hydrogels are called fixed-charge groups due to their inertance compared with the mobility of the freely mobile ions in the interstitial fluid. Figure 1.1 shows the microscopic structure of a polyelectrolyte hydrogel, in

which the fixed charge groups are attached onto the crosslinked macromolecular chains that construct a three-dimensional polymeric network. The network is a superporous structure filled with interstitial fluid, where the ions undergo Brownian motion and diffuse in and out of the hydrogel.

One of the most interesting properties of the polyelectrolyte hydrogels is their capability of responding to the environmental stimuli. Such polyelectrolyte hydrogels are called 'smart' or 'intelligent' materials, because the minute change in the environmental conditions or stimuli will trigger various behaviors of the hydrogels. One remarkable behavior is the volume phase transition that causes the swelling, shrinking or bending deformation of the hydrogels. The volume phase transition is the continuous or discontinuous volume change of the environmental-sensitive hydrogels responsive to a small change of local environmental conditions (Wang et al. 1993; Mow et al., 1999; Lowman and Peppas, 1999). When a stimulus is applied to a polyelectrolyte hydrogel, such as a change of buffer solution pH value, the mobile ions will diffuse in and out of the hydrogel to redistribute between the surrounding solution and the hydrogel, and the free energy of the system will correspondingly change, as shown in Figure 1.2 (Peppas and Merrill, 1977). As a result, an osmotic pressure is generated by the concentration difference at the interface between the solution and hydrogel, which drives the swelling or deswelling of the hydorgel. The deformation of the hydrogel will give rise to the redistribution of the diffusive ions and fixed charge groups, which generates a new concentration difference. The recurrent process will continue and finally stop until the system comprising the hydrogel and the solution

reaches an equilibrium state.

Due to the unique properties of the environmentally sensitive hydrogels, such as good mechanical properties, excellent sorption capacity, biocompatibility, permeability and surface properties, smart hydrogels have been used in diverse applications, such as biomedical and medicine microdevices, drug delivery systems, articular cartilage, wound scaffold and tissue engineering (Shahinpoor, 1998; Li et al., 2000; Qiu and Park, 2001).

The aforementioned environmental stimuli can be categorized into the physical and chemical stimuli. The physical stimuli include environmental temperature (Chen and Hoffman, 1995; Yoshida et al., 1995; Temtem et al., 2007), electric field (Tanaka et al., 1982; Kwon et al., 1991; Osada et al., 1992), light (Mamada et al., 1990; Kodzwa et al., 1999), pressure (Kato, 2000), and magnetic fields (Kato et al., 1997; Zrinyi et al., 1998), while the chemical or biochemical stimuli include environmental pH (Gehrke et al., 1988; Siegel et al., 1990; Brannon and Peppas, 1991; Chu et al., 1995; Ali and Hegazy, 2007), glucose (Miyata et al., 2002; Kabilan et al, 2004; Mano et al., 2005), chemicals species (Kokufuta et al., 1991; Kataoka et al., 1998; Petrova et al., 2007), antigen (Miyata et. al.,1999, 2002) and enzymes (Kataoka, et al, 1998; Mano, et al, 2005).

The environmental pH, electric field and glucose are the most important environmental signals, especially in applications of BioMEMS and biomedical fields. However, the influences of environmental pH, electric field and glucose on equilibrium behaviors of the environmental-sensitive hydrogels remain poorly

understood. Therefore, the objectives of this thesis are to develop multi-physics models with the capability of predicting the influences of the three environmental stimuli on smart hydrogels. Accordingly, the literature review on environmentally sensitive hydrogels will be made in detail in the next section for the stimuli of pH, electric field and glucose, respectively.

1.2 Literature Survey

1.2.1 pH-Sensitive Hydrogels

Solution pH is one of the commonest triggering signals for the environmentally sensitive hydrogels. Compared with thermosensitivity of smart hydrogels, their pH sensitivity gives more choices for their applications (Ni et al., 2007). Accordingly, the pH-sensitive hydrogels are widely investigated for various applications. All the pH-sensitive hydrogels are known as polyelectrolytes and contain a large number of pendant acidic groups, e.g. carboxylic and sulfonic acids or basic groups, e.g. ammonium salt, which either accept or release protons (H^+) in response to the change in environmental pH. In order to provide the research background of the hydrogels, a brief overview is given in the following subsections for the experimental work and existing theoretical models of the pH-sensitive hydrogels.

1.2.1.1 Brief review of experimental work and applications

Katchalsky (1949, 1950) may be the first researcher to synthesize a hydrogel, which can swell and shrink with change in solution pH. Based on his studies, many scientists continuously conducted investigations on this kind of material (Dusek and Patterson, 1968; Tanaka et al., 1978, 1981; Gehrke et al., 1988; Siegel, 1990b; Brannon-Peppas, 1991; Chu et al., 1995). In this field, Tanaka and his coworkers (1978, 1981) made the most outstanding investigation. They used the phase volume transition theory to describe the process, in which the hydrogels are stimulated by different environmental stimulus, including the solution pH. The phase volume transition theory successfully explains the conversion of chemical energy into mechanical energy. With this unique characteristic, the pH-sensitive hydrogels could be an ideal candidate for biomimetic actuators/sensors and drug delivery systems (Beebe et al., 2000).

It is well-known that the swelling of pH-sensitive hydrogels depends on the functional acidic or basic groups attached onto the crosslinked polymer backbone network, such as the carboxyl, sulfonic and amino groups. Due to the dissociation of the pendent groups and the influx of counterions, the concentration of ions within the hydrogel is higher than that in the surrounding solution, which generates osmotic pressure, resulting consequently in a swelling. The interaction and repulsion of charges along the polymeric chain may also affect the swelling (Siegel and Firestone, 1988). Equilibrium in the hydrogel system occurs when the elastic restoring force of the polymer network balances with the osmotic force (Tanaka and Fillmore, 1979; Tanaka, 1981). During the swelling process, the hydroxide ions transport into the gel, while during the shrinkage the protons H^+ diffuse into the hydrogel to neutralize the

negative charged acidic carboxylate groups. The diffusive ion flux induces an electrical potential difference that drives the electromigration of the ions in the direction opposite to that of the diffusion (Gerlach et al., 2005). The change of the electrical potential at the hydrogel-solution interface is a function of the pH value of the surrounding solution. Therefore, the coupled Poisson-Nernst-Planck equations and the mechanical equilibrium equations can be used to describe the gel swelling/shrinking process (Aluru et al., 2001; Li et al., 2004, 2005).

1.2.1.2 Review of existing theoretical models

In the modelling of the response of environmentally sensitive hydrogels to various stimuli, the ultimate goal is to elucidate the mechanism of the mobile ion diffusion, the degree of ionization, the polymer-solvent interaction and the swelling behavior. In order to realize the goal, numerous attempts were made in the theoretical studies for the responsive behaviors of the environmentally sensitive hydrogels under the stimuli of solution pH.

Essentially, the impetus for modeling of environmentally sensitive hydrogels stems from the two basic theoretical frameworks, Flory-Huggins theory and Flory-Rehner model. Brought forward independently by Flory (1941) and Huggins (1941), the Flory-Huggins theory is a mathematical model of the thermodynamics of polymer solutions which takes account of the great dissimilarity in molecular sizes in adapting the usual expression for the entropy of mixing solution. Although it makes the simplifying assumptions such as no chemical reaction, constant temperature and

external pressure, it can still provide some useful interpretation of experiments. Tanaka et al. (1982) used the Flory-Huggins theory to explain successfully the phenomenon that a hydrolyzed acrylamide collapses in an acetone/water binary mixture upon the application of an electric field. At swelling equilibrium, the elastic response of the network exactly offsets the difference in chemical potential of the solvent between the swollen network and the external solvent phase. Accordingly, several researchers obtained reasonable values of the polymer solvent interaction parameter χ by solving the Flory-Huggins equation to explain the experimental data of swelling hydrogels (English et al., 1997; Caykara and Aycicek, 2005).

The Flory-Rehner theory is similarly used to describe the equilibrium swelling of hydrogels, in which the swelling equilibrium is determined by a competition between the volume interactions of segments and elasticity of rubber-like gel (Flory, 1953; Orakdogen and Okay, 2006). The swelling ratio of a hydrogel depends on its network structure. Complemented by the Donnan equilibrium theory, the Flory-Rehner theory is modified to take into account the polymer volume fraction in the swollen state of hydrogel (Brannon-Peppas and Peppas, 1991; Okay and Sarusil, 2000; Caykara et al., 2003). The Flory-Rehner-Donnan equation can thus predict a region of bistability in the swelling of some hydrophilic pH-sensitive hydrogels (English et al., 1997; Gehrke, 2000; Caykara and Akcakaya, 2006; Emileh et al., 2007).

At present, there are few mathematical approaches applicable to descibe the swelling behavior of hydrogel instead. The two models are popularly used to qualitatively describe the swelling equilibrium, i.e. the thermodynamics model

developed by Siegel (1990a) and the triphasic mechanoelectrochemical model proposed by Lai et al. (1991). The thermodynamic model (Siegel, 1990a) assumes that the total free energy of hydrogel–solvent system contributes from the three sources, namely the hydrogel–solvent mixing, the deformation of polymer networks and the osmotic pressure. The mechanoelectrochemical model (Lai wt al., 1991) combines the physicochemical theory for ionic and polyionic solutions expressed in terms of their chemical potentials, where the gradients of chemical potentials are considered as the driving forces for the swelling of hydrogel. Comparing the two models, the mechanoelectrochemical model introduces the mechanical factor into the model with the assumption that the solid network deformation is linearly small. And the thermodynamic model doesn't consider the surface tension as an inevitable factor in a microsphere system. However, after adding a domain effect to the factor of osmotic pressure, the thermodynamic model is applicable (Tanaka et al., 1973).

In general, the volume phase transition results from the competitive balance between repulsive and attractive interactions (Li and Tanaka, 1992). According to the Flory's field theory for analysis of the swelling equilibrium of the hydrogels (Flory, 1953), the interactions may be presented mathematically by three contributions to the change of free energy, namely the polymer-solvent mixing, the elastic deformation of polymeric network matrix and the osmotic pressure due to ionic concentration difference. The polymer-solvent mixing contributes to either attractive or repulsive forces, depending on the relation between entropy change and heat associated with the mixing. The elastic deformation of polymeric network matrix is determined by

mechanical restoring force of the matrix due to material elasticity. The osmotic pressure is the driving source for expansion, resulting from the ionic concentration difference between the interior hydrogels and exterior bathing solution.

1.2.2 Electric-Sensitive Hydrogels

1.2.2.1 Brief review of experimental work and applications

Due to the ionizable groups binding to the network chains, the polyelectrolyte hydrogels can swell or shrink when induced the externally applied electric voltage. The phenomenon was first reported by Hamlen (1965), in which a PVA-PAA gel swells when an electric field of 5V is applied to the buffer solution in which the gel is immersed. Later, Fragala et al. (1972) fabricated electrically-controlled artificial muscles based on a weak acid polymer, which has attracted significant concerns about the application of the electric-stimulus hydrogels. Consequently, a series of foundational experiments were carried out for that in 1970s (Yannas and Grodzinsky, 1973; Glodzinsky 1974; Glodzinsky and Melcher, 1976). Based on the above experiments, many attempts were made extensively to investigate the swelling mechanism of the electric-sensitive hydrogels. Tanaka (1981) explained the sudden collapses of ionic polymer gels contacted the DC electrodes. Osada's team (1985, 1987, 1989, and 1991) developed an electrically activated artificial muscle with the hydrogels. Shiga et al (1990, 1992a, 1992b) investigated the swelling and bending deformation of PAA subjected to an electric field. Sagalman et al. (1992a, 1992b, 1993)

analyzed an electrically controlled ionizable hydrogel as active material in adaptive structures. Shahinpoor (1998) and Li (2000) fabricated the ionic polymer-metal composite (IMPC) to use for engineering tissue.

From the theoretical point of view, the response mechanism of the electric-sensitive hydrogels is similar to that of pH-sensitive hydrogels (Tanaka, 1981). When an electric field is applied to the bath solution, mobile ions will redistribute in the hydrogels and surrounding solution. The diffusion gives rise to the ionic concentration differences between the interior hydrogel and exterior solution because of the fixed charge groups that are bound to the crosslinked macromolecular chains. As a result, an osmotic pressure is generated by the concentration differences, which drives the swelling or shrinking of the hydrogel. The deformation of the hydrogel redistributes the diffusive ions and fixed charge groups, which causes new ionic concentration differences and the hydrogel deforms again. The recurrent kinetics will stop when the hydrogel reaches an equilibrium state. It can also explain the process how chemical energy converts to mechanical energy in the process.

1.2.2.2 Review of existing theoretical models

Despite many experiments in the past decades, few of them focused on the development of mathematical models for simulations of the responsive behaviors of electric-sensitive hydrogels.

Based on previous work (Mow et al., 1980; Myers et al., 1984; Lanir, 1987; Eisenberg and Grodzinsky, 1987), Lai et al. (1991) proposed a triphasic

mechano-electro-chemical theory for the responsive behaviors of hydrogel-like tissues. Although the theory explains explicitly the fixed charge density and diffusive ionic concentrations, it only partially accounts for the mechanical properties of tissues and is not successful in simulating the physiochemical and electrochemical phenomena in the hydrogels, such as the ions diffusion, mechanical expansion of solid matrix, and the effect of fixed charge groups on distribution of ionic concentrations. Recently, Wallmersperger et al. (2001) used the finite element method to simulate the deformation of the electic-sensitive hydrogels subjected to the externally applied electric voltage. However, the method by Wallmerspereger et al. assumes that the hydrogels undergo a small linear deformation even at high electric voltage. Comfirmed by experiments, the hydrogels will deform dramatically under a high voltage, and then the model faces difficulty and limitations. Zhou et al. (2002) developed a model to simulate the equilibrium behaviors of the electric-sensitive hydrogels, including the distributions of the diffusive ionic concentrations and electric potential. It partially considers the steady-state behaviors of the hydrogel and the computational domain of the model covers the hydrogel only, which will limit its study for the ionic transport.

1.2.3 Glucose-Sensitive Hydrogels

The glucose-sensitive hydrogels increasingly attract the attention of worldwide researchers because they are typically used as smart biomaterials to design self-regulated drug delivery systems (Qiu and Park, 2001; Eddington and Beebe, 2004).

The self-regulated systems are called closed-loop delivery systems, where the insulin infusion rate for the insulin-dependent diabetes mellitus (IDDM) is administered autonomously based on the physiological blood glucose levels, instead of depending on an external signal to trigger insulin delivery (Miyata et al., 2002; Sershen and West, 2002).

1.2.3.1 Brief review of experimental work and applications

So far the glucose-sensitive hydrogels are divided into three categories based on their different responses to the change of the glucose concentration.

The first kind is the glucose oxidase-loaded glucose-sensitive hydrogels, in which the glucose oxidase is immobilized in the pH-sensitive hydrogels to catalyze blood glucose to gluconic acid and regulate the insulin release. Many insulin delivery systems have been reported based on this kind of hydrogel. Ishihara et al. (1984, 1986) synthesized a DEA/HPMA crosslinked polymeric membrane and investigated the insulin release from the hydrogel membrane capsules containing insulin and glucose oxidase. Horbett el al. (1985, 1987 and 1995) fabricated the porous hydrogel membranes to obtain high insulin permeability. Peppas et al. (1997, 1999) studied the glucose-sensitive insulin release from the pH-sensitive hydrogels containing insulin and glucose oxidase.

The second is the lectin-loaded glucose-sensitive hydrogels. In this field, the research efforts are put on the concanavalin (Con A) loaded hydrogels, where Con A is a lectin possessing four binding sites of polymeric chains. Brownlee et al. (1979) and

Kim et al. (1989, 1990) developed the concanavalin-based glucose-sensitive systems for insulin release. Kokufuta et al. (1991) combined Con A with temperature-sensitive hydrogels to synthesize sachharide-sensitive hydrogels. Nakamae et al. (1994) investigated the complex formation of a Con A loaded hydrogel with pendant glucose groups. Park et al. (1996, 1997) prepared hydrogels capable of sol-gel phase-reversible transition responding to changes in glucose concentration, and also investigated the release of lysozyme and insulin from glucose-sensitive hydrogels.

The third is the glucose-sensitive hydrogels with phenylboronic acid moieties, which is a complex formation for the phenylboronic acid group and the glucose. Kikuchi et al. (1996) used an electrode coated with a poly(NVP-co-PBA)/PVA complex to develop glucose-sensitive devices. Kataoka et al. (1998) prepared totally synthetic hydrogels from NIPAAm and phenylboronic acid, which shows good glucose sensitivity.

Based on the brief literature review, it is known that most experiments mainly focus on the glucose oxidase-loaded glucose-sensitive hydrogels. Therefore, the present studies will try to develop a multiphysics model for simulation of the glucose oxidase-loaded glucose-sensitive hydrogels.

1.2.3.2 Review of existing theoretical models

In spite of numerous experimental studies done on the glucose-sensitive hydrogels, only a few studies found were made for theoretical modeling and numerical simulation. For example, Parker and Schwartz (1987) developed a ping-pong kinetics

model for the overall rate of reaction of the immobilized glucose oxidase. Albin et al. (1987) simulated the cationic glucose-sensitive membrane with the assumption that the diffusivity of each species within the membrane equal to that in the bulk solution and independent of the swelling or pH gradient of the membrane. Based on the work done by Albin et al. (1987), Klumb et al. (1992) discussed various design configurations to overcome the oxygen limitation in the insulin delivery system. Gough et al. (1985, 1988) simulated the steady-state and transient performance of a cylindrical glucose sensor. It is noted that the above models (Gough et al., 1985, 1988; Albin et al., 1987; Parker and Schwartz, 1987; Klumb et al., 1992) focus only on the diffuse and reaction of mobile species, or on the effect of the enzymes, but don't study the relation between the change of pH within the hydrogels and the mechanical deformation of the hydrogel. Abdekhodaie and Wu (2005) developed a theoretical model for the cationic glucose-sensitive membrane with consideration of the oxygen limitation and swelling-dependent diffusivities of the species involved in the membrane. The model developed by Abdekhodaie and Wu (2005) uses the mesh size of the polymeric network to define the volume swelling ratio, however, which requires lots of parameters and assumption for the calculation. In addition, it is widely accepted that the ionic strength of the surrounding solution and the externally applied electric field are two important factors affecting the swelling of the stimulus-sensitive polyelectrolyte hydrogels (Luo et al., 2007). In spite of this, all models mentioned above fail to take account of the two important factors for the simulation of the response of the glucose-sensitive hydrogels (Gough et al., 1985, 1988; Albin et al.,

1987; Parker and Schwartz, 1987; Klumb et al., 1992; Abdekhodaie and Wu, 2005). Therefore, developing a reliable model is crucial to investigate systematically the behaviors of the glucose-sensitive hydrogels.

1.2.4 Other Environmentally Sensitive Hydrogels

In addition to the three most important kinds of environmental-sensitive hydrogels discussed above, there are the environmentally sensitive hydrogels responsive to other stimuli, including environmental temperature, light, pressure, specific ions, thombin and antigen.

1.2.4.1 Temperature-sensitive hydrogels

Temperature is one common environmental stimulus to trigger smart hydrogels (Schild, 1992; Irie, 1993; Bromberg and Ron, 1998). This kind of hydrogel performing the property of temperature-responsive phase transition has hydrophobic groups in general, such as methyl, ethyl and propyl groups (Qiu and Park, 2001). According to the swelling behavior of the hydrogels in response to a stepwise temperature change, they are classified as negatively thermosensitive hydrogels which shrink as temperature increases above the lower critical solution temperature (LCST), positively thermosensitive hydrogels which swell at temperature higher than LCST and shrink at temperature lower than LCST, and the thermally reversible hydrogels which have different LCST values and biodegradability (Dong and Hoffman, 1990; Bromberg and

Ron, 1998). Due to their LCST around the body temperature, poly(N-iso-propylacrylamide) (PNIPAAm) and poly(N,N-diethylacrylamide) (PDEAAm) are the most widely used temperature-sensitive hydrogels (Okano et. al., 1990; Gutowska et al., 1992; Okuyama et al., 1993) in drug delivery systems (Yoshida et al., 1991; Dinarvand and Emanuele, 1995; Bromberg and Ron, 1998).

Only few models have been developed to simulate the response of thermal-stimulus responsive hydrogels. An early attempt is the interpolated affine model developed by Ten and Farasz (1984) which studied the compressibility and directional-specific interaction for responsive behaviors of temperature-sensitive hydrogels at the lower critical solution temperature. By assuming that the parameters related to the volume fraction can detail the polymer-solvent interaction, Erman and Flory (1986) studied discontinuous volume phase transition. Later, Otake et al. (1989) developed a model to investigate thermally induced discontinuous shrinking deformation of ionized hydrogels with considering the effects of hydrophobic hydration and interactions. The statistical thermodynamic model presented by Lele et al. (1995) considers the hydrogen bond interaction playing an essential role in the swelling equilibrium of PNIPA hydrogel immersed in water.

In addition, Hino and Prausnitz (1998) proposed a molecular thermodynamic model for simulation of volume phase transition of PNIPA hydrogels. More recently, Li et al. (2005b, 2005c) developed the multi-effect-coupling thermal-stimulus (MECtherm) model with consideration of multiphase and multiphysics effects to study the swelling equilibrium of ionic thermo-sensitive hydrogles.

1.2.4.2 Light-sensitive hydrogels

There are two kinds of light-sensitive hydrogels, UV-sensitive and visible light-sensitive hydrogels. Exposed to UV irradiation, the UV-sensitive hydrogels swell discontinuously at a given temperature, but shrink in the absence of UV (Mamada et al., 1990; Qiu and Park, 2001). When visible light is applied, the chromophore hydrogels can absorb light and convert it into heat to increase the local temperature of the hydrogels. The temperature increase causes a volume change in the hydrogels (Suzuki and Tanaka, 1990). Because light stimulus can be employed instantly and delivered in specific amounts with high accuracy, and the visible light is readily available, inexpensive, safe, clean and easily manipulated, light-sensitive hydrogels have desirable potentials in biomechanical engineering fields, such as optical switches, display units, photo-responsive artificial muscles and ophthalmic drug delivery devices (Suzuki and Tanaka, 1990; Rasmussen et al., 2002; Gupta et al., 2007).

1.2.4.3 Pressure-sensitive hydrogels

In general, the pressure-sensitive hydrogels expand at high pressure and shrink at low one. It is well known that this pressure sensitivity is related with the LCST and is a common characteristic of temperature-sensitive hydrogels, such as poly(*N*-isopropylacrylamide) (Lee et al., 1990), poly(*N*,*N*-diethylacrylamide) (Wang et al., 1996), poly(*N*,*N*-propylarcylamide) (Zhong et al., 1996). Zhang and Seitz (2002) demonstrated the performances of a new type of pH sensor by a pressure sensitive

resistor, which combines a bead of porous lightly crosslinked diethanolamine derivatized poly(vinylbenzyl chloride) with a strain gauge. Furthermore, a measurement concept is realized for the detection of carbon dioxide, where the CO_2 induced pressure generated in an enclosed pH-sensitive hydrogel is measured by a micro pressure sensor. The device can be applied to quantify the partial pressure of CO_2 (Pco_2) in the stomach as diagnosis for gastrointestinal ischemia (Herber et al., 2005).

1.2.4.4 Specific ion-sensitive hydrogels

Despite that most specific ion-sensitive hydrogels are ionizable and they are sensitive to the concentration of salt solution, there are some special neutral hydrogels responding to salt concentration. For example, the nonionic poly(*N*-isopropylacrylamide) hydrogel can swell at a critical concentration of sodium chloride in aqueous solution (Park and Hoffman, 1993). With the unique phase transition, this hydrogel can thus be used as the chloride ion-sensitive biosensors. By chemical modification of an ion-sensitive field-effect transistor, poly(vinyl chloride) (PVC) hydrogels containing lipophilic tetra-n-octal-ammonium ions are developed as sensors (chemfets) with the specific sensitivity to nitrate (Stauthamer et al., 1994). A holographic sensor fabricated by hydroxyethyl methacrylate (HEMA) and ethylene glycol dimethacrylate (EDMA) hydrogel matrix can have metal detection sensitivity to detect real-time divalent metal ions, such as Ca^{2+}, Mg^{2+}, Ni^{2+}, Co^{2+} and Zn^{2+} (Gonzalez et al., 2005).

1.2.4.5 Specific antigen-responsive hydrogels

The swelling behavior of the antigen-responsive hydrogels can be triggered and reduced the crosslinking density by higher competetivity of the free antigens than the polymer-bound antigen. This sol-gel phase transition caused by the antigen-antibody interactions is highly desirable and useful to develop devices for biomedical applications (Miyata et al., 1999). Novel antigen responsive hydrogels are copolymerized with crosslinked *N*-isopropylacrylamide (NIPAAm) and *N*,*N*'-methylenebis(acrylamide) (MBAAm) using redox initiators, and used for polymerizable antibody Fab fragment from monoclonal anti-fluorescein BDC1 antibody (IgG2a) (Lu et al., 2003). With loading grafted gentamycin, PVA hydrogels demonstrate significantly higher thrombin-like enzymatic activity toward a certain peptide sequence than exudates from non-infected wound (Suzuki et al., 1998). The hydrogels have sufficient specificity and excellent potential for applications of stimulus-responsive and controlled drug delivery systems (Tanihara et al., 1999).

1.2.5 Hermite-Cloud Method — A Meshless Numerical Technique

In order to solve the mathematical models in this thesis with challenges, for example, multi-energy domains, computational domain remeshing, coupled nonlinear partial differential governing equations, moving boundaries and localized high gradient, a truly meshless strong-form numerical technique, called the Hemite-cloud method, is employed for the simulation of the response of environmentally sensitive hydrogels.

1.2.5.1 A overview of meshless methods

In computational science and engineering, the finite element method (FEM) has become dominant numerical tool for modeling and simulation of a wide range of engineering problems for decades. However, in some cutting-edge areas, such as bio-micro-electro-mechanical systems (BioMEMS) which requires the multiphysical and multiscale studies, FEM faces certain limitations, including the tedious and iterative remeshing to track dynamic processes in large deformation problems and the requirement for large storage and memory due to the large number of element nodes involved in FEM discretization. In order to overcome these deficiencies resulting from FEM, various meshless numerical techniques are recently developed (Liu GR, 2003). According to the techniques to solve the governing partial differential equations, the meshless methods can be classified into two groups. One is based on the strong-form of partial differential equations (PDEs), such as the finite point method (Onate et al., 1996) and the smooth particle hydrodynamics (SPH) (Lucy, 1977). The other is based on the weak-form of PDEs, such as the element-free Galerkin method (EFG) (Belytschko et al., 1994) and the diffuse element method. (Nayroles et al., 1992)

It should be noted that in the field of meshless technique, Liu et al. have made significant contributions by developing several efficient approaches, including the point interpolation method (PIM) (Liu and Gu, 2001a), the meshless Petrov-Galerkin method (MLPG) (Liu et al., 2001b) and the local point interpolation method (LPIM) (Liu and Gu, 2001c).

The Hermite-cloud method is based on the classical reproducing kernel particle method (RKPM), except that a fixed reproducing kernel approximation is used instead (Aluru and Li, 2001). In this method, the Hermite theorem is employed for the construction of the interpolation functions, where the shape functions are constructed to correspond respectively to the unknown functions and their first-order derivatives. The point collocation technique is used for the discretization of the partial differential governing equations. Through the constructed Hermite-type interpolation functions, the approximate solutions of both the unknown functions and the first-order derivatives are computed directly. A set of differential-type auxiliary conditions are also required so as to construct a complete set of PDEs with the Dirichlet and/or Neumann boundary conditions. By scattering a set of points in the computational domain and its edges, the point collocation technique is then applied for the discretization of partial differential boundary value (PDBV) problems. The approximate solutions of both the unknown functions and their first-order derivatives are expressed in terms of the shape functions and unknown point values, resulting in a complete set of discrete algebraic equations. Finally, they are solved with respect to the unknown point values and the numerical solutions of the PDBV problem can be computed in a straightforward way.

1.2.5.2 Development of meshless Hermite-cloud method

The main characteristic of the reproducing kernel method is its ability to reproduce the unknown function by integration transform over the domain of interest. Let us take a two-dimensional case as example, the reproducing kernel expression can

be written as the product of the window function $\Phi_{window}(x-p, y-q)$ and the real function $f(x,y)$ which is integrated over the defined domain, Ω. In order to exactly reproduce the real function, an ideal window function required should fulfill two conditions: (1) it is orthogonal in nature, and (2) its integration over the Ω domain should be unity. However, a suitable window function that simultaneously satisfies the both conditions does not normally exist. Hence, only an approximation of the unknown function may be obtained in most cases.

The reproducing kernel approximation of unknown real function $f(x,y)$, designated as $\widetilde{f}(x,y)$, is thus written in the following form

$$\widetilde{f}(x,y) = \int_{\Omega} \Phi_{window}(x-p, y-q) f(p,q) dpdq \tag{1.1}$$

By following the idea of the classical RKPM and employing a correction function $C(x,y,p,q)$ and a kernel function $K(x-p, y-q)$, the real window function is $\Phi_{window}(x-p, y-q) = C(x,y,p,q)K(x-p, y-q)$. If a fixed kernel technique is used instead of the more classical $K(x-p, y-q)$, the approximate unknown function is rewritten as

$$\widetilde{f}(x,y) = \int_{\Omega} C(x,y,p,q)K(x_k - p, y_k - q) f(p,q) dpdq \tag{1.2}$$

where the kernels are centered at the point (x_k, y_k). The kernel function may be constructed by different forms of weighted window functions, depending on different PDBV problems. In this thesis, a form of cubic spline function is considered as

$$K(x_k - p, y_k - q) = \frac{1}{(\Delta x \Delta y)} W^*(\frac{x_k - p}{\Delta x}) W^*(\frac{y_k - q}{\Delta y}) \tag{1.3}$$

where $W^*(z)$ is a cubic-spline window function and is defined as

$$W^*(z)=\begin{cases}0 & z<-2\\ \dfrac{(2+z)^3}{6} & -2\le z<-1\\ \dfrac{2}{3}-z^2\left(1+\dfrac{z}{2}\right) & -1\le z<0\\ \dfrac{2}{3}-z^2\left(1-\dfrac{z}{2}\right) & 0\le z<1\\ \dfrac{(2-z)^3}{6} & 1\le z\le 2\\ 0 & z>2\end{cases} \tag{1.4}$$

where $z=(x_k-p)/\Delta x$ for the x-component, and $z=(y_k-q)/\Delta y$ for the y-component. Δx and Δy denote the cloud size of the fixed kernel point (x_k, y_k) in the x- and y-direction, respectively. The cloud size is more or less arbitrary and is adjusted according to the scattered point distribution and the accuracy requirements due to the consistency conditions of the reproducing kernel approach.

The correction function $C(x,y,p,q)$ is typically expressed as a combination of independent basis functions. The highest order polynomial terms in the correction function $C(x,y,p,q)$ will depend on the highest order derivative terms of the governing PDE of interest. Hence, the correction function is expressed here as a product of a β^{th}-order row basis function vector $\mathbf{B}(p,q)$ and a β^{th}-order column coefficient vector $\boldsymbol{C}^*(x,y)$, namely $C(x,y,p,q)=\mathbf{B}(p,q)\mathbf{C}^*(x,y)$, where β is the order of polynomial used as the basis function. A linearly independent basis is given for a one-dimensional quadratic PDE problem,

$$\mathbf{B}(p)=\{b_1(p),b_2(p),\ldots,b_\beta(p)\}=\{1,p,p^2\} \qquad (\beta=3) \tag{1.5}$$

and for a two-dimensional quadratic PDE problem,

$$\boldsymbol{B}(p,q)=\{b_1(p,q),b_2(p,q),\ldots,b_\beta(p,q)\}=\{1,p,q,p^2,pq,q^2\} \qquad (\beta=6) \tag{1.6}$$

The correction function coefficient is provided by

$$\mathbf{C}^{*T}(x,y)=\{c_1,c_2,\cdots,c_\beta\} \tag{1.7}$$

where $c_i\ (i=1,2,\cdots,\beta)$ are the unknown coefficients which can be determined to satisfy the following consistency conditions

$$b_i(x,y)=\int_\Omega \mathbf{B}(p,q)\mathbf{C}^*(x,y)K(x_k-p,y_k-q)b_i(p,q)dpdq \qquad (i=1,2,\cdots,\beta) \tag{1.8}$$

By employing the point collocation technique, the discretization of the equation (1.8) is achieved and the consistency conditions are defined in discrete form as

$$b_i(x,y)=\sum_{n=1}^{N_T}\mathbf{B}(p_n,q_n)\mathbf{C}^*(x,y)K(x_k-p_n,y_k-q_n)b_i(p_n,q_n)\Delta S_n \qquad (i=1,2,\cdots,\beta) \tag{1.9}$$

where N_T is the total number of points sprinkled over both the interior computational domain Ω and along its edges. The subscript n denotes the n^{th} point in the domain and ΔS_n is the cloud area associated with the n^{th} point.

It is observed that the basis functions in the equations (1.5) and (1.6) consist of known polynomials that follow a linear relation. This leads to the construction of a set of linear algebraic equations with respect to the coefficients c_i (i=1, 2, …, β). Thus, the equation (1.9) can be rewritten in matrix form to obtain the correction function coefficient,

$$\mathbf{B}^T(x,y)=\mathbf{A}(x_k,y_k)\mathbf{C}^*(x,y) \tag{1.10}$$

where $\boldsymbol{A}(x_k,y_k)$ is a symmetric matrix associated with the fixed kernel centered at point (x_k,y_k) defined as

$$A_{ij}(x_k,y_k)=\sum_{n=1}^{N_T}b_i(p_n,q_n)K(x_k-p_n,y_k-q_n)b_j(p_n,q_n)\Delta S_n \qquad (i,j=1,2,\cdots,\beta) \tag{1.11}$$

Based on the equation (1.10), the correction function coefficient is solved by

$$\mathbf{C}^*(x,y) = \mathbf{A}^{-1}(x_k, y_k)\mathbf{B}^T(x,y) \tag{1.12}$$

By substituting equation (1.12) into $C(x,y,p,q) = \mathbf{B}(p,q)\mathbf{C}^*(x,y)$, and substituting the resulting correction function into the equation (1.2), and then discretizing the resulting the equation (1.2), the approximation $\tilde{f}(x,y)$ of the unknown real function $f(x,y)$ can be obtained in the following discrete form,

$$\begin{aligned}\tilde{f}(x,y) &= \sum_{n=1}^{N_T}(\mathbf{B}(p_n,q_n)\mathbf{A}^{-1}(x_k,y_k)\mathbf{B}^T(x,y)K(x_k-p_n,y_k-q_n)\Delta S_n)f_n \\ &= \sum_{n=1}^{N_T} N_n(x,y)f_n\end{aligned} \tag{1.13}$$

where f_n is the unknown point value of the n^{th} point, and $N_n(x,y)$ are the shape functions defined as,

$$N_n(x,y) = \mathbf{B}(p_n,q_n)\mathbf{A}^{-1}(x_k,y_k)\mathbf{B}^T(x,y)K(x_k-p_n,y_k-q_n)\Delta S_n \tag{1.14}$$

It is distinct that the derivatives of the shape functions can be obtained in a straight forward manner by differentiating the polynomial terms in the basis functions $\boldsymbol{B}(x,y)$. Further, if $b_i(x,y)$ (i=1, 2, 3) are espressed as the discretized consistency conditions of the equation (1.9), we have

$$\begin{aligned} b_1(x,y) &= 1.0 = \sum_{n=1}^{N_T} N_n(x,y) \\ b_2(x,y) &= x = \sum_{n=1}^{N_T} N_n(x,y)x_n \\ b_3(x,y) &= y = \sum_{n=1}^{N_T} N_n(x,y)y_n \end{aligned} \tag{1.15}$$

Next, two additional unknown functions, $Gx(x,y)$ and $Gy(x,y)$ are introduced, as the first-order derivatives of the unknown real function $f(x,y)$,

$$Gx(x,y) = f_{,x}(x,y), \quad Gy(x,y) = f_{,y}(x,y) \tag{1.16}$$

in which a comma denotes a partial derivative with respect to the indicated spatial variable. It is known that the Hermite interpolation theorem requires the first-order derivatives of a real function to be treated as additional unknown functions. Hence, the first-order differential functions may also be computed in an analogous discretization procedure by the equation (1.13). Thus the discrete approximation is given by

$$\widetilde{G}x(x,y) = \sum_{m=1}^{N_s} M_m(x,y)Gx_m \ , \widetilde{G}y(x,y) = \sum_{m=1}^{N_s} M_m(x,y)Gy_m \tag{1.17}$$

where $N_S(\leq N_T)$ is the total number of points covering the interest domain. In similar form to the equation (1.14), Gx_m and Gy_m designate the unknown point values of m^{th} point. $M_m(x,y)$ is the shape function associated with the first-order differential functions of $\widetilde{f}(x,y)$. It is understood that there are differences between the shape functions $M_m(x,y)$ and $N_n(x,y)$. In particular, the former shape functions are composed of (β-1) order of polynomial in the construction of the basis functions.

According to the Hermite interpolation theorem, a meshless approximation $\widetilde{f}(x,y)$ of the unknown real function $f(x,y)$ can now be constructed as follows

$$\begin{aligned}\widetilde{f}(x,y) = \sum_{n=1}^{N_T} N_n(x,y)f_n + \sum_{m=1}^{N_S}(x - \sum_{n=1}^{N_T} N_n(x,y)x_n)M_m(x,y)Gx_m + \\ + \sum_{m=1}^{N_S}(y - \sum_{n=1}^{N_T} N_n(x,y)y_n)M_m(x,y)Gy_m\end{aligned} \tag{1.18}$$

With the implementation of the Hermite-based interpolation approximation, we can directly compute the approximate solutions of both the unknown function and its first-order differential function. It is noteworthy to point out the potential in improving the computational accuracy. Particularly, the solutions at discrete points in the domain

are much more refined than those of the classical RKPM. As a result, the increase of accuracy of the approximate solutions and its first-order derivatives balances the shortcoming of the current technique which is the requirement of additional unknown functions.

With the introduction of the additional unknown functions, $Gx(x,y)$ and $Gy(x,y)$, it is necessary to impose auxiliary conditions to formulate a complete set of PDBV equations. Based on the definitions of $Gx(x,y)$ and $Gy(x,y)$ in the equation (1.16), the auxiliary conditions are developed naturally by imposing the first-order partial derivative with respect to the indicated spatial variable on the approximate solution $\widetilde{f}(x,y)$ in the equation (1.18). By considering the equations (1.15) to (1.17), the auxiliary conditions are derived as,

$$\sum_{n=1}^{N_T} N_{n,x}(x,y) f_n - \sum_{m=1}^{N_S} (\sum_{n=1}^{N_T} (N_{n,x}(x,y) x_n)) M_m(x,y) Gx_m - \\ - \sum_{m=1}^{N_S} (\sum_{n=1}^{N_T} (N_{n,x}(x,y) y_n)) M_m(x,y) Gy_m = 0 \tag{1.19}$$

$$\sum_{n=1}^{N_T} N_{n,y}(x,y) f_n - \sum_{m=1}^{N_S} (\sum_{n=1}^{N_T} (N_{n,y}(x,y) y_n)) M_m(x,y) Gy_m - \\ - \sum_{m=1}^{N_S} (\sum_{n=1}^{N_T} (N_{n,y}(x,y) x_n)) M_m(x,y) Gx_m = 0 \tag{1.20}$$

So far we have completed the formulation of the Hermite-cloud method. In summary, based on the Hermite interpolation theorem, we need construct the approximate unknown function $\widetilde{f}(x,y)$ as in the equation (1.18), and introduce the first-order differential functions, $\widetilde{Gx}(x,y)$ and $\widetilde{Gy}(x,y)$ in the equation (1.17), and then couple the formulation with the presently developed auxiliary conditions (1.19) and (1.20).

As mentioned above, the point collocation technique is employed to dicretize the generic engineering partial differential problems, affiliating with boundary value problems. Thus let us examine the general case of

$$\boldsymbol{L}f(x,y) = P(x,y) \quad \text{in } \Omega \tag{1.21}$$

$$f(x,y) = Q(x,y) \quad \text{in } \Gamma_D \tag{1.22}$$

$$f_{,n} = R(x,y) \quad \text{in } \Gamma_N \tag{1.23}$$

where L is the differential operator, $f(x,y)$ an unknown real function, Ω the interior domain of the problem described by the PDE, Γ_D the section of the boundary where Dirichlet boundary conditions are imposed, and Γ_N the section of the boundary where Neumann boundary conditions are involved. By means of the point collocation technique, the PDBV equations are discretized as

$$\boldsymbol{L}\widetilde{f}(x_i,y_i) = P(x_i,y_i) \quad i=1,2,\ldots,N_\Omega \tag{1.24}$$

$$\widetilde{f}(x_i,y_i) = Q(x_i,y_i) \quad i=1,2,\ldots,N_D \tag{1.25}$$

$$\widetilde{f}_{,n} = R(x_i,y_i) \quad i=1,2,\ldots,N_N \tag{1.26}$$

where N_Ω, N_D and N_N are the numbers of scattered points in the interior computational domain, and along the Dirichlet and Neumann edges of the domain, respectively. The total number of scattered points is thus $N_T=(N_\Omega+N_D+N_N)$.

After substituting the approximations (1.17) and (1.18) into the equations (1.24) to (1.26), we can now construct a complete set of discretized governing equations for the PDBV problem with the introduction of the auxiliary conditions of the equations (1.19) and (1.20). By rearrangement, a set of discrete algebraic equations with respect to the unknown point values f_i, Gx_i and Gy_i is obtained and written in matrix

form as

$$[H_{ij}]_{(N_T+2N_S)\times(N_T+2N_S)}\{F_i\}_{(N_T+2N_S)\times 1}=\{d_i\}_{(N_T+2N_S)\times 1} \tag{1.27}$$

in which $\{d_i\}$ and $\{F_i\}$ are (N_T+2N_S)-order column vectors,

$$\{F_i\}_{(N_T+2N_S)\times 1}=\{\{f_i\}_{1\times N_T},\{Gx_i\}_{1\times N_S},\{Gy_i\}_{1\times N_S}\}^T \tag{1.28}$$

$$\{d_i\}_{(N_T+2N_S)\times 1}=\{\{P(x_i,y_i)\}_{1\times N_\Omega},\{Q(x_i,y_i)\}_{1\times N_D},\{R(x_i,y_i)\}_{1\times N_N},\{0\}_{1\times 2N_S}\}^T \tag{1.29}$$

and $[H_{ij}]$ is a $(N_T+2N_S)\times(N_T+2N_S)$ coefficient matrix

$$[H_{ij}]=\begin{bmatrix} [\boldsymbol{L}N_j(x_i,y_i)]_{N_\Omega\times N_T} & [\boldsymbol{L}((x_i-\sum_{n=1}^{N_T}N_n(x_i,y_i)x_n)M_j(x_i,y_i))]_{N_\Omega\times N_S} & [\boldsymbol{L}((y_i-\sum_{n=1}^{N_T}N_n(x_i,y_i)y_n)M_j(x_i,y_i))]_{N_\Omega\times N_S} \\ [N_j(x_i,y_i)]_{N_D\times N_T} & [0]_{N_D\times N_S} & [0]_{N_D\times N_S} \\ [0]_{N_N\times N_T} & [M_j(x_i,y_i)]_{N_N\times N_S} & [M_j(x_i,y_i)]_{N_N\times N_S} \\ [N_{j,x}(x_i,y_i)]_{N_S\times N_T} & [-(\sum_{n=1}^{N_T}N_{n,x}(x_i,y_i)x_n)M_j(x_i,y_i)]_{N_S\times N_S} & [-(\sum_{n=1}^{N_T}N_{n,x}(x_i,y_i)y_n)M_j(x_i,y_i)]_{N_S\times N_S} \\ [N_{j,y}(x_i,y_i)]_{N_S\times N_T} & [-(\sum_{n=1}^{N_T}N_{n,y}(x_i,y_i)x_n)M_j(x_i,y_i)]_{N_S\times N_S} & [-(\sum_{n=1}^{N_T}N_{n,y}(x_i,y_i)y_n)M_j(x_i,y_i)]_{N_S\times N_S} \end{bmatrix} \tag{1.30}$$

The above complete set of linear algebraic equations can be solved numerically to obtain (N_T+2N_S) point values for $\{F_i\}$. Accordingly, the approximate solutions of the PDBV problem, $\widetilde{f}(x,y)$ and the corresponding first-order differentials $\widetilde{G}x(x,y)$ and $\widetilde{G}y(x,y)$, can be computed through the equations (1.17) and (1.18).

1.3 Objectives and Working Scope

Modeling and simulation are very important tools of scientific research work. Experimental trial-and-error technique has dominated in the material research field, which is very costly and time-consuming, especially for some extreme environmental conditions, such as extremely low pressure and high temperature. However, computational-based simulation is cost-saving. The synthesis of hydrogels is very time-consuming and expensive. To fully study the influences of multi-parameters on

the responsive behaviors of the hydrogel to environmental change, it would need a lot of cost experiments. Furthermore, in order to precisely control the large deformation feature of the hydrogel, a model algorithm needs to be implemented.

The importance of such models for predicting the equilibrium state of the environmentally sensitive hydrogels responding to various stimuli also lies in their utility during both the design of a pharmaceutical formulation and the experimental verification of a release mechanism (Narasimhan and Peppas, 1997). To assist biodevice designers, material properties should be fully investigated to ensure functional and reliable structures, and to elucidate how the system responds to changes in the local environment. Additionally, there is a strong desire to better understand the underlying mechanisms for swelling in hydrogels so that more predictive models can be developed to guide the design process.

Furthermore, advanced modeling for the hydrogel volume transitions could be applied to optimize the design of smart biodevices. A detailed investigation of the hydrogel behaviour is crucial to establish reliable models for predicting the device characteristics (Thinh et al., 2006).

The objectives of this thesis are to model and simulate the responsive behaviors of the environmentally sensitive hydrogels in equilibrium state subject to the three stimuli, namely the externally applied electric field, the coupling pH-electric-stimuli and the blood glucose stimulus, respectively. The models presented in this thesis can explain theoretically the experimental phenomena such as the distribution of ionic concentrations, electric potential and network deformation.

The present mathematical models are termed as the refined multi-effect-coupling of electric-stimulus (rMECe) model, multi-effect-coupling of coupled pH-electric-stimulus (MECpHe) model and multi-effect-coupling of glucose-stimulus (MECglu) model. It is noted that the current numerical simulation involves only one-dimensional steady-state analysis of behaviors of the stimulus-sensitive hydrogels responsive to the change in local environmental stimulus. The three developed models should be able to predict numerically

- the distribution of diffusive ionic concentration in both the hydrogel and the surrounding solution, and the distribution of fixed charge density within the hydrogel;
- the distribution of electric potential in both the hydrogel and the surrounding solution;
- the equilibrium swelling ratio, the displacement and bending deformation of the environmental-sensitive hydrogels.

The modeling and simulation work would be useful for optimization of the design process for sensors/actuators, micro-fluidic valves and drug delivery systems which are based on the environment-responsive hydrogels.

1.4 Layout of Thesis

This thesis is divided into five chapters, and each of them consists of several subsections to make the thesis more systematic. The arrangement of thesis is as

follows:

Chapter 2 though Chapter 4 develop three models and describe the simulation of equilibrium behaviors of environmentally sensitive hydrogels to different stimulus.

In Chapter 2, the theoretical framework of the multi-effect-coupling of glucose-stimulus (MECglu) model is developed and the governing equations are presented with the swelling mechanism of the glucose-sensitive hydrogels. By discretizing the governing equations of MECglu model, the validation of the model is carried out by comparing the numerically simulated results with the experiments published in literature. Studies have been done to investigate the effects of several important parameters on the behaviors of the glucose-sensitive hydrogels. The last section summarizes some comments and remarks on this study.

Chapter 3 is organized as follows. The Multi-Effect-Coupling pH-Electric-Stimulus (MECpHe) Model is developed firstly for hydrogels responsive to the coupled pH-electric stimuli. Then the discretization is described for the governing equations and boundary conditions of the MECpHe model. Examination of the model is made by comparison between the simulation results and published experiments. Furthermore, the effects of the physical and chemical parameters on the response of the hydrogels are discussed. Some final remarks close this chapter.

Chapter 4 is outlined as follows. By modifying the two previously developed models, namely the multi-effect-coupling pH-stimulus (MECpH) and multi-effect-coupling electric-stimulus (MECe) models, the development of the refined multi-effect-coupling electric-stimulus (rMECe) model is presented in detail. The

governing equations are formulated and the boundary conditions are proposed. The model validation is conducted by comparison of the simulation results with experiments. Several studies are made for the influences of important physical conditions. Finally, some remarks are made on the model.

Chapter 5 as the last chapter will summarize the comments and conclusions and make suggestions for future studies on the modeling of the environmentally sensitive hydrogels.

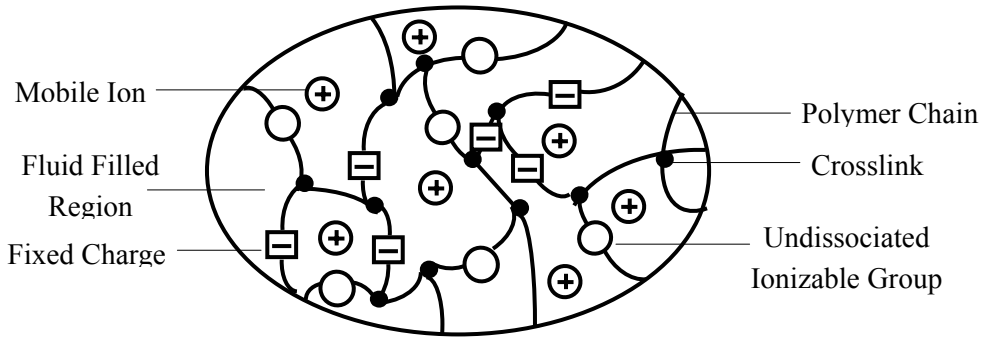

Figure 1.1 Microscopic structure of the charged hydrogel.

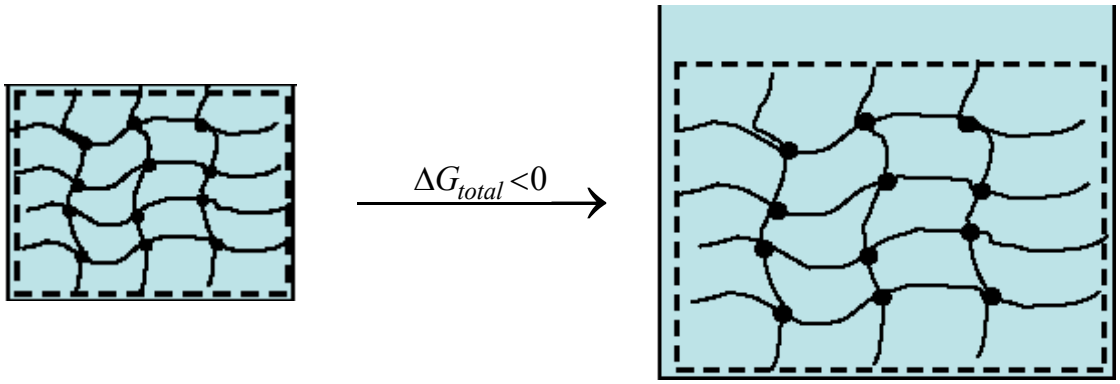

Figure 1.2 Thermodynamics of hydrogel swelling (Peppas and Merrill, 1977).

Chapter 2
Development of Multi-Effect-Coupling Glucose-Stimulus (MECglu) Model for Glucose-Sensitive Hydrogels

2.1 Introduction

As mentioned in Chapter 1, there are three broad categories of glucose-sensitive hydrogels, the glucose oxidase-loaded pH-sensitive-based hydrogels, the lectin-loaded hydrogels, and the hydrogels with phenylboronic acid moieties, which are investigated extremely in experiments due to their promiseful applications. One of them is the glucose oxidase-loaded pH-sensitive-based hydrogels based on their pH-sensitive property which will be studied in detail in this chapter. The glucose oxidase-loaded pH-sensitive-based hydrogels system is a kind of the pH-responsive polymeric hydrogel with the two immobilized enzymes, the glucose oxidase (GOD) and the catalase. When the hydrogel is immersed in a glucose buffer solution, the glucose in the solution diffuses into the hydrogel. The glucose oxidase then catalyzes the conversion of the glucose to the gluconic acid, thereby lowering the pH of the hydrogel and causing the deswelling of the hydrogel. The typical examples of those materials commonly include hydroxyethyl methacrylate (HEMA) and *N,N*-dimethylaminoethyl methacrylate (DMA), poly(HEMA-*co*-DMAEMA) (Ishihara et al., 1984, 1986; Kost et al., 1984; Albin et al., 1985, 1987; Traitel et al., 2000, 2003; Brahim et al., 2002), poly[(diethylaminoethyl methacrylate)-Hydroxyethyl

methacrylate-graft-(ethylene glycol)] poly(DEAEM-HEMA-*g*-EG) (Glodrich and Kost, 1993; Podual and Peppas, 2005), poly[(diethylaminoethyl methacrylate)-graft-(ethylene glycol)] poly(DEAEM-*g*-EG) (Podual and Peppas, 2005), poly(methacrylic acid-g-ethylene glycol) poly(MAAc-*g*-EG) (Hassan et al., 1997; Parker et al., 1999; Cao et al., 2001), *N*-Isopropylacrylamide, methacrylic acid, ethyleneglycol dimethacrylate (NIPA-MAA-EGDMA) (Zhang and Wu, 2002; Misra and Siegel, 2002; Dhanarajan and Siegel, 2005), *N,N*-dimethylacrylamide (DMAAm) (Kang, and Bae, 2003), p(MPBA-*co*-AAm) (Siegel et al., 2004.), and NIPA-MAA (Suzuki and Kumagai, 2003).

In spite of extensive experimental work, only a few studies focus on the development of mathematical models for simulation of the glucose-sensitive hydrogels. Parker et al. (1987) investigated theoretically the overall rate of reaction of the immobilized glucose oxidase and developed a steady-state model based on a ping-pong kinetic mechanism of the glucose oxidase. Horbett et al. (1987) developed a mathematical model to simulate the steady-state behavior of the cationic glucose-sensitive membrane, based on the assumption that the diffusivity of each species inside the membrane is equal to that in the bulk solution and independent of membrane swelling or pH gradient in the membrane. Based on the model developed by Horbett et al. (1987), Klumb et al. (1992) studied various design configurations to overcome the oxygen limitation in the insulin delivery system. Gough et al. (1984, 1985, and 1988) modeled the steady-state and transient response of a cylindrical glucose sensor. Abdekhodaie and Wu (2005) developed a theoretical model to describe

the steady-state behavior of the cationic glucose-sensitive membrane with consideration of oxygen limitation and swelling-dependent diffusivities of the involved species inside the membrane. However, in the above models developed by Parker et al. (1987), Horbett et al. (1987, 1992) and Gough et al. (1984, 1985, 1988), the diffusivity of species inside the membrane is assumed to be equal to the corresponding bulk value in aqueous solution, in which the diffusion is not a function of position within the membrane. In the model developed by Abdekhodaie and Wu (2005), the diffusivities of diffusive species are dependent on the swelling of the hydrogel, which is simply expressed by the volume swelling ratio of the polymer in equilibrium state. In brief, those models mentioned above cannot describe accurately the conversion of the chemical energy into mechanical energy, and also simulate difficultly the swelling deformation of the hydrogel system responding to the environmental glucose stimulus.

The chapter is organized as follows. The theoretical framework of the MECglu model is developed in Sections 2.2 and 2.3. The governing equations are presented in Section 2.2 based on the swelling mechanism of the glucose oxidase-loaded pH-sensitive-based hydrogels, and the formulations of the MECglu model is discretized in Section 2.3. Then a comparison is made in Section 2.4 between the numerically simulated results and the experiments published in literature to validate the MECglu model. The effects of several important parameters are investigated in Section 2.5 on the behaviors of the glucose-sensitive hydrogels. Finally, some comments and remarks are drawn in Section 2.6 on the study of modeling of the glucose-sensitive hydrogels.

2.2 Development of MECglu Model

2.2.1 Mechanism of Hydrogel Swelling

The swelling mechanism of the glucose-sensitive hydrogels in pH-dependent equilibrium can be characterized in the following steps: (a) diffusion of glucose into the hydrogel; (b) reactions occurring within the hydrogel; (c) ionization of the polymeric network; and (d) swelling of the hydrogel due to the derivation of osmotic pressures between the internal hydrogel and surrounding solution, illustrated in Figures 2.1 and 2.2. The theoretical model developed will describe the diffusion and reaction of glucose, oxygen and gluconic acid within the glucose oxidase-loaded pH-sensitive-based hydrogels. The stoichiometry of the reaction catalyzed by glucose oxidase (GOD) is given as (Whitaker, 1994),

$$\text{Glucose} + O_2 \xrightarrow{\text{GOD}} \text{Glucono} - \delta - \text{lactone} + H_2O_2 \tag{2.1}$$

The incorporated catalase then catalyzes the conversion of hydrogen peroxide (H_2O_2) to oxygen and water,

$$H_2O_2 \xrightarrow{\text{Catalase}} H_2O + \frac{1}{2}O_2 \tag{2.2}$$

The intermediate lactone species produced undergoes the spontaneous hydrolysis to gluconic acid,

$$\text{Glucono} - \delta - \text{lactone} + H_2O \longrightarrow \text{Gluconic Acid} \tag{2.3}$$

It is well known that the produced hydrogen peroxide can inhibit the glucose oxidase reaction (2.1) (Traitel et al., 2000). In addition, the incorporation of catalase

can reduce both the hydrogen peroxide inhibition and the oxygen limitation by an addition of 1/2mole of oxygen to the glucose oxidase reaction (Tse and Gough, 1987). Therefore, it is assumed that the excessive catalase incorporated in the hydrogel can reduce immediately all hydrogen peroxide (H_2O_2). Based on the assumption, the overall stoichiometry of glucose oxidation is thus written as,

$$\text{Glucose} + \frac{1}{2}O_2 \xrightarrow{\text{GOD/Catalase}} \text{Gluconic acid} \tag{2.4}$$

$$\text{Gluconic acid} \longrightarrow \text{Gluconate} + H^+ \tag{2.5}$$

$$\text{Glucose} + \frac{1}{2}O_2 \xrightarrow{\text{GOD/Catalase}} \text{Gluconate} + H^+ \tag{2.6}$$

The glucose and oxygen diffuse into the hydrogel from the medium and the glucose is converted to gluconic acid, which causes the pH dropping in the hydrogel and thereby triggers the deswelling deformation of the hydrogel.

In order to simplify the development of the mathematical model, the following assumptions are made as,

a) only steady state is considered;

b) the hydrogels are maintained in isothermal condition;

c) the enzymes are immobilized and distributed homogeneously within the hydrogels;

d) It is assumed that there is an excess of catalase contained in the hydrogel. As a result, the catalase reduces hydrogen peroxide H_2O_2, which is a byproduct if the glucose oxidase reaction, to O_2 and H_2O. Otherwise, the hydrogen peroxide produced will attack the glucose oxidase, deactivate the enzyme and finally inhibit the glucose oxidase

reaction (Malikkides and Wiland, 1982; Traitel et al., 2000);

e) if the hydrogels are placed in the unstirred solution and the pore of the hydrogels is very small, the ion transport by convection can be neglected reasonably (Nikonenko, et al., 2003). Therefore, the effect of the ion exchange and convection is neglected. Only passive diffusion is considered;

f) the diffusivity of each substrate, including glucose and oxygen, inside the hydrogel is assumed to be equal everywhere to its own diffusivity in bulk solution. Therefore, the diffusivities are independent of swelling or pH gradient. The diffusivity of gluconic acid is also assumed to be equal to that of glucose;

g) the acid/base reactions are assumed in local equilibrium, which is justified because these reactions are much faster than the glucose oxidase-catalyzed reaction;

h) the diffusivities of all the mobile ions and reactants in the hydrogel are assumed to be equal to their bulk values in aqueous solution due to the macroporous nature of the hydrogel, and, are listed in Table 2.1.

2.2.2 Formulation of MECglu Model

2.2.2.1 Diffusion and reaction

The diffusion problems can be solved based on the law of mass conservation

for a specific chemical species *k* in the hydrogel. For an appropriate system, such as in a differential volume element $\Delta x\Delta y\Delta z$, as shown in Figure 2.3, the law of mass conservation for the species *k* ($k = 1, 2, ..., N$) is written in the form,

$$\left\{\begin{array}{c}\text{rate of accumulation}\\ \text{of species } k \text{ per}\\ \text{unit volume}\end{array}\right\} = \left\{\begin{array}{c}\text{rate of}\\ \text{species } k\\ \text{flow in}\end{array}\right\} - \left\{\begin{array}{c}\text{rate of}\\ \text{species } k\\ \text{flow out}\end{array}\right\} \pm \left\{\begin{array}{c}\text{rate of}\\ \text{species } k\\ \text{generation/consumption}\end{array}\right\} \tag{2.7}$$

which is expressed mathematically as,

$$\frac{\partial c_k}{\partial t}\Delta x\Delta y\Delta z = J_{k,x}\Big|_x \Delta y\Delta z + J_{k,y}\Big|_y \Delta x\Delta z + J_{k,z}\Big|_z \Delta x\Delta y - J_{k,x}\Big|_{x+\Delta x} \Delta y\Delta z - J_{k,y}\Big|_{y+\Delta y} \Delta x\Delta z$$
$$- J_{k,z}\Big|_{z+\Delta z} \Delta x\Delta y + v_k r\Delta x\Delta y\Delta z \qquad (k = 1, 2, ..., N) \tag{2.8}$$

that is,

$$\frac{\partial c_k}{\partial t} = \left\{\frac{J_{k,x}\Big|_x - J_{k,x}\Big|_{x+\Delta x}}{\Delta x}\right\} + \left\{\frac{J_{k,y}\Big|_y - J_{k,y}\Big|_{y+\Delta y}}{\Delta y}\right\} + \left\{\frac{J_{k,z}\Big|_z - J_{k,z}\Big|_{z+\Delta z}}{\Delta z}\right\} + v_k r \qquad (k = 1, 2, ..., N) \tag{2.9}$$

where v_k are stoichiometric coefficients, for example, $v_g = -1$ for glucose, $v_{ox} = -1/2$ for oxygen, $v_a = 1$ for gluconic acid and $v_H = 1$ for hydrogen ion H^+.

If the limit of the differential volume is taken to zero by allowing $\Delta x \to 0$, $\Delta y \to 0$ and $\Delta z \to 0$, the partial differential governing equations are obtained as follows (Bird et al., 1960; Choy and Reible, 2000),

$$\frac{\partial c_k}{\partial t} = -\nabla \cdot J_k + v_k r = -\mathbf{div}\ J_k + v_k r \qquad (k = 1, 2, ..., N) \tag{2.10}$$

In the case of one-dimension diffusion, the conservation law of mass conservation is applied for each species *k* in the small element $A\Delta x$,

$A\Delta x\Delta c_k$ = Rate of Flow in -Rate of Flow out +reaction

$$= J_k(x)A\delta t - J_k(x+\delta x)A\delta t + v_k rA\delta x\delta t$$

$$= J_k(x)A\delta t - (J_k(x) + \frac{\partial J_k(x)}{\partial x}\delta x)A\delta t + v_k rA\delta x\delta t$$

$$= -\frac{\partial J_k(x)}{\partial x}\delta xA\delta t + v_k rA\delta x\delta t \qquad (k = 1,2,...,N) \tag{2.11}$$

Both sides are divided by $A\delta x\delta t$, and then taken the limit,

$$\frac{\partial c_k}{\partial t} = -\frac{\partial J_k(x)}{\partial x} + v_k r \qquad (k = 1,2,...,N) \tag{2.12}$$

Equations (2.10) and (2.12) are well known as the Nernst-Planck flux equation, which has been applied widely to describe the transport phenomena between membranes and solution systems (Alberty and Silbey, 1997; Sata, 2004).

In the formulation of the equations (2.7)-(2.12), J_k ($k = 1,2,...,N$) ($\mathrm{mol \cdot cm^{-2}s^{-1}}$) is defined as the flux of mass with respect to the mass average velocity. In a multispecies system, J_k ($k = 1,2,...,N$) can be expressed in terms of two contributions associated with mechanical driving forces, a contribution with the thermal driving force, and a contribution with an electrical driving force, where the charged species is required. These fluxes are strictly applicable to gases but can be simplified for liquids (Plawsky, 2001).

$$J_k = J_{k(D)} + J_{k(P)} + J_{k(T)} + J_{k(E)} \tag{2.13}$$

$J_{k(D)}$ ($\mathrm{mol \cdot cm^{-2}s^{-1}}$) is defined as the mass flux called ordinary or normal diffusion, which is driven by a concentration gradient. When ion species *k* diffuses through the hydrogel, where the *x*-axis is perpendicular to the surface of hydrogel membrane, the flux $J_{k(D)}$ can be characterized by a product of the gradient of the chemical potential, $-\nabla\mu_k$, and the concentration c_k of the species *k*,

$$J_{k(D)} = \frac{D_k}{RT}c_k(-\nabla\mu_k) \tag{2.14}$$

In general, the chemical potential of a component in liquid mixture can be expressed mathematically in term of the activity a_k, and given by (Alberty et al., 1997),

$$\mu_k = \mu_k^0 + RT \ln a_k \tag{2.15}$$

where D_k is the diffusion coefficient of the species *k*, *R* the gas constant, T the absolute temperature, and a_k activity of the species *k*, where $a_k = c_k \gamma_k$, (c_k and γ_k are the concentration and activity coefficient of the species *k*).

The mass flux is thus written as,

$$J_{k(D)} = \frac{D_k}{RT} c_k (-\nabla \mu_k) = -D_k c_k \nabla(\ln a_k) = -D_k c_k \nabla(\ln c_k + \ln \gamma_k)$$
$$= -D_k [\nabla c_k + c_k \nabla(\ln \gamma_k)] \tag{2.16}$$

It is noted that $\frac{d}{dx}\log_a u = \frac{\log_a e}{u}\frac{du}{dx}$, $\frac{d}{dx}\ln u = \frac{d}{dx}\log_e u = \frac{1}{u}\frac{du}{dx}$ (Spiegel and Liu, 1999).

In the equation (2.13), $J_{k(P)}$ is the diffusion term driven by pressure and it should be considered only when the system encounters high acceleration, such as in centrifuges. It was the fundamental mechanism exploited in the centrifugel method for separating U^{235} from U^{238}.

$$J_{k(P)} \propto \nabla P \tag{2.17}$$

In the present system, however, there are no high pressure and acceleration so that the term $J_{k(P)}$ is neglected.

In the equation (2.13), $J_{k(T)}$ is the mass flux resulting from the imposition of a temperature gradient, which is referred to as the Soret effect and is the analog of the Dufour effect (Mortimer and Eyring, 1980). The Soret coefficient is identical to the

Dufour coefficient. The mass flux resulting from thermal diffusion is given by,

$$J_{k(T)} = -D_k^T \nabla(\ln T) \tag{2.18}$$

However, the thermal diffusion flux generally depends on the gradient of the log of temperature and is very small. In the present isothermal system, the term $J_{k(T)}$ is thus neglected.

In the equation (2.13), $J_{k(E)}$ is the mass flux of charged species responding to electric potential gradient. When there is the gradient of electrical potential, the flux $J_{k(E)}$ of the species *k* is proportional to the gradient $\nabla\psi$ of the electrical potential, the concentration c_k, the valence z_k of ion *k* and the electrochemical mobility u_k, that is,

$$J_{k(E)} = -u_k z_k c_k \nabla\psi \tag{2.19}$$

The Nernst-Einstein equation is given as,

$$u_k = D_k \frac{F}{RT} \tag{2.20}$$

where F is the Faraday constant. One can thus have

$$J_{k(E)} = -D_k \frac{F}{RT} z_k c_k \nabla\psi \tag{2.21}$$

The hydrogel membranes with the ion exchange have a large number of hydrated counter-ions in the hydrogel. The counter-ions impart more momentum to the solvent than co-ions do, and solvent transfer takes place to the respective electrode chamber due to osmosis and electro-osmosis. If the hydrogel membrane has an anionic charge, the solvent transfer takes place from anolyte to catholyte. The velocity of this solvent transfer is proportional to the gradient of the electrical potential and is inversely proportional to the resistance to flow in the hydrogel membrane matrix. The

convection flux $J_{k(Conv)}$ of liquid in the membrane can be characterized by the velocity of the solvent flow is V and c_k is the concentration of counter-ion *k* in the membrane,

$$J_{k(Conv)} = c_k V \tag{2.22}$$

Therefore, the total flux of the ionic species *k* through the hydrogel membrane can be expressed as

$$J_k = J_{k(D)} + J_{k(E)} + J_{k(Conv)} = -D_k[\nabla c_k + z_k c_k \frac{F}{RT}\nabla\psi + c_k\nabla(\ln\gamma_k)] + \bar{c}_k v$$
$$= -D_k\left[\mathbf{grad}c_k + z_k c_k \frac{F}{RT}\mathbf{grad}\,\psi + c_k\mathbf{grad}(\ln\gamma_k)\right] + c_k V \quad (k = 1,2,...,N) \tag{2.23}$$

If the convection $J_{k(Conv)}$ is neglected in the hydrogel, the total flux of the species *k* is simplified to

$$J_k = J_{k(D)} + J_{k(E)} = -D_k[\nabla c_k + z_k c_k \frac{F}{RT}\nabla\psi + c_k\nabla(\ln\gamma_k)]$$
$$= -D_k\left[\mathbf{grad}c_k + z_k c_k \frac{F}{RT}\mathbf{grad}\,\psi + c_k\mathbf{grad}(\ln\gamma_k)\right] \tag{2.24}$$

The diffusion governing equation for the ionic species *k* is then written as,

$$\frac{\partial c_k}{\partial t} = -\nabla\cdot J_k + v_k r = -\mathbf{div}\ J_k + v_k r$$
$$= div\left\{D_k\left[\mathbf{grad}c_k + z_k c_k \frac{F}{RT}\mathbf{grad}\,\psi + c_k\mathbf{grad}(\ln\gamma_k)\right]\right\} - div(c_k V) + v_k r \tag{2.25}$$
$$(k = 1,2,...,N)$$

In steady-state case, the Nernst-Planck equations (2.25) can be written as,

$$div\left\{D_k\left[\mathbf{grad}c_k + z_k c_k \frac{F}{RT}\mathbf{grad}\,\psi + c_k\mathbf{grad}(\ln\gamma_k)\right]\right\} - div(c_k V) + v_k r = 0 \tag{2.26}$$
$$(k = 1,2,...,N)$$

For one-dimensional steady-state case, the above Nernst-Planck equations can

be further simplified to,

$$div\{D_k\left[\mathbf{grad}c_k + z_k c_k \frac{F}{RT}\mathbf{grad}\,\psi + c_k \mathbf{grad}(\ln\gamma_k)\right]\} - div(c_k V) + v_k r$$

$$= \frac{\partial}{\partial x}\left\{D_k\left[\frac{\partial c_k}{\partial x} + z_k c_k \frac{F}{RT}\frac{\partial \psi}{\partial x} + c_k \frac{\partial(\ln\gamma_k)}{\partial x}\right]\right\} - \frac{\partial}{\partial x}(c_k V) + v_k r$$

(where $RT\ln\gamma_k = -K_1 c_k + K_2 c_k^2$)

$$= \frac{\partial}{\partial x}\left\{D_k\left[\frac{\partial c_k}{\partial x} + z_k c_k \frac{F}{RT}\frac{\partial \psi}{\partial x} + \frac{c_k}{RT}\frac{\partial(-K_1 c_k + K_2 c_k^2)}{\partial x}\right]\right\} - \frac{\partial}{\partial x}(c_k V) + v_k r$$

(where D_k is assumed to be constant)

$$= D_k \frac{\partial}{\partial x}\left\{\left[\frac{\partial c_k}{\partial x} + z_k c_k \frac{F}{RT}\frac{\partial \psi}{\partial x} + \frac{c_k}{RT}(-K_1\frac{\partial c_k}{\partial x} + 2K_2 c_k \frac{\partial c_k}{\partial x})\right]\right\} - \frac{\partial}{\partial x}(c_k V) + v_k r$$

$$= \frac{\partial}{\partial x}\left[\frac{\partial c_k}{\partial x} + z_k c_k \frac{F}{RT}\frac{\partial \psi}{\partial x} + \frac{-K_1 c_k + 2K_2 c_k^2}{RT}\frac{\partial c_k}{\partial x}\right] - \frac{\partial}{D_k \partial x}(c_k V) + \frac{v_k}{D_k} r$$

$$= \left[\frac{\partial^2 c_k}{\partial x^2} + \frac{z_k F}{RT}\frac{\partial c_k}{\partial x}\frac{\partial \psi}{\partial x} + \frac{z_k F c_k}{RT}\frac{\partial^2 \psi}{\partial x^2}\right] + \frac{v_k}{D_k} r$$

$$- \frac{\partial}{D_k \partial x}(c_k V) + \left[\frac{(-K_1 + 4K_2 c_k)}{RT}(\frac{\partial c_k}{\partial x})^2 + \frac{(-K_1 + 2K_2 c_k)c_k}{RT}\frac{\partial^2 c_k}{\partial x^2}\right] \qquad (2.27)$$

$$= 0 \qquad (k = 1, 2, ..., N)$$

The stoichiometric coefficients of the reactants and products are given here, $v_g = -1$, $v_{ox} = -1/2$, $v_a = 1$ and $v_{H^+} = 1$.

Activity coefficient γ_k

In order to carry out quantitative modeling and simulations for nonideal solutions, it is convenient to introduce the activity coefficient γ_k (Moelwyn-Hughes, 1978).

The activity a_k is simply a means to express the chemical potential of a

species in a mixture. It is convenient to write the activity a_k as the product of an activity coefficient γ_k and a concentration.

The empirically corrected concentration, or called molar fraction (molality) is

$$a_k = c_k \gamma_k \tag{2.28}$$

$$a_k = x_k \gamma_k \tag{2.29}$$

The chemical potential of the component *k* in the solution is given by

$$G_k = G_k^0 + RT \ln a_k \tag{2.30}$$

then

$$G_k = G_k^0 + RT \ln c_k + RT \ln \gamma_k \tag{2.31}$$

or

$$G_k = G_k^0 + RT \ln x_k + RT \ln \gamma_k \tag{2.32}$$

It is clear that the activity coefficient of the equation (2.28) is unity when the solution obeys van't Hoff's law, and that γ_k of the equation (2.29) is unity when the solution obeys Raoult's law ($P_k = x_k P_k^*$) (Choy and Reible, 2000). The term $RT \ln \gamma_k$ is thus a measure of the difference between the chemical potential of an actual component of a solution and the chemical potential anticipated on the basis of either of these laws.

For binary systems, Van Laar's theory of isomegethic solutions provides an improved equation as (Moelwyn-Hughes, 1978),

$$G_k = G_{ik}^0 + RT \ln x_k + (1 - x_k)^2 \Delta U^0 \tag{2.33}$$

The activity coefficient of component *A* in a binary solution which obeys Van Laar's theory is given in terms of the interchange energy by

$$\ln \gamma_A = (1 - x_A)^2 (\Delta U^0 / RT) \tag{2.34}$$

The activity coefficient of ion in aqueous solution is given by

$$\ln \gamma_k = -(B / RT) c_i^{1/2} \tag{2.35}$$

The chemical potentials μ_1 and μ_2 in terms of the concentrations $n_1 = N_1 / V$ and $n_2 = N_2 / V$ are expressed as,

$$\begin{aligned} \mu_1 &= \mu_1^0 + kT \ln n_1 v_1 + kT n_2 (v_2 - v_1) + (P - P^0) v_1 + n_2^2 v_2 \sqrt{v_1 v_2} \Delta u^0 \\ \mu_2 &= \mu_2^0 + kT \ln n_2 v_2 + kT n_1 (v_1 - v_2) + (P - P^0) v_2 + n_1^2 v_1 \sqrt{v_1 v_2} \Delta u^0 \end{aligned} \tag{2.36}$$

where μ^0 is the chemical potential of the pure component at the temperature of the solution and at some reference pressure P^0.

Finally, to describe the significance of changing from one reference state to another, the equation (2.36) is applied to a solution containing the *A* and *S* types of molecules,

$$G_A = G_A^L + RT \ln \theta_A + (1 - \theta_A)^2 \sqrt{\frac{V_A}{V_S}} \Delta U^0 + RT (1 - \theta_A)(1 - \frac{V_A}{V_S}) \tag{2.37}$$

where θ_A is the volume fraction, ΔU^0 the exchange energy, V_A and V_S are the partial molar volume of component A and the solvent, respectively.

Here G_A^L manifestly stands for the free energy of one mole of pure component *A* in the liquid state at the temperature and pressure of the system. To examine the solution over the complete range of composition, there can be no better reference state. On the other hand, the nature of solutions is a limitation wherein the amount of S is always greatly in excess of the amount of *A*, i.e. a relatively dilute solution of *A* in *S* may a good try. The pure liquid is then a reference state to adopt, and may be replaced be one which, as far as numbers are concerned, is that of one gram-mole of *A* in a litre

of solution, but, as far as behaviour is concerned, is that corresponding to a zero value of the interchange energy ΔU^0. Let us replace θ_A by the product of the concentration c_A in moles per litre of solution, and the partial molar volume V_A adjusted by the necessary numerical factor,

$$\theta_A = c_A V_A / 1000 \tag{2.38}$$

The chemical potential of the solute now becomes

$$G_A = G_A^0 + RT \ln c_A - K_1 c_A + K_2 c_A^2 \tag{2.39}$$

where

$$G_A^0 = G_A^L + RT \ln(V_A / 1000) + \sqrt{\frac{V_A}{V_S}} \Delta U^0 + RT(1 - \frac{V_A}{V_S}) \tag{2.40}$$

$$K_1 = 2(V_A / 1000) \sqrt{\frac{V_A}{V_S}} \Delta U^0 + RT(V_A / 1000)(1 - \frac{V_A}{V_S}) \qquad (\mathrm{KJ} \times \mathrm{m}^3 / \mathrm{mol}) \tag{2.41}$$

$$K_2 = (V_A / 1000)^2 \sqrt{\frac{V_A}{V_S}} \Delta U^0 \qquad (\mathrm{KJ} \times \mathrm{m}^3 / \mathrm{mol}) \tag{2.42}$$

The equation (2.39) in more convenient form can be compared with the empirical extension of Van't Hoff's equation

$$G_A = G_A^0 + RT \ln c_A + RT \ln \gamma_A \tag{2.43}$$

giving us the result,

$$RT \ln \gamma_k = -K_1 c_k + K_2 c_k^2 \tag{2.44}$$

Chemical reaction ratio r:

There are two mechanisms for the conversion of glucose into gluconic acid by glucose oxidase. The chemical reaction ratio r can thus be expressed in the two corresponding formulas,

(a) Michaelis-Menten mechanism

The kinetics of many enzymes reactions can be described by Michaelis-Menten kinetics, which is named after Leonor Michaelis and Maud Menten (Michaelis and Menten, 1913). This kinetic model is assumed that the concentration of enzyme is much lower than the concentration of substrate (i.e. where enzyme concentration is the limiting factor), and the enzyme is not allosteric. It postulates that the complex of enzyme (catalyst) and substrate (reactant) exists in vary short time, which then dissociates fast to yield product and free enzyme. According to the quasi steady state approximation, the concentration of the enzyme namely does not change (Briggs and Haldane, 1925). Based on the Michaelis-Menten kinetics model, the chemical reaction ratio r of glucose oxidase reaction can thus be written as

$$r = \frac{c_{enz}}{\frac{c_{enz}}{v_{\max}} + \frac{k_1}{c_g} + \frac{k_2}{c_{ox}}} = \frac{V_{\max} c_g c_{ox}}{c_{ox}(c_g + \frac{k_1 V_{\max}}{c_{enz}}) + \frac{k_2 V_{\max}}{c_{enz}} c_g} \tag{2.45}$$

(b) The full Ping-Pong mechanism

Glucose oxidase exhibits the true ping-pong kinetics: moving from a fully oxidized state to a fully reduced form and back to the oxidized state in a catalytic cycle. By a combination of conventional and rapid reaction techniques, the overall reaction mechanism of glucose oxidase has been established to be (Parker and Schwartz, 1987; Robald T. Kurnik et al., 1998),

$$\text{(i)}\quad E_0 + G \underset{k_{-1}}{\overset{k_{+1}}{\rightleftarrows}} E_B \xrightarrow{k_{+2}} E_R + \text{D-gluconic acid}$$

$$\text{(ii)}\quad E_R + \mathrm{O_2} \xrightarrow{k_{+4}} E_0 + \mathrm{H_2O_2} \tag{2.46}$$

where E_0 is the oxidized form of glucose oxidase, E_R is the reduced form of glucose oxidase, G is glucose, and E_B is the enzyme substrate complex, ($E_0 - G$).

The reaction rate is given as (Klumb and Horbett, 1992),

$$r = \frac{r_m[E_T]}{\frac{\beta_g}{c_g} + \frac{\beta_0}{c_o} + 1} \tag{2.47}$$

where

$$r_m = k_{+2} \tag{2.48}$$

$$\beta_g = \frac{k_{-1} + k_{+2}}{k_{+1}} \tag{2.49}$$

$$\beta_0 = \frac{k_{+2}}{k_{+4}} \tag{2.50}$$

Therefore, the expression of the rate of full Ping-Pong reaction can be rewritten in the following form,

$$r = \frac{V_{\max} c_g c_o}{c_o(c_g + K_g) + K_o c_g} \tag{2.51}$$

where c_g and c_o are the concentrations of glucose and oxygen, respectively. $V_{\max}$ is the maximum velocity and $V_{\max} = r_m[E_T]$. K_g and K_o are the Michaelis constants for glucose and oxygen at infinite concentrations of the other substrate and $K_g = \beta_g$ and $K_o = \beta_o$, respectively.

The value of K_g reported for the soluble enzyme at 38℃ is 125 mM and similar values have been described over a wide range of temperature and pH values (Abdekhodaie and Wu, 2005). If the bulk glucose concentration is taken in the range of 0 to 5 mM, one can have

$$K_g + c_g \approx K_g \tag{2.52}$$

For the hydrogel membranes containing immobilized glucose oxidase and excess catalase, an approximate expression of the general Ping-Pong rate is thus expressed as (Leypoldt et al., 1984; Gough et al., 1985; Lusisano et al., 1988; Abdekhodaie and Wu, 2005),

$$r = \frac{V'_{\max} c_g c_o}{c_o + K_o' c_g} \tag{2.53}$$

where $V'_{\max} = V_{\max} / K_g$, and $K_o' = K_o / K_g$.

Average pH whinin the hydrogel $\langle \mathrm{pH} \rangle$*:*

A buffer solution consists of two components, a weak acid or a weak base and its salt. The solution has capability of resisting the change in pH upon the addition of small amounts of either acid or base. Buffer is very important to chemical and biological systems. The pH in the human blood is about 7.4, while the pH of the gastric juice in our stomachs is about 1.5. These pH values, which are crucial to proper enzyme function and the balance of osmotic pressure, are maintained by buffers in most cases (Kataoka et al., 1998).

A buffer solution should contain a relatively large concentration of acid to react with any OH^- ions added, and it should also contain a similar concentration of base to react with any added H^+ ions. Furthermore, the acid and base components of the buffer should not consume each other in a neutralization reaction. These requirements are satisfied by an acid-base conjugate pair, for example, a weak acid and its conjugate base (supplied by a salt) or a weak base and its conjugate acid (supplied by a salt).

The buffering capacity, i.e., the effectiveness of the buffer solution, depends on the amount of acid and conjugate base from which the buffer is made. The larger the amount is, the greater the buffering capacity is (Chang, 2002).

The pH profile is predicted from that of the hydronium ion [H_3O^+] concentration within the hydrogel. It is examined in terms of an average pH ($\langle \mathrm{pH} \rangle$), which is calculated based on the numerical solution of the pH profiles within the glucose sensitive hydrogel (Klumb et al., 1992, 1993):

$$\langle \mathrm{pH} \rangle = \frac{1}{\mathrm{Vol}} \int_{\mathrm{vol}} \mathrm{pH}(z, r, \theta) dV \tag{2.54}$$

The $\langle \mathrm{pH} \rangle$ is demonstrated previously to represent adequately the pH throughout the gel.

2.2.2.2 Poisson Equation

As a more rigorous approach, the Poisson equation is used to describe the spatial distribution of the electric potential in the whole domain and given as (Li et al., 2005a)

$$\nabla^2 \psi = -\frac{F}{\varepsilon \varepsilon_0} \left(\sum_k z_k c_k + z_f c_f \right) \tag{2.55}$$

In one-dimensional case,

$$\frac{\partial^2 \psi}{\partial x^2} = -\frac{F}{\varepsilon \varepsilon_0} \left(\sum_k z_k c_k + z_f c_f \right) \tag{2.56}$$

where ε is the relative dielectric constant of the surrounding medium and ε_0 is the vacuum permittivity or dielectric constant (8.85418×10^{-12} $\mathrm{C^2/Nm^2}$). It is observed that the electroneutrality and constant field hypotheses are in fact special cases for the

Poisson equation. The assumption of electroneutrality is applicable only when the concentrations are high while the hypothesis of constant field is valid for low concentrations.

2.2.2.3 Fixed charge density

Langmuir adsorption isotherm can be used to describe the fixed charge density of the polyelectrolyte hydrogels. In fact, there are two types of molecular adsorption, physical adsorption and chemisorption, distinguished conveniently by different adsorbed forces (Alberty and Silbey, 1997). The forces causing physical adsorption are the same type as those causeing the condensation of a gas to form a liquid and are generally referred to as van der Waals forces. The heat evolved in a physisorption process is the order of magnitude of the heat evolved in the process of condensing the gas, and the amount adsorbed may correspond to several monolayers at a high pressure. The extent of physisorption is smaller at higher temperature. On the other hand, the chemisorption involves the formation of chemical bonds. However, it is usually not possible to make a sharp distinction between these two kinds of adsorption. They may often be distinguished by the rates in which these processes occur. Compared to chemisorption, equilibrium in physical adsorption is generally achieved rapidly and is readily reversible. Physical adsorption is reversed by lowering the pressure of the gas or raising the temperature of the surface. The chemisorption, on the other hand, may not occur at an appreciable rate at low temperatures if the chemisorption reaction has an activation energy. In this case, the rate of chemisorption increases rapidly as the

temperature raises. In the chemisorption the bonding may be so tight that the original species may not adesorb. For example, heating a graphite surface after adsorbing atomic oxygen results in desorption of carbon monoxide.

The simplest equation for adsorption under equilibrium conditions is derived by Langmuir using kinetic theory (Moelwyn-Hughes, 1978), in which a surface is considered with a specific number of binding sites that are identical and each can adsorb one molecule. Thus, the adsorption is limited to a monolayer. In the Langmuir adsorption theory, it is also assumed that binding at a site has no influence on the properties of neighboring sites, this means that the enthalpy of adsorption is independent of coverage.

The hydrogen ion is bound by the fixed charge attached onto the polymeric chains of hydrogels stimulated by solution pH. This process is similar to monolayer absorption of the identical surface which has a specific number of binding sites. The each binding site can absorb one molecule only,

$$MS \xrightarrow{K} M + S \tag{2.57}$$

$$M + S \xrightarrow{Ka} MS \tag{2.58}$$

where *MS* is defined as the occupied fixed charge/site and c_f^b is the concentration of occupied fixed charge, *M* is mobile hydrogen ions such as c_{H^+} being the concentration of mobile molecules including hydrogen ions, *S* is the unoccupied fixed charge/site and defined as $c_f = c_f^0 - c_f^b$ being the concentration of the current concentration of the fixed charge group within the hydrogel membrane, c_f^0 is the total concentration of ionizable groups in the hydrogel, *K* is dissociation constant and K_a

is adsorption constant.

Anionic hydrogel ($\mathrm{R-COO^-}$ *or* $\mathrm{R\text{-}SO_2N\text{-}H^-}$*)*

$$\mathrm{R-COOH} \overset{K}{\rightleftharpoons} \mathrm{R-COO^- + H^+}$$

or (2.59)

$$\mathrm{R\text{-}SO_2NH_2} \overset{K}{\rightleftharpoons} \mathrm{R\text{-}SO_2NH^- + H^+}$$

According to the Langmuir monolayer adsorption isotherm, the equilibrium dissociation constant K can be expressed as

$$K = \frac{[\mathrm{R-COO^-}][\mathrm{H^+}]}{[\mathrm{R-COOH}]} = \frac{c_{\mathrm{H^+}}(c_f^0 - c_f^b)}{c_f^b} \tag{2.60}$$

The concentration c_f^b of the occupied fixed charge/site is thus obtained as

$$c_f^b = \frac{c_f^0 \cdot c_{\mathrm{H^+}}}{K + c_{\mathrm{H^+}}} \tag{2.61}$$

The current concentration c_f of fixed charge group is then expressed as follows,

$$c_f = c_f^0 - c_f^b = c_f^0 - \frac{c_f^0 \cdot c_{\mathrm{H^+}}}{K + c_{\mathrm{H^+}}} = \frac{c_f^0 \cdot K}{K + c_{\mathrm{H^+}}} \tag{2.62}$$

Based on the definition of concentration, the total concentration $c_{f,s}^0$ of the ionizable groups in the hydrogel in the relaxed state, and the current concentration c_f^0 of ionizable groups in the hydrogel can be written as follows

$$c_{f,s}^0 = \frac{n}{V^s} \tag{2.63}$$

$$c_f^0 = \frac{n}{V^w} = \frac{n}{V^s}\frac{V^s}{V^w} = \frac{c_{f,s}^0}{H} \tag{2.64}$$

where n is the moles of fixed-charge group, V^s and V^w are volumes of dry gel and

intramembrane fluid, V is current total volume ($V = V^s + V^w$) and H is local hydration of the hydrogel ($H = \frac{V^w}{V^s}$).

Therefore, a relation is developed between the fixed charge and diffusive hydrogen ion, whereby the concentration of the fix charged group can be calculated as a function of $c_{f,s}^0$ and c_H by

$$c_f = \frac{1}{H}\frac{c_{f,s}^0 K}{K + c_{\mathrm{H}^+}} \tag{2.65}$$

where c_f and z_f are the concentration and the valence of the fixed charge groups on the polymer chains, for example, $z_f = -1$ if the carboxylic acid groups are the pendent functional groups onto the polymer chains, *K* is then the dissociation constant of the carboxylic acid groups, $c_{f,s}^0$ is the total concentration of the ionizable groups in the hydrogel in the relaxed state, c_{H^+} is the concentration of hydrogen ions H^+ within the hydrogel and *H* is the local hydration of the hydrogel.

Cationic hydrogel ($\mathrm{R-NH_3^+}$*)*

$$\mathrm{R-NH_3^+} \underset{}{\overset{K}{\rightleftharpoons}} \mathrm{R-NH_2 + H^+} \tag{2.66}$$

The equilibrium constant K is expressed as

$$K = \frac{[\mathrm{R-NH_2}][\mathrm{H^+}]}{[\mathrm{R-NH_3^+}]} = \frac{c_f^b c_{\mathrm{H}^+}}{(c_f^0 - c_f^b)} \tag{2.67}$$

The concentration c_f^b of the occupied fixed charge/site is thus obtained as

$$c_f^b = \frac{c_f^0 \cdot K}{K + c_{\mathrm{H}^+}} \tag{2.68}$$

The current concentration c_f of fixed charge group is then expressed as

follows,

$$c_f = c_f^0 - c_f^b = c_f^0 - \frac{c_f^0 \cdot K}{K + c_{H^+}} = \frac{c_f^0 \cdot c_{H^+}}{K + c_{H^+}} \tag{2.69}$$

$$c_f^0 = \frac{n}{V^w} = \frac{n}{V^s}\frac{V^s}{V^w} = \frac{c_{f,s}^0}{H} \tag{2.70}$$

As a result, the fixed charge density of cationic hydrogel is characterized by

$$c_f = \frac{c_f^0 \cdot c_{H^+}}{K + c_{H^+}} = \frac{1}{H}\frac{c_{f,s}^0 \cdot c_{H^+}}{K + c_{H^+}} \tag{2.71}$$

According to the nature of the fixed charge groups presented in the polymeric chains, the glucose sensitive hydrogel responding to pH change may be classified as cationic or anionic hydrogel. The cationic hydrogels swell as pH decreases at higher glucose levels, while the anionic hydrogels shrink as pH decreases due to protonization of acidic groups (Podual et al., 2000; Abdekhodaie and Wu, 2005).

The typical cationic glucose sensitive hydrogels ($z_f = +1$) include hydroxyethyl methacrylate (HEMA) and *N,N*-dimethylaminoethyl methacrylate (DMA) poly(HEMA-*co*-DMAEMA) (Ishihara et al., 1984, 1986; Kost et al., 1984; Albin et al., 1985, 1987; Traitel et al., 2000,2003 ; Brahim et al., 2002), poly[(diethylaminoethyl methacrylate)-Hydroxyethyl methacrylate -graft-(ethylene glycol)] poly(DEAEM-HEMA-g-EG) (Glodrich and Kost, 1993; Podual and Peppas, 2005) and poly[(diethylaminoethyl methacrylate)-graft-(ethylene glycol)] poly(DEAEM-g-EG) (Podual and Peppas, 2005).

And the typical anionic glucose sensitive hydrogels ($z_f = -1$) include poly(methacrylic acid-g-ethylene glycol) poly(MAAc-*g*-EG) (Hassan et al., 1997; Parker et al., 1999; Cao et al., 2001) and *N*-isopropylacrylamide, methacrylic acid,

ethyleneglycol dimethacrylate (NIPA-MAA-EGDMA) (Zhang and Wu, 2002; Misra and Siegel, 2002; Dhanarajan and Siegel, 2005).

2.2.2.4 Finite deformation elastic theory

For geometrically nonlinear analysis, the governing equation for large mechanical deformation based on a total Lagrangian description is given as

$$\nabla \cdot \boldsymbol{P} + \rho \boldsymbol{f} - \rho \dot{\boldsymbol{V}} = \boldsymbol{F} \tag{2.72}$$

Where $\boldsymbol{P}$ is the first Piola-Kirchhoff stress tensor, ρ is the density of hydrogel membrane, $\boldsymbol{f}$ is the body force, $\dot{\boldsymbol{V}}$ is the acceleration, $\rho\dot{\boldsymbol{V}}$ is inertial force and $\boldsymbol{F}$ is the external force. In this system, there is no external force ($\boldsymbol{F} = \boldsymbol{0}$), and $\boldsymbol{f}$ and $\rho\dot{\boldsymbol{V}}$ are neglected. One can thus have

$$\nabla \cdot \boldsymbol{P} = 0 \qquad \text{in } \Omega \tag{2.73}$$

$$\boldsymbol{u} = \boldsymbol{G} \qquad \text{in } \Gamma_g \tag{2.74}$$

$$\boldsymbol{P} \cdot \boldsymbol{N} = \boldsymbol{H} \qquad \text{in } \Gamma_h \tag{2.75}$$

(a) For continuous solid material, the first Piola-Kirchhoff stress tensor $\boldsymbol{P}$ is given as

$$\boldsymbol{P} = \boldsymbol{S}\boldsymbol{F}^{\mathrm{T}} \tag{2.76}$$

(b) For porous mixture, the first Piola-Kirchhoff stress tensor $\boldsymbol{P}$ is (Li et al., 2005a)

$$\boldsymbol{P} = -J\boldsymbol{F}^{-1} p\boldsymbol{I} + \boldsymbol{S}\boldsymbol{F}^{\boldsymbol{T}} \tag{2.77}$$

where $\boldsymbol{F}$ is the deformation gradient tensor, J is the determinant of deformation gradient $\boldsymbol{F}$, $\boldsymbol{G}$ is the specified displacement vector on the boundary portion Γ_g, $\boldsymbol{H}$ is the surface traction vector on the boundary Γ_h, $\boldsymbol{N}$ is the unit outward normal vector. $\boldsymbol{u}$

is the displacement vector from the initial configuration $\boldsymbol{X}$ to the deformed configuration $\boldsymbol{x}$. $\boldsymbol{P}$ is the first Piola-Kirchhoff stress tensor that is a kind of expatriate, living partially in the deformed configuration $\boldsymbol{x}$ and partially in the reference configuration $\boldsymbol{X}$ (Where $\boldsymbol{x} = \boldsymbol{X} + \boldsymbol{u}$), p is the osmotic pressure $p_{osmotic}$, and $\boldsymbol{I}$ is identity tensor.

The deformation gradient tensor $\boldsymbol{F}$ is defined by

$$\boldsymbol{F} = F_{ij} = \frac{\partial x_i^{Deformed-configuration}}{\partial X_j^{initial-configuration}} = \frac{\partial (X_i + u_i)}{\partial X_j} = \delta_{ij} + \frac{\partial u_i}{\partial X_j} = \boldsymbol{I} + div(\boldsymbol{u}) \tag{2.78}$$

$$J = \det(\boldsymbol{F}) \tag{2.79}$$

The relationship between the first Piola-Kirchhoff stress tensor $\boldsymbol{P}$ and the second Piola-Kirchhoff stress tensor $\boldsymbol{S}$ is written as

$$\boldsymbol{P} = \boldsymbol{S}\boldsymbol{F}^{\mathrm{T}} \tag{2.80}$$

Due to $\boldsymbol{P}$ is unmeasurable and asymmetrical, the second Piola-Kirchhoff stress tensor $\boldsymbol{S}$ is required because $\boldsymbol{S}$ is symmetric and it is often used as the stress measure (Malvern, 1969),

$$\boldsymbol{S} = \boldsymbol{C} : \boldsymbol{E} \qquad \text{or} \qquad S_{ij} = C_{ijkl} E_{kl} \tag{2.81}$$

where $\boldsymbol{C}$ is the material moduli tensor, and $\boldsymbol{E}$ is the Green-Lagrangian strain tensor used as strain measure. Here the symbol (:) in $\boldsymbol{A} : \boldsymbol{B}$ is double contraction of inner indices, $\boldsymbol{A} : \boldsymbol{B}$ is given by $A_{ij} B_{ij}$. If $\boldsymbol{A}$ or $\boldsymbol{B}$ is symmetric, $\boldsymbol{A} : \boldsymbol{B} = A_{ij} B_{ji}$.

When the material is elastically isotropic,

$$S_{ij} = [\lambda \delta_{ij} \delta_{rs} + \mu(\delta_{ik}\delta_{jl} + \delta_{il}\delta_{jk})] E_{kl} \tag{2.82}$$

$$S_{11} = (\lambda + 2\mu)\left[\frac{1}{2}(2\frac{du}{dX} + (\frac{du}{dX})^2)\right] = (\lambda + 2\mu)\left[\frac{du}{dX} + \frac{1}{2}(\frac{du}{dX})^2\right] \tag{2.83}$$

For isotropic elastic material, therefore, the material moduli tensor can be written by

$$\boldsymbol{C} = \lambda \boldsymbol{I} \otimes \boldsymbol{I} + 2\mu \boldsymbol{I} \quad \text{or} \quad C_{ijkl} = \lambda \delta_{ij}\delta_{kl} + \mu(\delta_{ik}\delta_{jl} + \delta_{il}\delta_{jk}) \tag{2.84}$$

where λ and μ are the Lamé coefficients of solid phase. Here the symbol $\otimes$ as in $a \otimes b$ indicates vector product; in indicial notation, $a \otimes b \longrightarrow a_i b_j$; in matrix notation, $a \otimes b \longrightarrow \{a\}\{b\}^T$.

There are two types of typical states of two-dimensional solid, plane strain and plane stress, respectively.

In particular, the plane strain problems are solids whose thickness in the *z* direction is very large compared with dimensions in the *x* and *y* directions. External forces are applied uniformly along the *z*-axis, and the movement in the *z*-direction at any point is constrained. All the strain components in *z* direction (ε_{zz}, ε_{xz}, ε_{yz}) are equal to zero and there are only three in-plane non-zero strains (ε_{xx}, ε_{yy}, ε_{xy}) to be dealt with. For the plane strain problem,

$$\boldsymbol{C} = \frac{E}{(1+\nu)(1-2\nu)}\begin{bmatrix} 1-\nu & \nu & 0 \\ \nu & 1-\nu & 0 \\ 0 & 0 & (1-2\nu)/2 \end{bmatrix} \quad \text{or} \quad \boldsymbol{C} = \begin{bmatrix} \lambda+2\mu & \lambda & 0 \\ \lambda & \lambda+2\mu & 0 \\ 0 & 0 & \mu \end{bmatrix} \tag{2.85}$$

On the other hand, the plane stress problems are the solids whose thickness in the *z* direction is very small compared with dimensions in the *x* and *y* directions. As external forces are applied only in the *x*-*y* plane, and all the stresses in *z* direction (σ_{zz}, σ_{xz}, σ_{yz}) are equal to zero. Then there are only three in-plane no-zero stresses (σ_{xx}, σ_{yy}, σ_{xy}). For the plane stress problem,

$$C = \frac{E}{(1-\nu^2)}\begin{bmatrix} 1 & \nu & 0 \\ \nu & 1 & 0 \\ 0 & 0 & (1-\nu)/2 \end{bmatrix} \tag{2.86}$$

The two Lamé elastic constants, λ and μ, are related to the shear modulus G, Young's modulus E, and Poisson's ratio ν as follows:

$$\lambda = \frac{\nu E}{(1+\nu)(1-2\nu)} \quad \text{and} \quad \mu = G = \frac{E}{2(1+\nu)} \tag{2.87}$$

The Green-Lagrangian strain tensor $\boldsymbol{E}$ is given by

$$\boldsymbol{E} = \frac{1}{2}(\boldsymbol{F^T}\cdot\boldsymbol{F}-\boldsymbol{I}) \quad \text{or} \quad E_{ij} = \frac{1}{2}(F_{ik}^T F_{kj} - \delta_{ij}) = \frac{1}{2}(\frac{\partial u_i}{\partial X_j} + \frac{\partial u_j}{\partial X_i} + \frac{\partial u_k}{\partial X_i}\frac{\partial u_k}{\partial X_j}) \tag{2.88}$$

$$\boldsymbol{E} = E_{ij} = \frac{1}{2}\begin{bmatrix} 2\frac{\partial u_1}{\partial X_1} + (\frac{\partial u_1}{\partial X_1})^2 + (\frac{\partial u_2}{\partial X_1})^2 & \frac{\partial u_1}{\partial X_2} + \frac{\partial u_2}{\partial X_1} + \frac{\partial u_1}{\partial X_1}\frac{\partial u_1}{\partial X_2} + \frac{\partial u_2}{\partial X_1}\frac{\partial u_2}{\partial X_2} \\ \frac{\partial u_1}{\partial X_2} + \frac{\partial u_2}{\partial X_1} + \frac{\partial u_1}{\partial X_1}\frac{\partial u_1}{\partial X_2} + \frac{\partial u_2}{\partial X_1}\frac{\partial u_2}{\partial X_2} & 2\frac{\partial u_2}{\partial X_2} + (\frac{\partial u_2}{\partial X_2})^2 + (\frac{\partial u_1}{\partial X_2})^2 \end{bmatrix} \tag{2.89}$$

Therefore, the total momentum equation for the mixture can be rewritten as

$$div(-J\boldsymbol{F}^{-1}p_{osmotic}\boldsymbol{I} + \boldsymbol{S}\boldsymbol{F^T}) = 0 \tag{2.90}$$

$$\begin{aligned}
\boldsymbol{P} &= -J\boldsymbol{F}^{-1}p_{osmotic}\boldsymbol{I} + \boldsymbol{S}\boldsymbol{F}^T \\
&= -p_{osmotic}\begin{bmatrix} 1+\frac{\partial u_2}{\partial X_2} & -\frac{\partial u_1}{\partial X_2} \\ -\frac{\partial u_2}{\partial X_1} & 1+\frac{\partial u_1}{\partial X_1} \end{bmatrix} + \begin{bmatrix} S_{11} & S_{12} \\ S_{21} & S_{22} \end{bmatrix}\begin{bmatrix} 1+\frac{\partial u_1}{\partial X_1} & \frac{\partial u_2}{\partial X_1} \\ \frac{\partial u_1}{\partial X_2} & 1+\frac{\partial u_2}{\partial X_2} \end{bmatrix} \\
&= -p_{osmotic}\begin{bmatrix} 1+\frac{\partial u_2}{\partial X_2} & -\frac{\partial u_1}{\partial X_2} \\ -\frac{\partial u_2}{\partial X_1} & 1+\frac{\partial u_1}{\partial X_1} \end{bmatrix} + \begin{bmatrix} S_{11}(1+\frac{\partial u_1}{\partial X_1}) + S_{12}\frac{\partial u_1}{\partial X_2} & S_{11}\frac{\partial u_2}{\partial X_1} + S_{12}(1+\frac{\partial u_2}{\partial X_2}) \\ S_{21}(1+\frac{\partial u_1}{\partial X_1}) + S_{22}\frac{\partial u_1}{\partial X_2} & S_{21}\frac{\partial u_2}{\partial X_1} + S_{22}(1+\frac{\partial u_2}{\partial X_2}) \end{bmatrix} \\
&= \begin{bmatrix} S_{11}(1+\frac{\partial u_1}{\partial X_1}) + S_{12}\frac{\partial u_1}{\partial X_2} - p_{osmotic}(1+\frac{\partial u_2}{\partial X_2}) & S_{11}\frac{\partial u_2}{\partial X_1} + S_{12}(1+\frac{\partial u_2}{\partial X_2}) + p_{osmotic}\frac{\partial u_1}{\partial X_2} \\ S_{21}(1+\frac{\partial u_1}{\partial X_1}) + S_{22}\frac{\partial u_1}{\partial X_2} + p_{osmotic}\frac{\partial u_2}{\partial X_1} & S_{21}\frac{\partial u_2}{\partial X_1} + S_{22}(1+\frac{\partial u_2}{\partial X_2}) - p_{osmotic}(1+\frac{\partial u_1}{\partial X_1}) \end{bmatrix}
\end{aligned} \tag{2.91}$$

$$\begin{bmatrix} \frac{\partial}{\partial X_1} \\ \frac{\partial}{\partial X_2} \end{bmatrix}^{\mathrm{T}} \begin{bmatrix} S_{11}(1+\frac{\partial u_1}{\partial X_1}) + S_{12}\frac{\partial u_1}{\partial X_2} - p_{osmotic}(1+\frac{\partial u_2}{\partial X_2}) & S_{11}\frac{\partial u_2}{\partial X_1} + S_{12}(1+\frac{\partial u_2}{\partial X_2}) + p_{osmotic}\frac{\partial u_1}{\partial X_2} \\ S_{21}(1+\frac{\partial u_1}{\partial X_1}) + S_{22}\frac{\partial u_1}{\partial X_2} + p_{osmotic}\frac{\partial u_2}{\partial X_1} & S_{21}\frac{\partial u_2}{\partial X_1} + S_{22}(1+\frac{\partial u_2}{\partial X_2}) - p_{osmotic}(1+\frac{\partial u_1}{\partial X_1}) \end{bmatrix}$$

$$= \begin{bmatrix} \frac{\partial}{\partial X_1}(S_{11}(1+\frac{\partial u_1}{\partial X_1}) + S_{12}\frac{\partial u_1}{\partial X_2} - p_{osmotic}(1+\frac{\partial u_2}{\partial X_2})) + \frac{\partial}{\partial X_2}(S_{21}(1+\frac{\partial u_1}{\partial X_1}) + S_{22}\frac{\partial u_1}{\partial X_2} + p_{osmotic}\frac{\partial u_2}{\partial X_1}) \\ \frac{\partial}{\partial X_1}(S_{11}\frac{\partial u_2}{\partial X_1} + S_{12}(1+\frac{\partial u_2}{\partial X_2}) + p_{osmotic}\frac{\partial u_1}{\partial X_2}) + \frac{\partial}{\partial X_2}(S_{21}\frac{\partial u_2}{\partial X_1} + S_{22}(1+\frac{\partial u_2}{\partial X_2}) - p_{osmotic}(1+\frac{\partial u_1}{\partial X_1})) \end{bmatrix}^{\mathrm{T}} \quad (2.92)$$

Especially in one-dimensional case,

$$\nabla \cdot \boldsymbol{P} = \nabla \cdot (-J\boldsymbol{F}^{-1}p_{osmotic}\boldsymbol{I} + \boldsymbol{S}\boldsymbol{F}^{T}) = \frac{d}{dX}[-p_{osmotic} + S_{11}(1+\frac{du}{dX})] = 0$$

$$\frac{d}{dX}\left[-p_{osmotic} + (\lambda+2\mu)(\frac{du}{dX} + \frac{1}{2}(\frac{du}{dX})^2)(1+\frac{du}{dX})\right] = 0$$

$$\frac{d}{dX}[-p_{osmotic} + (\lambda+2\mu)(\frac{du}{dX} + \frac{3}{2}(\frac{du}{dX})^2 + \frac{1}{2}(\frac{du}{dX})^3)] = 0$$

$$(\lambda+2\mu)[\frac{d^2u}{dX^2} + 3\frac{du}{dX}\frac{d^2u}{dX^2} + \frac{3}{2}(\frac{du}{dX})^2\frac{d^2u}{dX^2}] - \frac{dp_{osmotic}}{dX} = 0 \quad (2.93)$$

Osmotic pressure $p_{osmitic}$

A Legendre transform is a linear change of variable that involves subtracting the product of conjugate variables from an extensive property of a system. The variables involved in work form conjugate pairs of intensive and extensive variables, as shown in Table 2.3.

To make Legendre transforms, we have introduced the intensive variables P and T as natural variables. This process can be continued to introduce the intensive variables μ_1, μ_2, …, μ_N by making the complete Legendre transform

$$U' = U + PV - TS - \sum_{k=1}^{N} n_k\mu_k = 0 \quad (2.94)$$

It is evident from equation

$$U = TS - PV + \sum_{k=1}^{N} n_k\mu_k \quad (2.95)$$

that this transformed internal energy U' is equal to zero. The differential of U' is

written as

$$dU + PdV + VdP - TdS - SdT - \sum_{k=1}^{N} n_k d\mu_k - \sum_{k=1}^{N} \mu_k dn_k = 0 \tag{2.96}$$

$$dU = TdS - PdV + \sum_{k=1}^{N} \mu_k dn_k \tag{2.97}$$

where $\mu_k = \left(\frac{\partial U}{\partial n_k} \right)_{S,V,n_j}$ for U fields

$$VdP - SdT - \sum_{k=1}^{N} n_k d\mu_k = 0 \tag{2.98}$$

which is known as the Gibbs-Duham equation. Note that it deals with changes only of the intensive variables for the system. Because of this relation, the intensive variables for a system are not independent.

The osmotic pressure $p_{osmitic}$ is the pressure difference across the hydrogel membrane required to prevent spontaneous flow of solvent in either direction across the membrane.

The Gibbs-Duham equation deals with changes of the intensive variables for this system,

$$Vdp - SdT - \sum_{k=1}^{N} n_k d\mu_k = 0 \tag{2.99}$$

If the temperature is constant,

$$Vdp - \sum_{k=1}^{N} n_k d\mu_k = 0 \tag{2.100}$$

So the pressure is

$$dp = \sum_{k=1}^{N} \frac{n_k}{V} d\mu_k = \sum_{k=1}^{N} c_k d\mu_k \tag{2.101}$$

The chemical potential for the species k is

$\mu_k = \mu_k^0 + RT \ln a_k = \mu_k^0 + RT \ln(c_k \gamma_k)$. Thus one can have

$$dp = \sum_{k=1}^{N} c_k d[RT \ln(c_k \gamma_k)] = RT \sum_{k=1}^{N} [c_k d(\ln c_k) + c_k d(\ln \gamma_k)]$$

$$= RT \sum_{k=1}^{N} [dc_k + c_k d(\ln \gamma_k)] \tag{2.102}$$

where γ_k is the activity coefficient of the species *k*, c_k^0 is the concentration of the species *k* in the stress-free state, and c_k the concentration of k^{th} species within the hydrogel in swelling state.

The current study focuses on the one-dimensional steady-state analysis for the response of the glucose-sensitive hydrogels. In sum, the governing equations for the MECglu model in one-dimensional case are expressed as,

Nernst-Planck equations,

$$div\left\{ D_k \left[\mathbf{grad} c_k + z_k c_k \frac{F}{RT} \mathbf{grad}\, \psi + c_k \mathbf{grad}(\ln \gamma_k) \right] \right\} + v_k r = 0 \tag{2.26}$$

$$(k = 1, 2, ..., N)$$

Rate of enzyme reaction,

$$r = \frac{V_{\max} c_g c_o}{c_o (c_g + K_g) + K_o c_g} \tag{2.51}$$

Poisson equation,

$$\frac{\partial^2 \psi}{\partial x^2} = -\frac{F}{\varepsilon \varepsilon_0} \left(\sum_k z_k c_k + z_f c_f \right) \tag{2.56}$$

Fixed charge density,

$$c_f = \frac{1}{H} \frac{c_{f,s}^0 K}{K + c_{H^+}}, \qquad \text{for anionic hydrogel} \tag{2.65}$$

$$c_f = \frac{1}{H}\frac{c_{f,s}^0 \cdot c_{H^+}}{K + c_{H^+}} \qquad \text{for cationic hydrogel} \qquad (2.71)$$

Mechanical deformation equation,

$$(\lambda + 2\mu)\left[\frac{d^2u}{dX^2} + 3\frac{du}{dX}\frac{d^2u}{dX^2} + \frac{3}{2}\left(\frac{du}{dX}\right)^2\frac{d^2u}{dX^2}\right] - \frac{dp_{osmotic}}{dX} = 0 \qquad (2.93)$$

2.2.2.5 Boundary conditions

For one-dimensional steady-state analysis,

$$c_{ox} = c_{ox}^* \;,\quad c_g = c_g^* \;,\quad c_a = 0 \;,\quad c_k = c_k^* \;,\quad \psi = 0 \qquad \text{at} \quad x = L \qquad (2.103)$$

In the central no-reaction zone, the reaction rate is zero. For the glucose and gluconic acid, therefore, the governing equation for diffusion is simplified to $J_g = J_{ox} = 0$,

$$\frac{\partial c_k}{\partial x} = 0 \qquad \text{at} \quad x = 0 \qquad (2.104)$$

At the interface between the solution and the hydrogel,

$$\frac{du}{dx} = \frac{p_{osmotic}}{E} \qquad (2.105)$$

In addition, to prevent the hydrogel from undergoing rigid body motion in the applied electric field, a point constraint is introduced in the middle of the hydrogel ($x = L/2$):

$$u = 0 \qquad \text{at} \quad x = 0 \qquad (2.106)$$

The osmotic pressure in any given point inside the hydrogel can be determined by

$$p^{\text{interface}} = RT\sum_k (c_k^{\text{in-interface}} - c_k^{\text{out-interface}}) - p_0 \qquad (2.107)$$

with $c_k^{out-interface}$ denotes the ionic concentration in exterior solution near the interface, and p_0 is the fluid pressure at a reference state.

2.3 Validation of MECglu Model

Validation of the MECglu model is carried out by the comparison between the simulation results and the experimental data from published literature (Kang and Bae, 2003). As shown in Figure 2.2, a typical glucose-sensitive hydrogel, poly(*N*,*N*-dimethylacrylamide) gel (PDMAAm), covalently immobilized glucose oxidase (GOD) and catalase, is immersed in an isotonic phosphate buffered saline (PBS) solution with pH 7.4. It is well-known that pH-sensitive hydrogels exhibit the volume transition in a narrow range of pH, which is depended by the pK_a of the pendant ionic groups containing on the crosslinked networks (Katchalsky and Michaeli, 1955; Richa and Tanaka, 1984; Peppas et al., 2000). PDMAAm hydrogel contains the sulfonic acid, $-SO_2N-H^-$, which are attached onto the polymeric networks, and shows sudden changes in the dynamic and equilibrium swelling behavior responding to the change of external pH. For this hydrogel, ionization occurs when the environmental pH is above the pK_a of the ionizable sulfonic group (Kang and Bae, 2002). With selecting appropriate pK_a, PDMAAm hydrogel can be controlled for the transition of solubility and swelling at a desired pH (near 7.4). As glucose diffuses into the hydrogel from the solution, the glucose oxidase will catalyze its conversion to gluconic acid, thereby lowering the pH within the hydrogel and then the osmotic pressure is changed, resulting in the swelling deformation of the hydrogel.

The material properties and other parameters used for simulation are given in

Table 2.1. The oxygen concentration in the body fluid always remains saturated all the time, i.e. $c_{ox} = 0.247$ mM, because the oxygen pressure in the capillary blood is higher than that in the tissue (Guyon, 1991). The global decrease of Young's modulus with enhancement of swelling has been confirmed experimentally (Kidoaki et al., 2001; Johnson et al., 2002; Isayava et al., 2002). The experimental values of Young's modulus are fit with a triple-line function by assuming a semi-linear transition in modulus between the range of pH=6.5 and 7.5, (Kidoaki et al., 2001; Sudipto et al., 2002) as shown in Figure 2.5, which is employed as input data for the present simulation based on the MECglu model.

Figures 2.6-2.8 show the comparison between experimental and simulating results for the equilibrium response of the glucose-sensitive hydrogels. In Figure 2.6, the pH-dependent swelling curve profile for PDAAm hydrogel shows a gradual increase in solubility as pH increases. It is found that the simulation results marked by circles consist qualitatively and quantitatively with the published experimental data marked by squares (Kang and Bae, 2003). The ionization of fixed charge groups is altered by the changing environmental pH. Figure 2.6 shows the distinguished volume transition in the range of pH from 6.5 to 8.0. In this range of pH, the swelling ratio of the hydrogel increases with increasing pH. Because the polymeric complexes are broken and the fixed charge groups of PDMAAm hydrogel are ionized, the osmotic pressure increases and then causes the hydrogel swelling. When pH is lower than 6.5 (around the pK_a of the sulfonic acid), the volume change of the hydrogel is tiny, that is, the hydrogel network is collapsed and the swelling ratio is low. Probably the reason

is that the certain interaction between ionized and un-ionized fixed charge groups in a solid state prevents the solubilization of crosslinked polymeric network until the number of ionized groups becomes dominant (Kang and Bae, 2001). It can also be found that the simulation results are slightly larger than that the experimental data in the range of pH higher than 7.0, which may be attributable to the immobilized glucose oxidase and catalase. The existing of enzymes will make the hydrogel thicker and stronger (Dhanarajan and Siegel, 2005). The effect of enzymes in the MECglu model should be further investigated in future work.

Figures 2.7 and 2.8 demonstrate the glucose dependent swelling and corresponding internal average pH of the hydrogel to make the comparison between the simulation results and experimental data (Kang and Bae, 2003). The swelling ratio of the hydrogel decreases with increasing the glucose concentration from 0 to 16.5mM, associated with the drop of internal pH of the gel. The process involves the conversion of glucose to gluconic acid by the enzyme glucose oxidase. Meanwhile, the catalase reaction is to prevent the accumulation of peroxide and to partially regenerate the oxygen. The important product of the reaction is a free proton, hydrogen ion H^+, which lowers the local pH and causes the pH-dependent volume phase transition to occur, enlarging the swelling of the hydrogel. The swelling deformation simulated also coincides quantitatively and qualitatively with the experimental results observed in Figure 2.8. The swelling ratio of the hydrogel nearly linearly drops from 12 to 8 in the same pace for both the experimental and simulation curves. In Figure 2.7 however, the decrease of simulated internal average pH within the hydrogel from 7.4 to 7.28 is

smaller than that of experimental results from 7.4 to 7.24. Despite the fact that the MECglu model may not accurately predict the accurate drop of average pH achieved in the glucose-sensitive hydrogel, the phenomena and the trends demonstrated here confirm and support the experiment, which is the first and most important step in the design of a glucose sensitive hydrogel system.

Nonetheless, the simulations match closely with the experimental results. This proves that the MECglu model can satisfactorily predict the swelling behavior of the glucose-sensitive hydrogel.

2.4 Parameters Studies

There have been increased research interests in the development of glucose-sensitive hydrogel systems that deliver appropriate amounts of insulin in response to changing glucose levels, so as to mimic the natural response of the body (Krall and Beaser, 1989; Jennedy, 1991). This could lead to better control of blood glucose levels for diabetic patients. This approach involves an enzyme-substrate reaction that results in a pH change and the swelling of the pH-sensitive hydrogel responding to the change. Glucose reacts with glucose oxidase (GOD) forming gluconic acid (GlucA), and thus decreasing the pH of the environment. With the change of pH, the hydrogels swell ore collapse depending on the characteristics of the particular polymer of the systems. Insulin is released from this system with the change in the size of the pores of the polymer (Heller, 1993). To elucidate the mechanisms of

these systems, it is vital to investigate the effects of the various parameters on the equilibrium behaviors of the glucose-sensitive hydrogels.

2.4.1 Influences of Oxygen Concentration

Compared with the blood glucose concentration and owning to its low solubility in aqueous solution, the sparse availability of oxygen is known to be a fundamental limitation of all implanted glucose oxidase-based sensitive devices (Parker and Schwartz, 1987; Traitel et al., 2000). In order to investigate the vital role of oxygen in the glucose-sensitive hydrogel systems, the numerical simulations are shown in Figures 2.9-2.18 for the effect of the oxygen concentration in the environmental solution on the equilibrium behaviors of the glucose-sensitive hydrogel with the input parameters $c_f^0 = 10.0$ mM, $z_f = -1$, $c^* = 138.0$ mM, $E = 0.64$ MPa, $L = 4.0$ mm, $LGel0 = 600$ μm, $pH = 7.4$, $c_g^* = 8.0$ mM, $c_{ox} = 0.1$, 0.15, 0.2 and 0.247mM, respectively, and others shown in Table 2.1.

Figure 2.9 illustrates the distributive profile of hydrogen ion concentration with the various oxygen concentrations. It is found that the H^+ concentration within hydrogel obviously increases with the increasing oxygen supply, and the hydrogel shrinks dramatically with the increase of oxygen concentration, especially from 0.1mM to 0.15mM. Figure 2.10 shows the dependence of the average pH in hydrogel on the concentration of oxygen in the media. It is noticed that pH decreases monotonically with the increase of oxygen supply. As expected, due to $c_g^* \gg c_{ox}$,

greater oxygen supply will produce more hydrogen ions, which thus reduces pH in the hydrogel. Figures 2.11 and 2.12 show the effect of the oxygen concentration on the distributive profiles of diffusive ions, Na^+ and Cl^-. The concentration of sodium Na^+ in the hydrogel decreases with increasing of the concentration of oxygen, while the concentration of chloride Cl^- in the hydrogel increases conversely. Consequently, the concentration difference reduces over the interface between the hydrogel and surrounding solution.

Figure 2.13 shows that the distribution of glucose depends on the variation of oxygen concentration. Figure 2.14 shows the distributive profile of oxygen concentration within the hydrogel. Figure 2.15 illustrates the distribution of the product of enzyme reaction, gluconic acid, with different oxygen concentrations. With increasing of oxygen concentration, more glucose is converted into gluconic acid. As a result, the concentration of glucose decreases and that of gluconic acid increases accordingly. The results of the MECglu model show that due to the low solubility and slow diffusion of oxygen in the aqueous solution, the supply of oxygen controls the enzyme reaction (Clark et al., 1987).

Figure 2.16 shows the effect of oxygen concentration on the distributive profile of the electric potential. The electric potential in the hydrogel increases with increasing of the concentration of oxygen. It can be explained that the increasing of hydrogen ions hinders the protonization of the fixed groups and the diffusion of mobile ions into the hydrogel. Figures 2.17 and 2.18 show that the change of mechanical deformations of the glucose-sensitive hydrogel with the effect of the oxygen concentration. It is shown

in Figure 2.17 that the hydrogel strip shrinks as increasing of oxygen concentration. Figure 2.18 shows the effect of oxygen concentration on the swelling ratio of hydrogel with different glucose concentrations. The swelling ratio decreases with the increase of the oxygen concentration, especially for lower glucose concentration.

2.4.2 Influences of Enzyme Concentration

Enzyme concentration is one of the major factors in an enzyme-mediated reaction. In enzyme-mediated reactions, the rate of reaction increases in proportion to enzyme concentration (Tozeren and Byers, 2004). It is thus very important to investigate the effect of the enzyme concentration in the local environment on the equilibrium behavior of the glucose-sensitive hydrogel. The input parameters in the simulation are $c_f^0 = 10.0\,\text{mM}$, $z_f = -1$, $c^* = 138.0\,\text{mM}$, $E = 0.64\,\text{MPa}$, $L = 4.0\,\text{mm}$, $LGel0 = 600$ μm, $pH = 7.4$, $c_g^* = 8.0$ mM, $c_{ox} = 0.247$ mM, $c_{enz} = 2.0$, 2.5 and 25.0μM, respectively.

The effect of the loading enzyme concentrations on the concentration of hydrogen ions is firstly concerned and the distributive profile is shown in Figure 2.19. The concentration of H^+ ions increases in the hydrogel owning to the accumulation of gluconic acid with the converting of higher enzyme concentration. The reusability of enzyme immobilized onto the hydrogels and the applicability to continuous processes can significantly enhance the accumulation of hydrogen ions and minimize pH (Blandino et al., 2002).

The effect of the enzyme concentrations on the distributive profiles of Na^+ and Cl^- is illustrated in Figures 2.20 and 2.21, and the concentration of Na^+ in the hydrogel decreases slightly while that of Cl^- increases. This comes to a drop of concentration difference over the interface between the hydrogel and the surrounding solution and furthermore reduces the osmotic pressure, which finally results in the shrinking of the hydrogel strip.

As shown in Figure 2.22, the glucose concentration decreases from 8.0mM at the edge of solution boundary to a much lower value towards the centre of hydrogel, and the change is much steeper with higher enzyme concentration. Similarly, the oxygen concentration decreases while the concentration of gluconic acid increases towards the centre of hydrogel, as shown in Figures 2.23 and 2.24.

Figure 2.25 shows the effect of enzyme concentration on the distributive profile of the electric potential. It is found that electric potential in the hydrogel increases with the increment of enzyme concentration. Figure 2.26 shows the effect of enzyme concentration on the distributive profile of the fixed charge group density. It is seen that the density of fixed change groups increases as the enzyme concentration increases, which is the result of shrinking of hydrogel owning to the decrease of concentration difference (Kratz et al., 2000).

It is shown in Figure 2.27 that the displacement u of the hydrogel strip slightly drops with the increase of enzyme concentration. And so does the swelling ratio of hydrogel with different glucose concentrations under the effect of enzyme concentration as shown in Figure 2.28. It is shown in Figure 2.29 that the change of

enzyme concentration influences the average pH in the hydrogel. The pH in hydrogel drops imperceptibly with the increase of enzyme concentration. Actually, the enzyme GOD is stale ($\leq 20\%$ loss of activity after 180 h at 25°C) in solutions within a broad pH range between 4 and 9 (Rehor et al., 2005). It is important to show that the enzyme concentration does not change reaction equilibria in the enzyme-mediated catalysis, because both the forward and reverse reactions are catalyzed equally well (Tozeren and Byers, 2004).

2.4.3 Influences of Initially Fixed Charge Group Density

A number of experiments show the volume phase transition of hydrogels depends strongly on the fixed charge density on the crosslinking chains (Katayama et al., 1992; Sarkyt and Vladimir, 1999; Chen et al., 2004). Numerical simulations on the effect of fixed charge density will study well the properties of the glucose-sensitive hydrogels and optimize the design of drug delivery system based on these hydrogel. In the following, Figures 2.30-2.39 show the simulations for the effect of the initially fixed charge group density on the equilibrium behavior of the glucose-sensitive hydrogel with the input parameters $c_f^0 = 10.0$ mM, $z_f = -1$, $c^* = 138.0$ mM, $E = 0.64$ MPa, $L = 4.0$ mm, $LGel0 = 600$ μm, $pH = 7.4$, $c_g^* = 8.0$ mM, $c_{ox} = 0.247$ mM, $c_{enz} = 2.5\,\mu$M, $c_f^0 = 5.0$, 10, 15 and 20mM, respectively.

Figure 2.30 illustrates the distributive profile of hydrogen ion H^+ concentration with the various initially fixed charge group densities. A higher fixed charge density

triggers the increase of H^+ concentration in the hydrogel. Figures 2.31 and 2.32 show the effect of the initially fixed charge group density on the distributive profiles of Na^+ and Cl^-. As the initially fixed charge density increases linearly, both the concentrations of Na^+ and Cl^- increase rapidly within the hydrogels. The three figures also clearly show that the domain of hydrogel for the distribution of ions decrease, which reveal the shrinking largely of the hydrogel with the change of fixed charge group densities. It is shown in Figure 2.33 that the change of initially fixed charge group density influences the average pH in the hydrogel. With increase of fixed charge group densities, the average pH in the hydrogel decreases gradually and the result accords with Figure 2.30.

Figures 2.34-2.36 are plotted for the effect of fixed charge group density on the distribution of chemical reaction substrates and product, glucose, oxygen and gluconic acid. These figures show that the concentration of substrate glucose increases while that of gluconic acid decreases. It suggests that the enzyme reaction has been inhibited, which may be due to greater H^+ concentration enhanced by the increase of fixed charge density.

Figure 2.37 shows that the absolute value of the electric potential distributing in the hydrogel decreases as the initially fixed charge group density increases from 5 to 20mM. It is shown in Figure 2.38 that the change of initially fixed charge group densities influences the displacement of the hydrogel strip. The displacement increases with the increase of initially fixed charge density.

Figure 2.39 shows the effect of enzyme concentration on the swelling ratio of

hydrogel with different initially fixed charge group densities. As a given c_g, the hydrogel with higher fixed charge density gains lower swelling ratio. Meanwhile, the simulation result is indicative of a good glucose response for the hydrogel with bigger fixed charge density.

2.4.4 Influences of Ionic Strength

To significantly improve the lives of diabetic patients and decrease their risk of hypoglycemia, the insulin delivery systems and glucose sensors based on the pH-sensitive hydrogels must be developed accurate, reliable, continuous, have to operate reliably at the physiological pH values and ionic strengths of body fluids and would have to be immune from interference by other species present (Pickup et al., 1999; Asher, 2003). Due to their inherent nature, the polyelectrolyte hydrogels respond spontaneously to the change of the ionic strength (IS) of environmental solution. The swelling of anionic or cationic hydrogels decreasing upon increasing ionic strength is called polyelectrolyte effect (Oppermann, 1992; Valencia and Pierola, 2007). In order to understand the effect of the ionic strength on the equilibrium behavior of the glucose-sensitive hydrogel, the dependence of the response of hydrogel on IS in the environmental solution are investigated with the input parameters $c_f^0 = 10.0$ mM, $z_f = -1$, $E = 0.64$ MPa, $L = 4.0$ mm, $LGel0 = 600$ μm, $pH = 7.4$, $c_g^* = 8.0$ mM, $c_{ox} = 0.247$ mM, $c_{enz} = 2.5$ μM, $I = 30.0$, 60.0, 90.0 and 120.0mM, respectively.

Figure 2.40 illustrates the distributive profile of hydrogen ion concentration

with the various ionic strengths. The H^+ concentration decreases with the increase of ionic strength of surrounding solution. Figure 2.41 shows that the distribution of glucose depends on the variation of ionic strengths. The glucose concentration also decreases with increasing of the ionic strength of surrounding solution. While the concentration of the product of chemical reaction, gluconic acid increases conversely, as shown in Figure 2.43. The effect of ionic strength on the distributive profile of oxygen concentration in the system is plotted in Figure 2.42. With increment of ionic strength (IS) of surrounding solution, the O_2 concentration in the hydrogel increases. The simulation result consists with the experimental phenomena (Schroder et al., 2007).

Figure 2.44 is plotted for the change of ionic strength influences the average pH in the hydrogel. With the increment of ionic strength, the average pH in the hydrogel will decrease obviously. The ionic strength may affect the association state of pendent fixed charge groups and their hydration affinity in solutions. For the glucose concentration sensors based on the pH-sensitive hydrogles, the sensitivity may dramatically decrease with increasing ionic strength (Zhang and Anslyn, 2007).

Figure 2.45 shows the effect of ionic strengths on the distributive profile of the electric potential. The electric potential of ionic hydrogels was mainly related to the valence of fixed charge, the ionic concentration and charge number of the external solution. As the concentration of cations in swelling medium enhanced, a charge screening effect of the additional cations resulted in a nonperfect anion-anion electrostatic repulsion, which may hinder the diffusion of mobile ions into hydrogel

(Flory, 1953). Therefore, the absolute value of electric potential ψ in the hydrogel decreases with the enhancement of ionic strength.

Figure 2.46 shows the effect of ionic strengths on the distributive profile of the fixed charge group density. As the ionic strength increases, the difference in concentration of mobile ions between the inside and the outside of the gel diminish. As a result, the repulsive electrostatic pressure and the osmotic pressure decrease inside the gel. The equilibrium ratio of shrinkage depends upon the ionic strength of buffer solution. The higher the ionic strength is, the larger the equilibrium shrinking ratio is (Suzuki and Kumagai, 2003). That is the reason for increasing of fixed charge density in the hydrogel with the increase of ionic strength, as shown in Figure 2.46.

Increasing ionic strength of swelling medium may enhance hydrophobic bonding and polymer-polymer interaction with hydrogel, increase consequently crosslink density, and then result in Young's modulus increasing (Wang and Wu, 2005).

It is shown in Figure 2.47 that the change of ionic strength influences the displacement of the hydrogel strip. With larger ionic strength, the hydrogel has lower displacement. Figure 2.48 shows the effect of ionic strength on the length of hydrogel strip with different glucose concentrations. It is clear that the equilibrium swelling decreases by increasing the ionic strength of the solution. In current simulations, we assumed the diffusive ions have the same size. If these ions have comparatively different sizes, their diffusions appear different. Increasing concentration of bigger ions will cause the hydrogel shrinking more dramatically (Bajpai and Kankane, 2007). This is consistent with the finding that when the matrix is immersed in aqueous buffer

solutions of the same pH, but of increased ionic strength, the swelling equilibrium reduces (Siegel, 1993).

It is known that at the same ionic strength, the electrochemomechanical response of the hydrogel depends on the three factors, the size of the hydrated counter ion, the ionic mobility, and the valence and concentration of the solution ions (El-Hag Ali et al., 2006). In present studies, the valence and concentration of the solution ions, H^+, Na^+ and Cl^- are considered in the MECglu model. The others two factors, the size of the hydrated counter ion, the ionic mobility will be investigated in the future work.

2.4.5 Influences of Environmental pH

For normal blood, there is no significant pH change expected, because the pH of blood is usually in a narrow range of around 7.4 (Suzuki and Kumagai, 2003). However, when people get a sick, the physiological pH will be changed, for instance, the acidosis can cause the pH value to drop down to 6.7, or alkalosis can target it up to 7.8 (Hoffman, 1970; Varley et al., 1980). It is known that the reversible and remarkable volume transition of pH-sensitive hydrogels is associated strongly with the environmental solution pH (Kang and Bae, 2001), and the large pH variations may hinder the use of the insulin delivery system based on the hydrogels (Rehor et al., 2005). In order to investigate the effect of the pH of surrounding solution on equilibrium behaviors of the glucose-sensitive hydrogels, the simulations are carried

out with the input parameters $c_f^0 = 10.0\,\text{mM}$, $z_f = -1$, $c^* = 138.0\,\text{mM}$, $E = 0.64\,\text{MPa}$, $L = 4.0$ mm, $LGel0 = 600$ μm, $c_g^* = 8.0$ mM, $c_{ox} = 0.247$ mM, $c_{enz} = 2.5$ μM $pH = 6.8$,7.0, 7.2 and 7.4, respectively.

Figure 2.49 illustrates the distributive profile of pH in the whole domain. It is found that pH value in the hydrogel is smaller than that in the surrounding solution. Typically, the pH drop is attributed to that glucose reacts with oxygen in the presence of the enzyme glucose oxidase forming gluconic acid and, thus, increasing the hydrogen concentration within the hydrogel (Hassan et al., 1997). Besides the more hydrogen ions accumulated by the chemical reaction and diffused from solution, the diffusion of glucose into and gluconic acid out of the hydrogel could attribute to a gradual pH change (Albin et al., 1987; Zhang and Wu, 2002). The result is consisted with the published simulations (Klumb and Horbett TA, 1992, 1993).

Figures 2.50 and 2.51 show the effect of the environmental pH on the distributive profiles of Na^+ and Cl^-. It is found that the concentration of Na^+ within the hydrogel decreases with increasing of the environmental pH, while the concentration of Cl^- in the hydrogel increases conversely. The degree of ionization of the fixed charge groups in the hydrogel is modified by the pH of the surrounding solution. As microenvironmental pH increases over the pK_a of ionizable groups, more and more ionizable groups become deprotonated. The formation of charged groups on the polymer backbone will affect the ionic diffusion (Podual et al., 2000). The increase of the negative charged groups will attract more counterions Na^+ diffusing into the hydrogel to satisfy electroneutrality condition, while the negative

charged groups will restrain Cl^- entering the hydrogel.

Figures 2.52 and 2.53 show the distribution profiles of glucose and oxygen concentrations depending on the varying of environmental pH. Both the concentrations of glucose and oxygen decrease within the hydrogel as the environmental pH increases. Increase of pH within the hydrogel means few hydrogen ions, which will activate the enzyme reaction and then consume more reactants, glucose and oxygen. The pH of media solution affecting enzymatic activity may be another factor. Moderate changes in pH may also have effects on the ionic state of the enzyme and the substrate. Changes in pH could alter the charge distribution on the binding sites, resulting in a change in the efficiency of catalytic activity (Tozeren and Byers, 2004). Figure 2.54 illustrates the distribution of the product of chemical reaction, gluconate acid, with various environmental pH. It is found that the concentration of gluconic acid increases with the environmental pH. The conversion of glucose will accumulate the gluconic acid in the hydrogel. The concentration of gluconic acid thus decreases in the hydrogel.

Figure 2.55 shows the effect of environmental pH on the distributive profile of the electric potential. The absolute value of electric potential in the hydrogel enhances with the increase of environmental pH. Figure 2.56 shows the effect of environmental pH on the distributive profile of the fixed charge group density. With higher environmental pH, the fixed charge density gradually increases due to the deprotonation of ionizable groups.

It is shown in Figure 2.57 that the change of environmental pH influences the displacement of the hydrogel strip. The hydrogel strip gains larger displacement with

higher environmental pH value. Equilibrium swelling characteristics is obtained by exposing polymer samples to different pH solutions and yielding their swelling ratio as a function of pH. Figures 2.58 and 2.59 illustrate the effect of environmental pH on the swelling ratio of hydrogel strip with different glucose concentrations. When pH increases, the concentration differences between the interior hydrogel and the surrounding solution will enhances, which can be observed in Figures 2.50 and 2.51. It augments the osmotic pressure and accordingly drives the hydrogel to swell. The simulations agree well with the experimental results (Kang and Bae, 2001) As a given c_g, the hydrogel immersed in solution with higher pH value gains larger swelling ratio. Furthermore, the simulation result suggests a good glucose response for the hydrogel in surrounding solution with higher pH value.

2.4.6 Influences of Initial Hydrogel Length

A hydrogel system in general, and especially those designed for drug delivery and tissue implantation, must fulfill the following minimum criteria: appropriate biocompatibility properties and size (McMahon et al., 2006). A hydrogel with suitable size can response fast to the external stimuli, maintain high mechanical strength and develop better physical integrity and storage capacity (Suzuki and Kumagai, 2003; Ziaie et al., 2004). Since the responsive nature of the hydrogel is limited by diffusion of chemical signals into the gel matrix, decreasing the size of the hydrogel will decrease the response time (Beebe et al., 2000). The size of hydrogels affects not only

the transient response, but also the equilibrium behaviors (Zhou et al., 2002; De and Aluru, 2004). Therefore, it is very important to assess the effect of the initial hydrogel length on the equilibrium behavior of the glucose-sensitive hydrogel. The following simulation are carried out with the input parameters $c_f^0 = 10.0$ mM, $z_f = -1$, $c^* = 138.0$ mM, $E = 0.64$ MPa, $pH = 7.4$, $c_g^* = 8.0$ mM, $c_{ox} = 0.247$ mM, $c_{enz} = 2.5\,\mu$M, $L = 4.0$ mm, $LGel0 = 600$, 700, 800, 900, 1000, 1100 and 1200μm, respectively.

Figure 2.60 illustrates the distributive profile of hydrogen ion with the effect of initial length of hydrogel strip. The concentration of hydrogen ions decreases with the growth of length of hydrogel strip. Figures 2.61 and 2.62 show the effect of the initial length of hydrogel strip on the distributive profiles of Na^+ and Cl^-. The concentration of Na^+ in the hydrogel decreases with increasing of the initial length of hydrogel strip, while the concentration of Cl^- in the hydrogel increases conversely. The average pH in the hydrogel increases with the increase of the initial length of hydrogel strip, as shown in Figure 2.63. Transport for countions of negative fixed charge groups is limited to the regions containing fluid in the gel. The effective path is longer than the hydrogel thickness and affected by it, therefore the ions must weave its way through the hydrogel (Weiss et al., 1986). Because the increase of hydrogel length means the presence of more polymer chains, which are impenetrable to mobile ions, and increases the path length an ion travels, resulting in a slower diffusion rate (De and Aluru, 2004).

Figures 2.64 and 2.65 show that the distributions of reaction substrates depend

on the variation of the initial length of hydrogel strip. Figure 2.66 illustrates the distribution of the product of chemical reaction, gluconate acid, with various initial length of hydrogel strip. From the three figures, it is found that the increasing of initial length of hydrogel strip retards the enzyme reaction, which results in the glucose accumulating in the hydrogel and less gluconic acid being produced.

Figure 2.67 shows the effect of initial length of hydrogel strip on the distributive profile of the electric potential. The absolute value of the electric potential ψ decreases with the growth of the hydrogel strip length. Figure 2.68 shows the effect of initial length of hydrogel strip on the distributive profile of the fixed charge group density. The fixed charge density decreases, due to the swelling of the hydrogel strip. It is shown in Figure 2.69 that the displacement of the hydrogel increases with the increase of initial length of hydrogel strip. Figure 2.70 shows the effect of initial length of hydrogel strip on the swelling ratio of hydrogel strip with different glucose concentrations. The equilibrium swelling reatio decreased reversely with the increase of diameter of hydrogel fibers (Fei et al., 2002).

2.4.7 Influence of Young's Modulus

It is known that the mechanical properties of polymers result from the chain structure of the materials (Arridge, 1975). Experimental results show that the Young's modulus of the hydrogel is improved by increasing the concentration of crosslinking agents, meaning that stiffness of the hydrogel is enhanced by the additional

crosslinking bonds (Sun et al., 2000). Therefore, the influence of crosslink density of hydrogel can be elucidated by investigating the equilibrium behaviors of the glucose-sensitive hydrogel with different Young's modulus. Figures 2.71-2.81 show the effect of the Young's modulus of the hydrogel on the equilibrium behavior of the glucose-sensitive hydrogel with the input parameters $c_f^0 = 10.0$ mM, $z_f = -1$, $c^* = 138.0$ mM, $L = 4.0$ mm, $LGel0 = 600$ μm, $pH = 7.4$, $c_g^* = 8.0$ mM, $c_{ox} = 0.247$ mM, $c_{enz} = 2.5$ μM, $E = 1.0 \times 0.64$, 1.5×0.64, 2.0×0.64 and 2.5×0.64 MPa, respectively.

Figure 2.71 illustrates the distributive profile of hydrogen ion with the effect of Young's modulus of the hydrogel. The concentration of hydrogen ions decreases when the hydrogel strip becomes much stiffer. Figures 2.72 and 2.73 show the effect of the Young's modulus of the hydrogel on the distributive profiles of Na^+ and Cl^-. The concentration of Na^+ in the hydrogel decreases slightly which that of Cl^- increasing. This comes to a drop of concentration difference over the interface between the hydrogel and the surrounding solution and furthermore leads the osmotic pressure decreasing, which finally results in the shrinking of the hydrogel strip. The average pH in the hydrogel increases with the growth of the Young's modulus of the hydrogel, as shown in Figure 2.74.

Figure 2.75 shows that the distribution of glucose depends on the variation of Young's modulus of the hydrogel. Figure 2.76 shows the distributive profile of oxygen concentration in the system. Figure 2.77 illustrates the distribution of the product of chemical reaction, gluconate acid, with various Young's modulus. For the three

components, glucose, oxygen and gluconic acid, their concentrations change very tiny as shown in those figures. It implies that the change of Young's modulus of the hydrogel strip has insignificant influence on the enzyme-catalyzed chemical reaction.

Figure 2.78 shows the effect of Young's modulus of the hydrogel on the distributive profile of the electric potential. Figure 2.79 shows the effect of Young's modulus of the hydrogel on the distributive profile of the fixed charge group density. Both the electric potential and fixed charge density increase with increasing of Young's modulus.

It is shown in Figure 2.80 that the change of Young's modulus of the hydrogel influences dramatically the displacement of the hydrogel strip. The hydrogel displays smaller displacement with higher Young's modulus. Figure 2.81 shows the effect of Young's modulus of the hydrogel on the swelling ratio of hydrogel strip with different glucose concentrations. The high Young's modulus reveals that hydrogel chains highly crosslink. The equilibrium swelling ratio tended to decrease with increasing Young's modulus because the hydrogel chains are enriched by crosslinking and the free volume in the network is reduced and thus restrained the expandability of the network. It yields good correlation with reported experimental results (Fei et al., 2002).

2.5 Remarks

The chapter has be successful modeled and simulated the equilibrium responsive behaviors of glucose oxidase-loaded pH-sensitive hydrogels subject to the blood

glucose concentration. The model can explain the experimental phenomena theoretically of the distribution of ionic concentration, electric potential and network deformation. It is noted that the current numerical simulation are conducted for the one-dimensional steady-state responsive behaviors of the glucose-sensitive hydrogels. The developed model has studied numerically the distribution of diffusive ionic concentration both in the hydrogel and the surrounding solution, the distribution of electric potential both in the hydrogel and the surrounding solution, the degree of equilibrium swelling, the displacement and swelling ratio of the glucose-sensitive hydrogels.

The equilibrium analysis for the glucose-sensitive hydrogel by MECglu model is very valuable, especially for the comparison with experimental data. First, we obtain an enhanced understanding of the swelling mechanisms, such as the differing rate of entry of water and protons into the matrix, and equilibrium swelling of the hydrogel being attained when protonation of the fixed charge groups was complete. Second, the simulations will solve and explain some questions arising from experiments. Ultimately, the model will enable simulation of results of future experiments thus hastening the development process of new controlled delivery devices. The MECglu model could be used to simulate various combinations of the parameters, the important parameters involved account for differences in the physical structure of the hydrogels as well as variations in the swelling media investigated. Thus the present model enables better design of bench experiments in the optimization process of developing new drug delivery systems.

It is noted to point out that the glucose-sensitive systems based on the pH-responsive hydrogels have a series of unique characteristics, (1) they respond abruptly to glucose concentration, (2) they expand and contract abruptly because of pH changes, (3) they are mechanically strong and (4) they can contain large amounts of insulin dispersed uniformly in the hydrogels. According to these characteristics, such systems are promising candidates for insulin delivery for diabetics.

Table 2.1 Material properties and constants for the simulations by MECglu model

Parameters	Value
Diffusion coefficient at infinite dilution in aqueous solution (25 °C) (m^2/s)	
hydrogen ion (Plawsky, 2001)	$D_H = 9.31\times10^{-9}$
gluconic acid and glucose (Albin et al., 1987; Klumb and Horbett, 1992)	$D_a = D_g = 6.75\times10^{-10}$
oxygen (Albin et al., 1987; Klumb and Horbett, 1992; Abdekhodaie and Wu, 2005)	$D_{ox} = 2.29\times10^{-9}$
Faraday's constant(C/mol)	$F = 9.645\times10^{4}$
universal gas constant(J/mol.K)	$R = 8.314$
absolute temperature(K)	T=310
the vacuum permittivity or dielectric constant (Li et al., 2005)	$\varepsilon_0 = 8.854\times10^{-12}\ C^2/Nm^2$,
the relative dielectric constant of the surrounding medium (Li et al., 2005)	$\varepsilon = 80$
kinetics constant (mol/cm^3) (Abdekhodaie and Wu, 2005)	$K_{ox} = 6.992\times10^{-3}$; $K_g = 6.178\times10^{-7}$
the maximum velocity	$V_{\max}(mol/s\times cm^3) = 860(s^{-1})\times c_{enz}(mol/cm^3)$
the equilibrium dissociation constant (Kang and Bae, 2002)	$K = 10^{-6.17}$ mM.
Young's modulus (MPa) (Kidoaki et al., 2001; Sudipto et al., 2002)	E=0.6~1.5
the initial water volume fraction (Li et al., 2004)	$\phi_0^w = 0.8$

Initially fixed charge density and	$c_f^0 = 10\ \text{mM}$
valence of fixed charge groups	$z_f = -1$
Boundary conditions	$c^* = c_{\text{Na}^+} = c_{\text{Cl}^-} = 138.0\ \text{mM}$
Geometry size	$L = 4000\mu\text{m}$;
	$LGel0 = 600\ \mu\text{m}$

Table 2.2 The gradient operator in Cartesian, Cylindrical and Spherical Coordinates (Plawsky, 2001).

Coordinate System	Gradient Equation
Cartesian	$\nabla J = (\frac{\partial}{\partial x}\boldsymbol{i} + \frac{\partial}{\partial y}\boldsymbol{j} + \frac{\partial}{\partial z}\boldsymbol{k})J$
Cylindrical	$\nabla J = (\frac{\partial}{\partial r}\boldsymbol{e}_r + \frac{1}{r}\frac{\partial}{\partial r}\boldsymbol{e}_\theta + \frac{\partial}{\partial z}\boldsymbol{e}_z)J$
Spherical	$\nabla J = (\frac{\partial}{\partial r}\boldsymbol{e}_r + \frac{1}{r}\frac{\partial}{\partial \theta}\boldsymbol{e}_\theta + \frac{1}{r\sin\theta}\frac{\partial}{\partial \varphi}\boldsymbol{e}_\varphi)J$

Table 2.3 Conjugate Pairs of Thermodynamic Variables (Alberty and Silbey, 1996)

Type of Work	Intensive variable	Extensive Variable	Differential Work
Hydrostatic	Pressure, P	Volume, V	$-PdV$
Surface	Surface tension, γ	Area, A_s	γdA_s
Elongation	Force, f	Length, L	fdL
Electrical	Potential difference, ϕ	Electric charge, Q	ϕdQ
Gravitational	Gravitational potential, ψ	Mass, m	ψdm

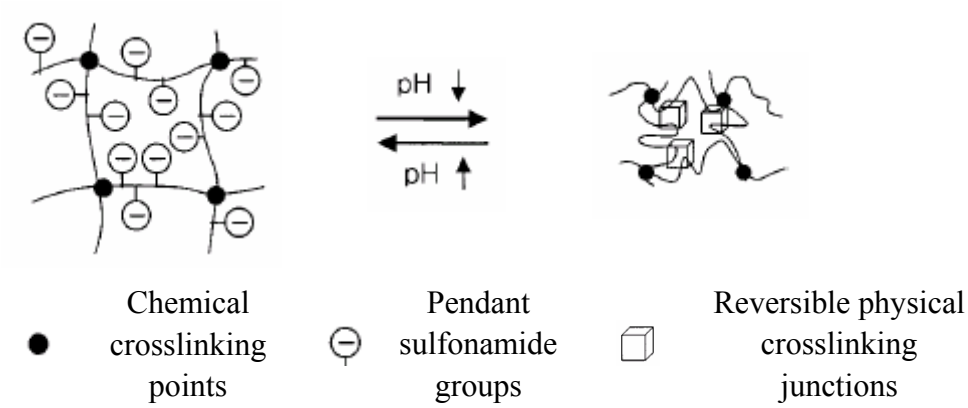

Figure 2.1 Schematic for volume-phase transition of pH-sensitive hydrogel. The hydrogel expands when the sulfonamide groups are fully charged negatively at high pH and completely collapse by protonation of sulfonamide groups at low pH (Kang and Bae, 2001).

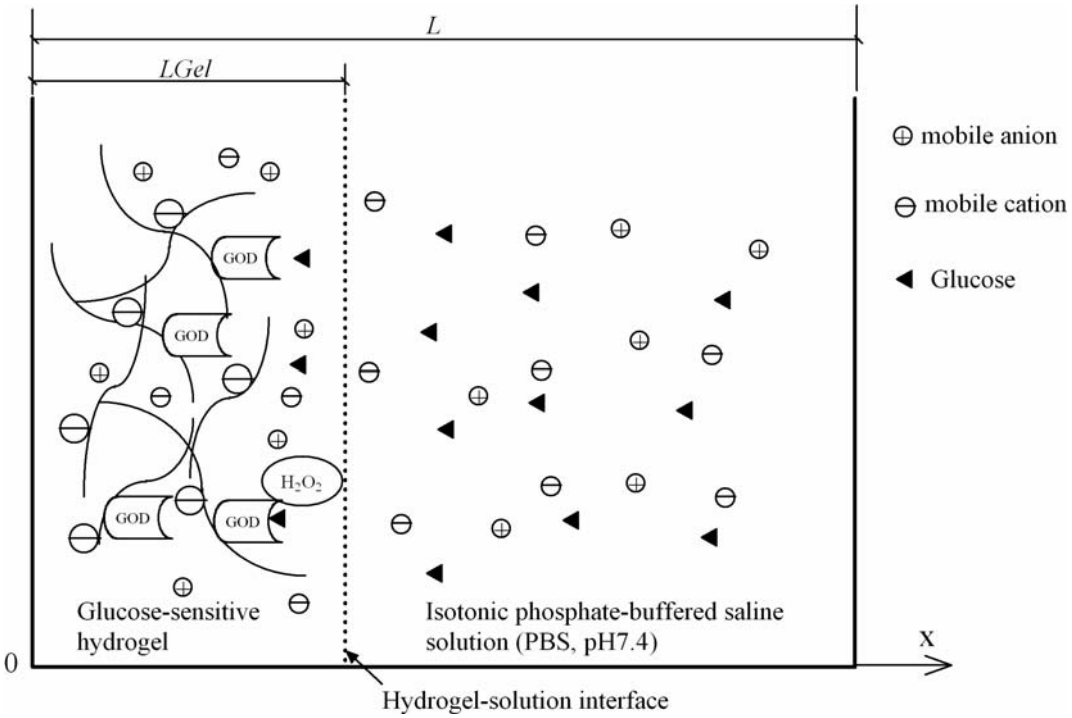

Figure 2.2 Schematic for ions transport and reaction in glucose-sensitive hydrogel systems

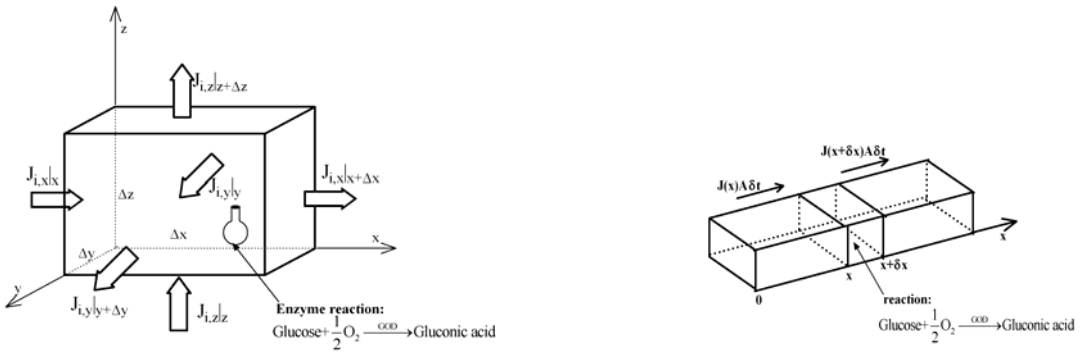

Figure 2.3 Ionic species flux and reactions in a differential volume element in (a) three-dimensional and (b) one-dimension domains.

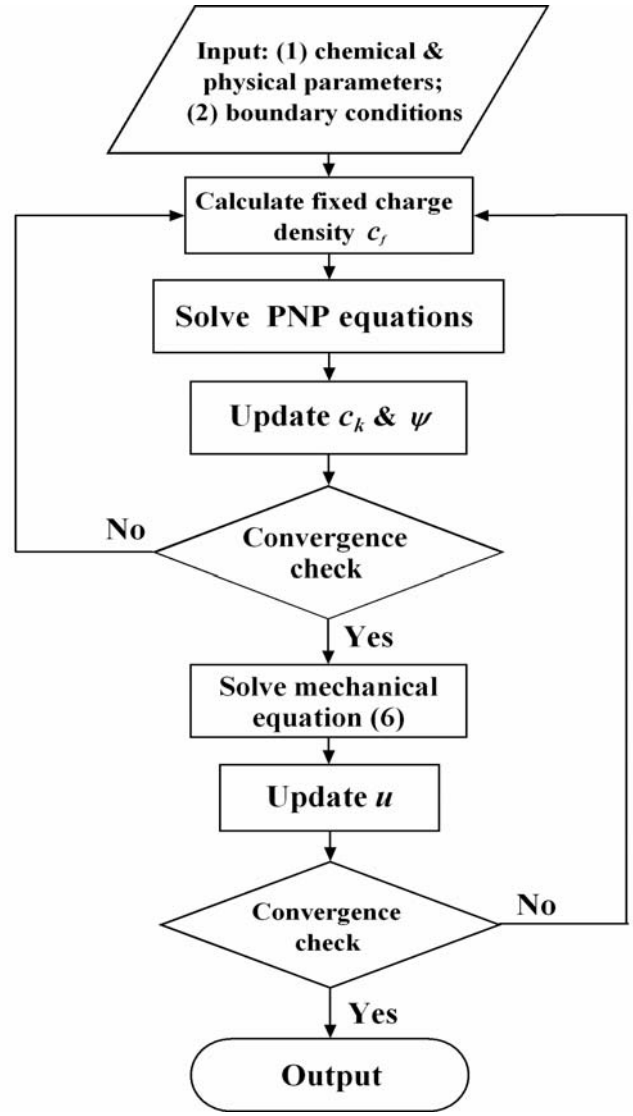

Figure 2.4 Flowchart for the MECglu model.

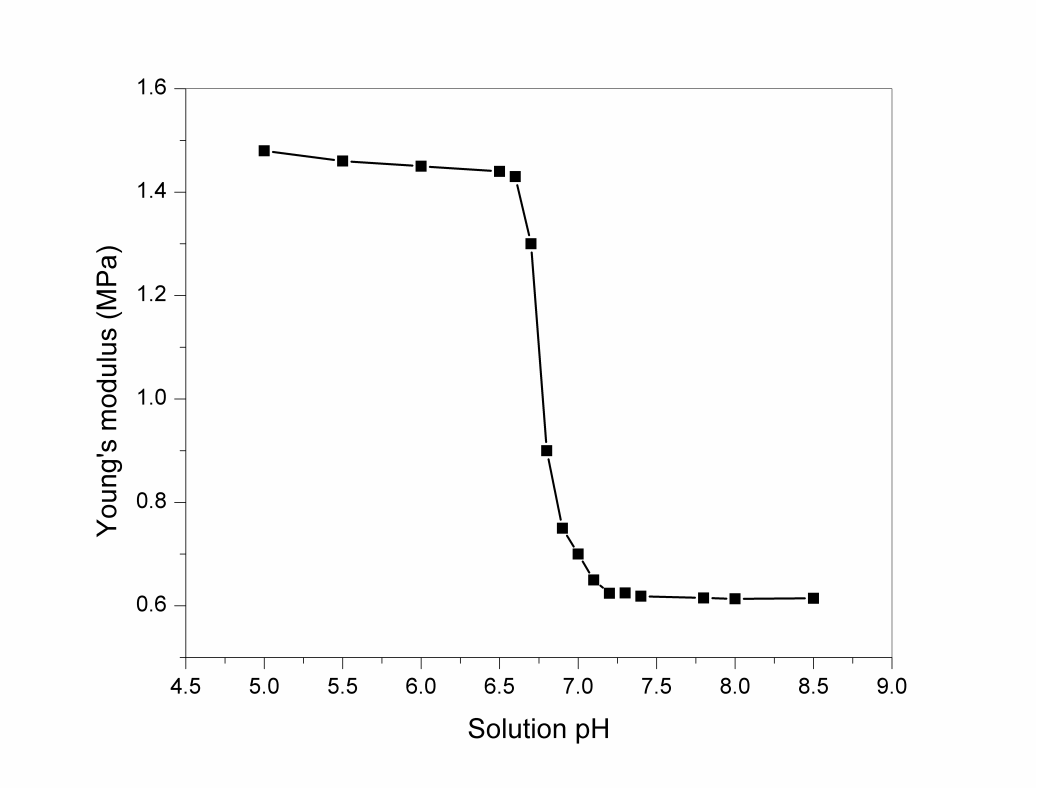

Figure 2.5 Input of Young's modulus for simulation based on the present MECglu model.

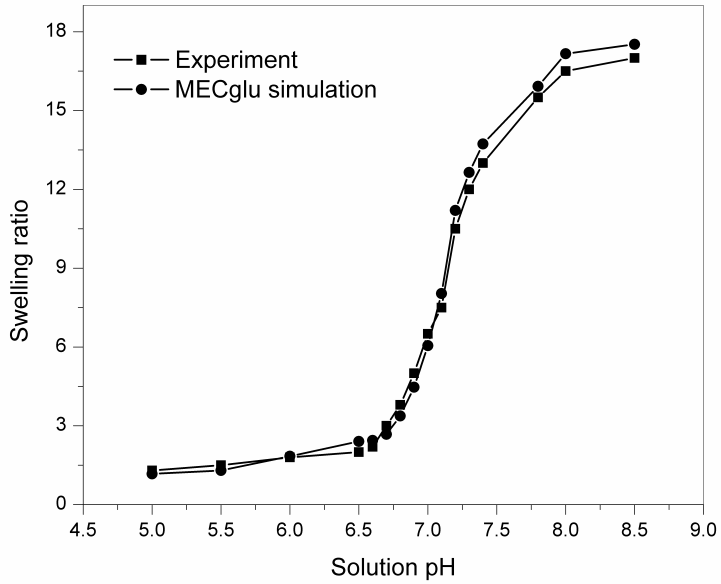

Figure 2.6 Swelling ratio of the hydrogel at 37°C in pH buffer solution.

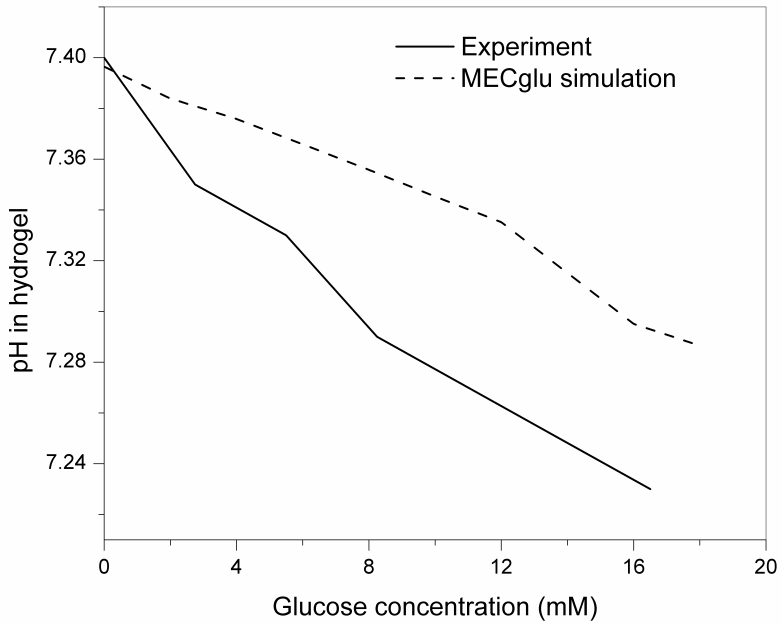

Figure 2.7 Average pH within the hydrogel strip.

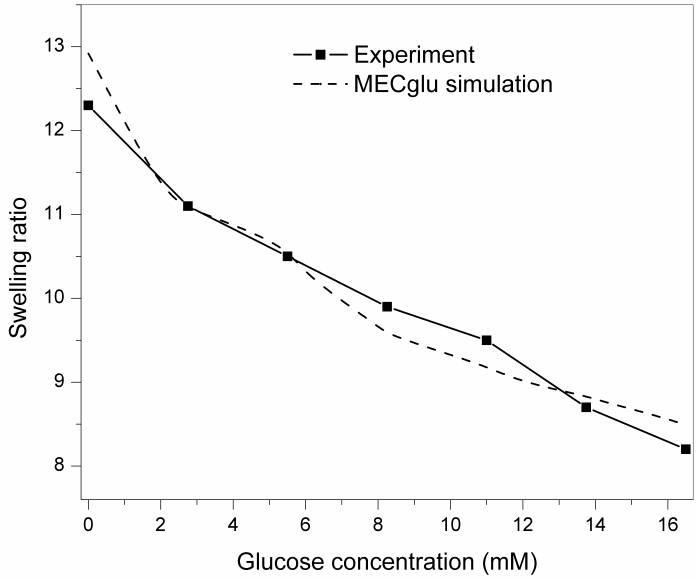

Figure 2.8 Glucose dependent swelling of the glucose-sensitive hydrogel at 37°C in pH buffer solution.

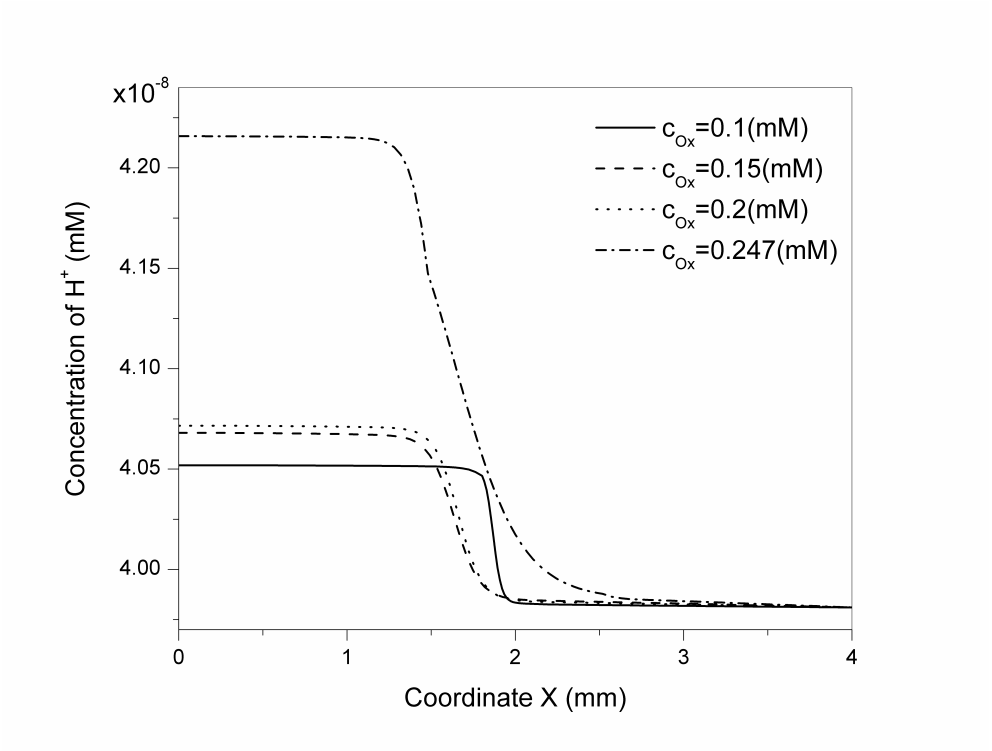

Figure 2.9 The distributive profile of hydrogen ion concentration with the various oxygen concentrations.

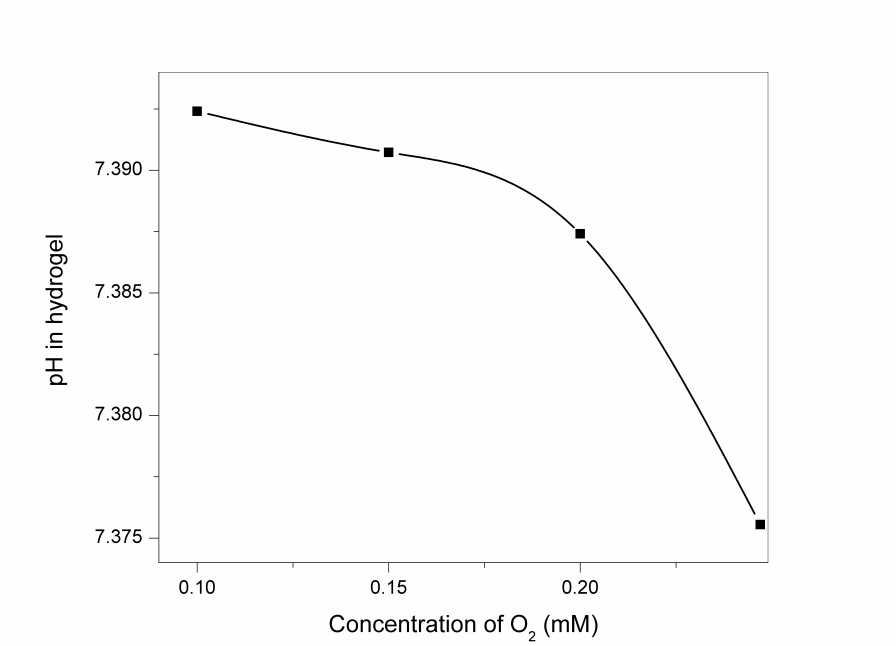

Figure 2.10 The average pH in hydrogel drops when increasing the oxygen supply in the media.

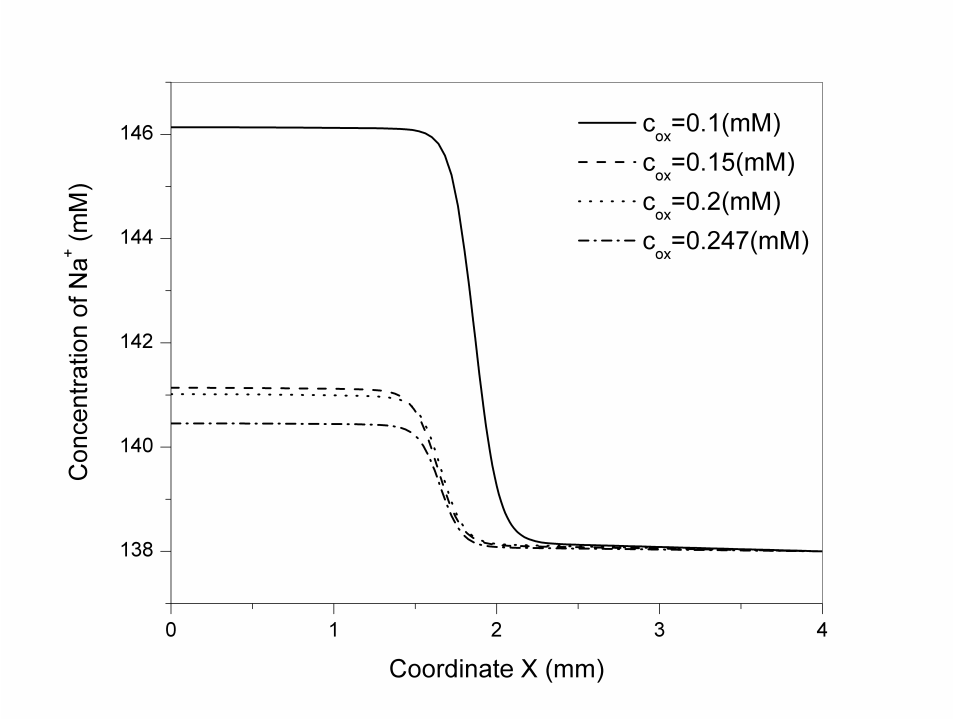

Figure 2.11 Effect of the oxygen concentration on the distributive profiles of Na^+.

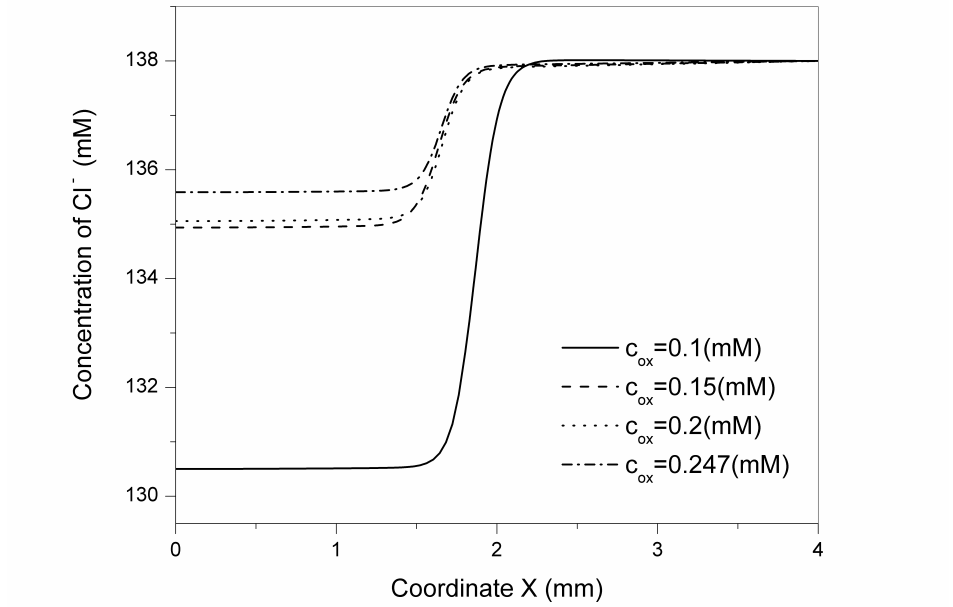

Figure 2.12 Effect of the oxygen concentration on the distributive profiles of Cl^-.

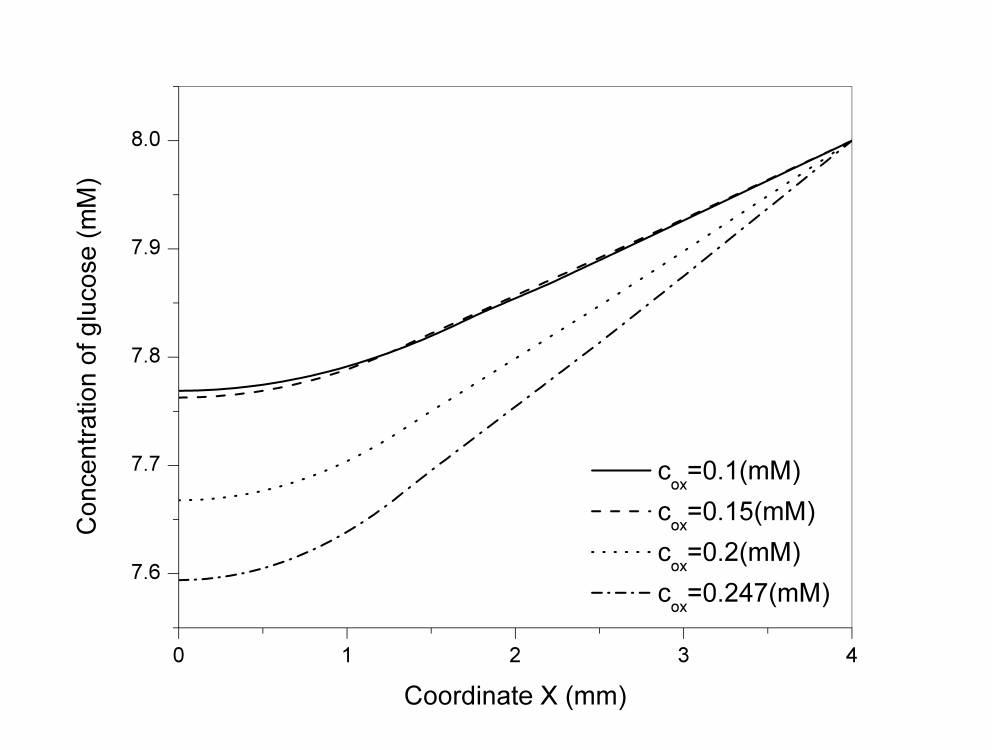

Figure 2.13 Distribution of glucose depends on the varying of oxygen concentration.

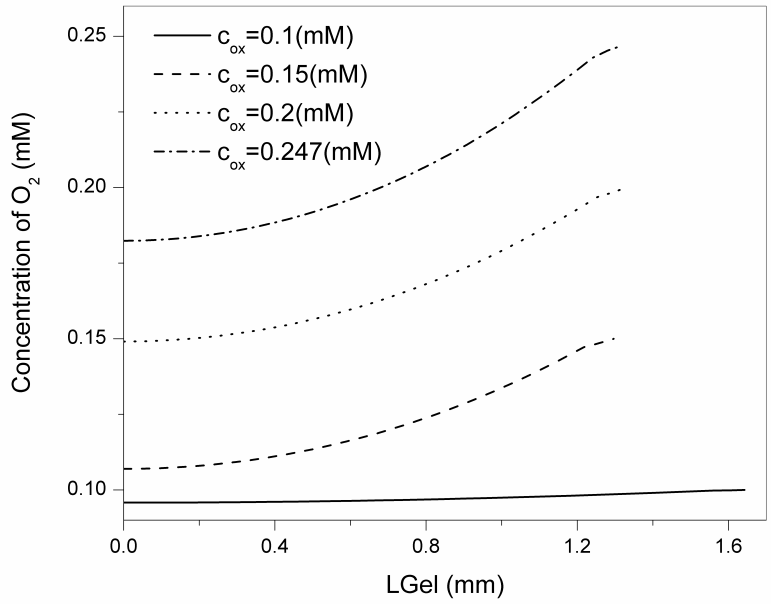

Figure 2.14 The distributive profile of oxygen concentration in the system.

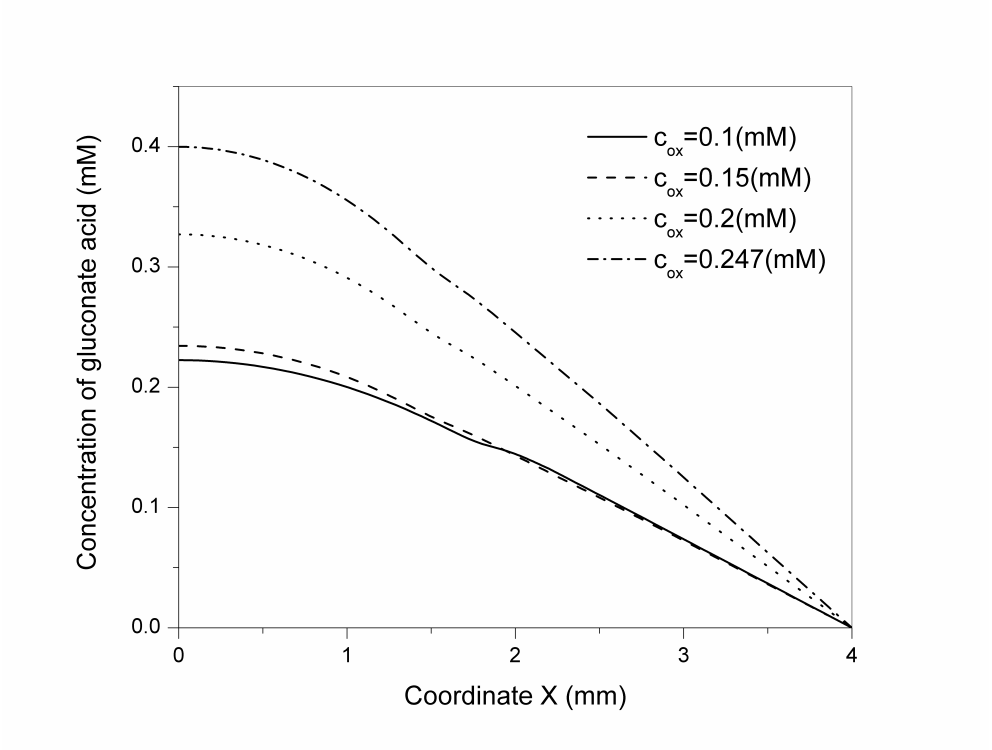

Figure 2.15 Distribution of the product of chemical reaction, gluconate acid, with various oxygen concentrations.

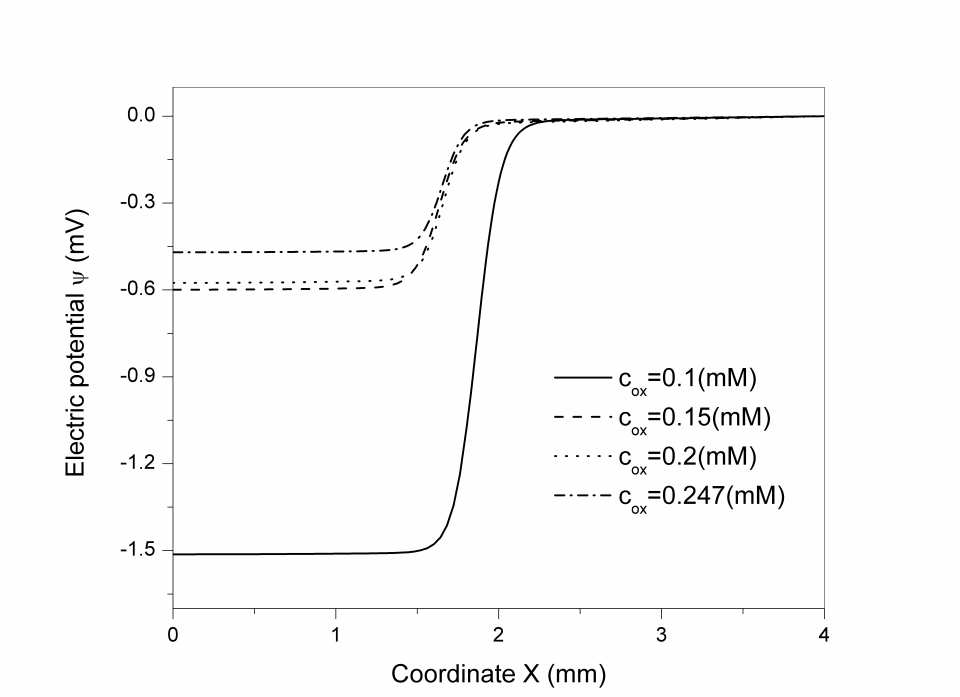

Figure 2.16 Effect of oxygen concentration on the distributive profile of the electric potential.

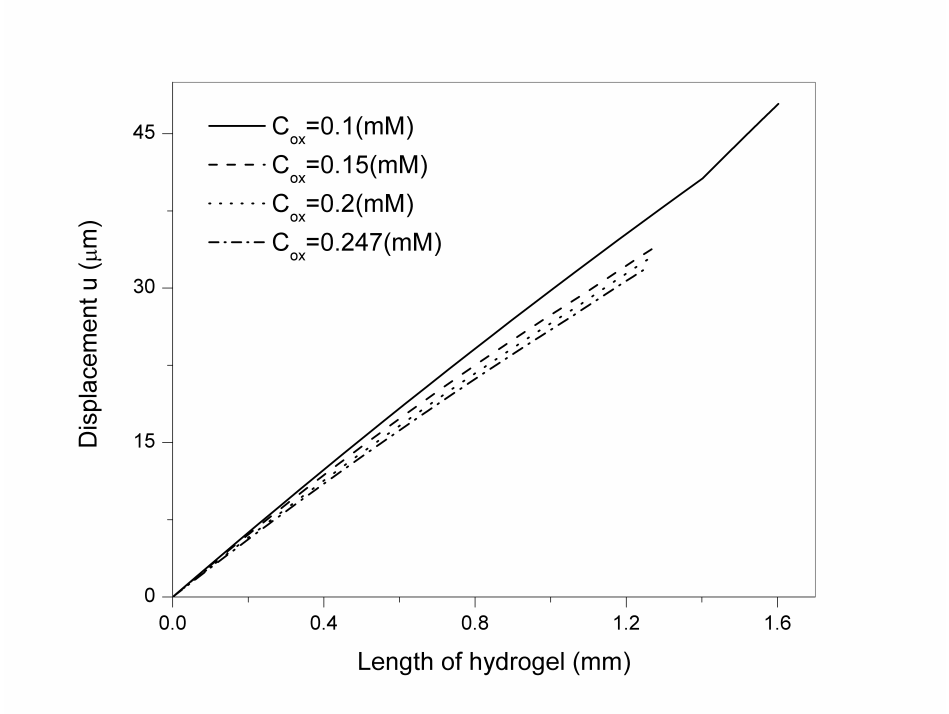

Figure 2.17 Displacement of the glucose-sensitive hydrogel with the effect of the oxygen concentration.

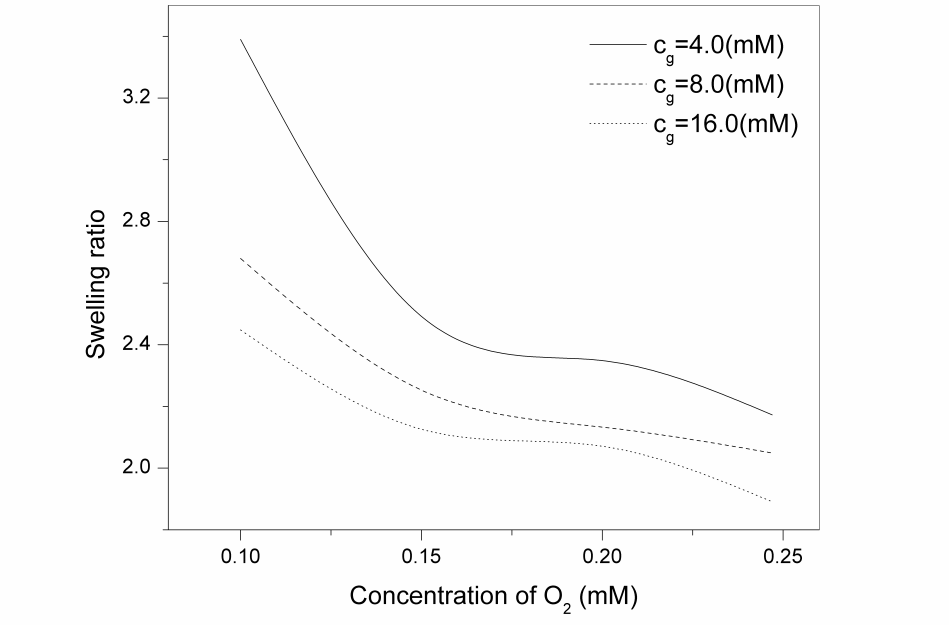

Figure 2.18 Effect of oxygen concentration on the swelling ratio of hydrogel with different glucose concentrations.

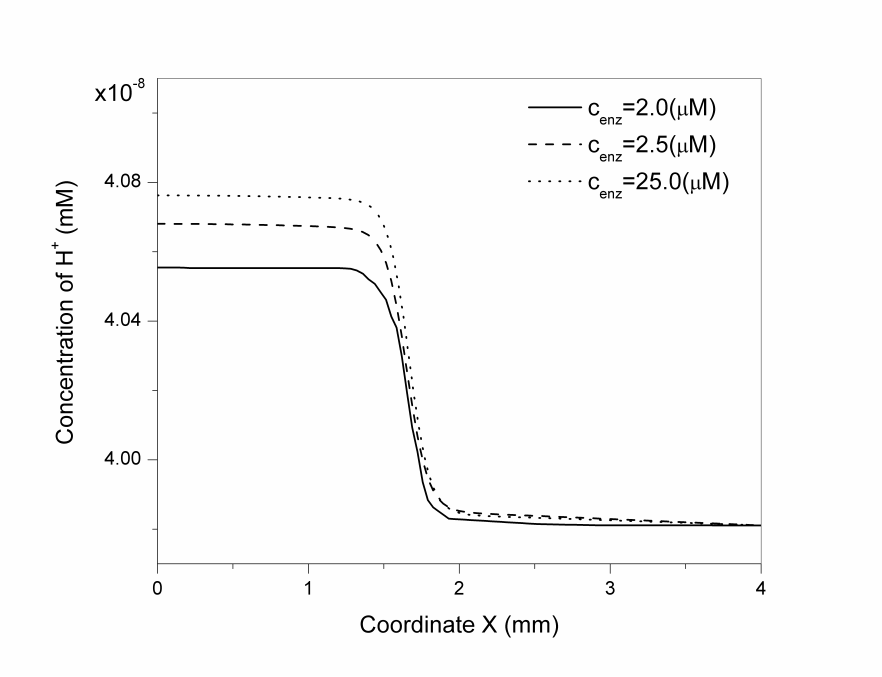

Figure 2.19 Distributive profile of hydrogen ion concentration with the various enzyme concentrations.

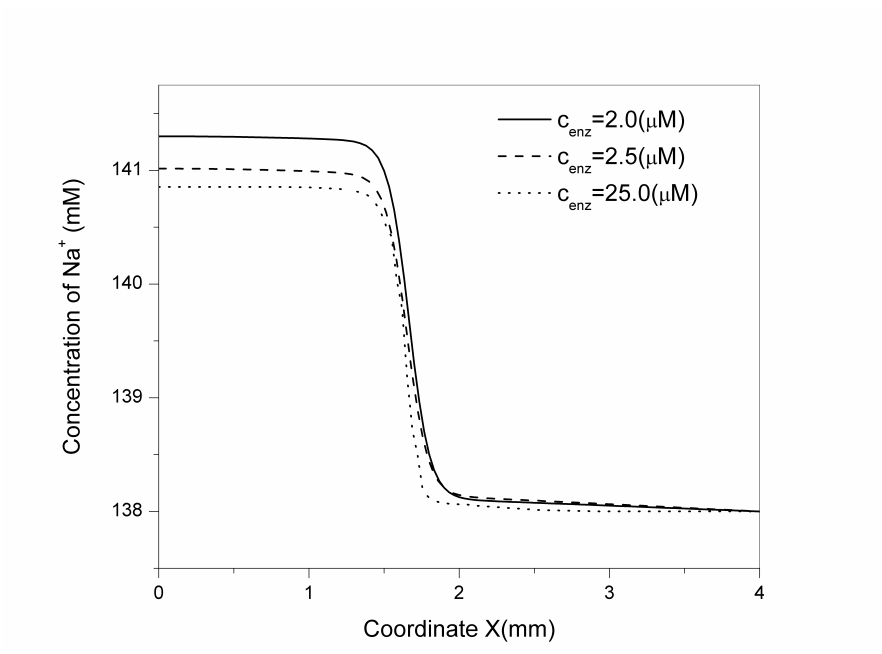

Figure 2.20 Effect of the enzyme concentrations on the distributive profiles of Na^+.

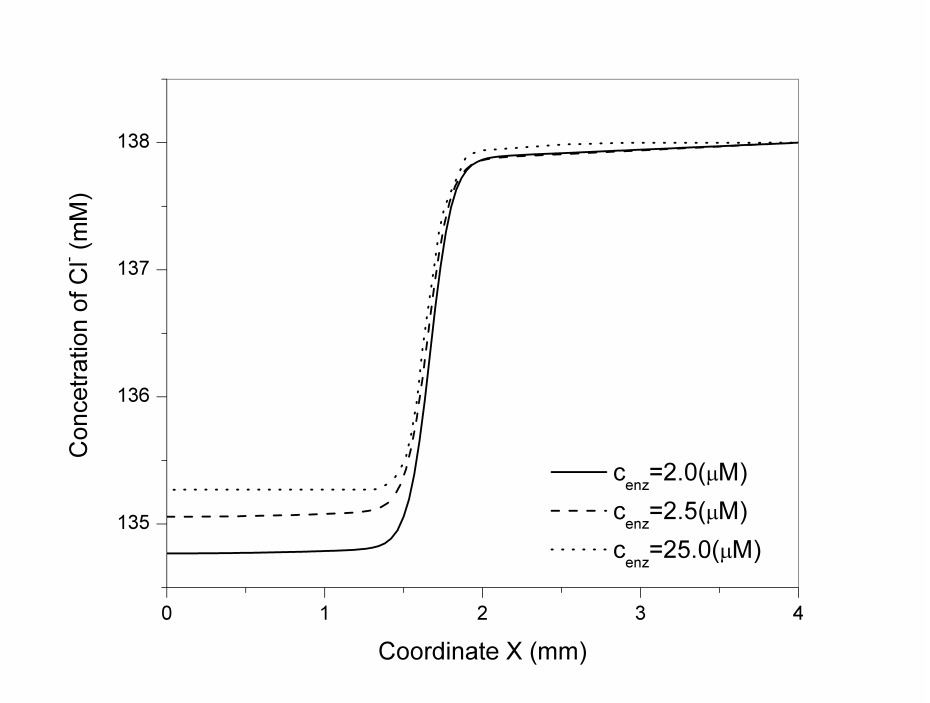

Figure 2.21 Effect of the enzyme concentrations on the distributive profiles of Cl^-.

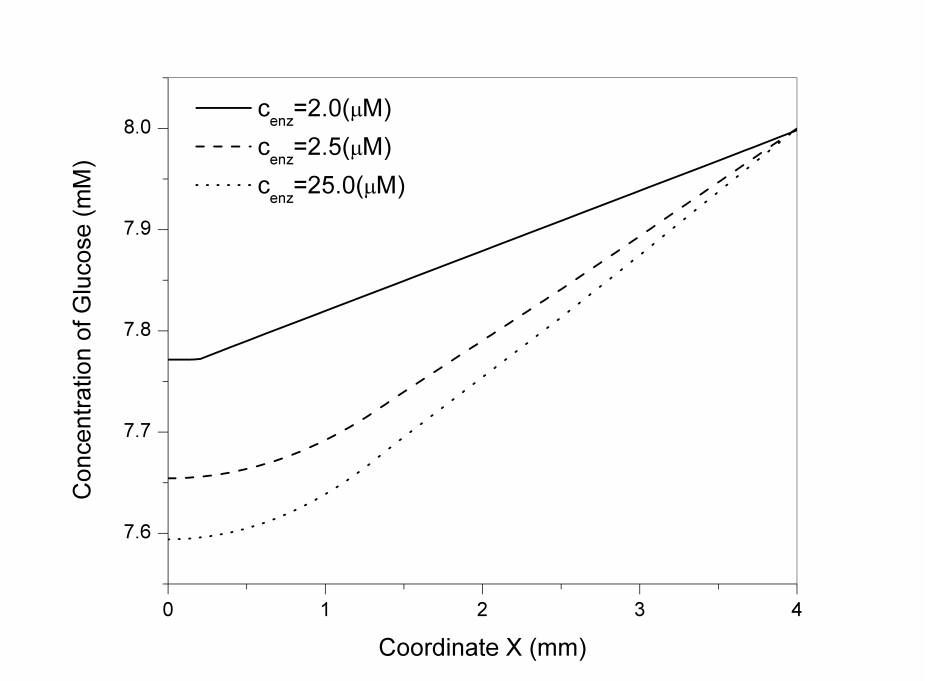

Figure 2.22 Distribution of glucose depends on the varying of concentrations.

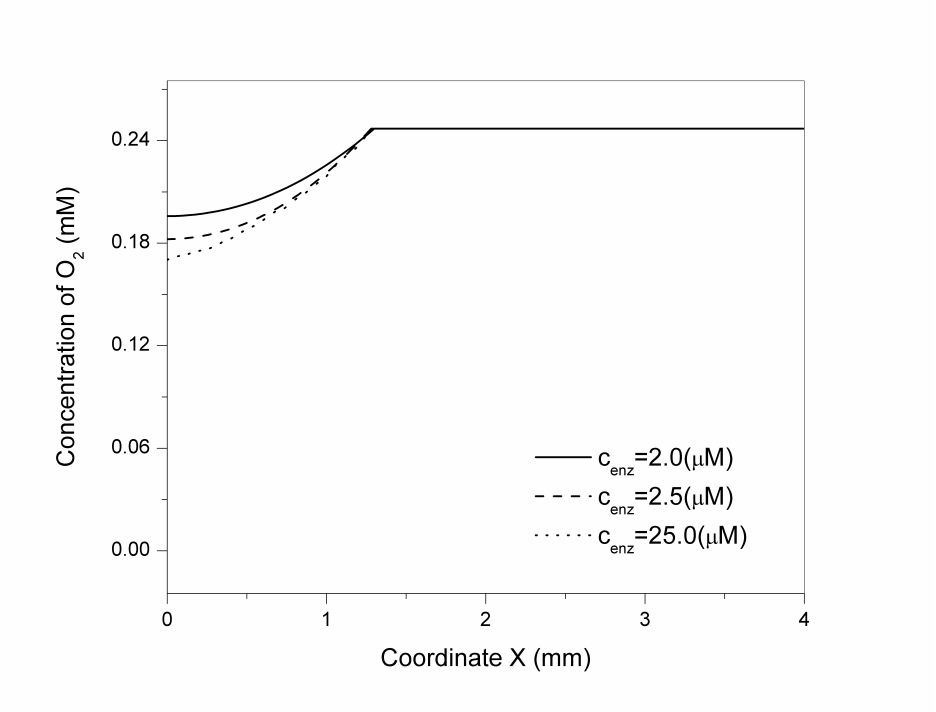

Figure 2.23 Distributive profile of oxygen concentration in the system.

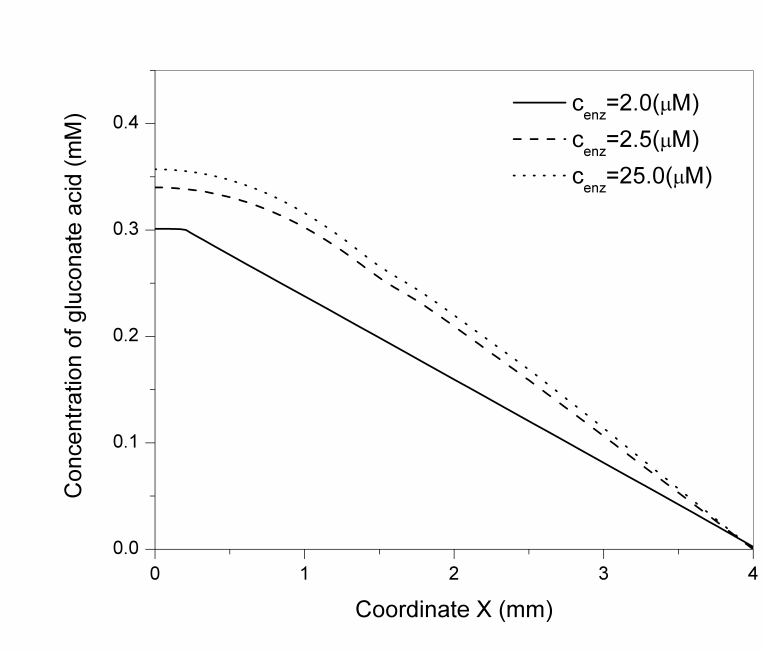

Figure 2.24 Distribution of the product of chemical reaction, gluconate acid, with various enzyme concentrations.

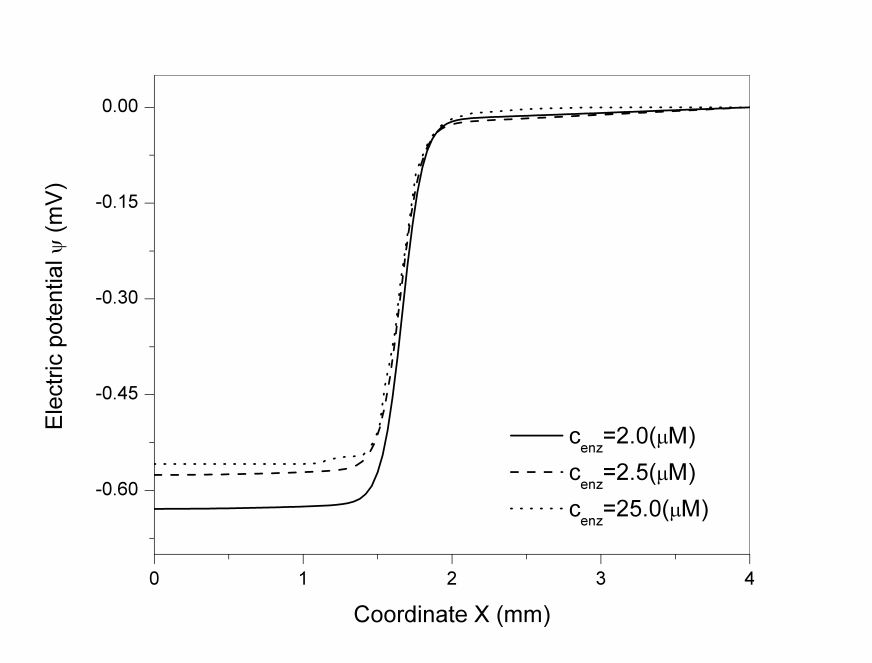

Figure 2.25 Effect of enzyme concentration on the distributive profile of the electric potential.

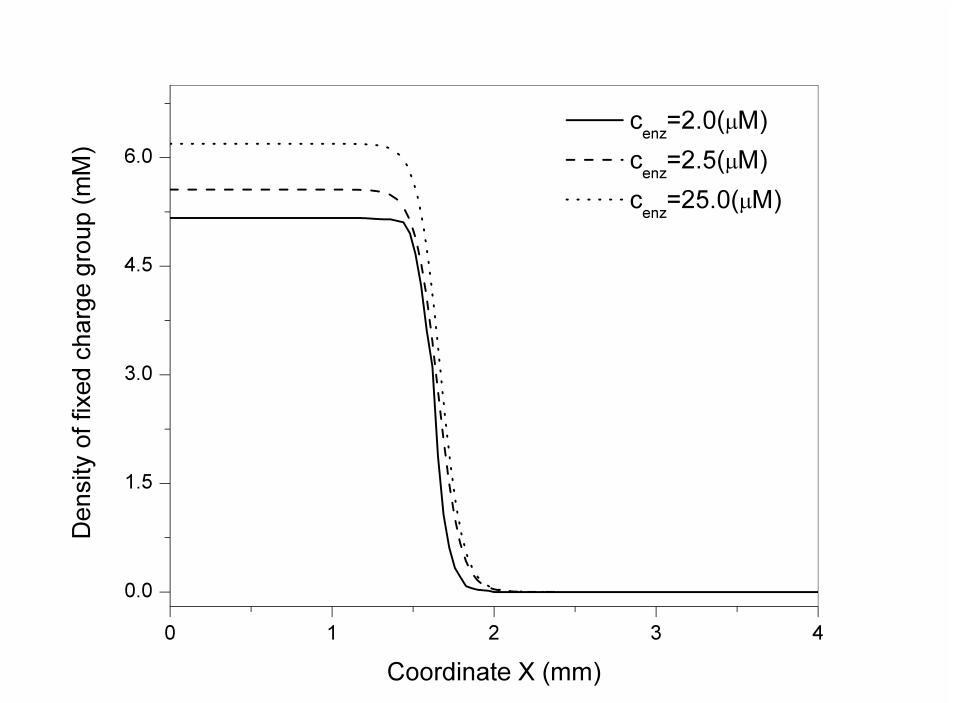

Figure 2.26 Effect of enzyme concentration on the distributive profile of the fixed charge group density.

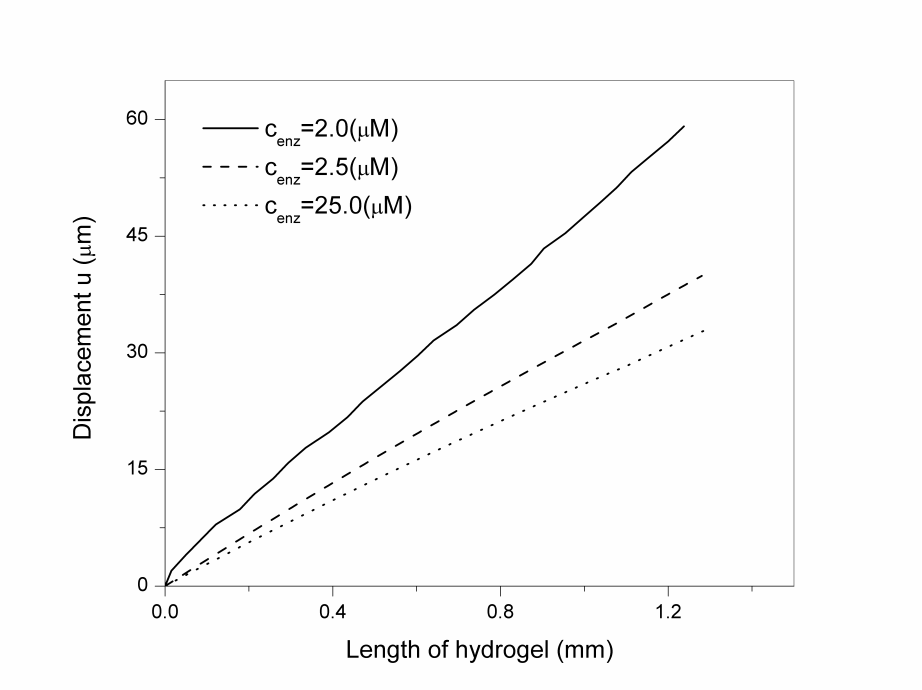

Figure 2.27 Change of enzyme concentration influences the displacement of the hydrogel strip.

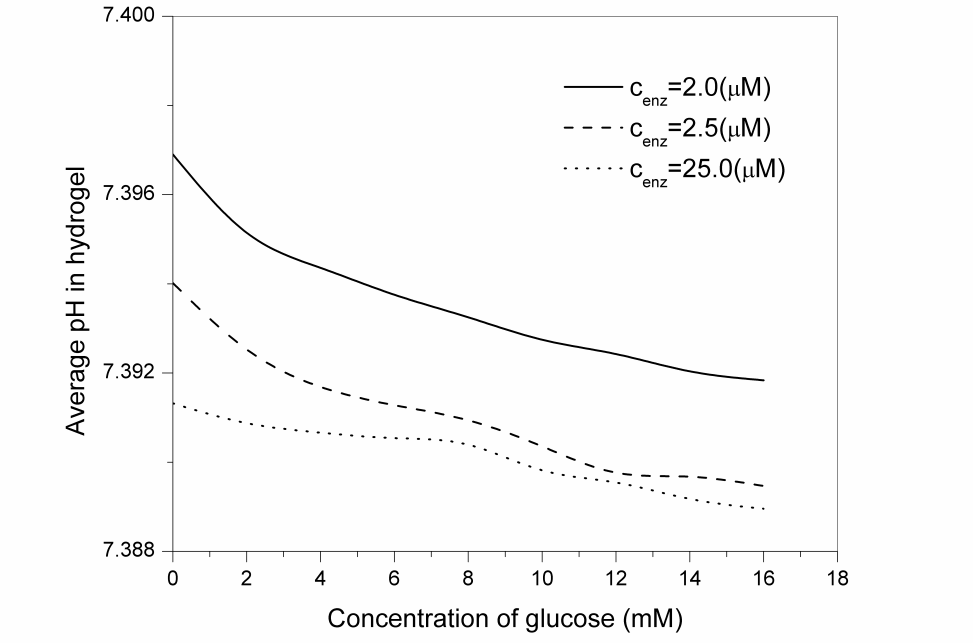

Figure 2.28 Change of enzyme concentration influences the average pH in the hydrogel.

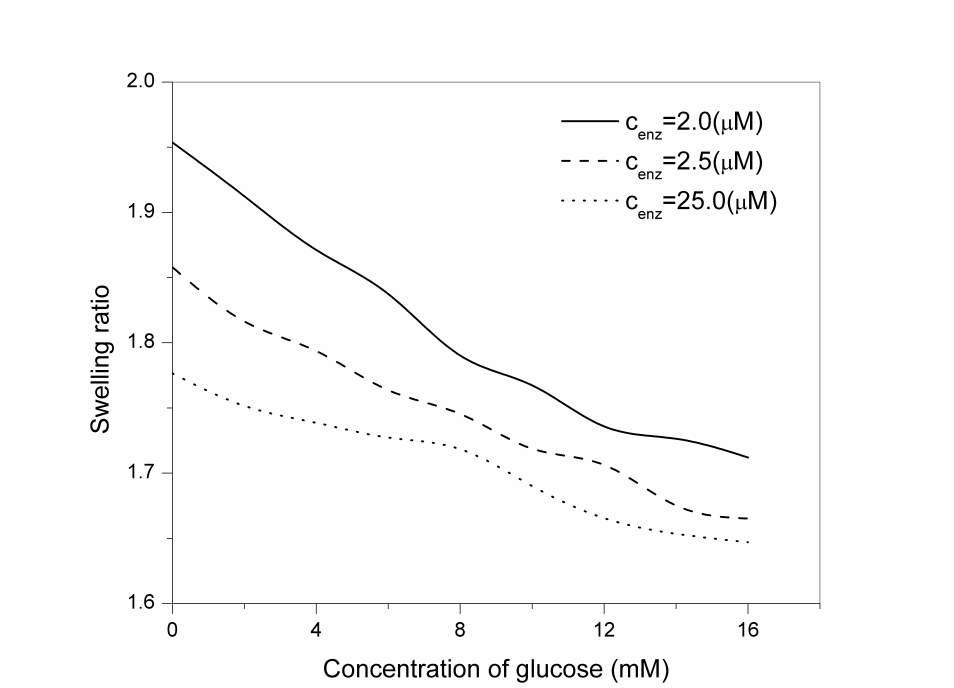

Figure 2.29 Effect of enzyme concentration on the swelling ratio of hydrogel with different glucose concentrations.

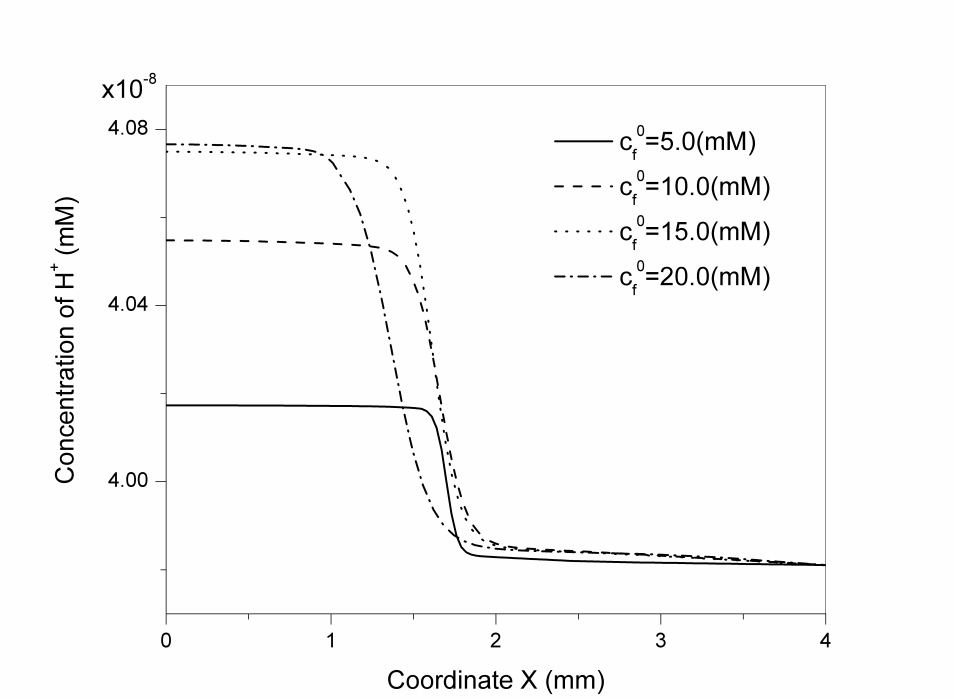

Figure 2.30 Distributive profile of hydrogen ion concentration with the various initially fixed charge group densities.

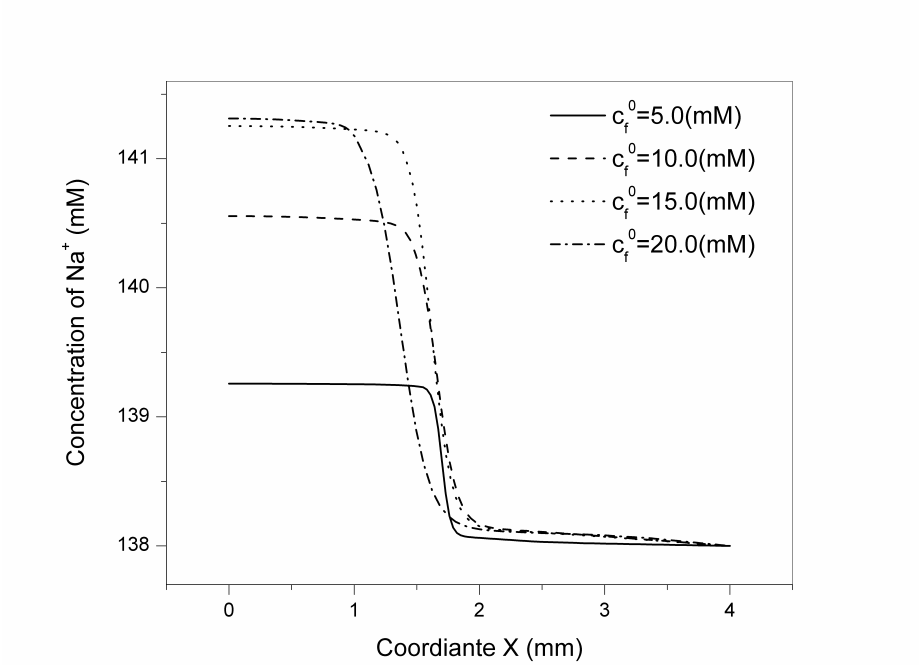

Figure 2.31 Effect of the initially fixed charge group density on the distributive profiles of Na^+.

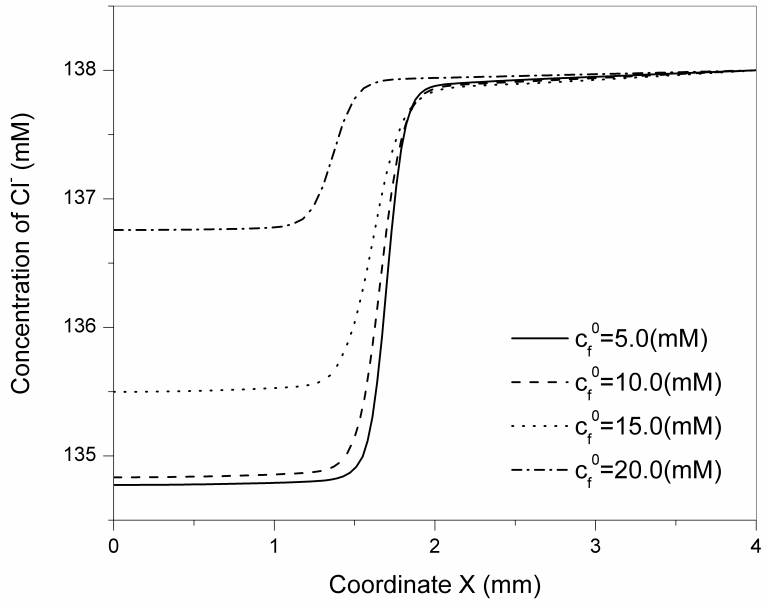

Figure 2.32 Effect of the initially fixed charge group density on the distributive profiles of Cl^-.

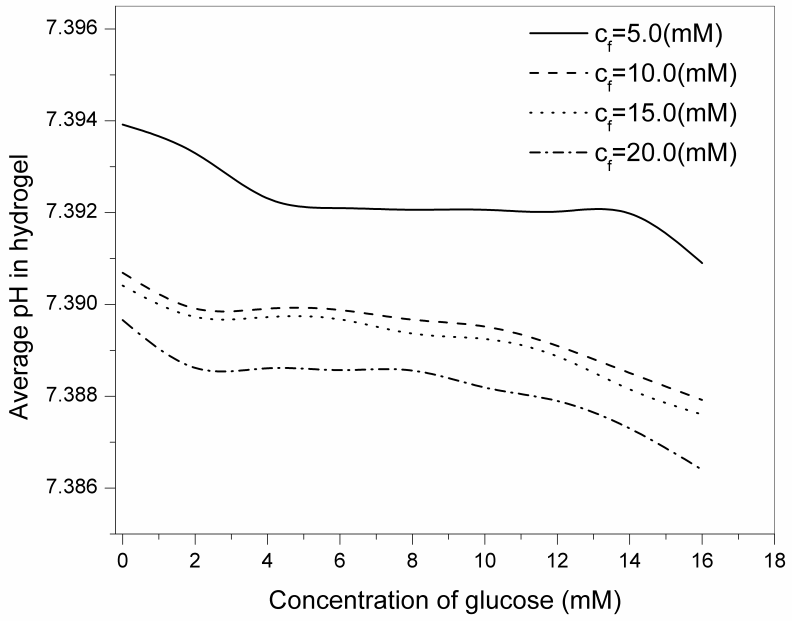

Figure 2.33 Change of initially fixed charge group density influences the average pH in the hydrogel.

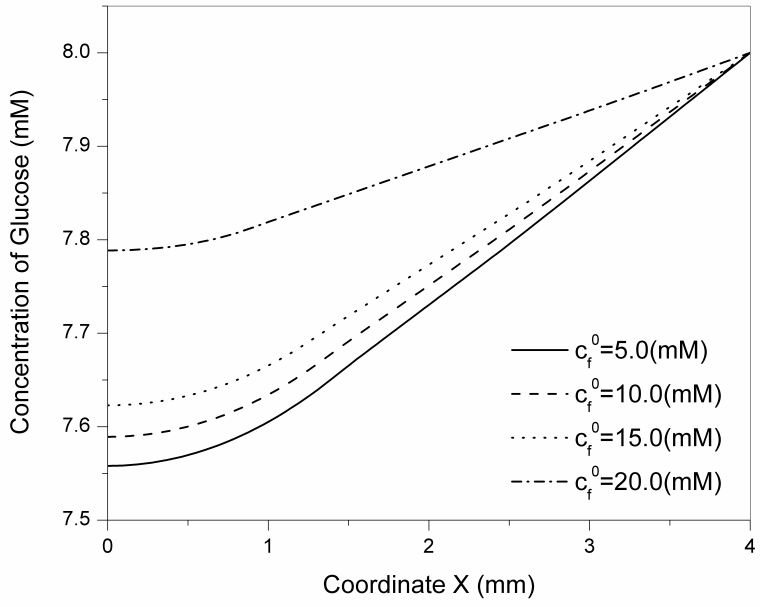

Figure 2.34 Distribution of glucose depends on the varying of initially fixed charge group densities.

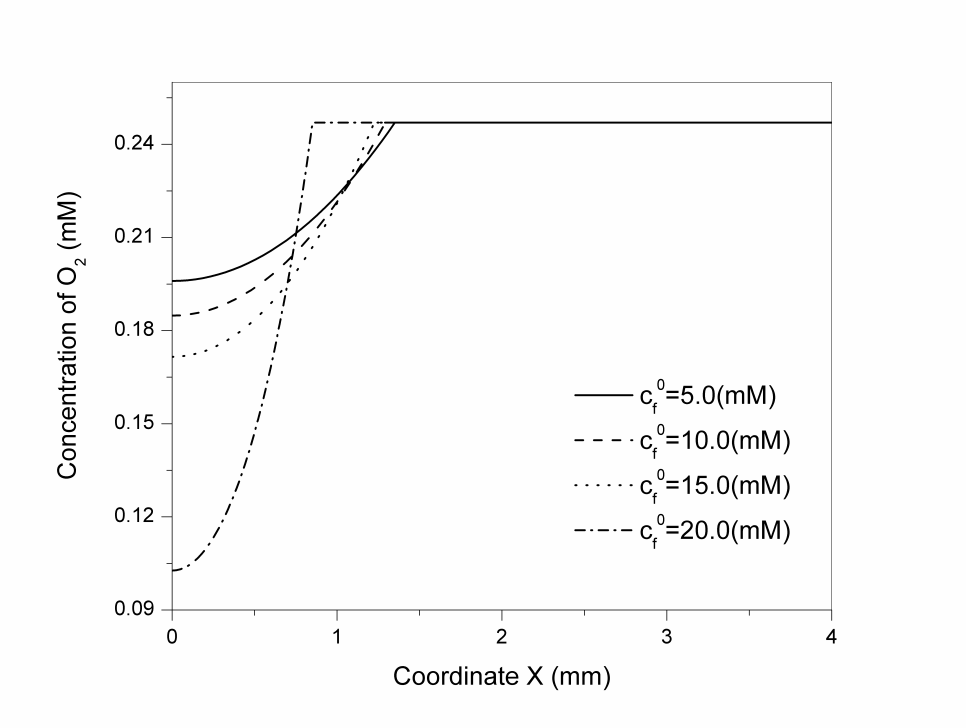

Figure 2.35 Distributive profile of oxygen concentration in the system.

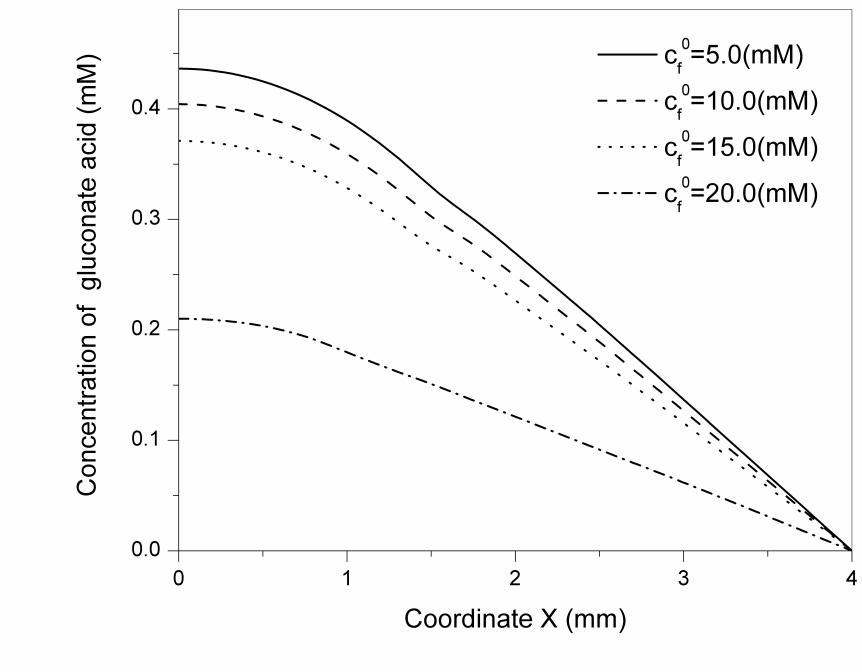

Figure 2.36 Distribution of the product of chemical reaction, gluconate acid, with various initially fixed charge group densities.

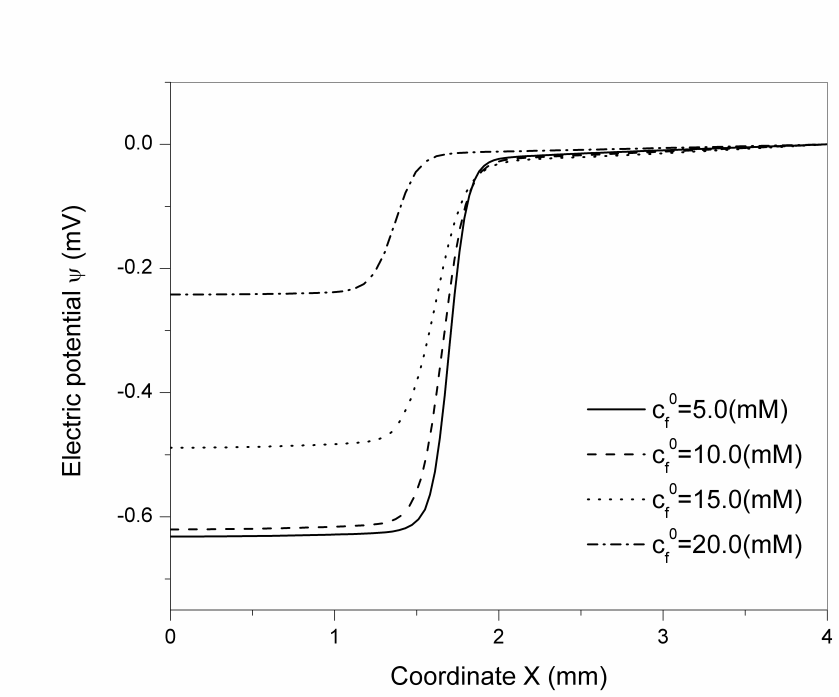

Figure 2.37 Effect of initially fixed charge group densities on the distributive profile of the electric potential.

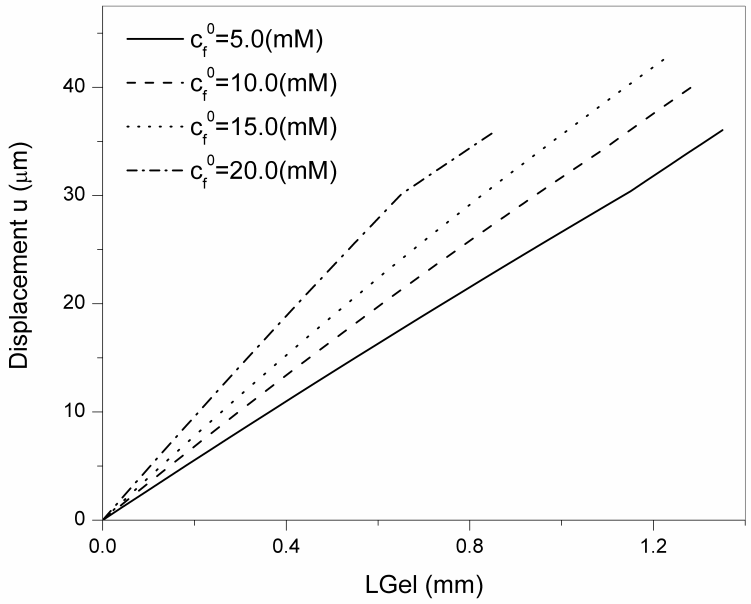

Figure 2.38 The change of initially fixed charge group densities influences the displacement of the hydrogel strip.

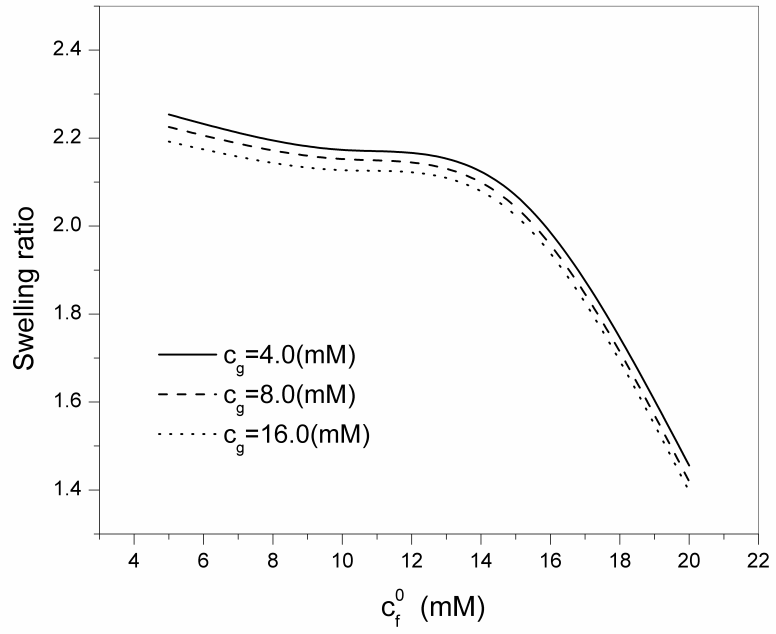

Figure 2.39 Effect of enzyme concentration on the swelling ratio of hydrogel with different initially fixed charge group densities.

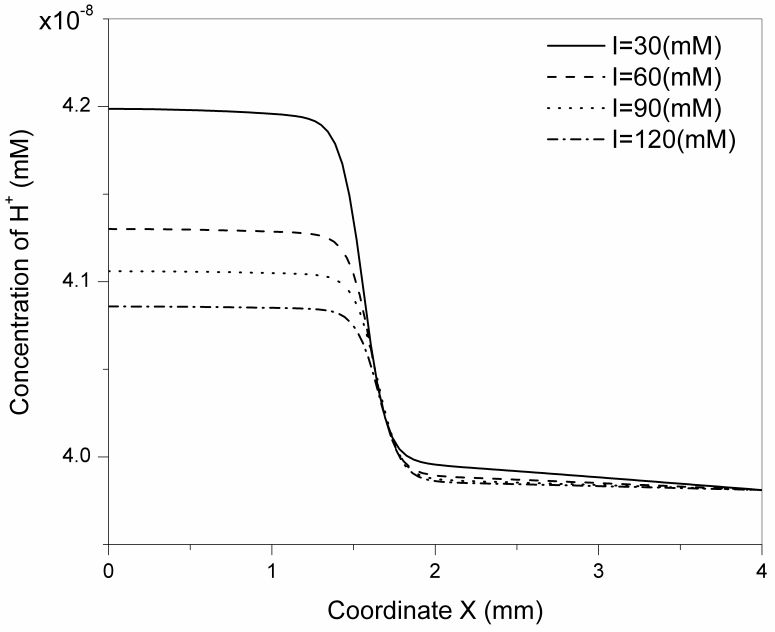

Figure 2.40 Distributive profile of hydrogen ion concentration with the various ionic strengths.

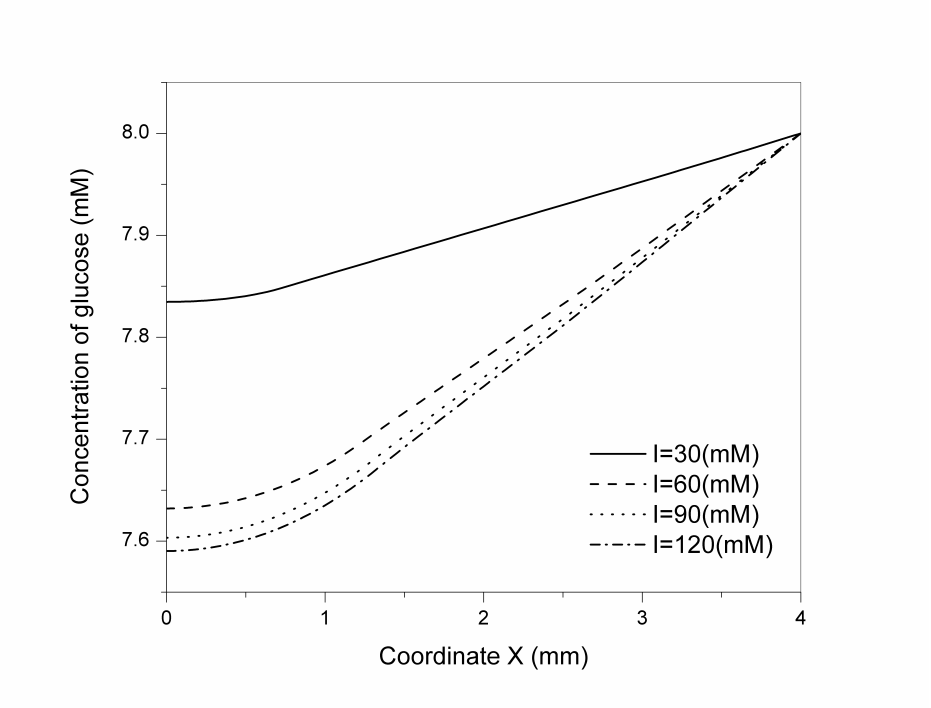

Figure 2.41 Distribution of glucose depends on the varying of ionic strengths.

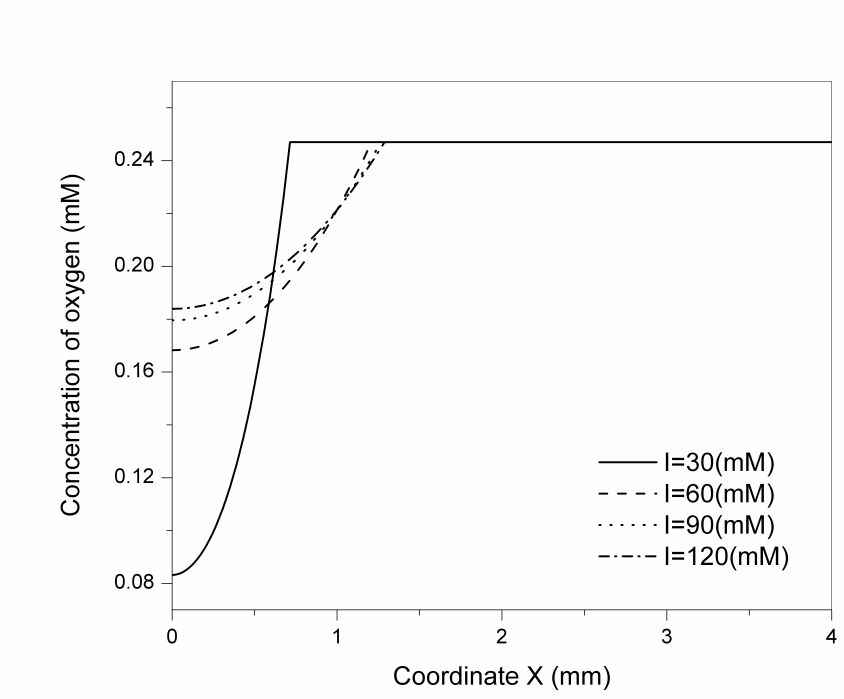

Figure 2.42 Distributive profile of oxygen concentration in the system.

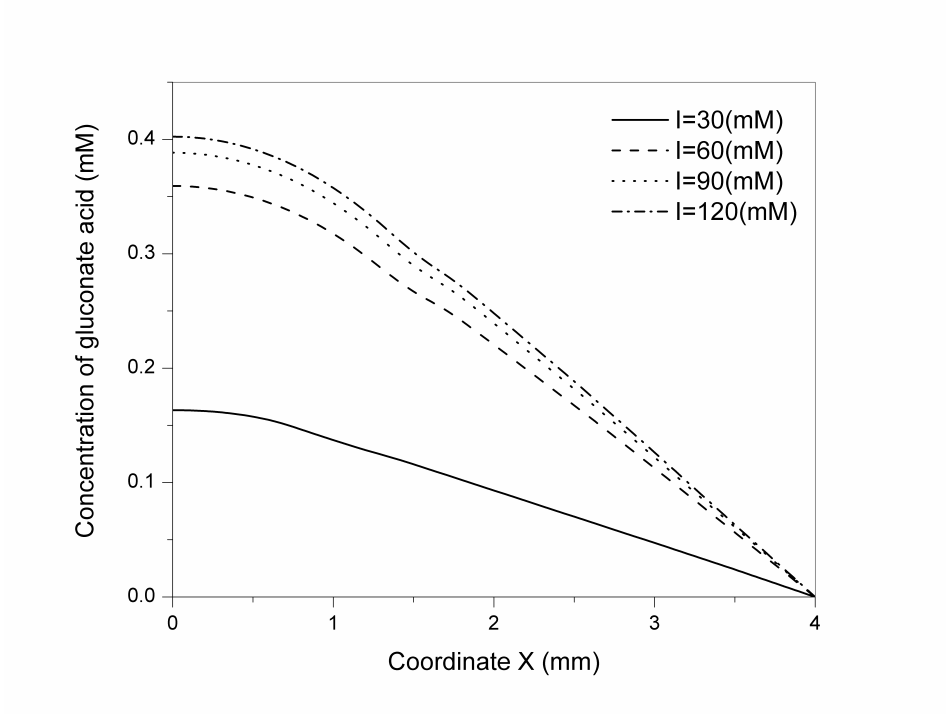

Figure 2.43 Distribution of the product of chemical reaction, gluconate acid, with various ionic strengths.

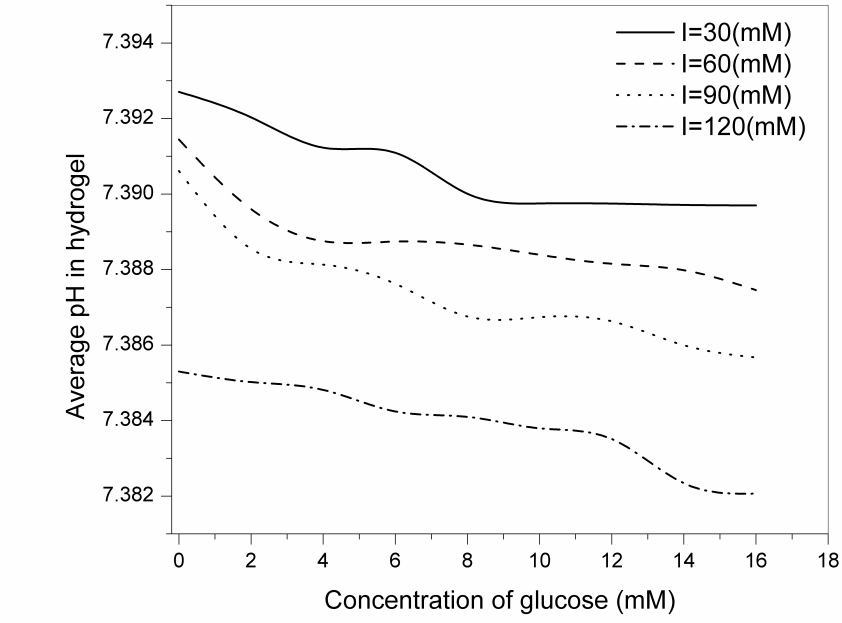

Figure 2.44 The change of ionic strength influences the average pH in the hydrogel.

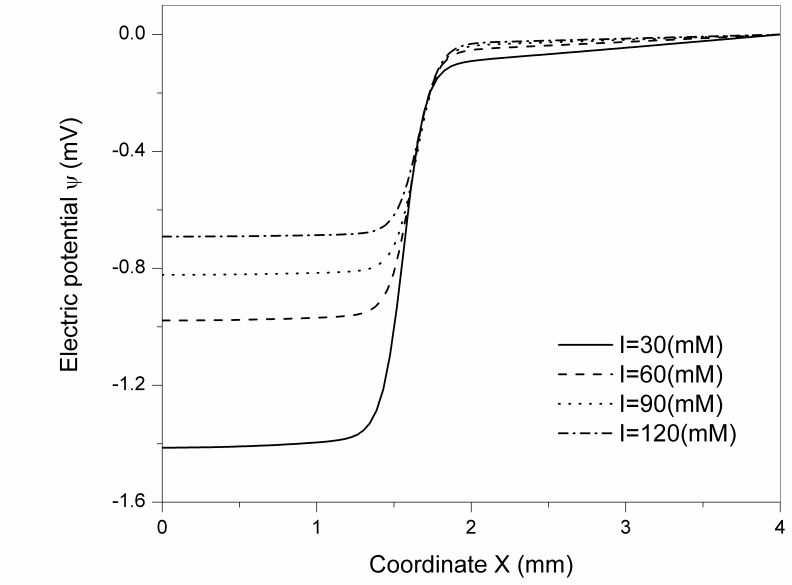

Figure 2.45 Effect of ionic strengths on the distributive profile of the electric potential.

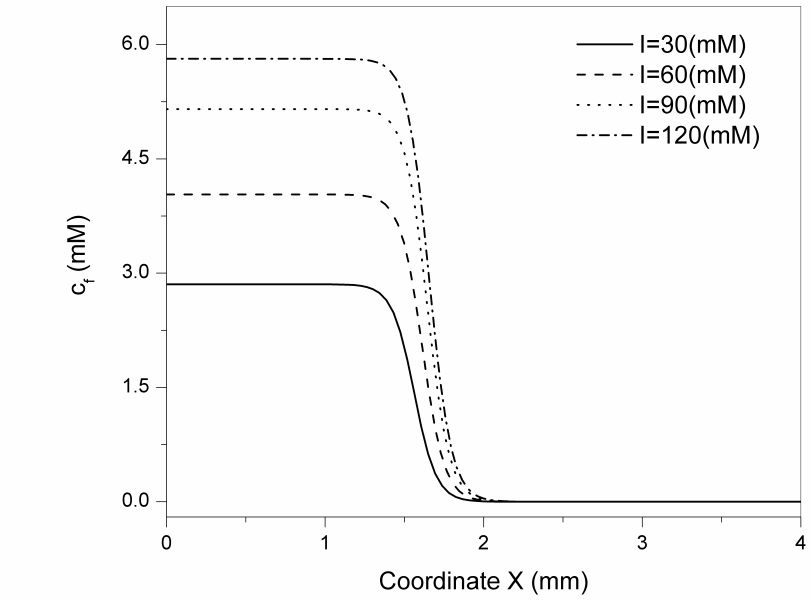

Figure 2.46 Effect of ionic strengths on the distributive profile of the fixed charge group density.

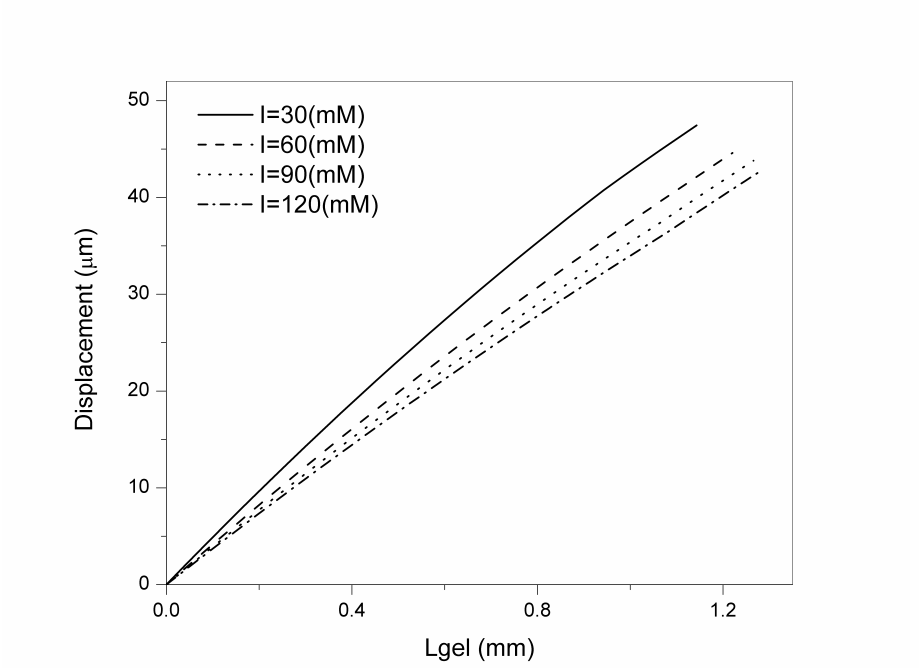

Figure 2.47 The change of ionic strength influences the displacement of the hydrogel strip.

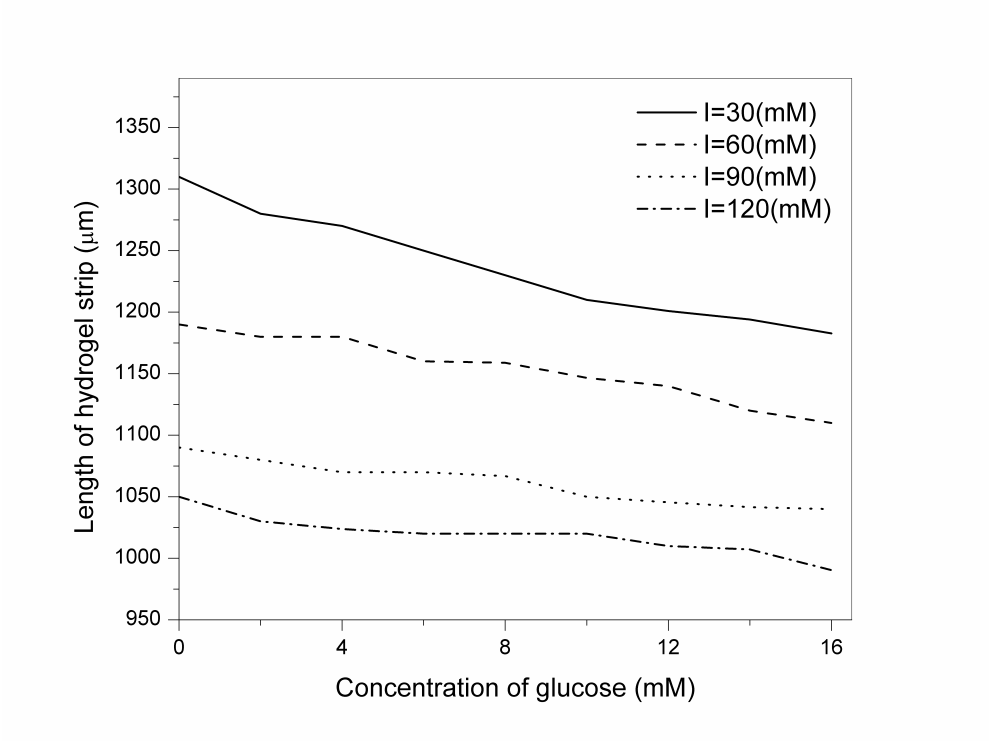

Figure 2.48 Effect of ionic strength on the length of hydrogel strip with different glucose concentrations.

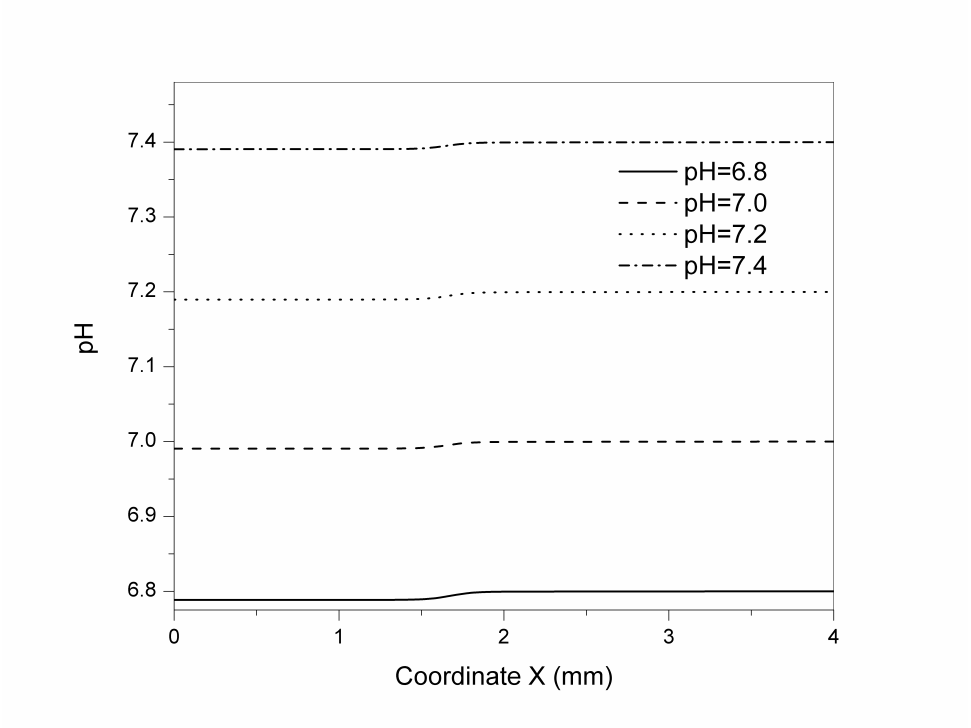

Figure 2.49 Distributive profile of pH in the whole domain.

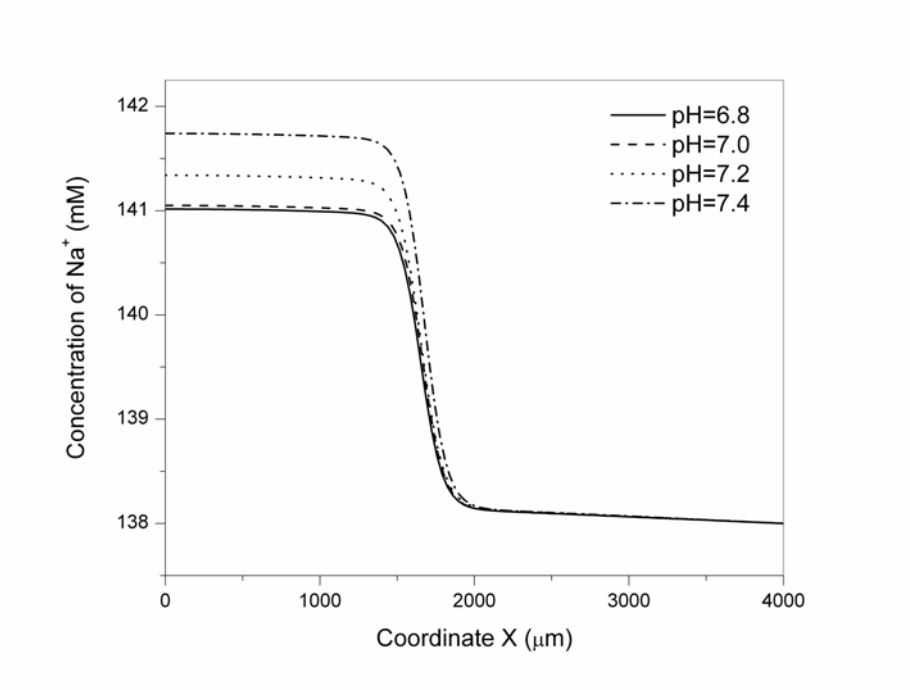

Figure 2.50 Effect of the environmental pH on the distributive profiles of Na^+.

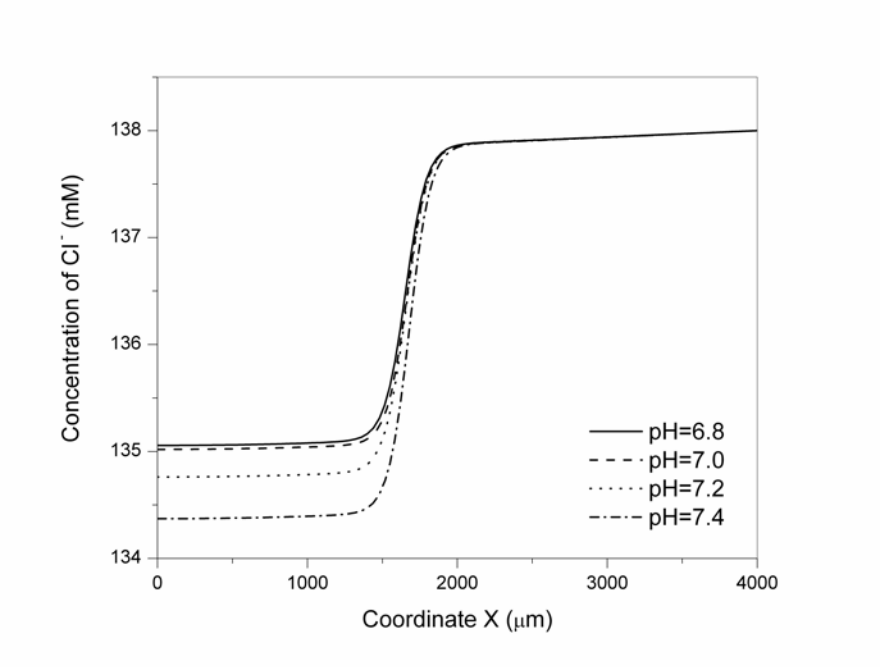

Figure 2.51 Effect of the environmental pH on the distributive profiles of Cl^-.

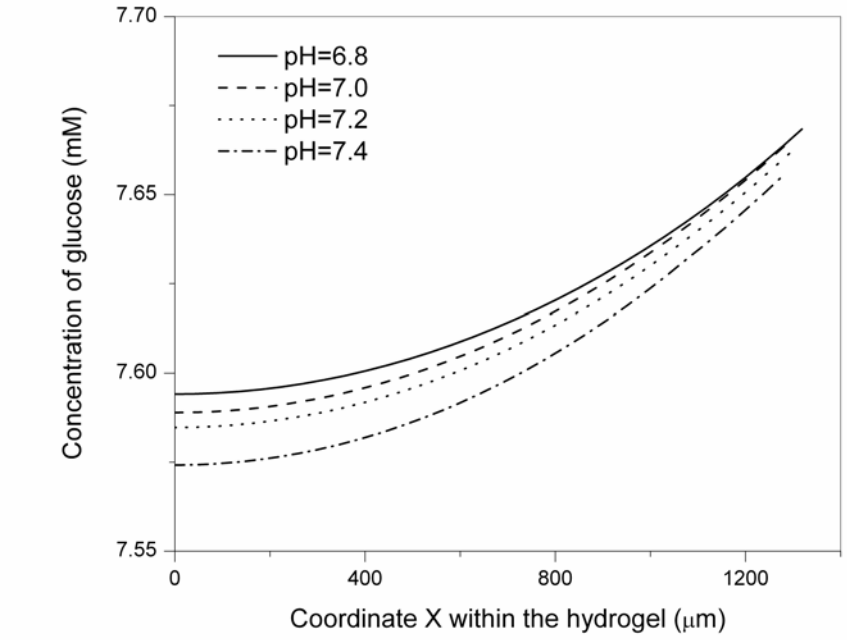

Figure 2.52 Distribution of glucose depends on the varying of environmental pH.

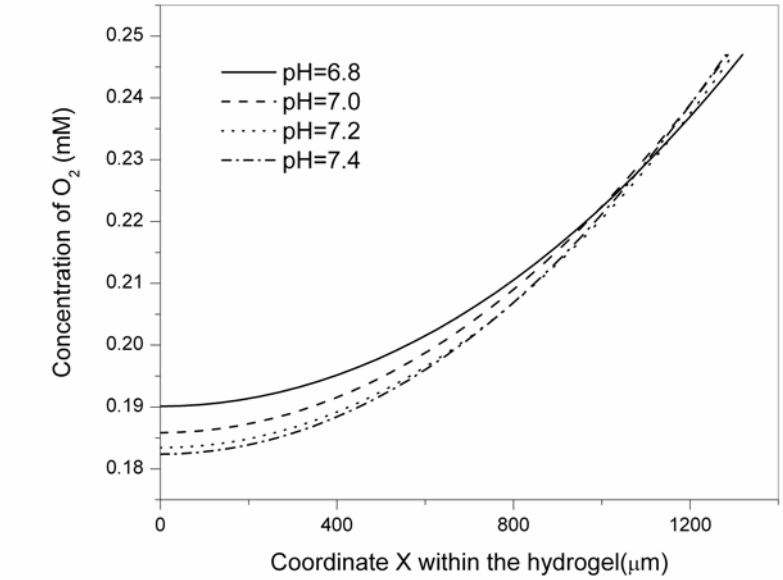

Figure 2.53 Distributive profile of oxygen concentration in the system.

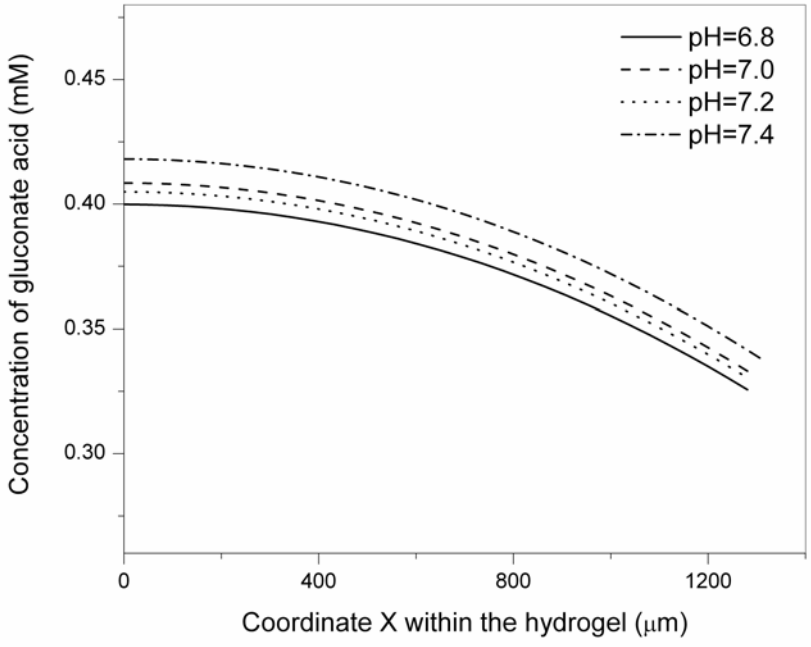

Figure 2.54 Distribution of the product of chemical reaction, gluconate acid, with various environmental pH.

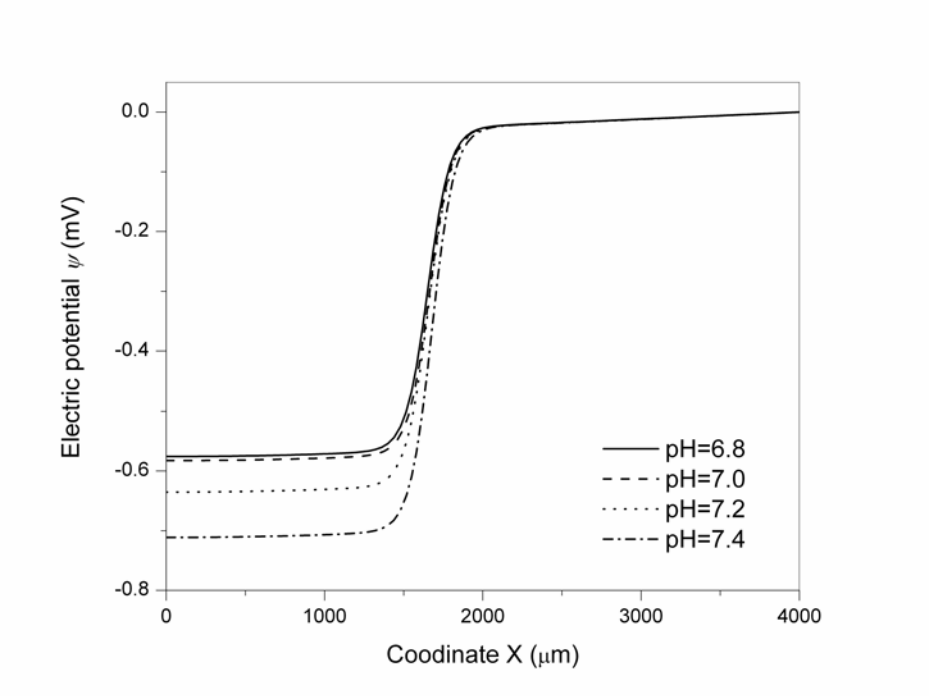

Figure 2.55 Effect of environmental pH on the distributive profile of the electric potential.

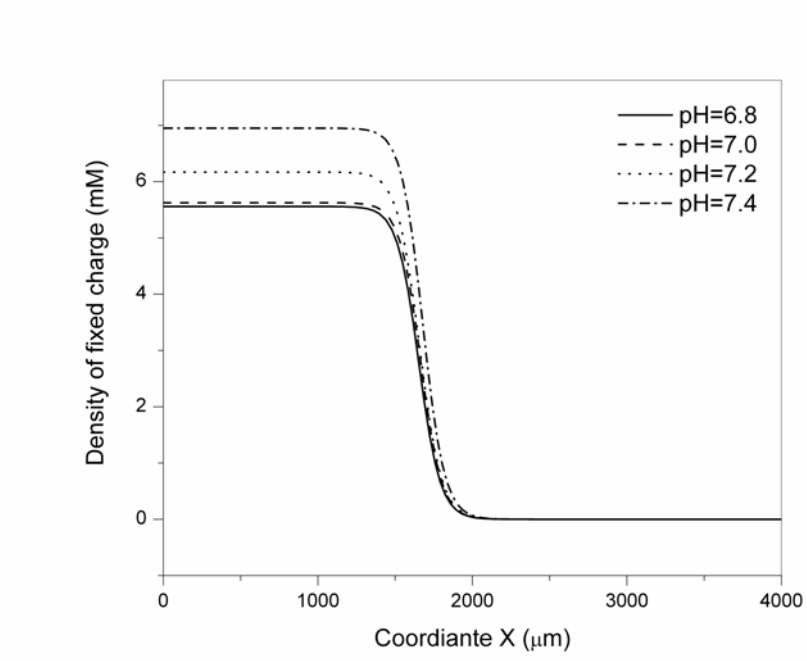

Figure 2.56 Effect of environmental pH on the distributive profile of the fixed charge group density.

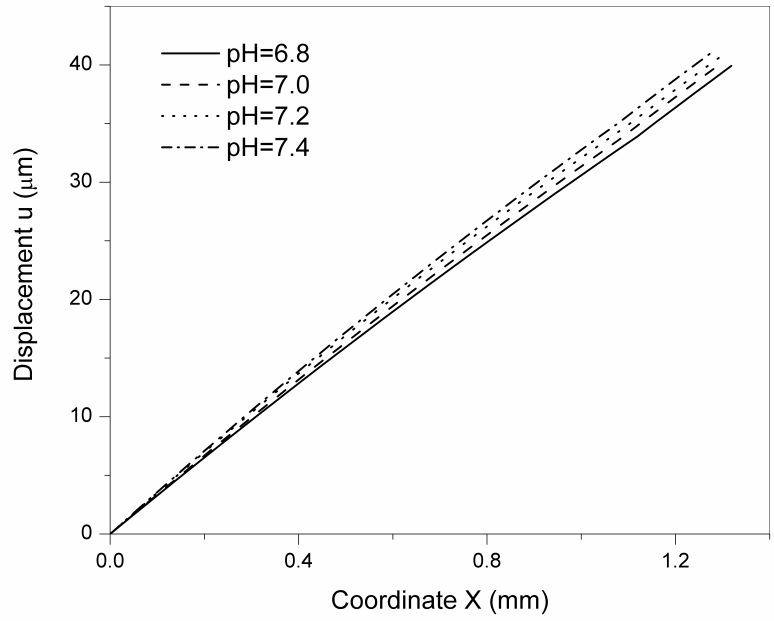

Figure 2.57 Change of environmental pH influences the displacement of the hydrogel strip.

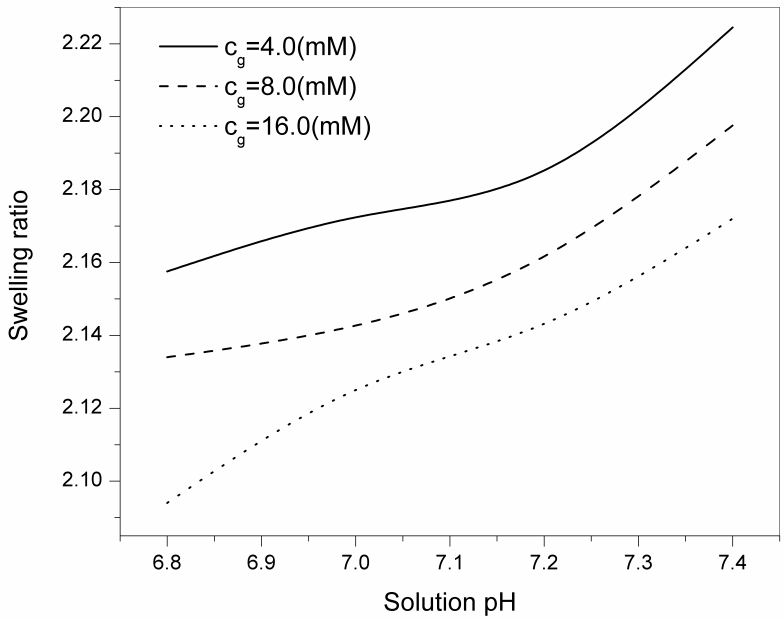

Figure 2.58 Effect of glucose concentrations on the swelling ratio of hydrogel strip with different environmental pH.

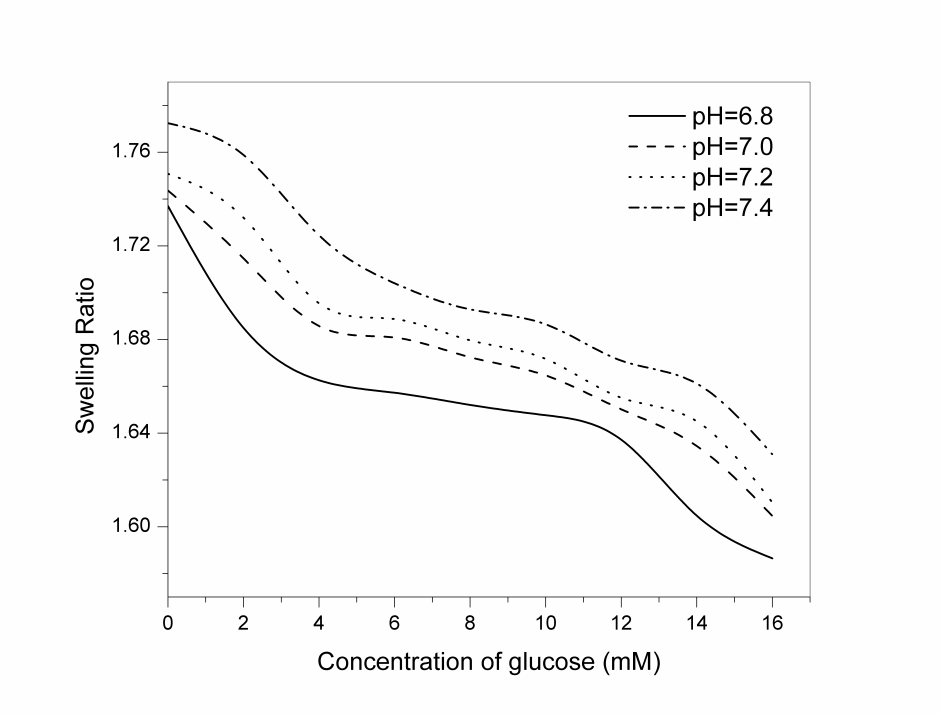

Figure 2.59 Effect of environmental pH on the swelling ratio of hydrogel strip with different glucose concentrations.

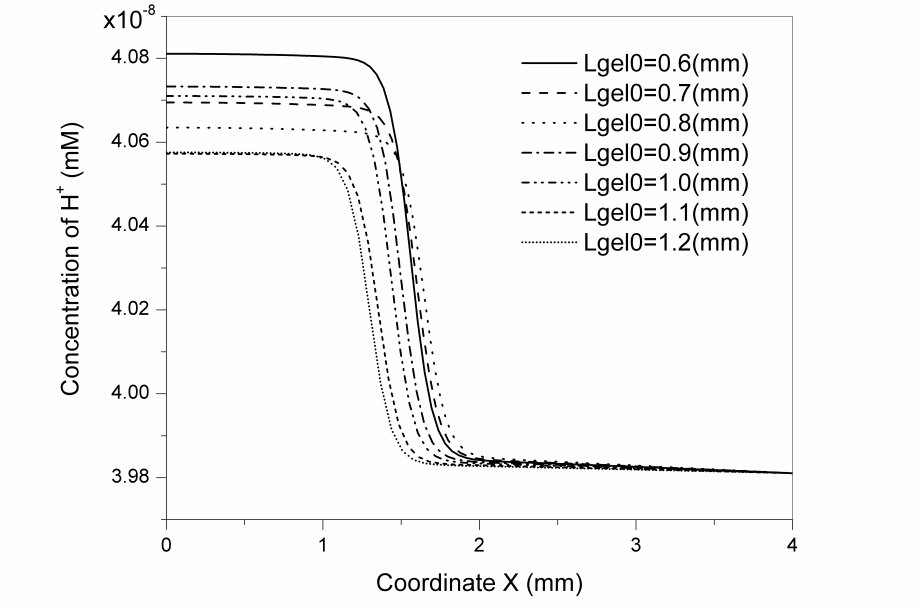

Figure 2.60 Distributive profile of hydrogen ion with the effect of initial length of hydrogel strip.

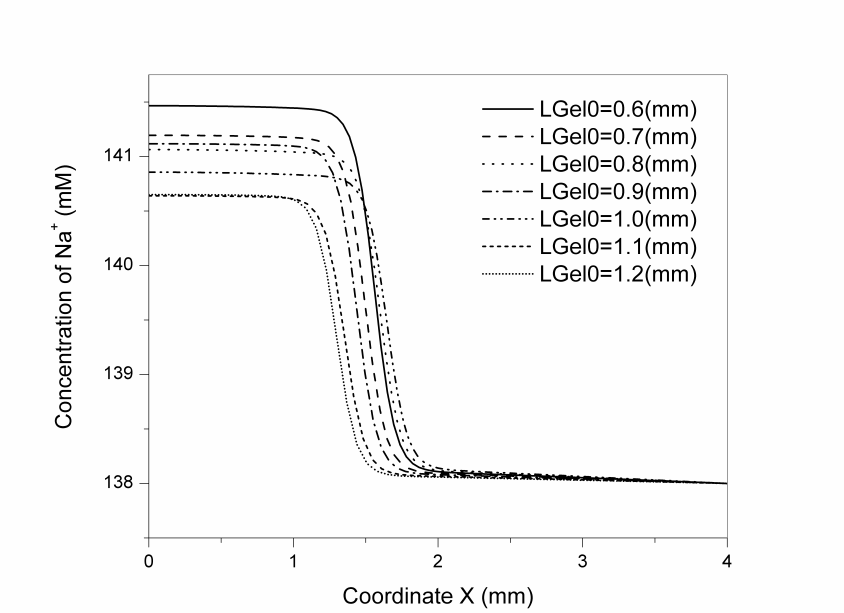

Figure 2.61 Effect of the initial length of hydrogel strip on the distributive profiles of Na^+.

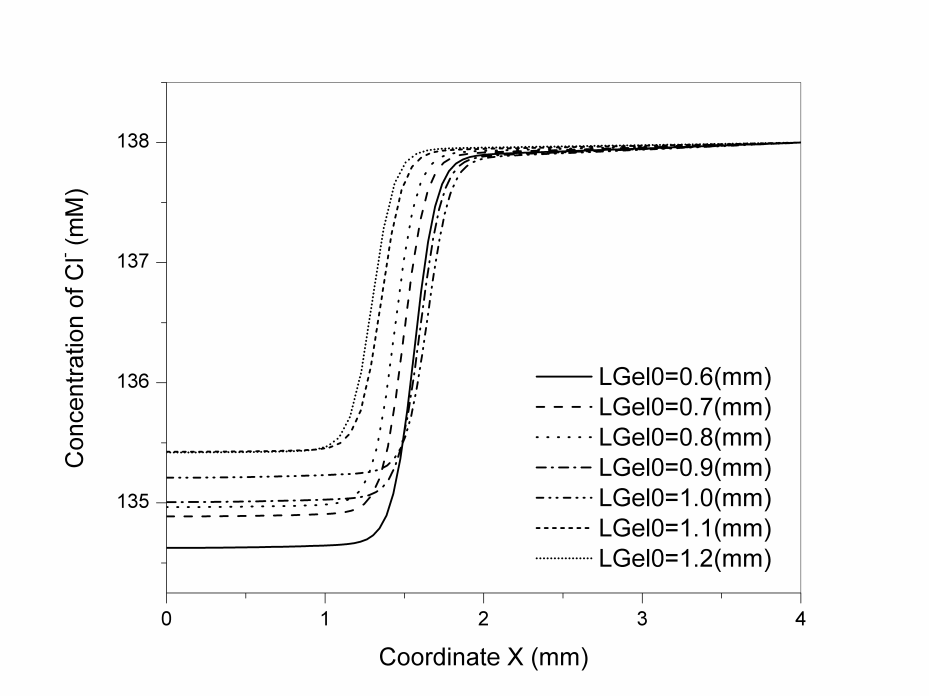

Figure 2.62 Effect of the initial length of hydrogel strip on the distributive profile of Cl^-.

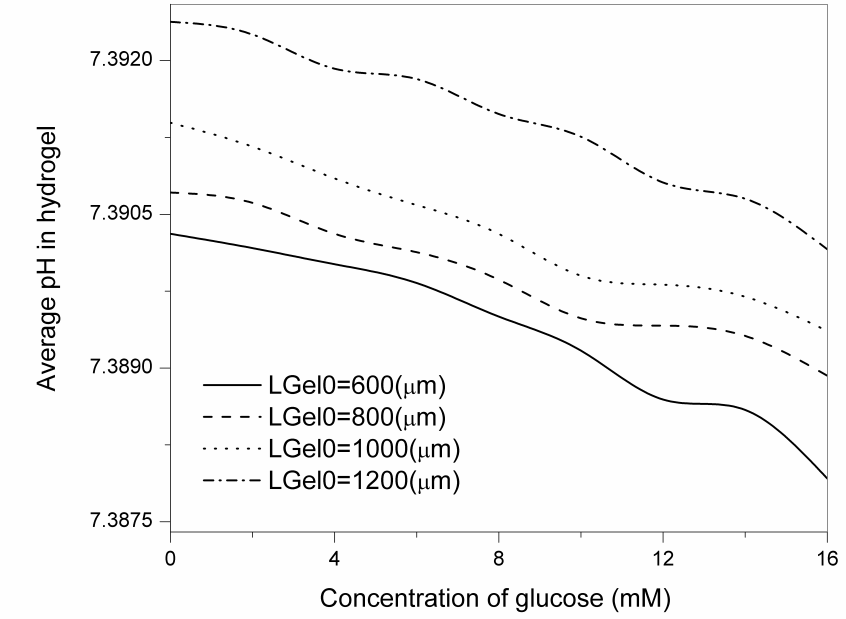

Figure 2.63 Variations of average pH in the hydrogel with the effect of the initial length of hydrogel strip.

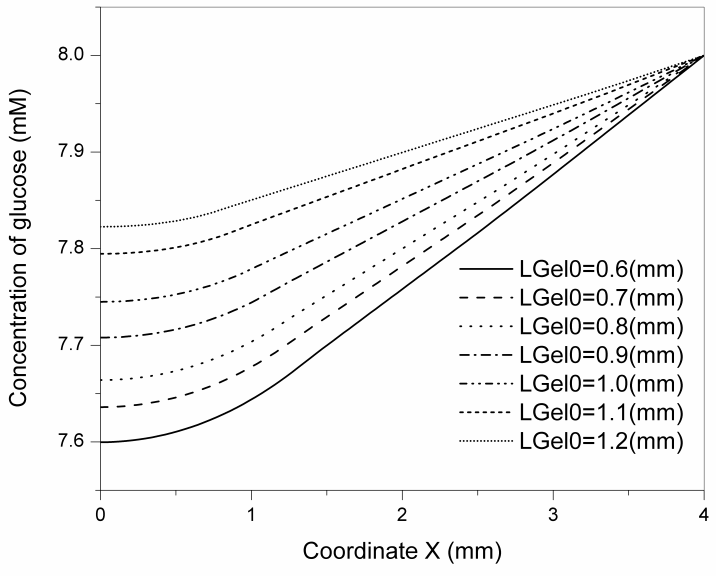

Figure 2.64 Distribution of glucose depends on the varying of initial length of hydrogel strip.

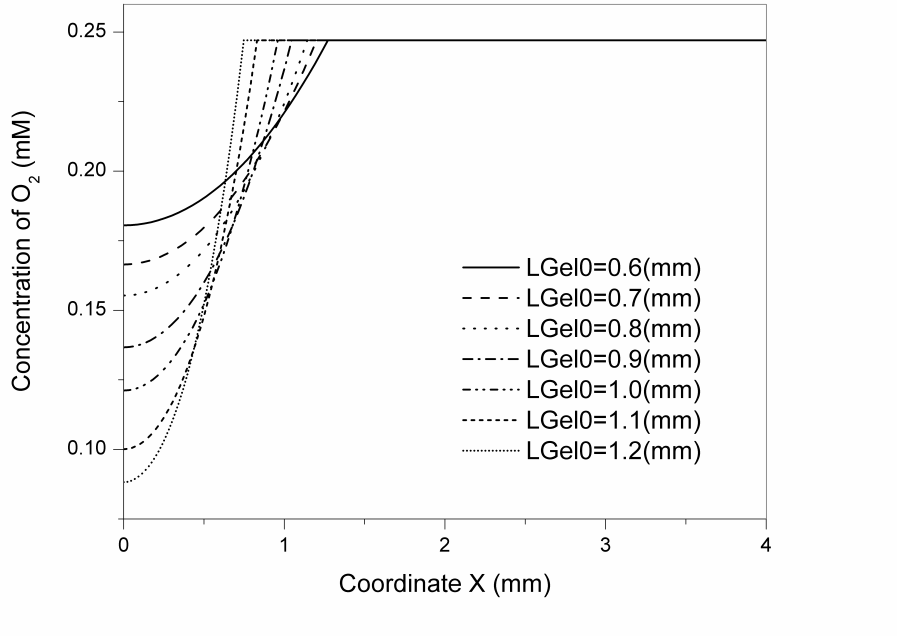

Figure 2.65 Distributive profile of oxygen concentration in the system.

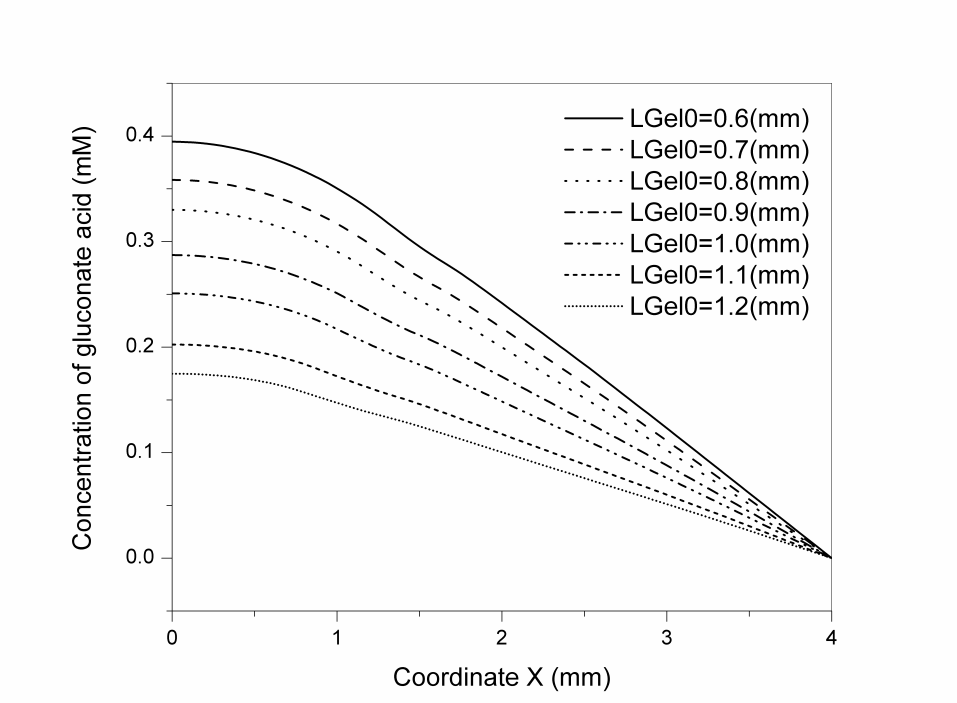

Figure 2.66 Distribution of the product of chemical reaction, gluconate acid, with various initial length of hydrogel strip.

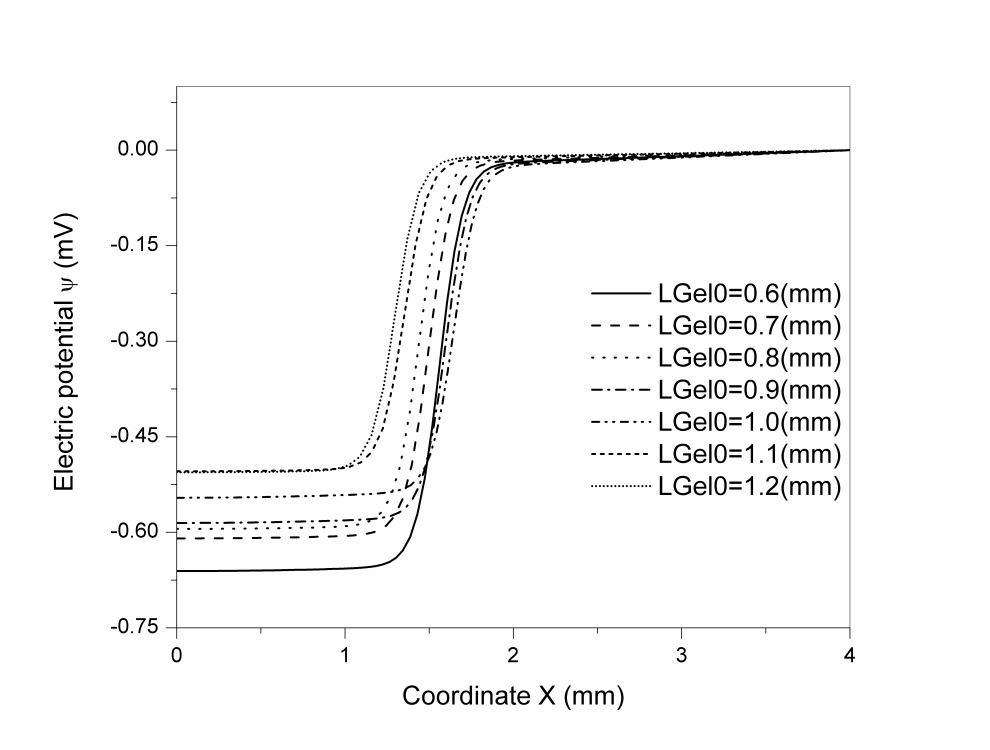

Figure 2.67 Effect of initial length of hydrogel strip on the distributive profile of the electric potential.

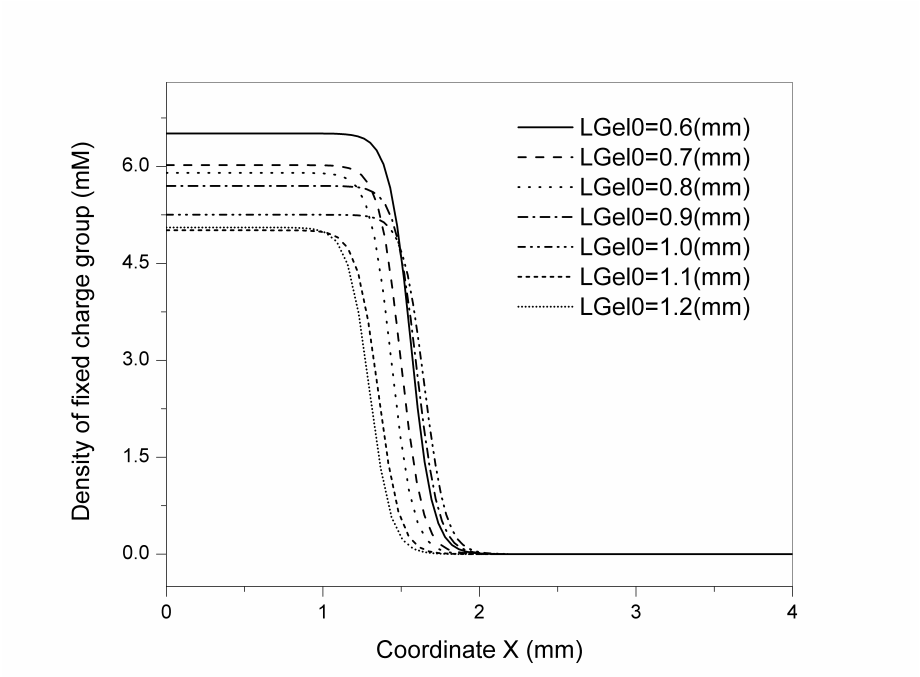

Figure 2.68 Effect of initial length of hydrogel strip on the distributive profile of the fixed charge group density.

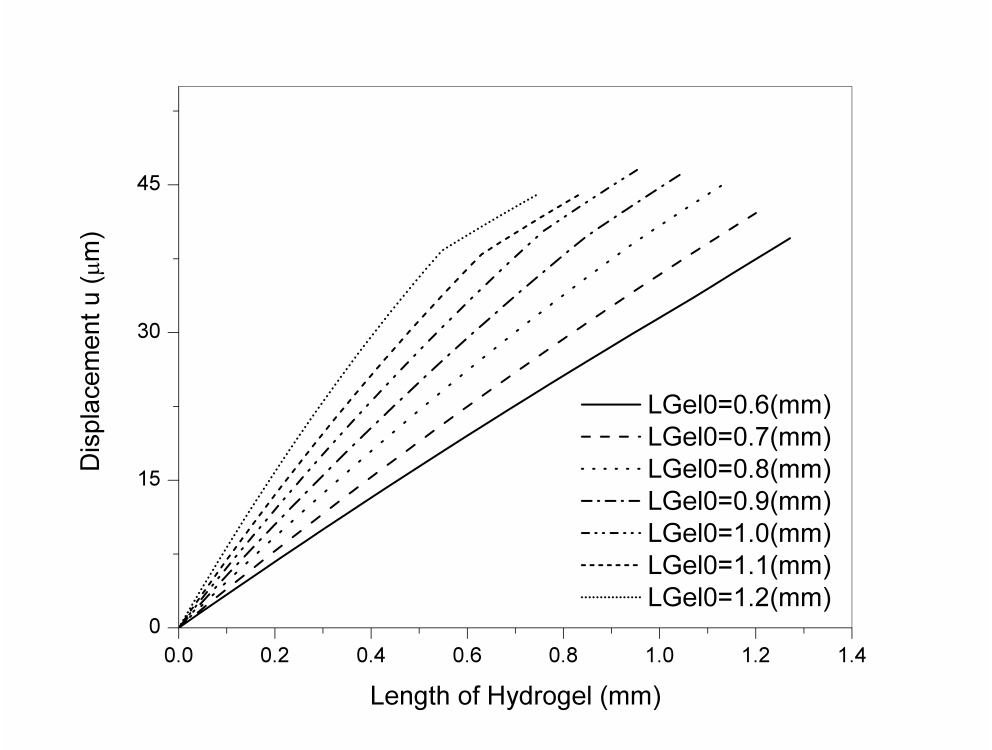

Figure 2.69 The change of initial length of hydrogel strip influences the displacement of the hydrogel strip.

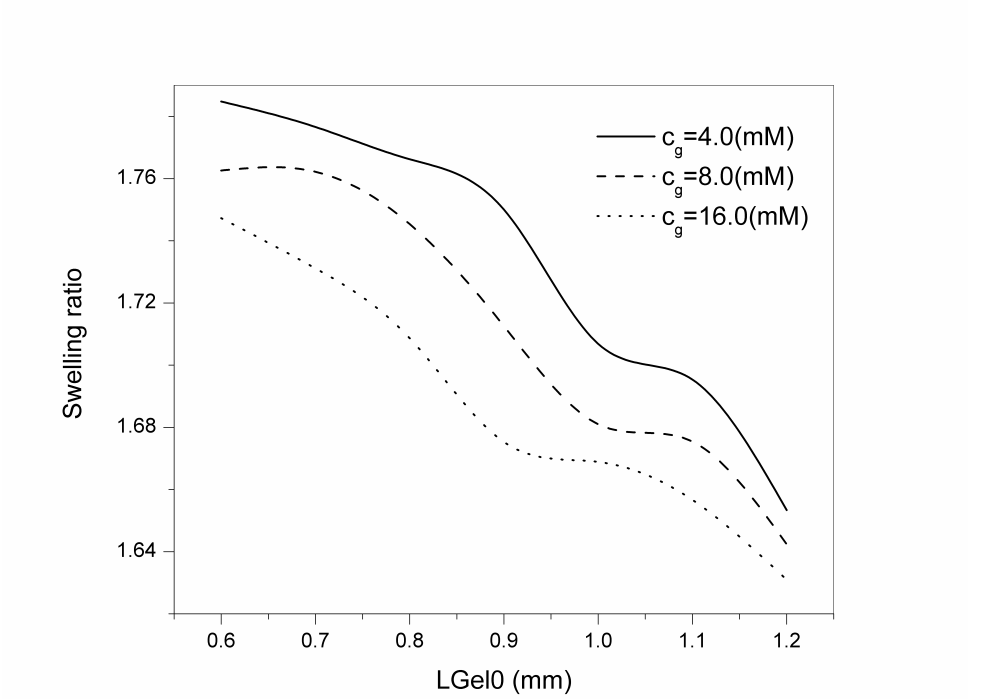

Figure 2.70 The effect of initial length of hydrogel strip on the swelling ratio of hydrogel strip with different glucose concentrations.

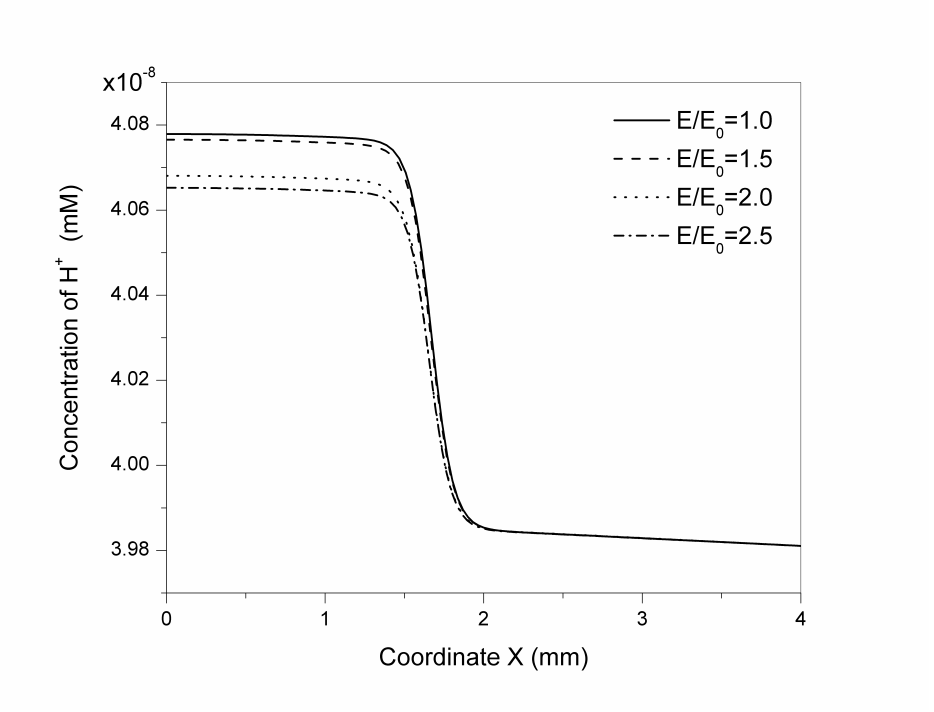

Figure 2.71 Distributive profile of hydrogen ion with the effect of Young's modulus of the hydrogel.

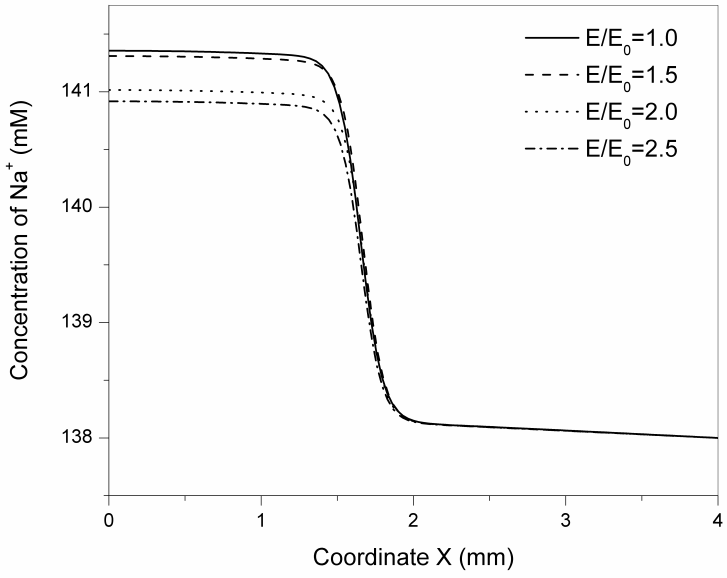

Figure 2.72 Effect of the Young's modulus of the hydrogel on the distributive profiles of Na^+.

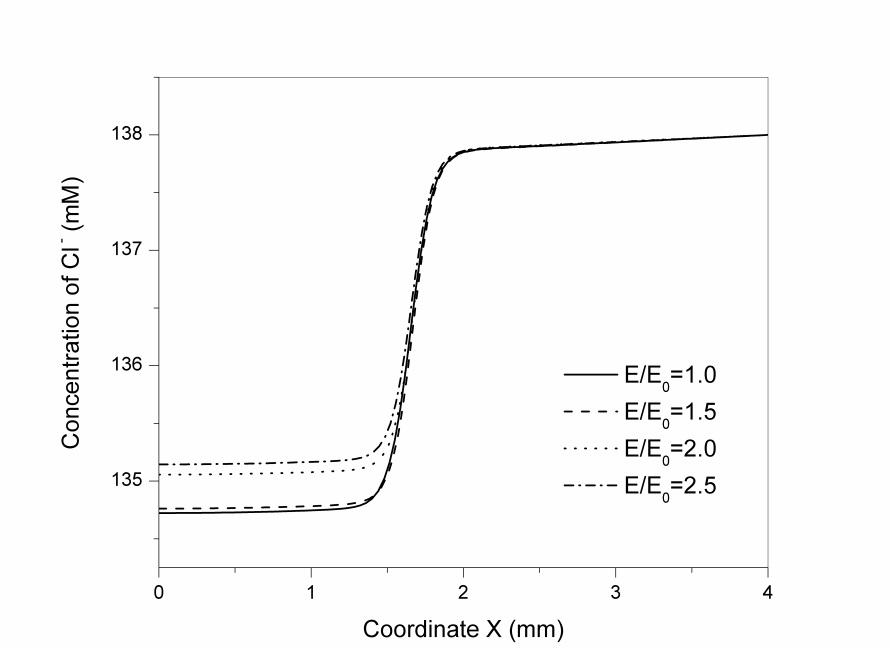

Figure 2.73 Effect of the Young's modulus of the hydrogel on the distributive profiles of Cl^-.

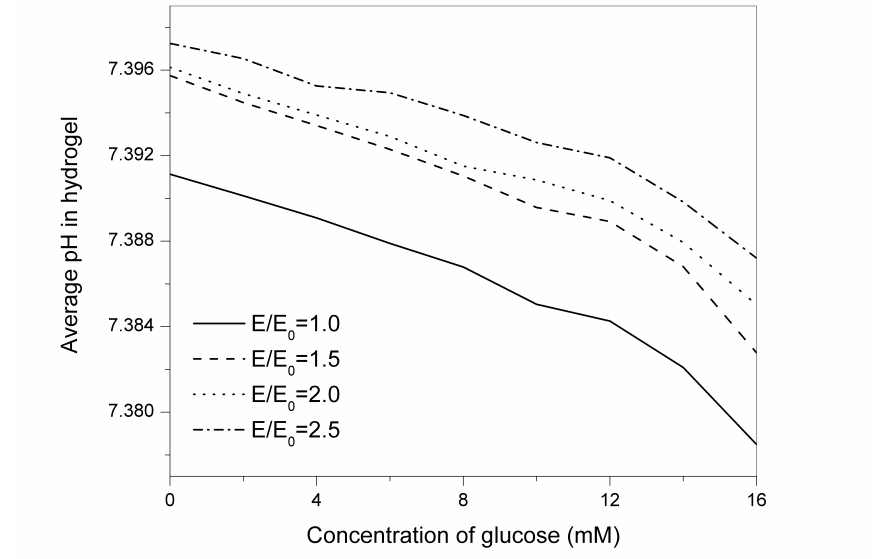

Figure 2.74 The variations of average pH in the hydrogel with the effect of the Young's modulus of the hydrogel.

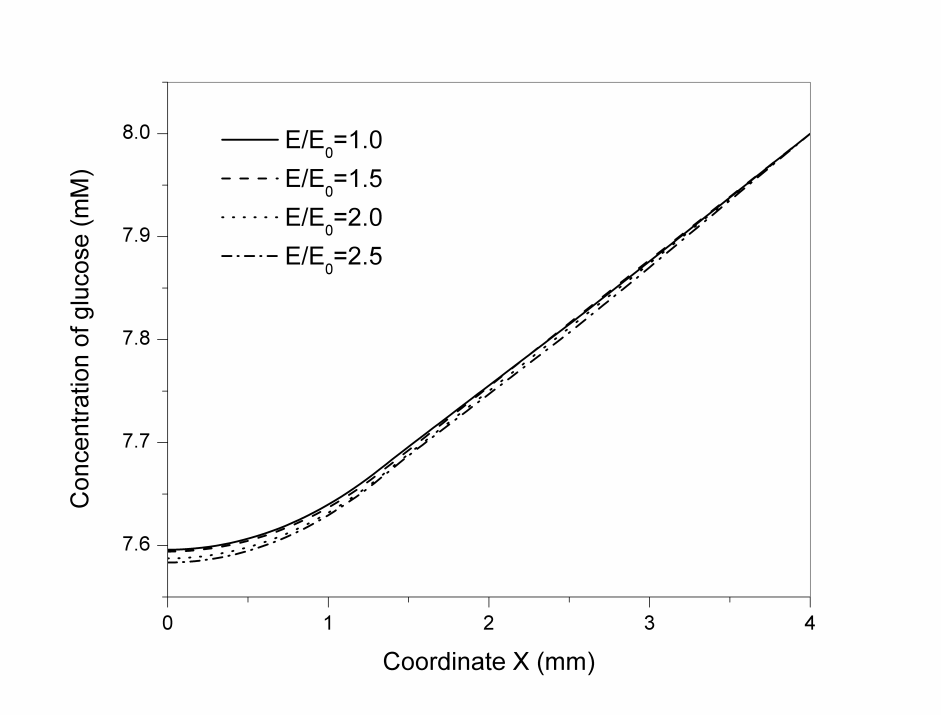

Figure 2.75 Distribution of glucose depends on the varying of Young's modulus of the hydrogel.

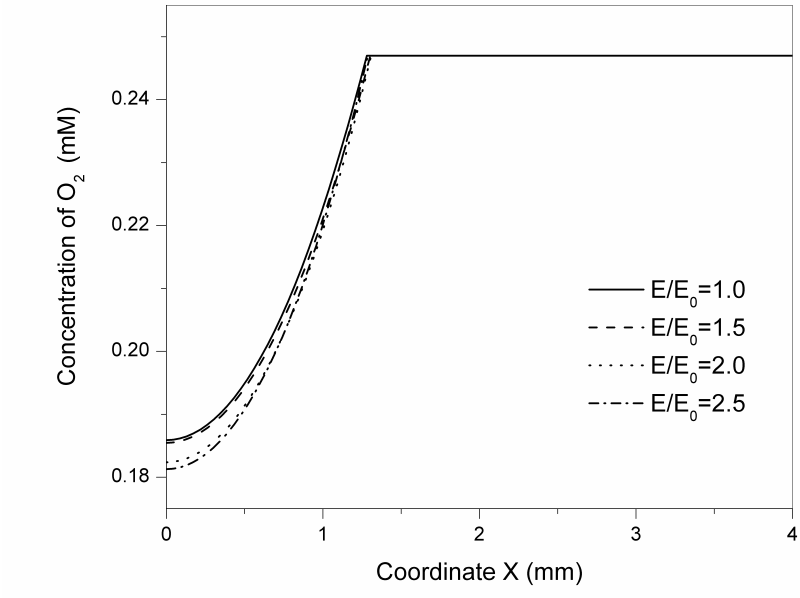

Figure 2.76 Distributive profile of oxygen concentration in the system.

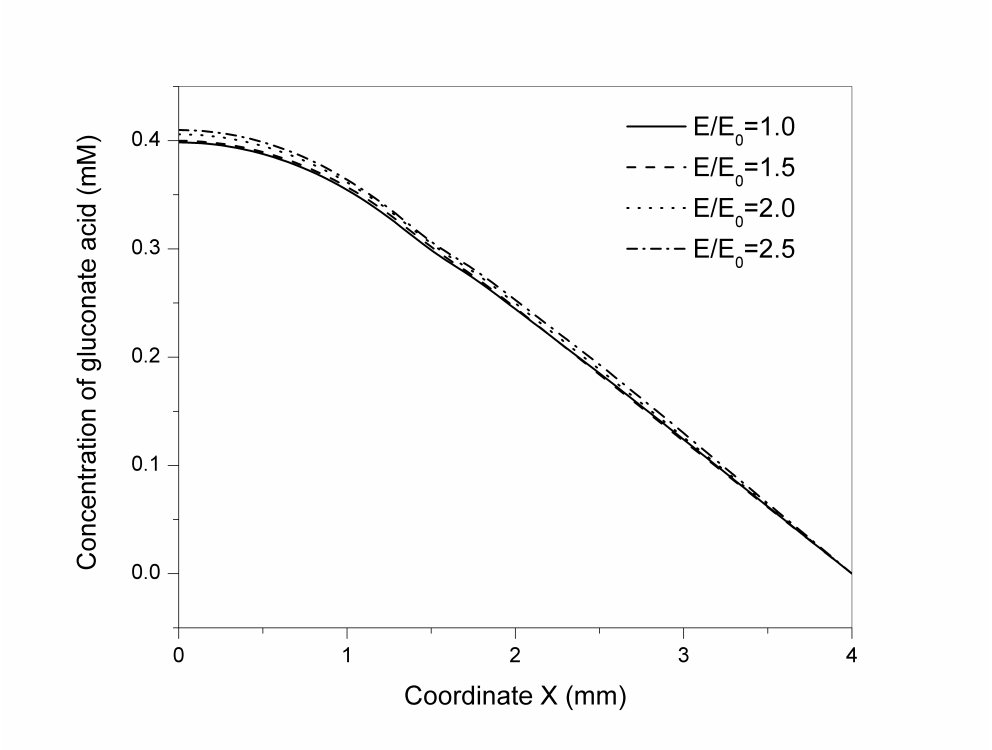

Figure 2.77 Distribution of the product of chemical reaction, gluconate acid, with various initial length of hydrogel strip.

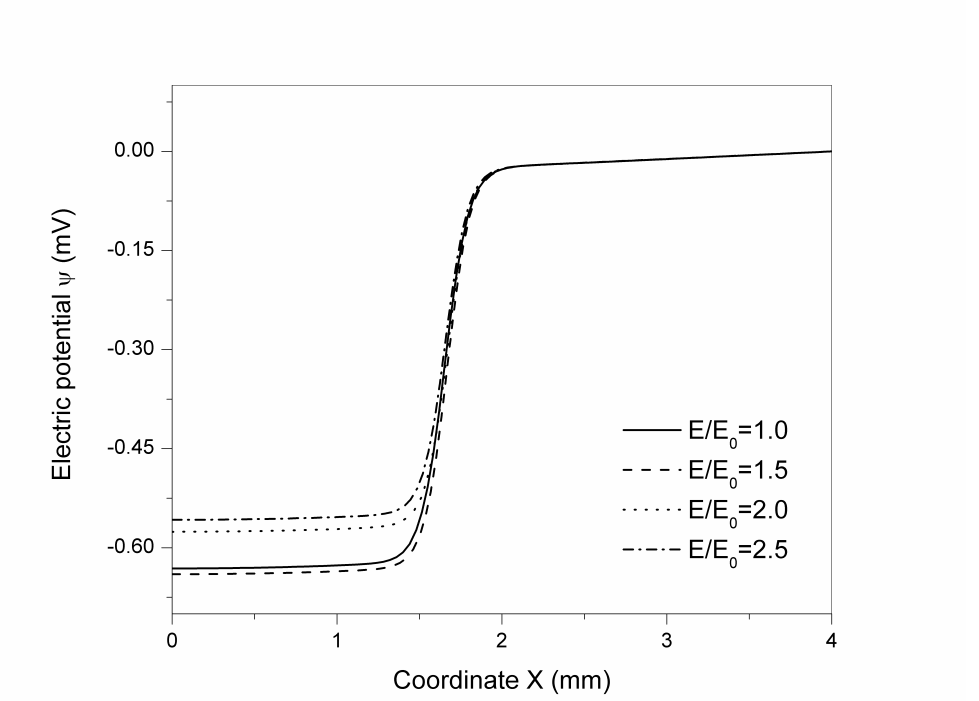

igure 2.78 Effect of Young's modulus of the hydrogel on the distributive profile of the electric potential.

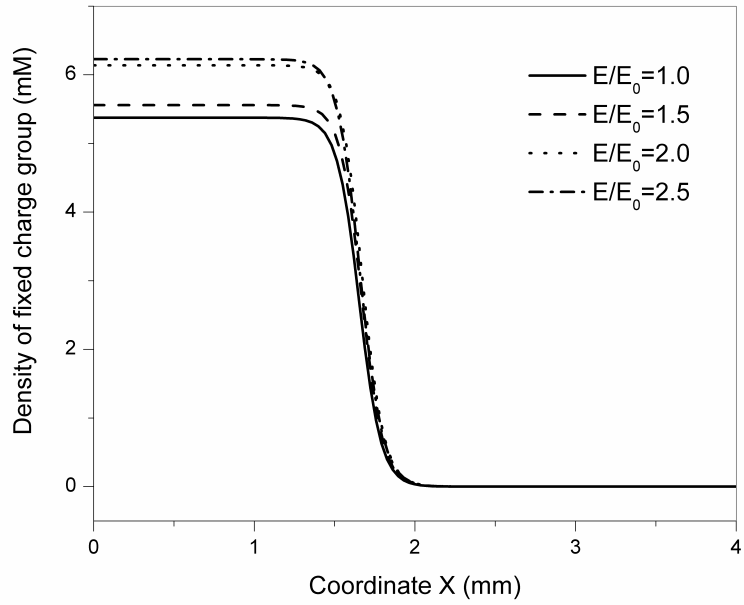

Figure 2.79 Effect of Young's modulus of the hydrogel on the distributive profile of the fixed charge group density.

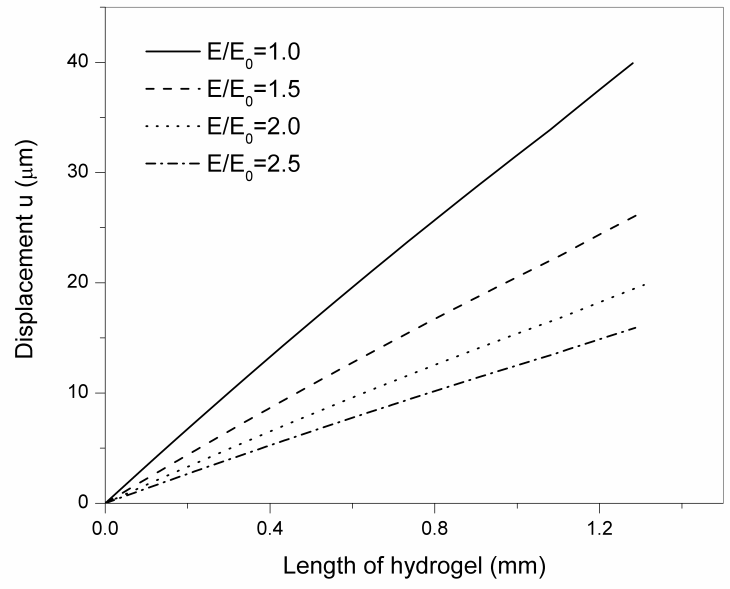

Figure 2.80 The change of Young's modulus of the hydrogel influences the displacement of the hydrogel strip.

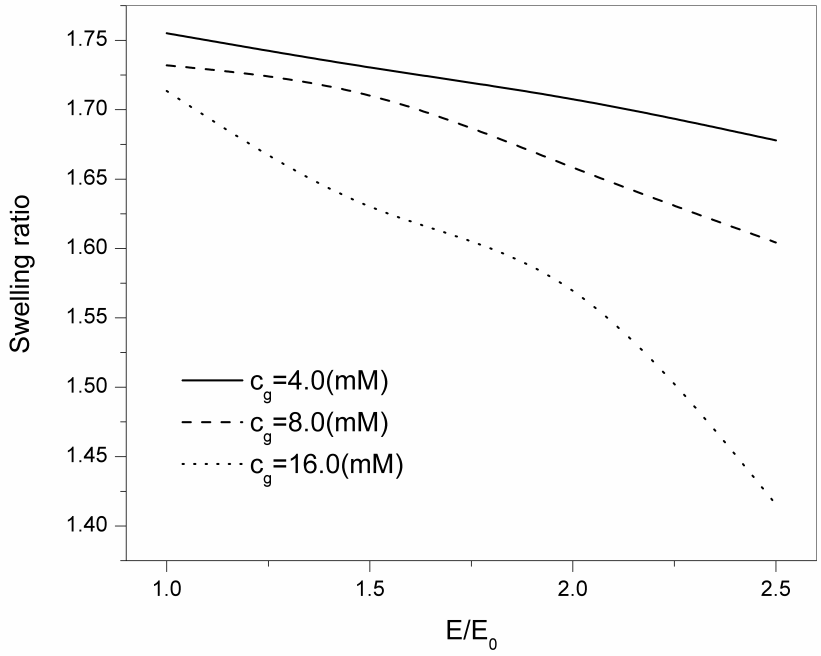

Figure 2.81 Effect of Young's modulus of the hydrogel on the swelling ratio of hydrogel strip with different glucose concentrations.

Chapter 3

Development of Multi-Effect-Coupling pH-Electric-Stimulus (MECpHe) Model for Hydrogels Responsive to The Coupled pH-Electric Stimuli

3.1 Introduction

Theoretically, the mechanism of the smart hydrogels responding to the electric-stimulus is similar to that to solution pH (Tanaka, 1981; Qiu and Park, 2001). After an electric field is applied to the bath solution, ions will diffuse between the hydrogels and surrounding solution. The diffusion gives rise to the ionic concentration differences between the interior hydrogel and exterior solution because of the fixed charge groups bound to the crosslinked macromolecular chains. As a result, an osmotic pressure is generated due to the concentration differences, which drives the swelling or shrinking of the hydrogel. The deformation of the hydrogel results in the redistribution of the diffusive ions and fixed charge groups, which causes new ionic concentration differences and then the hydrogel deforms again. The recurrent kinetics will continue and finally stop when the hydrogel reaches an equilibrium state. It explains well how the chemical energy converts to the mechanical energy.

The majority of studies on the hydrogels generally focused on a single stimulus at a time. However, one can expect that the hydrogel in a given application might

experience more then one stimuli. One of examples is the poly(*N*-iso-propylacrylamide) (PNIPAAm) hydrogel, which is sensitive to both temperature and pH for applications of drug delivery (Dong and Hoffman, 1990, 1991; Brazel and Peppas, 1996; Shin et al., 2003). Other examples are the typical pH-sensitive hydrogels for electric-sensitive applications, for example, Poly(2-acrylamido-2-methylpropane sulfonic acid) (PAMPS), Poly(acrylic acid) (PAA), and poly(methacrylic acid-*co*-vinyl alcohol) PMAA/PVA IPN hydrogel (Schreyer et al., 2000; Jin and Hsieh, 2005). When the hydrogel is subjected to a single particular stimulus at a time, one often faces the problems such as long response time and limited deformation. To overcome these limitations, thinner and smaller hydrogels are possible solutions. Unfortunately, this approach generally compromises the mechanical strength and leads to more fragile systems (Schreyer et al., 2000; Qiu and Park, 2001). An alternative is to perturb the hydrogel with multiple stimuli, in which the multiple stimuli will shorten the response time and increase swelling ratios. Kim et al. demonstrated this improvement in a string of experiments for the hydrogels subjected to simultaneous changes in both pH and applied electric field (Kim et al., 2003, 2004a, 2004b). They can reduce response time of swelling and shrinking down to a few seconds or less. With this performance, fast response actuators and artificial muscles become more feasible (Sawahata et al., 1990; Otake et al., 2002; Shihinpoor, 2003).

With the emergence of various applications that relies on the swelling behavior of the hydrogels, a convincing need comes for physically accurate theories and numerical simulations capable of capturing, analyzing, and predicting the behavior. To

design micro-actuation and sensing devices based on the smart hydrogels, it is critical to predict the relationship between the swelling time and the environmental stimuli. These theories and models must provide sufficient physical understanding of the various processes associated with the swelling of hydrogels (Dolbow et al., 2007). With the knowledge, the performance characteristics of the hydrogels can be optimized during the fabrication of the hydrogels.

This chapter is organized as follows. In Section 3.2, the Multi-Effect-Coupling pH-Electric-Stimulus (MECpHe) model is developed in details for the hydrogels responsive to the coupled pH-electric stimuli. Section 3.3 describes the discretization of the governing equations and boundary conditions of the MECpHe model. Section 3.4 validates the present MECpHe model by comparison between the simulation results and experiments. Section 3.5 discusses the effect of the several important physical and chemical parameters on the response of the hydrogels. Section 3.6 closes this chapter with some final remarks.

3.2 Development of MECpHe Model

The hydrogels responsive to the coupled pH-electric stimuli are able to convert chemical energy to mechanical energy. They are applied in controlled drug delivery in which the release pattern is affected by the externally applied electric field and solution pH (Qiu and Park, 2001). In order to simulate the responsive behaviors of hydrogels under the coupled pH-electric stimuli, based on the rMECe model which will be mentioned in Chapter 4, a new model is developed in this chapter, and called

multi-effect-coupling pH-electric-stimuli (MECpHe) model. The main contribution of the MECpHe model is the reformulation of the fixed charge density with simultaneous considerations of solution pH, electric potential and hydrogel large deformation.

3.2.1 Nernst-Planck Equations for Ionic Transportation

For simplicity of describing the flux of k^{th} ionic species in solution, the convective transport of the ionic species is neglected here. Thus, the flux of k^{th} ionic species in the systems consisting of the hydrogel and the surrounding solution can be given as

$$\boldsymbol{J}_k = -[D_k]\left(\operatorname{grad}(c_k) + \frac{z_k F}{RT} c_k \operatorname{grad}(\psi) + c_k \operatorname{grad}(\ln \gamma_k) \right) \qquad (k = 1,2,\ldots,N) \qquad (3.1)$$

where $\boldsymbol{J}_k$, $[D_k]$, c_k and z_k are the flux (mM/s), the diffusivity tensor, the concentration (mM) and the valence number of the k^{th} diffusive ionic species, ψ is the electrostatic potential (V) and γ_k is the chemical activity coefficient. F, R and T are the Faraday's constant (9.6487×10^4 C/mol), universal gas constant (8.314 J/mol$\cdot$K) and absolute temperature (K), respectively.

The three terms on the right hand side of the equation (3.1) represent the diffusive flux due to the concentration gradient, the migration flux due to the gradient of the electrical potential and chemical flux related to the chemical activity coefficient.

Based on the law of mass conservation, the change of the species k contained in the volume with respect to time t is given by the difference between the fluxes entering and leaving the reference volume. Thus, Nernst-Planck type of the mass conservation

is derived as

$$\frac{\partial c_k}{\partial t} + div(\boldsymbol{J}_k) = \frac{\partial c_k}{\partial t} + div\left\{-\left[D_k\right]\left(\boldsymbol{grad}(c_k) + \frac{z_k F}{RT} c_k \boldsymbol{grad}(\psi)\right)\right\} = 0 \tag{3.2}$$

3.2.2 Poisson Equation for Electric Potential

As more rigorous approach, the Poisson equation is used to describe the spatial distribution of the electric potential in the domain and is given as

$$\nabla^2 \psi = -\frac{F}{\varepsilon \varepsilon_0}\left(\sum_k z_k c_k + z_f c_f\right) \tag{3.3}$$

where ε is the relative dielectric constant of the medium and ε_0 is the vacuum permittivity or dielectric constant (8.85418×10^{-12} C^2/Nm^2). It is observed that the electroneutrality and constant field hypotheses are in fact special cases of the Poisson equation.

Based on Langmuir adsorption isotherm theory (Grimshaw et al., 1990), a relation between the fixed charge and diffusive hydrogen ion concentration can be developed to complete the Poisson equation, whereby the concentration of the fix charged group is calculated as a function of c_f^0 and c_{H^+} by

$$c_f = c_f^0 - c_f^b = c_f^0 - \frac{c_f^0 \cdot c_{H^+}}{K + c_{H^+}} = \frac{c_f^0 \cdot K}{K + c_{H^+}} \tag{3.4}$$

where c_f and z_f are the concentration and the valence of the fixed charge groups attached onto the polymeric chains within the hydrogel. For example, if the carboxylic acid groups are used as the fixed charges on the polymer chains, $z_f = -1$. K is the dissociation constant of the carboxylic acid groups, c_f^0 is the total concentration of

the ionizable groups in the hydrogel, c_{H^+} is the concentration of hydrogen ions H^+ within the hydrogel and H is the local hydration of the hydrogel.

In the presently developed MECpHe model, the total concentration of the fixed charge groups in the hydrogel at the relaxed state $c_{f,s}^0$ is defined as follows

$$c_{f,s}^0 = \frac{n}{V^s} \tag{3.5}$$

Then the total concentration of the ionizable groups in the hydrogel is derived by

$$c_f^0 = \frac{n}{V} = \frac{n}{V^s + V^w} = \frac{n}{V^s}\frac{V^s}{V^s + V^w} = \frac{n}{V^s}\frac{V^s}{V^s + HV^s} = \frac{n}{V^s}\frac{V^s}{(H+1)V^s} = \frac{c_{f,s}^0}{H+1} \tag{3.6}$$

Substituting the equation (3.6) into the equation (3.4), one can obtain,

$$c_f = \frac{c_f^0 \cdot K}{K + c_H} = \frac{1}{H+1} \cdot \frac{c_{f,s}^0 \cdot K}{K + c_H} \tag{3.7}$$

As mentioned above, the local hydration of the hydrogel is defined as $H = \frac{V^w}{V^s}$, namely

$$1 + H = 1 + \frac{V^w}{V^s} = \frac{V^s + V^w}{V^s} = \frac{V}{V^s} = \frac{1}{\phi^s} = \frac{1}{1 - \phi^w} \tag{3.8}$$

From the equation (3.8), the volume fractions of water and solid phases can be written as, respectively

$$\phi^w = \frac{H}{1+H} \tag{3.9}$$

$$\phi^s = \frac{1}{1+H} \tag{3.10}$$

Here the volume fraction of ions ϕ^i is assumed to be comparatively very small, and then the saturation equation is given as

$$\phi^w + \phi^s \approx 1 \tag{3.11}$$

The relationship between of the volume fractions of water and solid phases is thus given by

$$\phi^w \approx 1-\phi^s = 1-\frac{V^s}{V} = 1-\frac{V^s}{V_0}\frac{V_0}{V} = 1-\phi_0^s \cdot J \tag{3.12}$$

where J **(** $J = dV_0 / dV$ **)** is the volume ratio of apparent solid phase and can be expressed by the Green strain tensor $\boldsymbol{E}$ of the apparent solid phase as follows (Hon et al., 1999),

$$\frac{1}{J} = \sqrt{1+2F_1(\boldsymbol{E})+4F_2(\boldsymbol{E})+8F_3(\boldsymbol{E})} \tag{3.13}$$

where $F_1(\boldsymbol{E}) = tr(\boldsymbol{E})$, $F_2(\boldsymbol{E})$ and $F_3(\boldsymbol{E})$ are the first, second and third invariant of Green strain tensor $\boldsymbol{E}$, respectively.

The Green strain tensor can be expressed in terms of displacement gradients by (Belytschko et al., 1995),

$$E_{ij} = \frac{1}{2}\left(\frac{\partial u_i}{\partial X_j}+\frac{\partial u_j}{\partial X_i}+\frac{\partial u_k}{\partial X_i}\frac{\partial u_k}{\partial X_j}\right) \tag{3.14}$$

where X_i, X_j are the components of the position vector in the initial configuration, u_i, u_j and u_k are the displacements. In one-dimensional case,

$$E_{11} = \frac{1}{2}\left(\frac{\partial u_1}{\partial X_1}+\frac{\partial u_1}{\partial X_1}+\frac{\partial u_1}{\partial X_1}\frac{\partial u_1}{\partial X_1}\right) = \frac{1}{2}\left[2\frac{du}{dx}+\left(\frac{du}{dx}\right)^2\right] \tag{3.15}$$

Three invariants of the deformation gradient tensor are defined as follows (Lai et al., 1974),

$$F_1 = E_{11}+E_{22}+E_{33} \tag{3.16}$$

$$F_2 = \begin{vmatrix} E_{11} & E_{12} \\ E_{21} & E_{22} \end{vmatrix} + \begin{vmatrix} E_{11} & E_{13} \\ E_{31} & E_{33} \end{vmatrix} + \begin{vmatrix} E_{22} & E_{23} \\ E_{32} & E_{33} \end{vmatrix} \tag{3.17}$$

$$F_3 = \left|E_{ij}\right| = \begin{vmatrix} E_{11} & E_{12} & E_{13} \\ E_{21} & E_{22} & E_{23} \\ E_{31} & E_{32} & E_{33} \end{vmatrix} \tag{3.18}$$

For one-dimension special case,

$$F_1 = E_{11} = \frac{1}{2}[2\frac{du}{dx} + (\frac{du}{dx})^2] = \frac{du}{dx} + \frac{1}{2}(\frac{du}{dx})^2 \tag{3.19}$$

From the equations (3.9) and (3.12), one can have

$$\phi^w = \frac{H}{1+H} = 1 - \phi_0^s J \tag{3.20}$$

Then the local hydration of the hydrogel H is expressed as follows,

$$H = \frac{1-\phi_0^S J}{\phi_0^S J} \tag{3.21}$$

Substituting the equations (3.13) and (3.21) into the equation (3.7), the density of fixed charge groups is then rewritten as

$$c_f = \frac{c_{m0}^s \cdot K \cdot \phi_0^s}{(K + c_H)\sqrt{1 + 2F_1(\boldsymbol{E}) + 4F_2(\boldsymbol{E}) + 8F_3(\boldsymbol{E})}} \tag{3.22}$$

In one-dimensional case, by substituting the equation (3.19) into the equation (3.22), the expression of density of fixed charge groups is reduced to

$$c_f = \frac{c_{m0}^s \cdot K \cdot \phi_0^s}{(K + c_H)\sqrt{1 + 2\frac{du}{dx} + (\frac{du}{dx})^2}} \tag{3.23}$$

3.2.3 Nonlinear Mechanical Equation for Finite Deformation

The first Piola-Kirchhoff stress tensor ***P*** is a kind of expatriate, living partially in the deformed (current) configuration ***x*** and partially in the reference configuration ***X*** (where $\mathbf{x} = \mathbf{X} + \mathbf{u}$), and is unable to measure. For this reason and because of the

absence of symmetry in the first Piola-Kirchhoff stress tensor ***P***, it is seldom used in constitutive equations. However, the second Piola-Kirchhoff stress tensor ***S*** is symmetric and is often used as the stress measure, and then the second Piola-Kirchhoff stress tensor ***S*** is chosen to analyze the large deformation. The relationship between the first Piola-Kirchhoff stress tensor ***P*** and the second Piola-Kirchhoff stress tensor ***S*** is given as,

$$\mathbf{P} = \mathbf{S}\mathbf{F}^{\mathrm{T}} \tag{3.24}$$

where $\mathbf{F}$ is the deformation gradient tensor and defined as,

$$\mathbf{F} = \mathbf{I} + \nabla \mathbf{u} \tag{3.25}$$

The second Piola-Kirchhoff stress tensor ***S*** is given by,

$$\mathbf{S} = \mathbf{C}\mathbf{E} - p_{osmotic}\mathbf{I} \tag{3.26}$$

where $\mathbf{C}$ is the material tensor and ***E*** is the Green-Lagrangian strain tensor that is used as the strain measure,

$$\mathbf{E} = \frac{1}{2}(\mathbf{F}^{\mathrm{T}}\mathbf{F} - \mathbf{I}) \tag{3.37}$$

Then, the governing equation for large deformation can be written as follows

$$\nabla \cdot [(\mathbf{C}\mathbf{E} - p_{osmotic}\mathbf{I})\mathbf{F}^{\mathrm{T}}] = 0 \tag{3.38}$$

So far the development of MECpHe model is completed. For the present one-dimensional study, the full governing equations of the model consist of the Nernst-Planck convention-diffusion equations for ion concentration, Poisson equation for the electric potential, and nonlinear mechanical equation for the hydrogel large displacement, namely

$$\frac{\partial c_k}{\partial t} + div(\mathbf{J}_k) = \frac{\partial c_k}{\partial t} + div\left\{-\left[D_k\right]\left(\text{grad}(c_k) + \frac{z_k F}{RT} c_k \text{grad}(\psi)\right)\right\} = 0 \tag{3.2}$$

$$\nabla^2 \psi = -\frac{F}{\varepsilon \varepsilon_0}\left(\sum_k z_k c_k + z_f c_f\right) \tag{3.3}$$

$$c^f = \frac{c_{m0}^s \cdot K \cdot \phi_0^s}{(K + c_H)\sqrt{1 + 2\frac{du}{dx} + (\frac{du}{dx})^2}} \tag{3.23}$$

$$(\lambda + 2\mu)[\frac{d^2u}{dX^2} + 3\frac{du}{dX}\frac{d^2u}{dX^2} + \frac{3}{2}(\frac{du}{dX})^2\frac{d^2u}{dX^2}] - \frac{dp_{osmotic}}{dX} = 0 \tag{3.38}$$

Boundary conditions are given as follows

$$c\big|_{Anode} = c\big|_{Cathode} = c^* \tag{3.39}$$

$$\psi\big|_{Anode} = 0.5V_e \text{ and } \psi\big|_{Cathode} = -0.5V_e \tag{3.40}$$

where c^* is the initial ionic concentration of the bath solution and V_e the externally applied electric voltage.

At the solvent/hydrogel interfaces ($x = (L \pm h)/2$):

$$\frac{du}{dx} = \frac{p_{osmotic}}{E} \tag{3.41}$$

In addition, to prevent the hydrogel from undergoing translational motion in the applied electric field, a point constraint is introduced in the middle of the hydrogel ($x = L/2$):

$$u = 0 \tag{3.42}$$

3.3 Discretization of MECpHe Model

For computational convenience, a set of non-dimensional variables are defined as,

$$\bar{x}=\frac{x}{L_{ref}},\quad \bar{u}=\frac{u}{L_{ref}},\quad \bar{c}_k=\frac{c_k}{c_{ref}},$$
$$\bar{c}_f=\frac{c_f}{c_{ref}},\quad \bar{\psi}=\frac{\psi}{\psi_{ref}}=\frac{F\psi}{\eta RT},\quad \bar{p}_{osmotic}=\frac{p_{osmotic}}{\xi c_{ref}RT} \tag{3.46}$$

Then, the non-dimensional forms of partial differential governing equations of the MECpHe model are written as

$$\frac{d^2\bar{c}_k}{d\bar{x}^2}+\eta z_k\frac{d\bar{c}_k}{d\bar{x}}\frac{d\bar{\psi}}{d\bar{x}}+\eta z_k\bar{c}_k\frac{d^2\bar{\psi}}{d\bar{x}^2}=0 \qquad (k=1,2,\cdots,N) \tag{3.47}$$

$$\frac{d^2\bar{\psi}}{d\bar{x}^2}=-\frac{F^2}{\varepsilon\varepsilon_0 RT}\frac{L_{ref}^2c_{ref}}{\eta}(z_f\bar{c}_f+\sum_{k=1}^{N}z_k\bar{c}_k) \tag{3.48}$$

$$[\frac{d^2\bar{u}}{d\bar{x}^2}+3\frac{d\bar{u}}{d\bar{x}}\frac{d^2\bar{u}}{d\bar{x}^2}+\frac{3}{2}(\frac{d\bar{u}}{d\bar{x}})^2\frac{d^2\bar{u}}{d\bar{x}^2}]-\frac{\xi c_{ref}RT}{f_1}\frac{d\bar{p}_{osmotic}}{d\bar{x}}=0 \tag{3.49}$$

The non-dimensional of the osmotic pressure equation is given as

$$\bar{p}_{osmotic}=\frac{1}{\xi}\sum_k(\bar{c}_k-\bar{c}_k^0) \tag{3.50}$$

Based on the Hermite-cloud method, the unknown variables are discretized as

$$\bar{c}_k(\bar{x}_i)=\sum_{j=1}^{np}N_j(\bar{x}_i)\bar{c}_{kj}+\sum_{m=1}^{np}(\bar{x}_i-\sum_{j=1}^{np}N_j(\bar{x}_i)\bar{x}_j)M_m(\bar{x}_i)\bar{c}_{km,x} \tag{3.51}$$

$$\bar{\psi}(\bar{x}_i)=\sum_{j=1}^{np}N_j(\bar{x}_i)\bar{\psi}_j+\sum_{m=1}^{np}(\bar{x}_i-\sum_{j=1}^{np}N_j(\bar{x}_i)\bar{x}_j)M_m(\bar{x}_i)\bar{\psi}_{m,x} \tag{3.52}$$

$$\bar{u}(\bar{x}_i)=\sum_{j=1}^{npGel}N_j(\bar{x}_i)\bar{u}_j+\sum_{m=1}^{npGel}(\bar{x}_i-\sum_{j=1}^{npGel}N_j(\bar{x}_i)\bar{x}_j)M_m(\bar{x}_i)\bar{u}_{m,x} \tag{3.53}$$

Finally, the discrete forms of the non-dimensional 1-D steady-state partial differential governing equations of the MECpHe model and auxiliary conditions are obtained as

$$\sum_{j=1}^{np}N_{j,xx}(\bar{x}_i)\bar{c}_{kj}+\eta z_k[\sum_{m=1}^{np}M_m(\bar{x}_i)\bar{c}_{km,x}][\sum_{m=1}^{np}M_m(\bar{x}_i)\bar{\psi}_{m,x}]+$$
$$+\eta z_k[\sum_{j=1}^{np}N_j(\bar{x}_i)\bar{c}_{kj}-\sum_{m=1}^{np}(\bar{x}_i-\sum_{j=1}^{np}N_j(\bar{x}_i)\bar{x}_j)M_m(\bar{x}_i)\bar{c}_{km,x}][\sum_{j=1}^{np}N_{j,xx}(\bar{x}_i)\bar{\psi}_j]=0 \tag{3.54}$$

$$\sum_{j=1}^{np} N_{j,xx}(\bar{x}_i)\bar{\psi}_j + \frac{F^2}{\varepsilon\varepsilon_0 RT}\frac{L_{ref}^2 c_{ref}}{\eta}\{z_f c_f + \sum_{k=1}^{N} z_k[\sum_{j=1}^{np} N_j(\bar{x}_i)\bar{c}_{kj} -$$

$$\sum_{m=1}^{np}(\bar{x}_i - \sum_{j=1}^{np} N_j(\bar{x}_i)\bar{x}_j)M_m(\bar{x}_i)\bar{c}_{km,x}]\} = 0 \tag{3.55}$$

$$f_1\{\sum_{j=1}^{npGel} N_{j,xx}(\bar{x}_i)\bar{u}_j + 3[\sum_{m=1}^{npGel} M_m(\bar{x}_i)\bar{u}_{m,x}][\sum_{j=1}^{npGel} N_{j,xx}(\bar{x}_i)\bar{u}_j]$$

$$+\frac{3}{2}[\sum_{m=1}^{npGel} M_m(\bar{x}_i)\bar{u}_{m,x}][\sum_{m=1}^{npGel} M_m(\bar{x}_i)\bar{u}_{m,x}][\sum_{j=1}^{npGel} N_{j,xx}(\bar{x}_i)\bar{u}_j]\}$$

$$-\frac{1}{\xi}\sum_k[\sum_{m=1}^{npGel} M_m(\bar{x}_i)\bar{c}_{km,x}] = 0 \qquad (k = 1,2,\cdots) \tag{3.56}$$

$$\sum_{j=1}^{np} N_{xj}(\bar{x}_i)\bar{c}_k - [\sum_{j=1}^{np} N_{xj}(\bar{x}_i)\bar{x}_j]\sum_{m=1}^{np} M_m(\bar{x}_i)\bar{c}_{km,x} = 0 \tag{3.57}$$

$$\sum_{j=1}^{np} N_{xj}(\bar{x}_i)\bar{\psi} - [\sum_{j=1}^{np} N_{xj}(\bar{x}_i)\bar{x}_j]\sum_{m=1}^{np} M_m(\bar{x}_i)\bar{\psi}_{m,x} = 0 \tag{3.58}$$

$$\sum_{j=1}^{npGel} N_{xj}(\bar{x}_i)\bar{u} - [\sum_{j=1}^{npGel} N_{xj}(\bar{x}_i)\bar{x}_j]\sum_{m=1}^{npGel} M_m(\bar{x}_i)\bar{u}_{m,x} = 0 \tag{3.59}$$

where *np* is the number of the scattered points in the whole domain covering the hydrogel and surrounding solution, and *npGel* is that within the hydrogel domain only.

3.4 Examination of MECpHe Model

In order to examine the MECpHe model, a numerical comparison is made between the computed results and experimentally measured bending data extracted from the publication (Kim et al., 2004b), where Kim et al. measured experimentally the deformation of the PMAA/PVA IPN hydrogel strip which was immersed in the pH buffer solution, as shown in Figure 3.2. When the pH is low, the carboxylic acid groups in PMAA are in the form of $R-COOH$. As the pH increases, $R-COOH$ is

dissociated to $R-COO^-$, the hydrogel strip swells uniformly (Kim et al., 2004b). When the electric field is applied, the electric potential will cause the non-uniform distribution of ionic concentrations, leading to the unequal concentration differences at both the interfaces between the hydrogel and surrounding solution near to the anode and cathode, respectively. The unequal concentration differences result in the unequal osmotic pressure at both the interfaces near the anode and cathode, which makes the hydrogels bent (Wallmersperger and Kroeplin, 2001; Homma et al., 2001).

The proposed hydrogels contain carboxylic groups and undergo drastic change in swelling capacity with pH of the external media. The minimum swelling in the media of low pH may be attributed to the fast that the –COOH groups present along the macromolecular chains in the matrix remain almost unionized (since pK_a of the acrylic acid is 5.4), thus resulting in almost nil osmotic swelling pressure as there is no difference of mobile/counter ions concentration inside/outside of the gel matrix. Moreover, there occur H-bonding interactions among the carboxylic groups within the matrix, thus providing a compact H-bonded structure to the hydrogel, which ultimately restricts the movements of polymeric segments and highly discourages the solvent entrance. However, when the hydrogel is put in the medium of pH higher than pK_a, the ionization of –COOH groups not only increases the osmotic swelling pressure but it also results in relaxation of polymeric chains due to repulsion among similarly charged $R-COO^-$ groups along the macromolecular chains. This causes extensive swelling of the hydrogel as indicated by higher swelling ratio of the gel (Bajpai and Dubey, 2005).

The parameters used for examination of the model include R=8.314 J/mol·K, $F = 9.648\times10^4$ C/mol, T=278K, $\varepsilon_0 = 8.854\times10^{-12}$ C^2/Nm^2, $\varepsilon = 80$, $c^* = 137.1$ mM, $z_f = -1$, $c_f^0 = 200$ mM, the initial water volume fraction $\phi_0^w = 0.8$. In general, the elastic modulus of the polymer PMAA varies with change in buffer solution pH (Yin et al., 1997; Bashir et al., 2002; Rong et al., 2004). The elastic modulus is taken here as 3MPa according to the experiment (Yin et al., 1997). The distance between the two carbon electrodes $L = 30$ mm and the hydrogel strip is tailed in $20\times5\times0.2$mm^3. The simulating results are illustrated in Figure 3.3 for the bending behavior of the hydrogel subject to the electric voltage ($V_e = 15$ V) coupled with solution pH stimuli. In order to measure the bending deformation of the hydrogel, an equilibrium bending angle (EBA), α, is defined as $\alpha = 45L_0(e_1 - e_2)/\pi h$ in the unit of degree (Kim et al., 2004b), where e_1 and e_2 are the strains of the hydrogel strip at the two ends in thickness direction, L_0 and h are the length and thickness of the hydrogel strip, respectively. At the higher electric voltage $V_e = 15$ V, the profile of α increasing gradually with buffer solution pH value may be divided into three stages. When the pH is lower than pH=4.0 or higher than pH=6.0, the α achieves in increasing gradual rate. However, it will increase rapidly in the range from pH=4.0 to 6.0. Basically the deformation mechanism of the hydrogel may be explained by the Flory's osmotic pressure theory (Shiga and Kurauchi, 1990; Yang and Engberts, 2000). When external electric field is applied, mobile ions will move toward their counter electrode. As a result, an ion concentration gradient is developed. The osmotic pressure due to the ion concentration difference is generated at both the interfaces between the hydrogel and the surrounding

solution. The cation Na^+ diffuses into the hydrogel more than the anions Cl^-, and move toward the cathode. Since the increase of osmotic pressure at the interface near the anode is larger than that at the interface near the cathode, the hydrogel near the anode swells greater than that near the cathode, which results in the bending toward the cathode. Figure 3.3 demonstrates that the simulating results agree well with the experimental data (Kim et al., 2004b). This validates the MECpHe model with capability of efficiently simulating hydrogels responsive to coupled pH-electric stimuli.

3.5 Simulation for Effects of Various Parameters

For further understanding of the influences of various physical parameters on the responsive behaviors of the hydrogels subject to the solution pH and electric field coupled stimuli, several simulations are carried out with the parameters R=8.314 J/mol·K , $F = 9.648\times10^4$ C/mol, T=278K, $\varepsilon_0 = 8.854\times10^{-12}$ C^2/Nm^2, $\varepsilon = 80$, $c^* = 4.0$ mM, $c_f^s = 10.0$ mM, $z_f = -1$, $\phi_0^w = 0.8$, $L = 2400$ μm, $h = 800$ μm, and the Young's modulus is 3.0MPa. The simulation results are illustrated in the following subsections, in which the influences of the several important parameters are discussed in detail on the responsive distribution of the diffusive ionic concentrations c_k, the electric potential ψ, and the fixed charge density c_f as well as the mechanical deformation of hydrogel, including the hydrogel strip displacement u, swelling ratio R_s and average curvature K_a. In the present simulations, an average

curvature, K_a, is defined as $K_a = 2(e_1 - e_2)/[h(2 + e_1 + e_2)]$ (e_1 and e_2 are the strains of the hydrogel strip at the two ends) at the fixed point of hydrogel thickness axis for measurement of the bending deformation of the hydrogel (Li et al., 2007).

3.5.1 Coupled Effects of pH and Electric Voltage

Figures 3.4 and 3.5 show the influence of surrounding solution pH on the distribution of diffusive ionic species concentrations of the system in response to the coupled stimuli of solution pH and electric voltage, with V_e=0, 0.08, 0.16 and 0.32, respectively. When no external electric field is applied, i.e. $V_e = 0$, the distributions of the diffusive ionic concentrations are simulated and shown in Figures 3.4(a) and 3.5(a), respectively. It is observed from the figures that the electroneutrality phenomenon exists in the bath solution and the hydrogel strip. The concentrations of the diffusive ionic species, Na^+ and Cl^-, are distributed uniformly within hydrogels and symmetrically in the whole computational domain. The same profiles of concentration differences at the both interfaces between the hydrogels and surrounding solution occur near to the anode and cathode. This makes the hydrogel strip swell uniformly without bending deformation. Once an electric field is applied however, such as $V_e = 0.16$ V, the distributions of the diffusive ionic species Na^+ and Cl^- concentrations are no longer uniform in the hydrogels and bath solution, and also no longer symmetric in the whole domain. It is noted that the simulated hydrogel is assumed to be charged negatively.As the electric field is applied, the mobile cations

Na^+ transport from anode region to cathode one until the equilibrium state is achieved. Therefore, the diffusive Na^+ concentration increases at the hydrogel edge near the cathode and decreases near the anode. When the electric current is constant in equilibrium state, it is understood that the electroneutrality conserves at every local point in the solution and the global flow of all ions across the boundary yields a null current. As a result, the Cl^- concentration also increases at the hydrogel edge near the cathode and decreases near the anode. With increasing the distance from the cathode, the concentrations of the diffusive ionic species Na^+ and Cl^- decrease within the hydrogels. It can also be observed from Figures 3.4(b)-(d) and 3.5(b)-(d) that the differences of ionic concentrations at the hydrogel-solution interfaces between the interior hydrogel and exterior bath solution near the anode are larger than that near the cathode. Along the pH-axis direction, the profile of concentration distributions forms a slant for the cation Na^+ concentration over the hydrogel-solution interface near the anode and a trench near the cathode, while the distributive profile of the anion Cl^- concentration forms a trench near the anode and a slant near the cathode. Moreover, the distributive profiles of ionic concentrations change significantly from pH 1.0 to 6.0, while the distributions vary gradually from pH 6.0 to 10.0. In brief, it is known that the simulations shown in Figures 3.4 and 3.5 are consistent qualitatively with the experimental phenomena (Doi et al., 1992).

Figures 3.6(a)-(d) demonstrate the coupled influences of the solution pH and electric voltage on the distribution of electric potential ψ of the system. If $V_e = 0$, the distribution of electric potential ψ is symmetric in the whole domain and uniform

in the hydrogel strip, as shown in Figure 3.6(a). As an electric voltage is applied to the system as shown in Figures 3.6(b)-(d), the distribution of the electric potential ψ is unsymmetrical and non-uniform, where the gradients of electric potential ψ are observed over the hydrogel-solution interfaces. The larger difference of electric potential ψ near the anode leads to the larger concentration difference over the interfaces near the anode. Furthermore, the larger concentration difference near the anode, relatively compared with that near the cathode, results in the higher osmotic pressure near the anode. In addition, the collapse within the hydrogel domain will diminish with the increase of applied voltage. Thus the unequal osmotic pressures near to the anode and cathode cause the hydrogel bending (Homma et al., 2001).

Figures 3.7(a)-(d) illustrate the influence of pH on the distribution of fixed charge density c_f of the hydrogel responding to different electric voltages. It is known from these figures that the distribution of fixed charge density c_f of the hydrogel decreases when the voltage is applied to the system. The increase of the electric voltage makes the hydrogel strip swell and then the fixed charge groups redistribute within the hydrogel. The fixed charge groups redistribute and its corresponding density decreases since the electric voltage V_e causes the hydrogel strip to swell and bend. Along the pH-axis direction, the distributive profiles of fixed charge group increase rapidly from pH=1.0 to 6.0, and then gradually from pH 6.0 to 10.0, similarly to those of the diffusive ionic species Na^+ and Cl^- concentrations and electric potential ψ.

Figures 3.8(a)-(d) show the influence of the buffer solution pH on the

distribution of displacement u of the hydrogel under different electric voltages. It is seen from the figures that the displacement of the hydrogel strip changes dramatically with the electric-pH coupled stimuli. In the range of pH=2 to 6, if an electric voltage is applied, such as $V_e = 0.32$ V, the hydrogel strip swells obviously and the displacement is about 10 times larger than that of the hydrogel strip without electric stimulus. When pH is higher than 6, the effect of solution pH on the displacement of the hydrogel is insignificant and the displacement is distributed almost uniformly. This is a good example to demonstrate that the smart hydrogels responsive to the solution pH and electric voltage coupled stimuli can gain larger deformation and perform better mechanical strength. Thus they have a great potential for application as linear actuator in BioMEMS (Schreyer et al., 2000).

Figures 3.9-3.13 show the coupled effect of solution pH and electric voltage V_e on the variation of swelling ratio R_s and average curvature K_a of the hydrogel strip. Figure 3.9 illustrates that the effect of solution pH on the variation of swelling ratio R_s with $V_e = 0.4$ V. Figure 3.10 shows that the coupled effect of solution pH and external electric voltage V_e stimuli on the swelling ratio. It is observed from the figure that the swelling ratio R_s increases with the applied voltage V_e. Theoretically it is known that, the increment of the applied voltage V_e amplifies the osmotic pressure and makes the hydrogels swell. It is also seen that the swelling ratio R_s of the hydrogel strip changes dramatically with the coupled pH-electric stimuli, especially in the range of pH=1.0 to 6.0. In the range of pH=6.0 to 9.0 however, the effect of solution pH on the swelling ratio R_s is insignificant.

Figures 3.11 and 3.12 illustrate the coupled influences of the solution pH and the electric voltage on the average curvature K_a of the hydrogel. It is observed that the average curvature K_a of the hydrogel increases with the externally applied voltage V_e, especially under higher electric voltage V_e. Then the hydrogel in equilibrium state gains larger bending deformation, which is different from the behavior of the hydrogel responsive to the single stimulus, i.e. solution pH only. At the same level of electric voltage, the average curvature K_a increases dramatically from pH=1.0 to 4.0. However, it gains tiny increase in the range of pH=5.0 to 9.0. The deformation of the hydrogel may be produced by changes of two physical parameters (Kim et al., 2003; Lam et al., 2006). One is the change of the osmotic pressure due to the difference of ion concentrations between the inside and the outside hydrogel. It is the main driving force to make the hydrogel have swelling and bending deformations. The other is the change of applied electric voltage. The higher voltage results in the larger difference of the ionic concentration over the interfaces of the hydrogel. The concentration differences cause differences of the osmotic pressures at the two interfaces of the hydrogel, which makes the hydrogel bent. As a result, higher voltage V_e makes larger average curvature K_a, as shown in Figure 3.39. The predictions by the present simulations are consistent with the experimental phenomena (Bajpai, 2001).

3.5.2 Effect of Initially Fixed Charge Group Density

For discussion of the effect of initially fixed charge group density on the responsive behaviors of the hydrogels subject to the solution pH and electric field coupled stimuli, several simulations are carried out numerically with the input parameters required by the MECpHe model, R=8.314 J/mol·K , $F = 9.648\times10^4$ C/mol, T=298K, $\varepsilon_0 = 8.854\times10^{-12}$ C^2/Nm^2, $\varepsilon = 80$, $c^* = 4.0$ mM, $|z_k| = 1$, $c_f^s = 10.0$ mM, $z_f = -1$, $K = 10^{-2.1}$ mM, $\phi_0^w = 0.8$, $L = 2400$ μm, $h = 800$ μm, and the Young's modulus is 3.0MPa.

Figures 3.14 and 3.15 are plotted for the distribution of mobile ions Na^+ and Cl^- with coupled influences of solution pH and external electric voltage V_e ($V_e = 0.16$V) as well as initially fixed charge density, c_f^0=2.0, 4.0, 8.0 and 16.0mM, respectively. As shown in Figures 3.14(a)-(d), when the initially fixed charge density c_f^0 increases, the concentration distributions of the cation Na^+ increase within the hydrogel, and the gradient of ionic concentration within the hydrogel increases, which will enhance the osmotic pressure to swell the hydrogel strip. The increase of the initially fixed-charge density c_f^0 increases the concentrations of the cation within the hydrogels, which makes main contribution into the increment of the ionic concentration differences between the hydrogel-solution interfaces. Similarly, this leads to the increase of osmotic pressure and then the swelling of the hydrogel. The simulated results are consistent with the experimental phenomena (Fei et al., 2002).

Figures 3.16 and 3.17 show that coupled influences of solution pH and external electric voltage V_e ($V_e = 0.16$V) as well as initially fixed charge density on the profiles of electric potential ψ and fixed charge density c_f, where c_f^0=2.0, 4.0, 8.0

and 16.0mM, respectively. It is found that the collapse of electric potential ψ within the hydrogel enhances as the initially fixed charge density c_f^0 increases, while the gradient of ψ within the hydrogel diminishes, as shown in Figures 3.16(a)-(d). Additionally, it is found in Figures 3.17(a)-(d) that the fixed charge density increases obviously.

Figures 3.18-22 show that the coupled influences of solution pH and electric voltage V_e as well as initially fixed charge density c_f^0 on the mechanical deformation of the stimuli-sensitive hydrogel.

Figures 3.18(a)-(d) illustrates that the distributive profile of displacement u with the coupled influences of solution pH and electric voltage (V_e=0.16V) as well as initially fixed charge density c_f^0=2.0, 4.0, 8.0 and 16.0mM, respectively. It is seen that the displacement u increases dramatically with increment of the initially fixed charge density c_f^0. For example, the displacement increases about 10 times as c_f^0 changes from 2mM to 16.0mM.

Figures 3.19 and 22 illustrate the coupled influences of the solution pH and the electric voltage V_e as well as the initially fixed charge density c_f^s on the hydrogel curvature K_a, when the solution pH changes from 1.0 to 9.0 and the electric voltages V_e varies from 0 to 0.4V, and the initially fixed charge densities c_f^0=2.0, 4.0, 8.0 and 16.0mM, respectively. It is observed from the three figures that the average curvature K_a of the hydrogel strip increases with the externally applied voltage V_e. If the electric voltage V_e is higher, the hydrogel strip gains larger equilibrium bending deformation, which is different from the behavior of the hydrogel strip responsive to

the solution pH. At the given electric voltage V_e, the average curvature K_a increases dramatically from pH=1.0 to 4.0. However, it gains tiny increase in the range of pH=5.0 to 9.0. The deformation of the hydrogel may be produced by changes of two factors (Kim et al., 2003). One is the change of the osmotic pressure due to the difference of ionic concentrations between the inside and the outside hydrogels, which is the dominated driving source for swelling and bending deformations of the hydrogel strip. The increase of electric voltage results in the larger difference of the ionic concentration over the interfaces of the hydrogel. The ionic concentration differences cause differences of the osmotic pressures at the two interfaces of the hydrogel, which makes the hydrogel strip bent. As a result, the increase of electric voltage V_e makes larger average curvature K_a, as shown in Figures 3.29-31. The other is the conformational change of crosslinked polymer chains due to the pH change in the hydrogel. The increase of pH within the hydrogel leads to the change of the carboxylic acid groups from $\mathrm{R-COOH}$ to $\mathrm{R-COO^-}$. The change from weak polyelectrolyte to strong one means the increase of the electrorepulsive interaction between the carboxylic acid groups. Therefore, the conformation of the polymeric chains changes from the compact state to the expanded one, and then the hydrogel swells. A close look into the figures reveals that the significant increase of the equilibrium swelling and bending of the hydrogel in micro-scale occur in the range of solution pH=2.0 to 4.0, which is close to the dissociation constant of the hydrogel, $pK_a = 2.1$. The carboxylic groups at $\mathrm{pH} \geq 4.0$ are totally ionized, which may be the reason for the tiny increase of K_a in the range of pH=5.0 to 9.0. The predictions by the present simulations are

consistent with the experimental phenomena (Bajpai, 2001), in which it is reported that the local pH gradient attributed to water electrolysis may be additional factor to influence the bending deformation (Lam et al., 2006).

Figures 3.20 and 3.21 are plotted for the coupled effect of the initially fixed charge density c_f^0 and electric voltage V_e as well as solution pH on variation of the swelling ratio R_s with pH=4.0 and $V_e = 0.4$ V. It is shown from the figures that the swelling ratio R_s increases with the initially fixed charge density c_f^0. The present simulation results qualitatively agree well with the experimental results (Fei et al., 2002).

3.5.3 Effect of Ionic Strength

As promising materials for sensors, actuators and artificial muscles for biomedical engineering applications, the mechanical properties of pH-electric-sensitive hydrogels are particularly concerned. It is known that the mechanical force is generated by osmotic pressure, which is governed by the ionic transport through the system, and is affected by the hydrogel architecture (Chiarelli and Rossi, 1996; Carlson et al., 2003). In order to investigate the effect of the ionic strength I ($I = 0.5 * \sum_k c_k z_k^2$) on the bending deformation of the hydrogels, several simulations are conducted numerically with the input parameters for the MECpHe model, R=8.314 J/mol·K , $F = 9.648 \times 10^4$ C/mol, T=298K, $\varepsilon_0 = 8.854 \times 10^{-12}$ C^2/Nm^2, $\varepsilon = 80$, $z_f = -1$, $K = 10^{-2.1}$ mM, $\phi_0^w = 0.8$, $L = 2400$ μm, $h = 800$ μm, and the

Young's modulus is equal to 3.0MPa.

Figures 3.23 and 3.24 illustrate that the distributive profiles of the electric potential ψ and fixed charge density c_f with coupled influences of solution pH and external electric voltage (V_e=0.16V) as well as ionic strength I=2.0, 4.0, 8.0 and 16.0mM. It is found that as the ionic strength I increases, the gradient of electric potential ψ increases within the hydrogel, while the collapse of ψ diminishes and the electric potential ψ distributes linearly in the whole domain covering the hydrogel and bathing solution, especially at high ionic strength *I*. Theoretically, the higher ionic strength makes the mobile ions diffuse more into the hydrogel, then the conductivity of hydrogels is almost equal to that of surrounding solutions, which results in the electric potential ψ quasi-linearly distribute in the whole domain. From Figure 3.24, it is known that the fixed charge density c_f and the corresponding gradient in the hydrogel increase with the ionic strength *I*. It is noted that the dissociation of carboxylic groups in the polymeric chains imparts ionic character to the hydrogels and affects the ion osmotic swelling pressure (Bajpai, 2001). In fact, the enhancement of the ionic strength *I* endows more to the increase of the concentration in the surrounding solution, relatively compared with the contribution to that in the hydrogels. This reduces the concentration differences of diffusive ions between the hydrogel-solution interfaces. The reduction of concentration differences decreases the osmotic pressure. It is also observed from the experimental swelling phenomena of polyelectrolyte gels that the osmotic pressure reduces ultimately the equilibrium swelling capacity of the hydrogels (Khare and Peppas, 1995). Thus the hydrogels

shrink.

Figures 3.25-34 show that the coupled influences of solution pH and electric voltage V_e as well as initially fixed charge density c_f^0 on the mechanical deformation of the stimuli-sensitive hydrogel.

Figures 3.25(a)-(d) illustrate that the distributive profiles of displacement u with the coupled influences of solution pH and electric voltage (V_e=0.16V) as well as ionic strength I. The displacement u decreases with increase of ionic strength. As mentioned above, the increase of I will reduce the osmotic pressure and thus cause the hydrogel deswelling. However, the average curvature K_a increases with the enhancement of ionic strength. Figures 3.26(a)-(d) show the coupling influences of the solution pH, the electric voltage V_e and the solution ionic strength *I* on the hydrogel curvature K_a, in which $c_f^s = 10.0$ mM, the range of solution pH is from 1.0 to 9.0, the range of electric voltages V_e from 0 to 0.4V, and the different solution ionic strengths *I* =2.0, 4.0, 8.0 and 16.0mM, respectively. Figures 3.27-3.30 illustrate the influence of the ionic strength *I* on the average curvature K_a at pH=4.0 and V_e=0.4V, respectively. It is observed that the average curvature K_a of the hydrogel increases with the externally applied voltage V_e, namely the hydrogel gains larger equilibrium bending deformation at higher electric voltage V_e. But the characteristics of the hydrogels in response to the solution pH are different. The average curvature K_a under the same electric voltage increases dramatically from pH=1.0 to 4.0. However, it gains the slight increment in the range of pH=5.0 to 9.0. The deformation of the hydrogel may be mainly driven by the change in the osmotic pressure (Shiga et al., 1992), which is

generated by the difference of ion concentrations between the interior hydrogels and exterior solution. The higher voltage results in the larger ionic concentration differences over the interfaces between the hydrogel and solution. The differences of ion concentration result in the difference of the osmotic pressures at the two sides of the hydrogel, which makes the hydrogel bent. Therefore, the higher voltage V_e gains the larger average curvature K_a, as shown in the Figures 3.26(a)-(d). A numerical observation from the figures reveals that a significant increase in the equilibrium swelling and bending of the hydrogel occurs in the range of solution pH= 2.0-4.0, which is associated with the dissociation constant $pK_a = 2.1$ of the hydrogels. If the solution pH is larger than 4.0, the carboxylic groups may be totally ionized, which could be the reason for the tiny increase of K_a in the range of pH=5.0-9.0. The simulation results are consistent with the experimental phenomena (Bajpai, 2001). It is found from the four figures that, under the solution pH and externally applied electric voltage V_e coupled stimuli, the average curvature K_a of the hydrogel increases with the ionic strength *I*, in which the increment K_a is not linear and will be slow down with the ionic strength *I*. It is known that, with increase of the ionic strength of the system medium, the osmotic pressure decreases, and ultimately reduces the equilibrium swelling capacity of the hydrogels (Lam et al., 2006). However, the increase of the ionic strength (electrolyte concentration) induces the increase of mobile counterions diffusing into the hydrogel. Due to the fixed charge groups existing in the hydrogel subject to electric field, the redistribution of the counterions makes the larger difference of ionic concentrations at both the ends of the hydrogel, which enlarges the

difference of the osmotic pressures over the two interfaces between the hydrogel and the surrounding solution. Therefore, the bending deformation of the hydrogel increases further and the average curvature K_a increases as well. The influence of ionic strength I may be weakened by the shielding effect of the fixed charge groups (Kim et al., 2004), and the average curvature K_a decreases gradually under higher ionic strength, as shown in Figure 3.29. The simulations agree well qualitatively with the published experimental studies (Kim et al., 2004a, 2004b).

Figures 3.31-34 are plotted for the coupled effect of the ionic strength I and electric voltage V_e as well as solution pH on the variation of swelling ratio R_s at pH=4.0 and $V_e = 0.4$ V, respectively. It is found that the swelling ratio R_s decreases with increment of the ionic strength I. In fact, the increase of ionic strength I makes more contribution to the increase of the concentration in the surrounding solution, relatively compared with the contribution to that in the hydrogels. This reduces the concentration differences of diffusive ions between the hydrogel-solution interfaces, and thus it decreases the osmotic pressure, which causes the hydrogels shrinking. The details how ionic strength influences the pH sensitivity of the hydrogels will require more systematic investigation, particularly in the case of multivalent ions (Mao and McShane, 2006).

3.5.4 Effect of Ionic Valence

In order to gain further insight into the effects of various physical parameters

on the responsive behaviors of the hydrogels to the coupled stimuli of the solution pH and electric field, several simulations are carried out numerically with the input parameters required by the MECpHe model, R=8.314 J/mol·K , $F = 9.648\times10^{4}$ C/mol, T=298K, $\varepsilon_0 = 8.854\times10^{-12}$ C^2/Nm^2, $\varepsilon = 80$, $c^* = 4.0$ mM, $c_f^0 = 10.0$ mM, $z_f = -1$, $K = 10^{-2.1}$ mM, $\phi_0^w = 0.8$, $L = 2400$ μm, $h = 800$ μm, and the Young's modulus is 3.0MPa. The simulation results are illustrated as follows for the influence of the ionic valence $|z_k|$ on the responsive distributions of the diffusive ionic concentrations c_k, the electric potential ψ, the fixed charge density c_f and the mechanical deformation of hydrogel strip.

Figures 3.35 and 3.36 show that the coupled effects of solution pH and external electric voltage (V_e=0.16V) as well as ionic valence ($|z_k|$=1, 2 and 3) on the distributive profiles of mobile cation and anion concentrations. It is noted that the distributive concentrations of diffusive cation species within the hydrogel reduces when $|z_k|$ increases. In fact, in order to maintain the electroneutrality within the hydrogel, the cations diffuse into the hydrogel to neutralize the fixed charges ($c_f^0 = 10.0$ mM, $z_f = -1$) on the network chains. Simply considering the ion-exchange process, it needs 10.0mM monovalent cations to neutralize the fixed charge on the chains. However, it needs 5.0mM divalent cations only. Therefore, when the surrounding solution is changed from monovalent electrolyte to bivalent or trivalent one, the concentration difference of diffusive cations decreases significantly between the hydrogel and solution, the variation of the concentration distributions is relatively small for the diffusive anions. This gives rise to the smaller osmotic pressure and then

makes the hydrogels shrinking.

Figures 3.37 and 3.38 show that the distributive profiles of the electric potential ψ and fixed charge density c_f with coupled influences of solution pH and external electric voltage (V_e=0.16V) as well as ionic valence ($|z_k|$=1, 2 and 3). It is found that as the ionic valence $|z_k|$ increases, the gradient of electric potential ψ increases within the hydrogel, while the collapse of ψ diminishes and the electric potential ψ distributes linearly in the whole domain covering the hydrogel and bathing solution, especially at larger ionic valence.

Figures 3.39-43 show that the coupled influences of solution pH and electric voltage V_e as well as ionic valence $|z_k|$ on the mechanical deformation of the stimuli-sensitive hydrogel.

Figures 3.39(a)-(c) illustrate the profile of displacement u of the hydrogel strip. It is noted that, when the surrounding solution is changed from monovalent electrolyte to bivalent or trivalent one, the osmotic pressure decreases dramatically over the interface between the hydrogel and surrounding solution. Thus, the displacement u of the hydrogel decreases, especially when monovalent electrolyte changes to divalent one, as shown in the figures.

Figures 3.40-41 are plotted for the coupled effect of the ionic valence $|z_k|$ and electric voltage V_e as well as solution pH on the variation of the average curvature K_a at pH=4.0 and $V_e = 0.4$ V, respectively. It is found that the average curvature K_a increase slightly with increment of the ionic valence $|z_k|$. However, it is found that the swelling ratio R_s decreases with increment of the ionic valence $|z_k|$,

as shown in Figures 3.42 and 3.43. Similar results are also reported elsewhere (Horkay et al., 2001; Bajpai and Dubey, 2005). From the above study it can be concluded that presence of divalent ions in the intestinal fluid may cause a great volume transition in the swollen gel. This in turn may affect the drug releasing capacity of the hydrogel.

3.6 Remarks

In this chapter, the equilibrium responsive behaviors of stimulus-sensitive hydrogels have been modeled and simulated subject to coupled stimuli of the solution pH and the externally applied electric field. The results obtained by the present MECpHe model agree well with published experimental data, both qualitatively and quantitatively. The influence of various physical parameters on the degree of swelling is investigated. Specifically, by increasing the externally applied electric voltage and the fixed charge density or by lowering the ionic strength of the solution, the swelling deformation can be improved.

The MECpHe model can be used theoretically to explain the experimental phenomena of the distribution of ionic concentration, electric potential and network deformation. The developed model can predict numerically the distribution of diffusive ionic concentration in both the hydrogel and the surrounding solution, the distribution of electric potential in both the hydrogel and the surrounding solution, the degree of equilibrium swelling, the displacement and curvature of the pH-electric-sensitive hydrogels. The modeling and simulation work would be useful for design optimization

of the sensors/actuators, micro-fluidic valves and drug delivery systems based on the pH-electric-sensitive hydrogels.

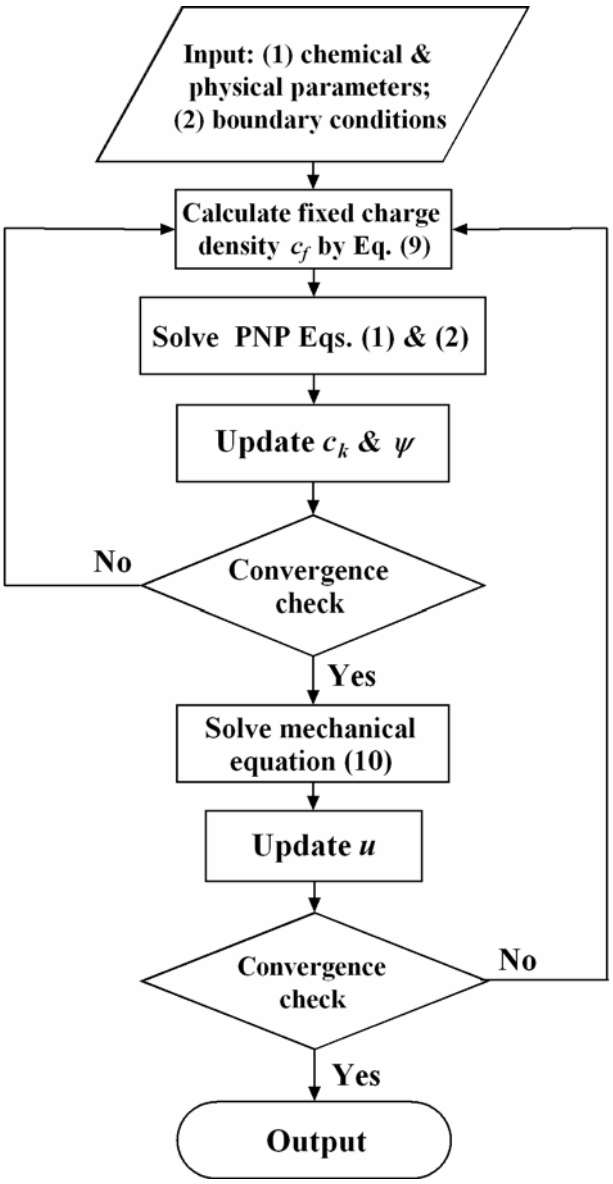

Figure 3.1 Computational flowchart of the developed MECpHe model.

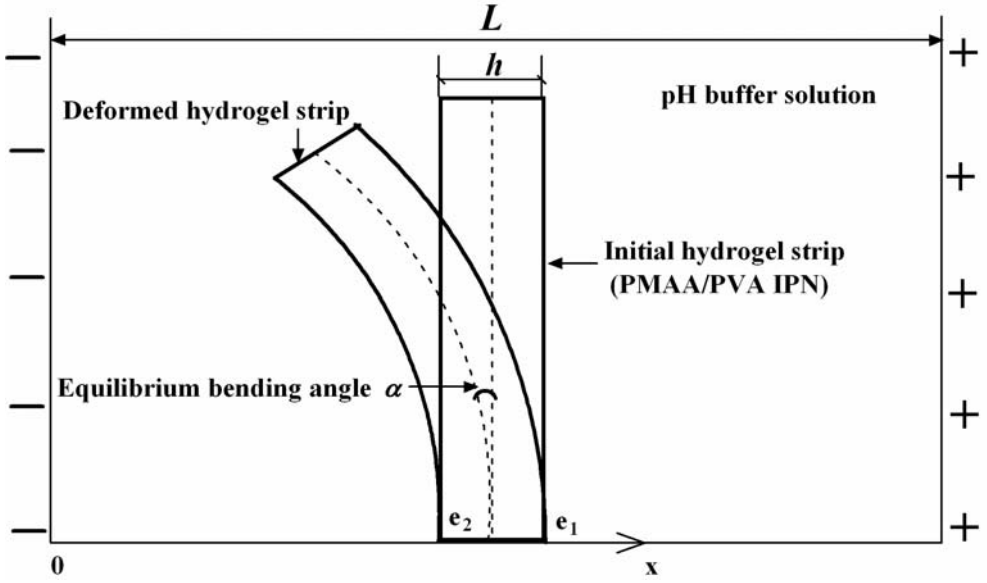

Figure 3.2 Schematic diagram for a hydrogel strip immersed in pH buffer solution subject to an externally applied electric field.

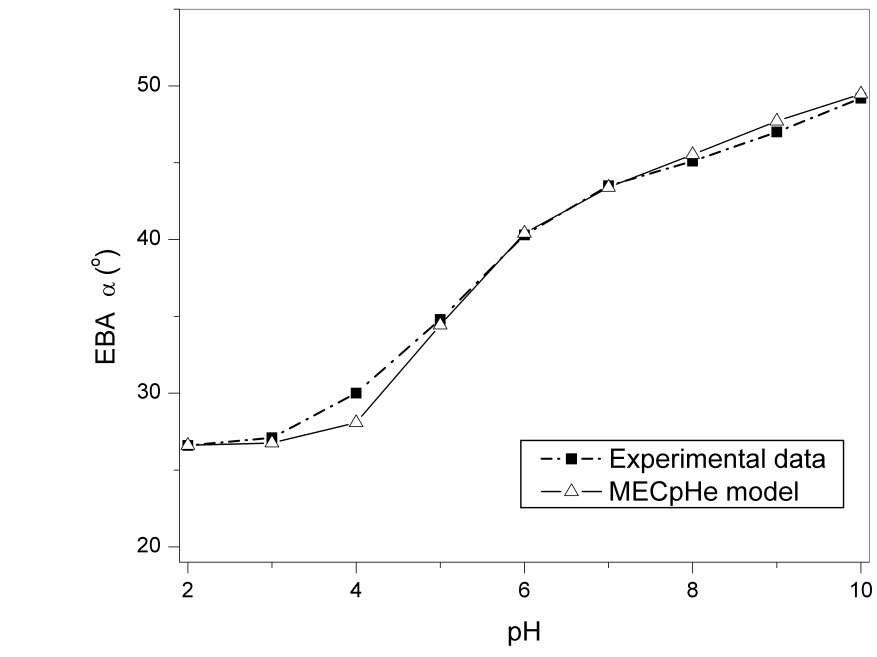

Figure 3.3 Comparison of numerically computed results with experimental data (Kim et al., 2004b).

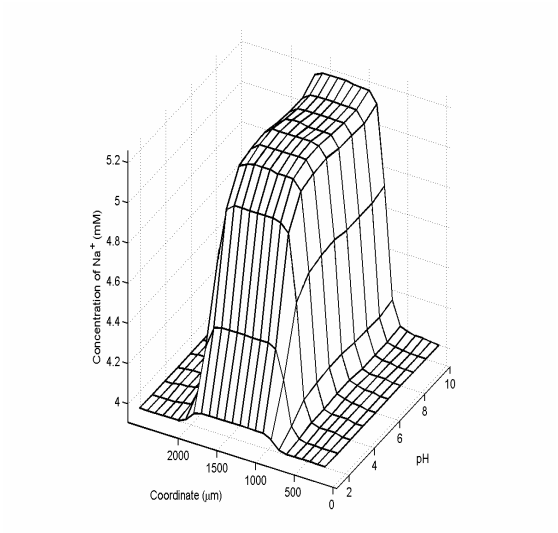

(a) $V_e = 0$

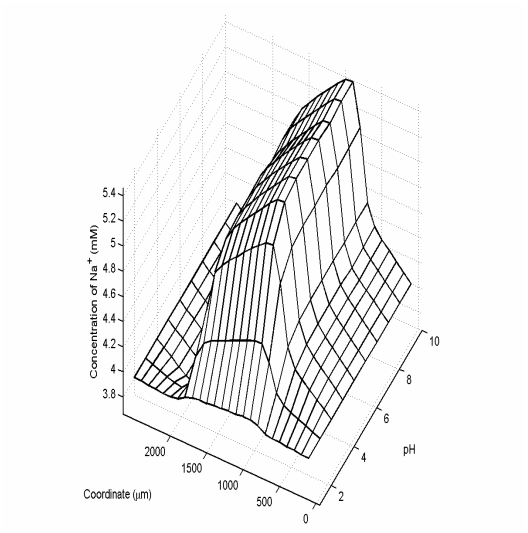

(b) $V_e = 0.08\text{V}$

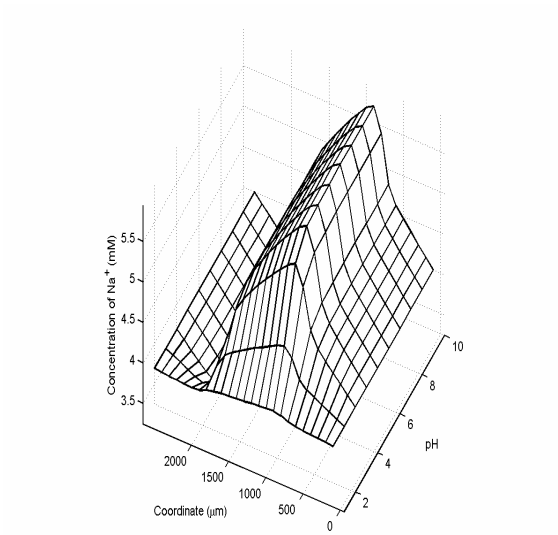

(c) $V_e = 0.16\text{V}$

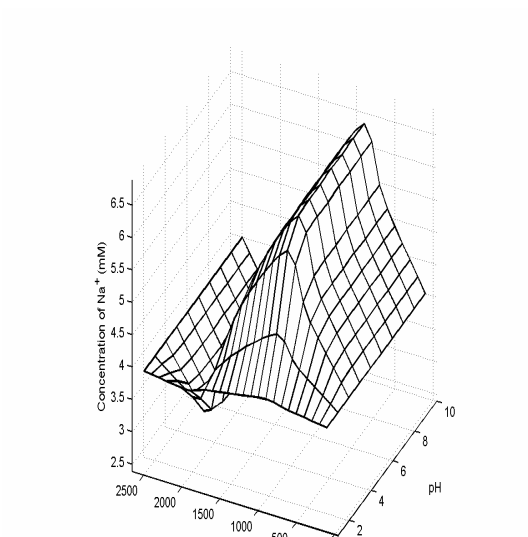

(d) $V_e = 0.32\text{V}$

Figure 3.4 Coupled effects of solution pH and external electric voltage V_e on distributive profiles of Na^+.

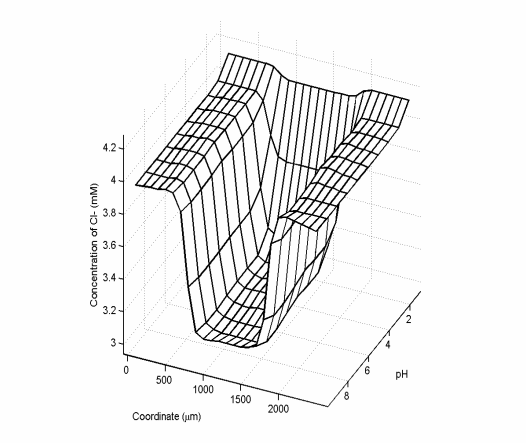

(a) $V_e = 0$

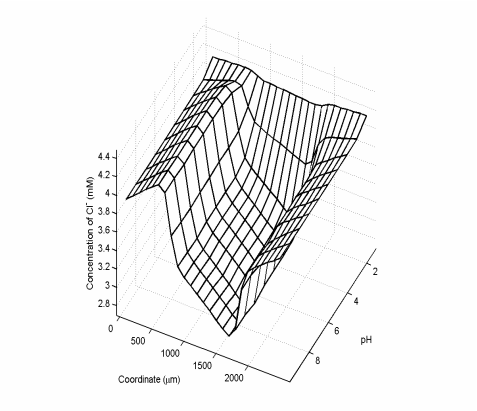

(b) $V_e = 0.08\text{V}$

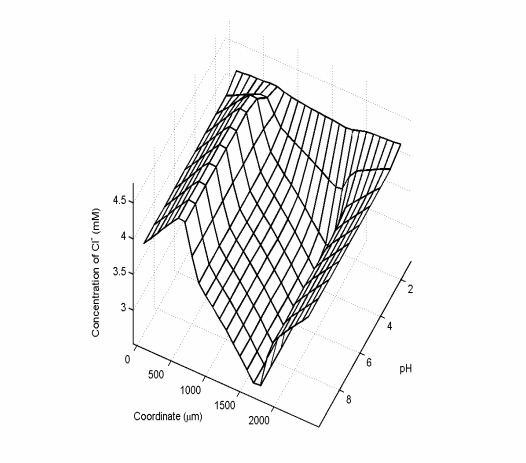

(c) $V_e = 0.16\text{V}$

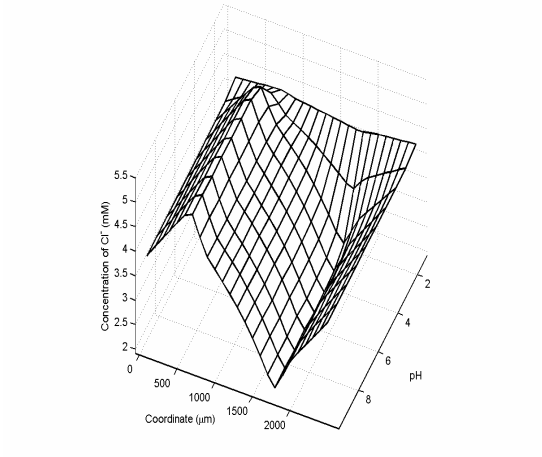

(d) $V_e = 0.32\text{V}$

Figure 3.5 Coupled effects of solution pH and external electric voltage V_e on distributive profiles of Cl^-.

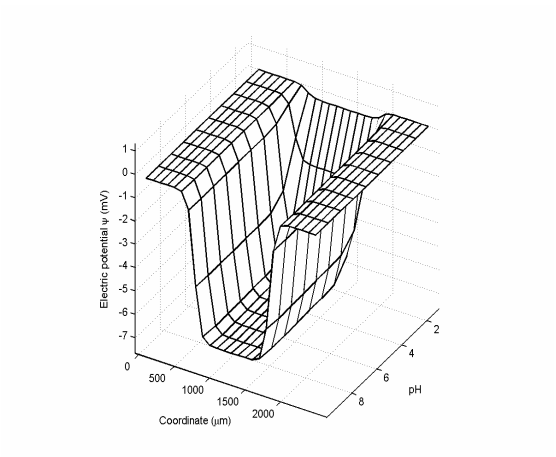

(a) $V_e = 0$

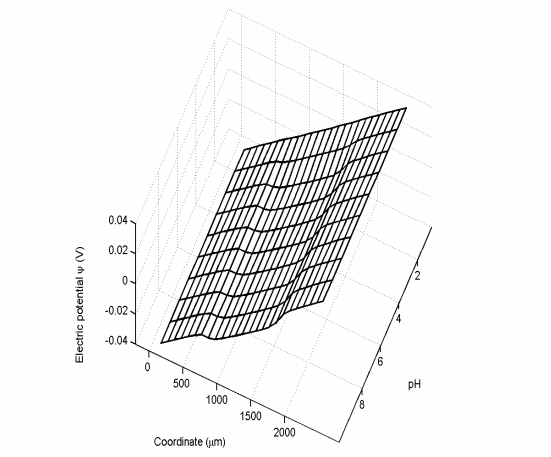

(b) $V_e = 0.08\text{V}$

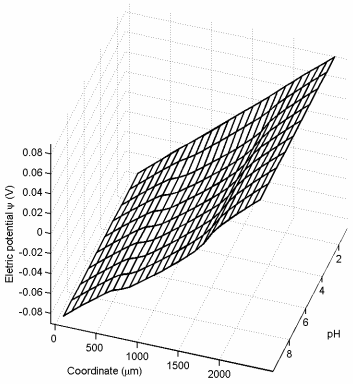

(c) $V_e = 0.16\text{V}$

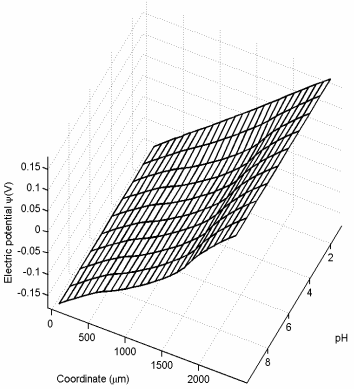

(d) $V_e = 0.32\text{V}$

Figure 3.6 Coupled effects of solution pH and external electric voltage V_e on distributive profiles of electric potential ψ.

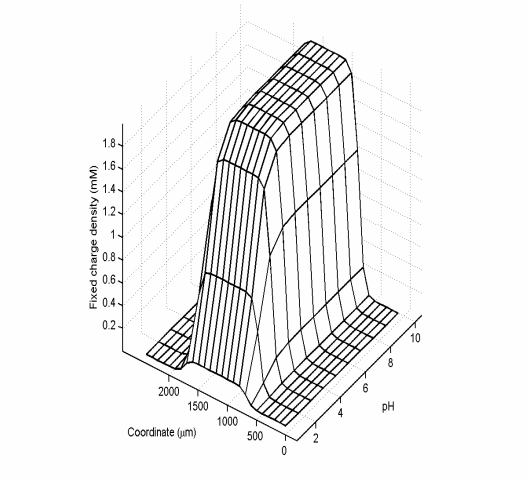

(a) $V_e = 0$

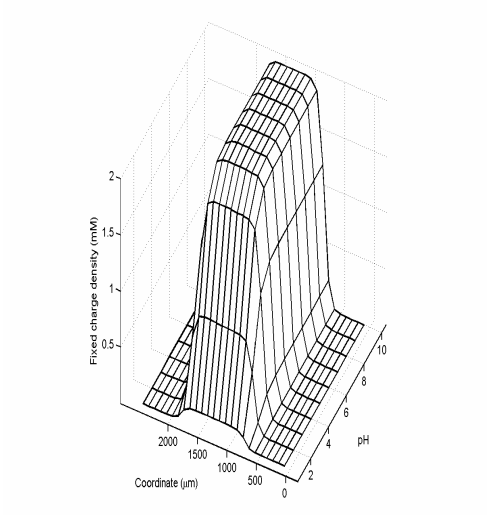

(b) $V_e = 0.08\text{V}$

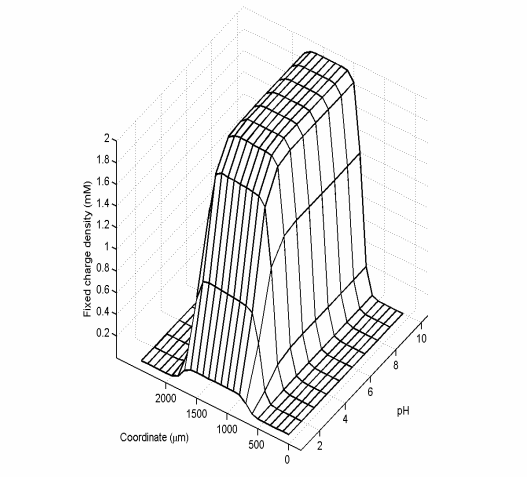

(c) $V_e = 0.16\text{V}$

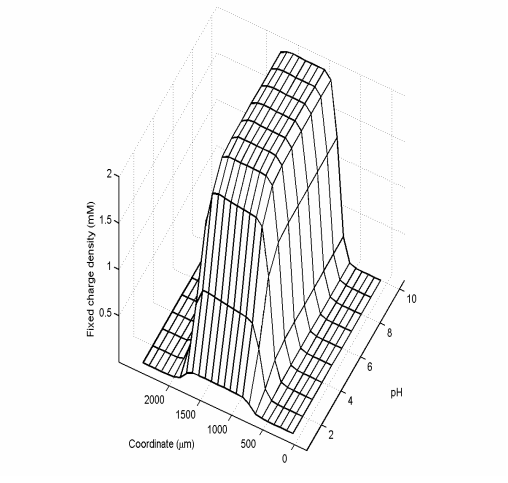

(d) $V_e = 0.32\text{V}$

Figure 3.7 Coupled effects of solution pH and external electric voltage V_e on distributive profiles of fixed charge density c_f.

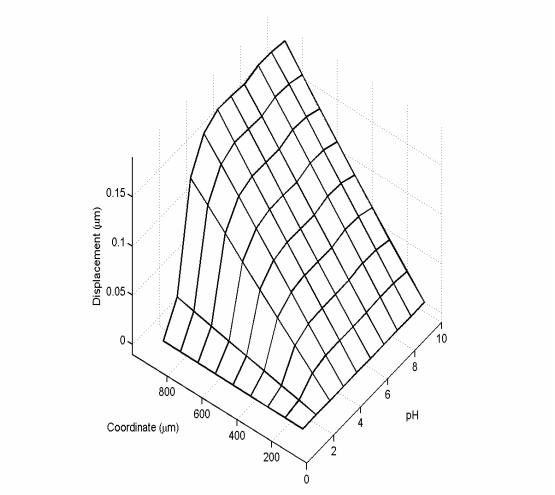

(a) $V_e = 0$

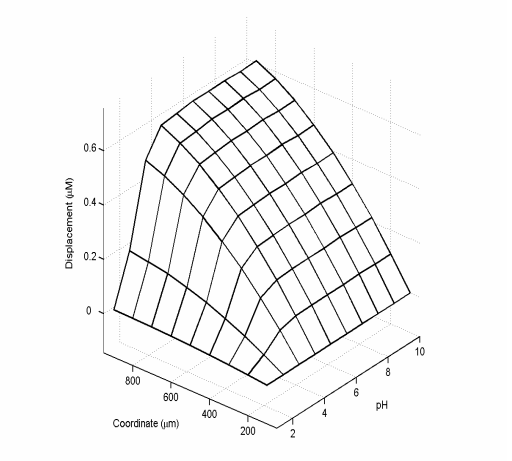

(b) $V_e = 0.08\text{V}$

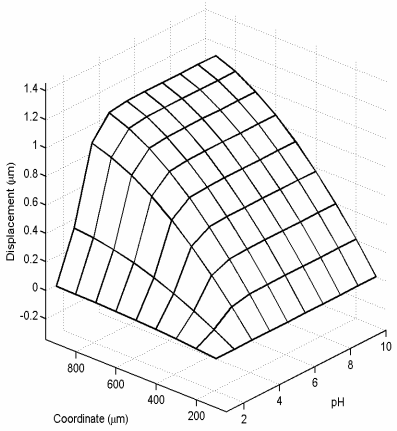

(c) $V_e = 0.16\text{V}$

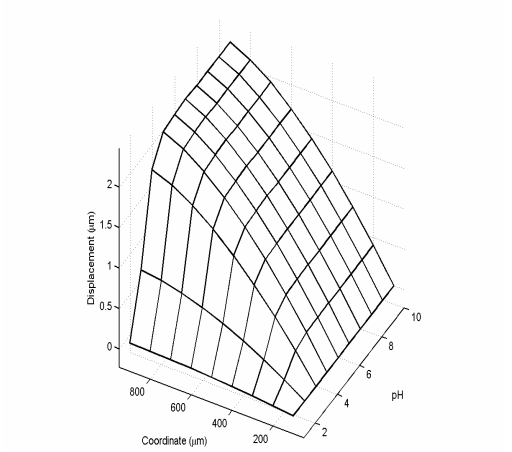

(d) $V_e = 0.32\text{V}$

Figure 3.8 Coupled effects of solution pH and external electric voltage V_e on distributive profiles of displacement u of the hydrogel strip.

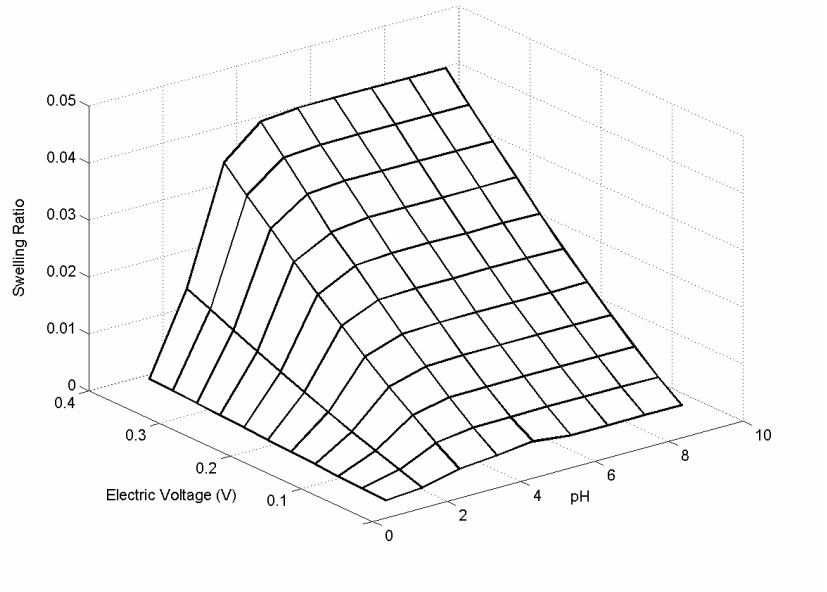

Figure 3.9 Coupled effects of electric voltage V_e and solution pH stimuli on variation of swelling ratio R_s.

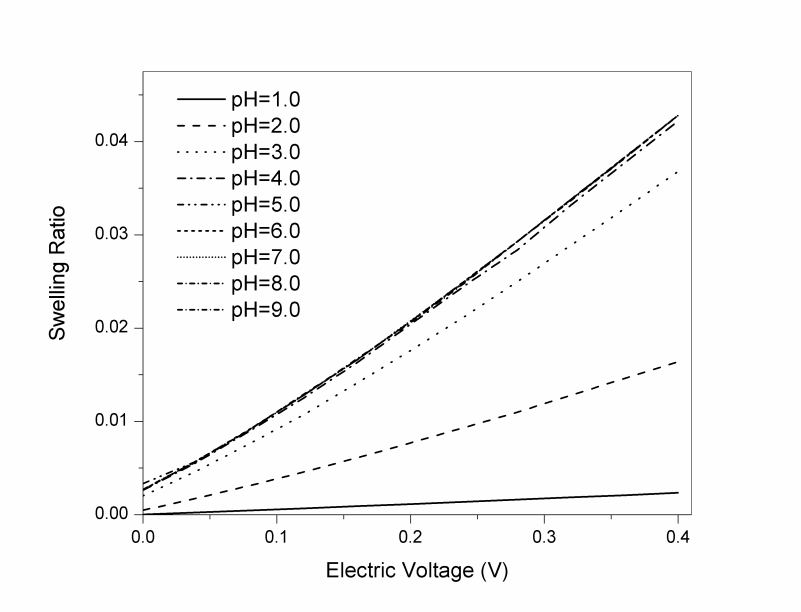

Figure 3.10 Distribution of swelling ratio R_s of hydrogel strip responding to the coupled stimuli of solution pH and external electric field V_e.

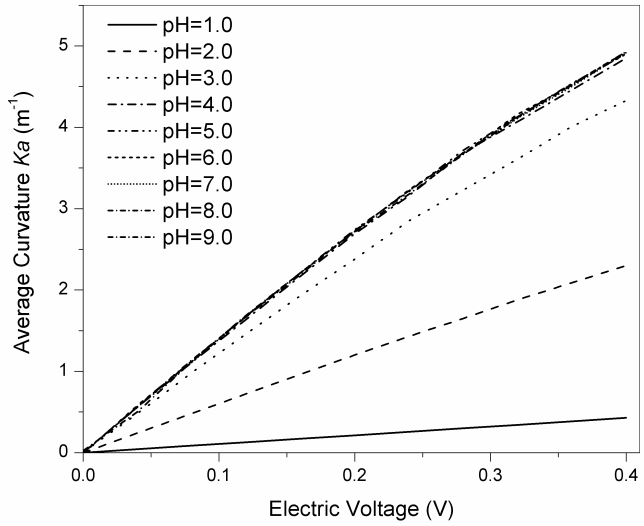

Figure 3.11 Profile of curvature K_a of hydrogel strip responding to the coupled stimuli of solution pH and external electric field V_e.

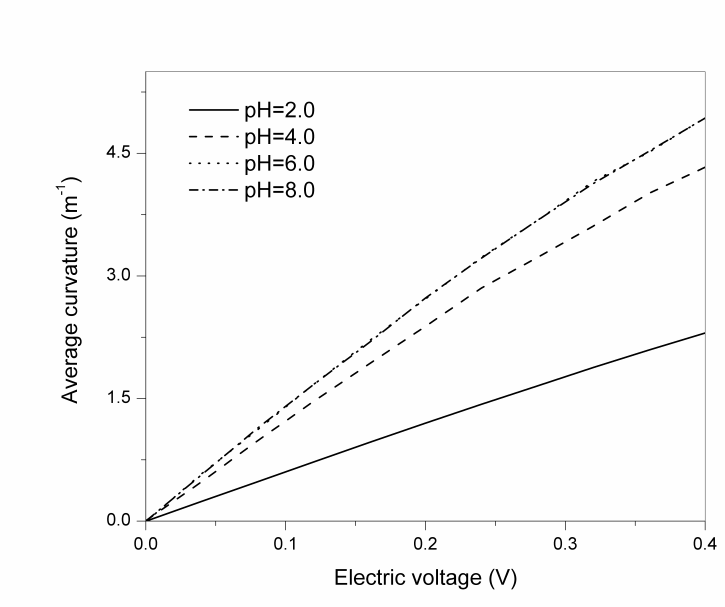

Figure 3.12 Variation of curvature K_a of hydrogel strip responding to the stimulus of external electric field V_e.

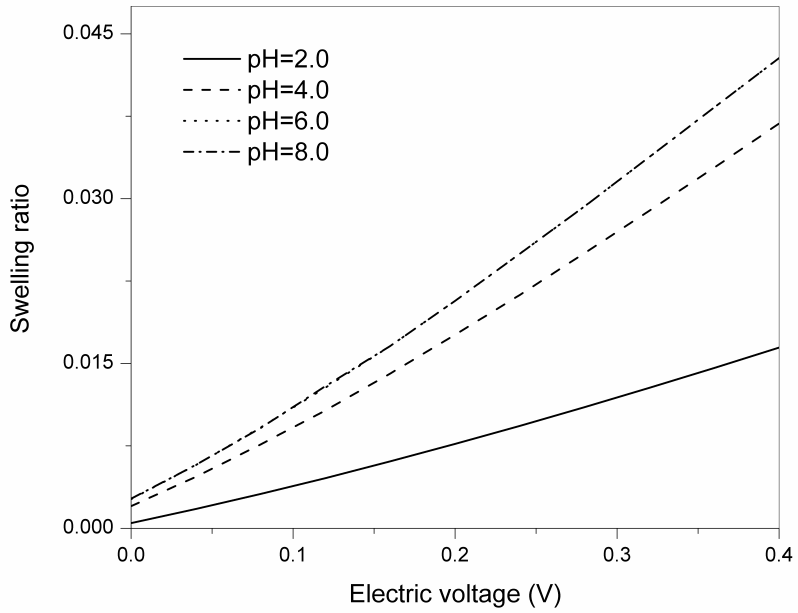

Figure 3.13 Variation of swelling ratio R_s of hydrogel strip responding to the stimulus of external electric field V_e.

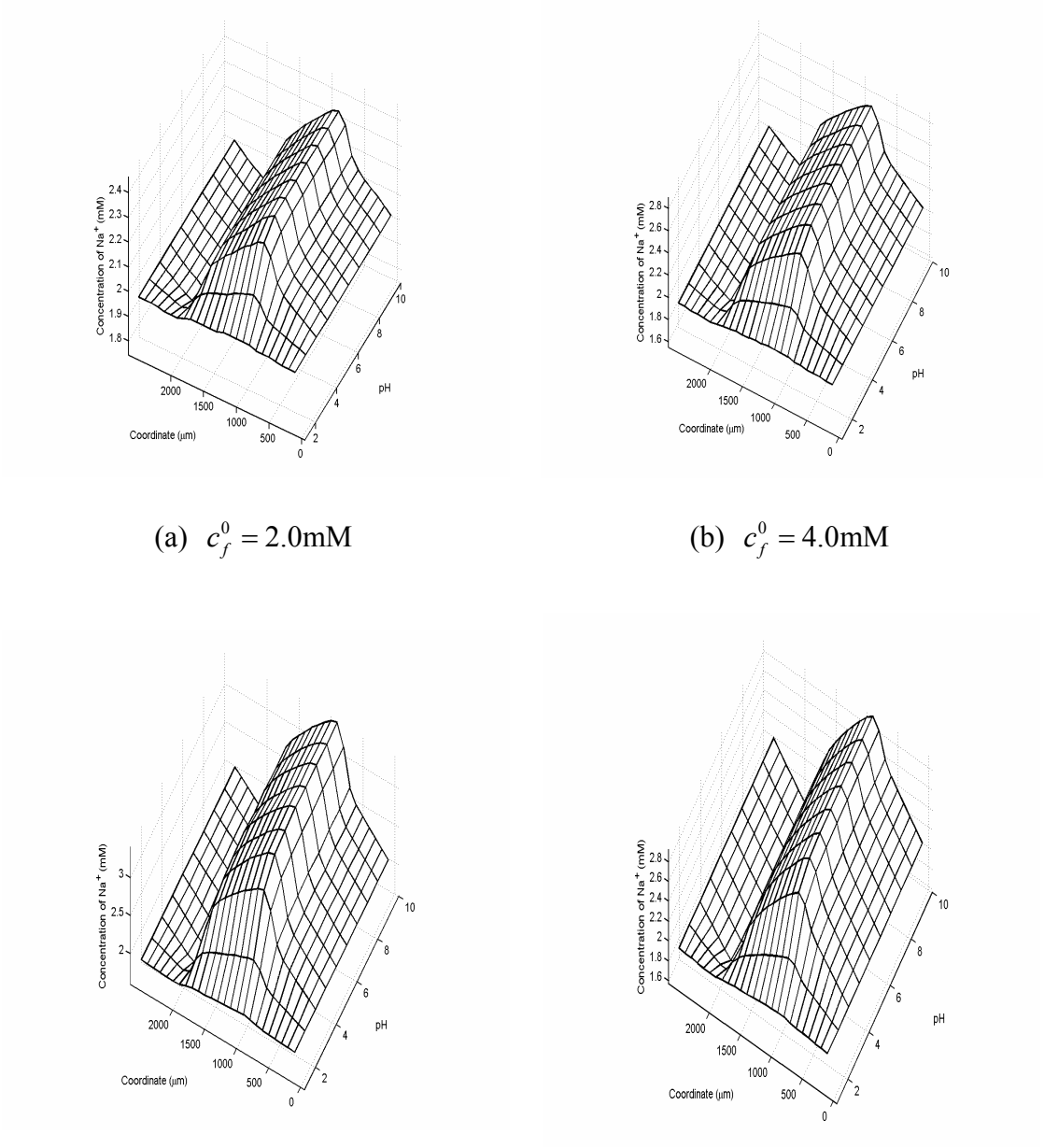

(a) $c_f^0 = 2.0\text{mM}$ (b) $c_f^0 = 4.0\text{mM}$

(c) $c_f^0 = 8.0\text{mM}$ (d) $c_f^0 = 16.0\text{mM}$

Figure 3.14 Distributive profiles of Na^+ with coupled influences of solution pH and external electric voltage V_e as well as initially fixed charge density c_f^0 (V_e=0.16V).

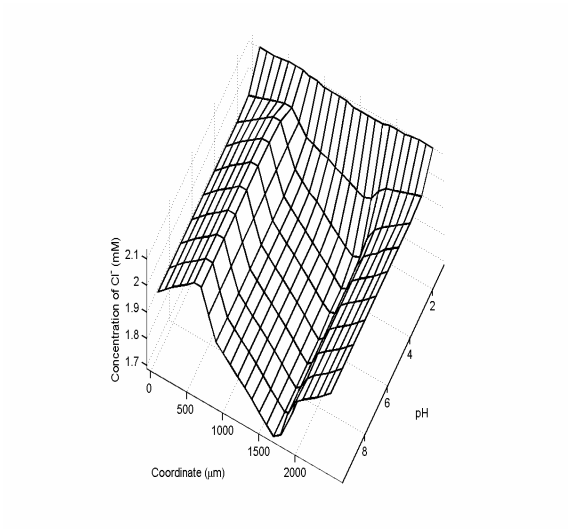

(a) $c_f^0 = 2.0\text{mM}$

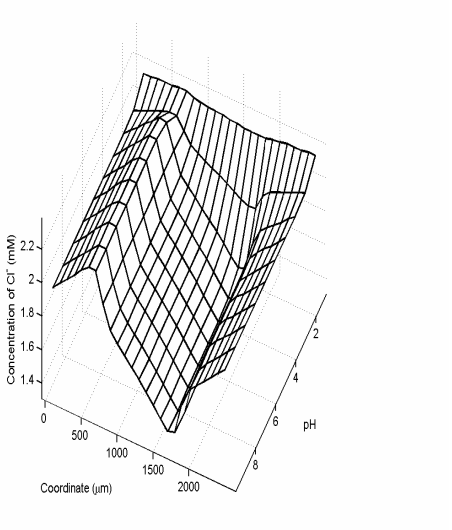

(b) $c_f^0 = 4.0\text{mM}$

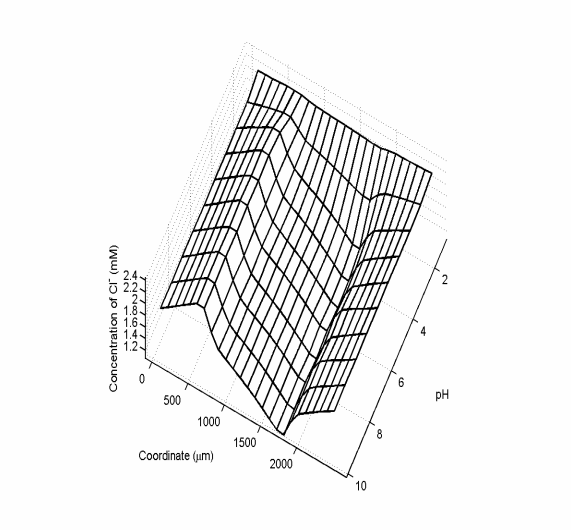

(c) $c_f^0 = 8.0\text{mM}$

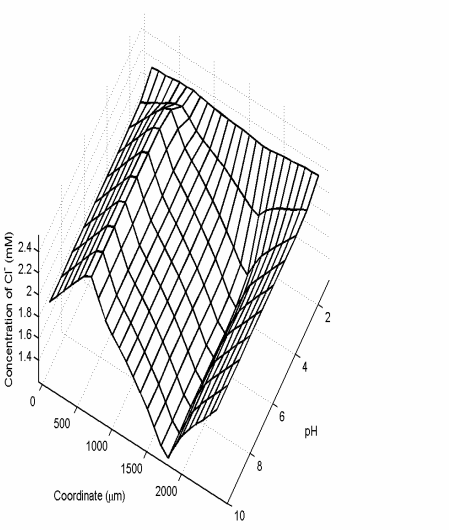

(d) $c_f^0 = 16.0\text{mM}$

Figure 3.15 Distributive profiles of Cl^- with coupled influences of solution pH and external electric voltage V_e as well as initially fixed charge density c_f^0 (V_e=0.16V).

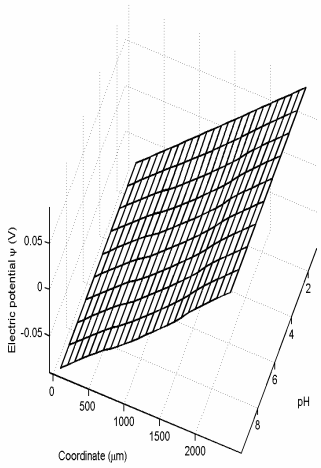

(a) $c_f^0 = 2.0\text{mM}$

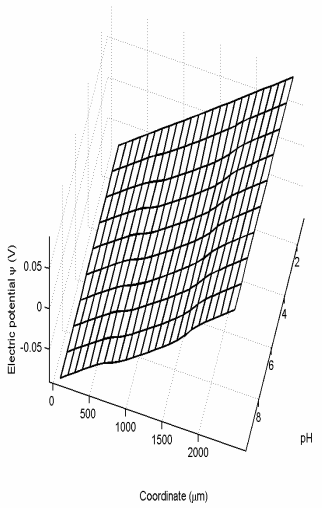

(b) $c_f^0 = 4.0\text{mM}$

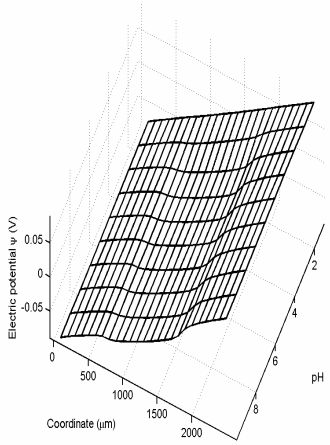

(c) $c_f^0 = 8.0\text{mM}$

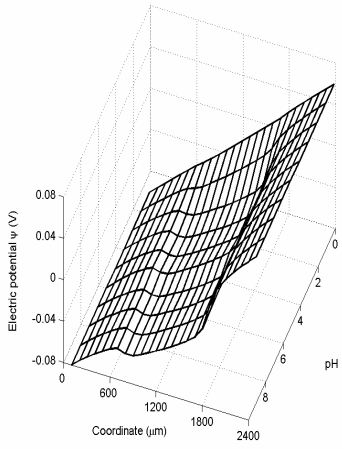

(d) $c_f^0 = 16.0\text{mM}$

Figure 3.16 Distributive profiles of electric potential ψ with coupled influences of solution pH and external electric voltage V_e as well as initially fixed charge density c_f^0 (V_e=0.16V).

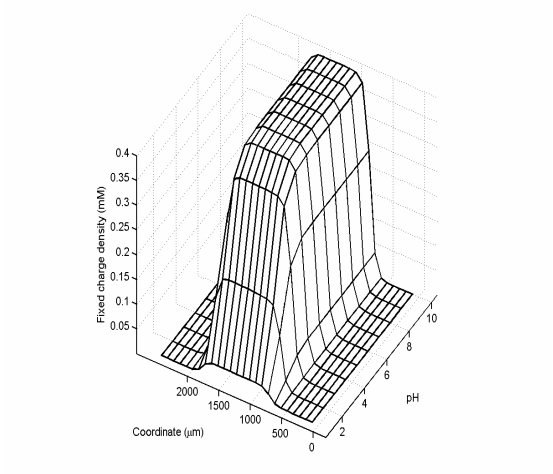

(a) $c_f^0 = 2.0\text{mM}$

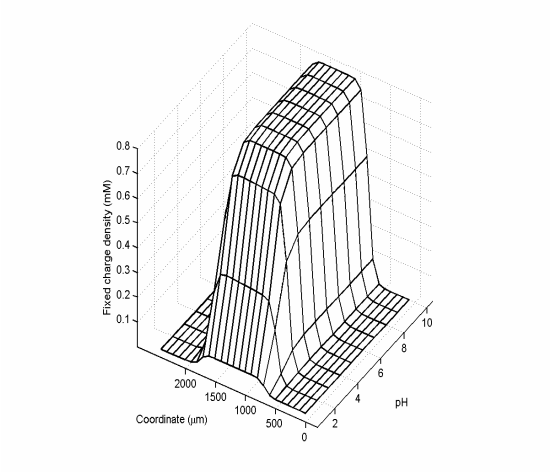

(b) $c_f^0 = 4.0\text{mM}$

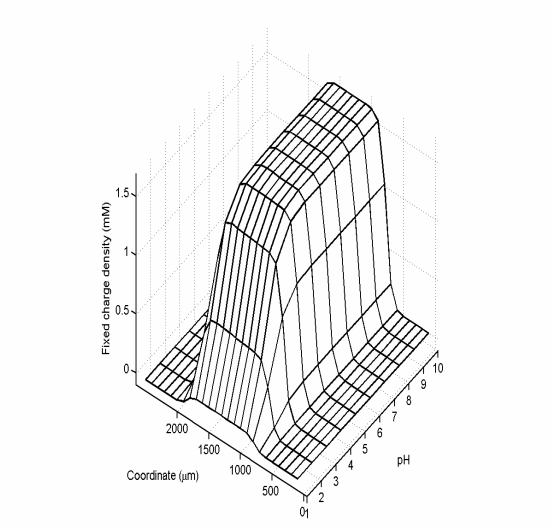

(c) $c_f^0 = 8.0\text{mM}$

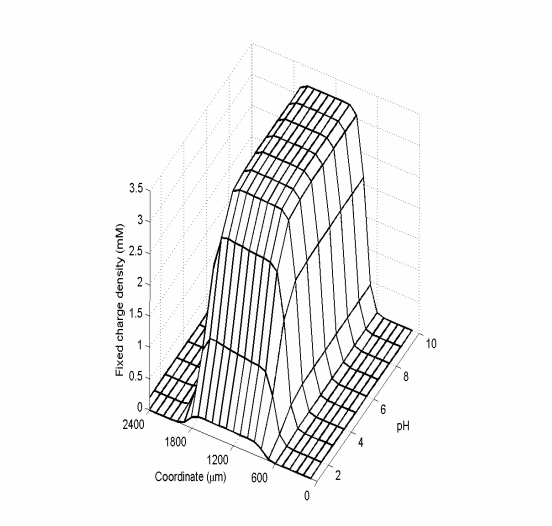

(d) $c_f^0 = 16.0\text{mM}$

Figure 3.17 Distributive profiles of fixed charge density c_f with coupled influences of solution pH and external electric voltage V_e as well as initially fixed charge density c_f^0 (V_e=0.16V).

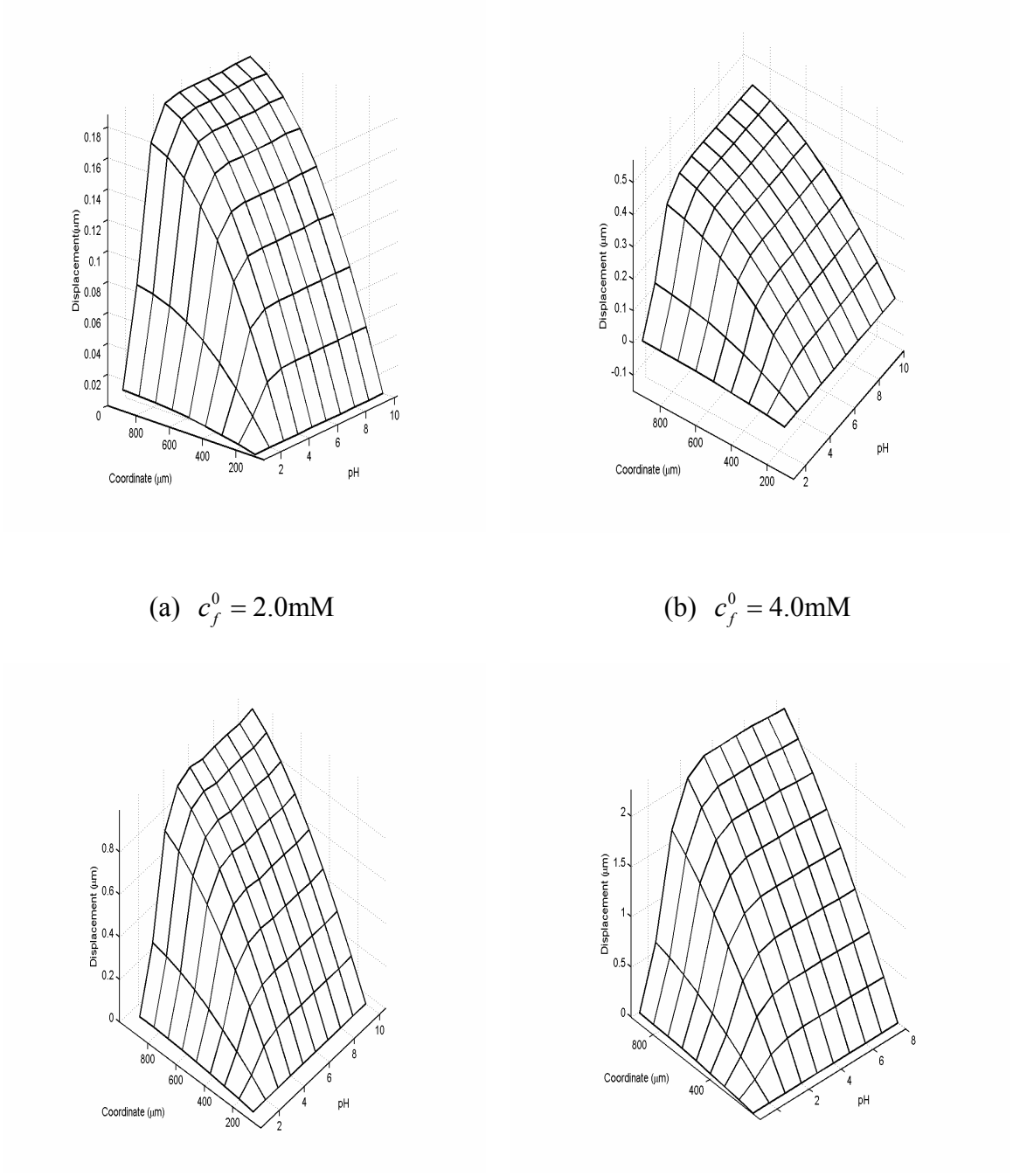

(a) $c_f^0 = 2.0\text{mM}$ (b) $c_f^0 = 4.0\text{mM}$

(c) $c_f^0 = 8.0\text{mM}$ (d) $c_f^0 = 16.0\text{mM}$

Figure 3.18 Distributive profiles of displacement u with coupled influences of solution pH and external electric voltage V_e as well as initially fixed charge density c_f^0 (V_e=0.16V).

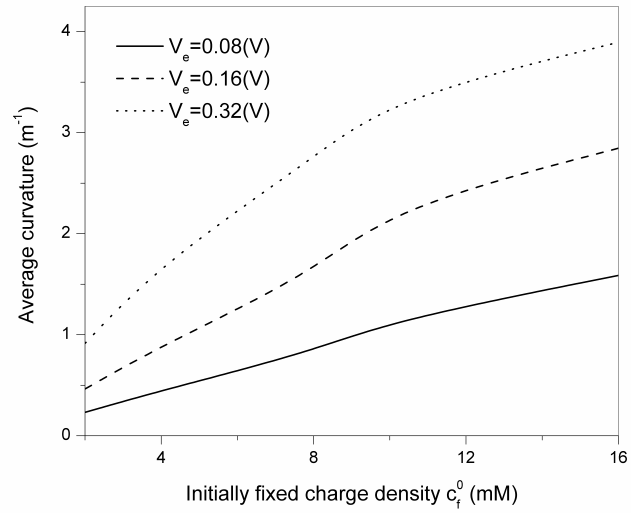

Figure 3.19 Coupled effect of initially fixed charge density c_f^0 and electric voltage V_e as well as solution pH on variation of average curvature K_a (pH=4.0).

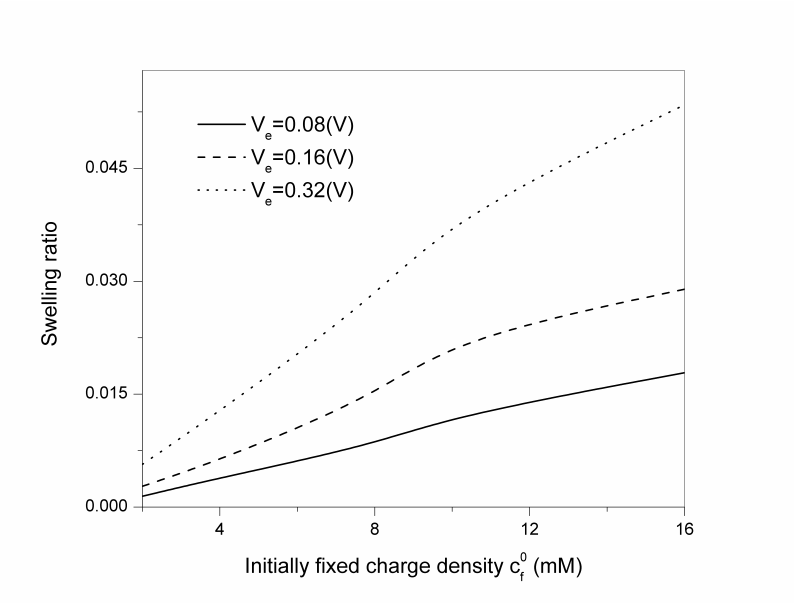

Figure 3.20 Coupled effect of initially fixed charge density c_f^0 and electric voltage V_e as well as solution pH on variation of swelling ratio R_s (pH=4.0).

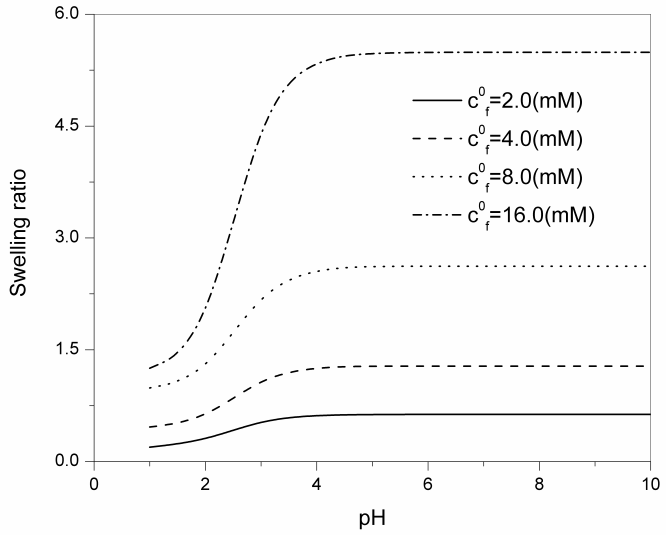

Figure 3.21 Coupled effect of initially fixed charge density c_f^0 and electric voltage V_e as well as solution pH on variation of swelling ratio R_s (Ve=0.4V).

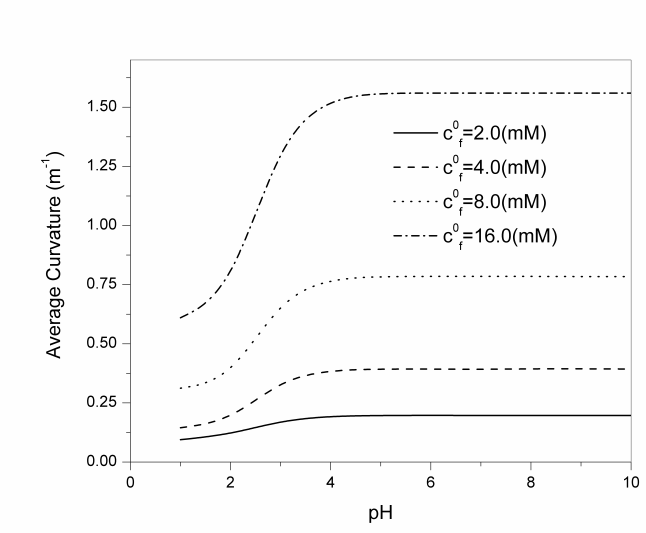

Figure 3.22 Coupled effect of initially fixed charge density c_f^0 and electric voltage V_e as well as solution pH on variation of swelling ratio R_s (V_e=0.4V).

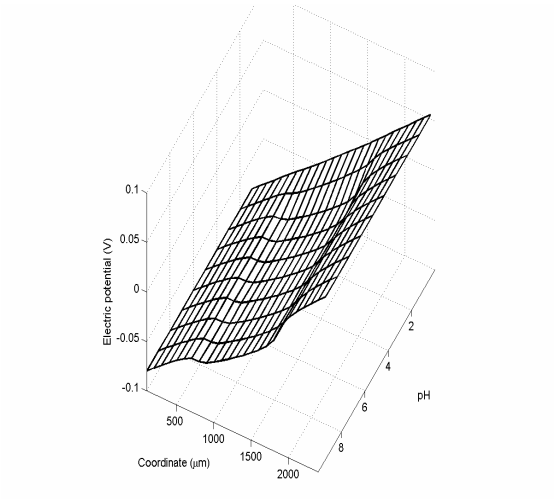

(a) $I = 2.0\text{mM}$

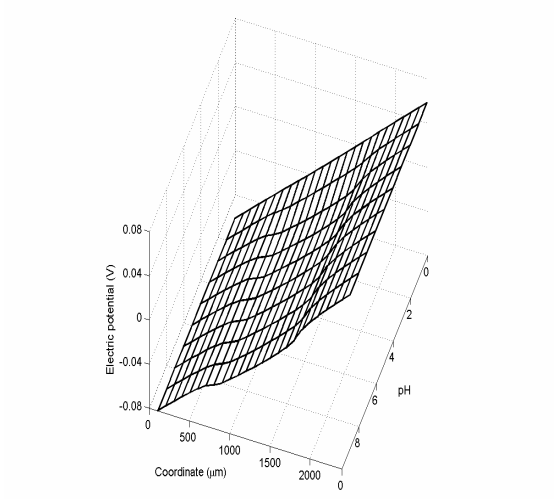

(b) $I = 4.0\text{mM}$

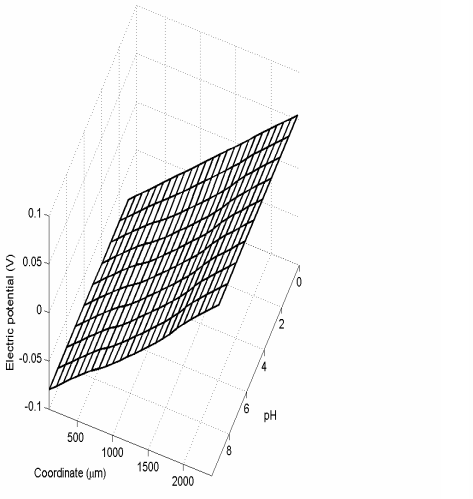

(c) $I = 8.0\text{mM}$

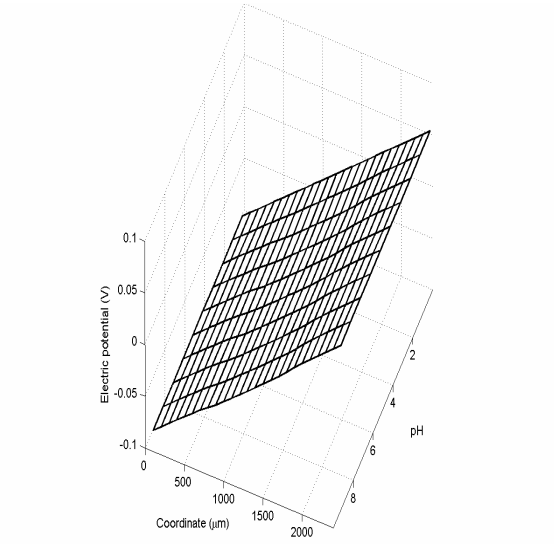

(d) $I = 16.0\text{mM}$

Figure 3.23 Distributive profiles of electric potential ψ with coupled influences of solution pH and external electric voltage V_e as well as ionic strength I (V_e=0.16V).

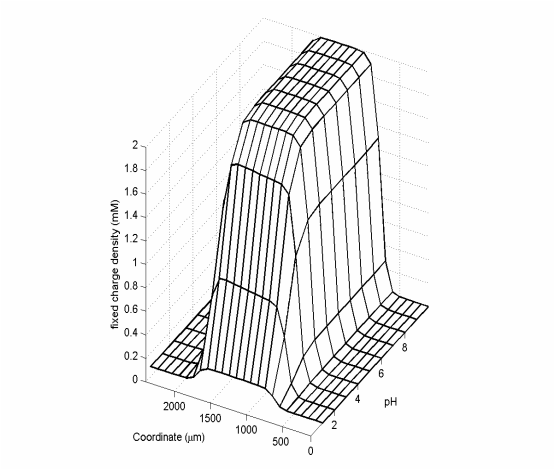

(a) $I = 2.0\text{mM}$

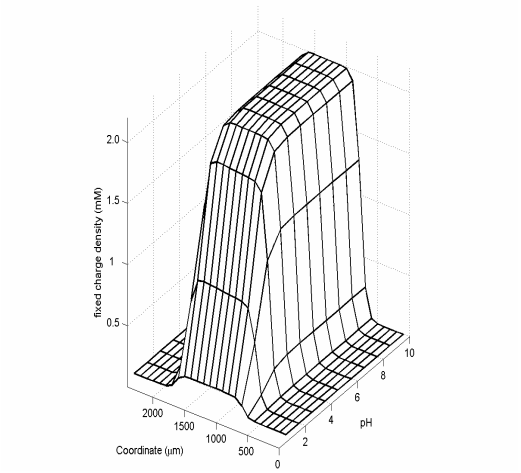

(b) $I = 4.0\text{mM}$

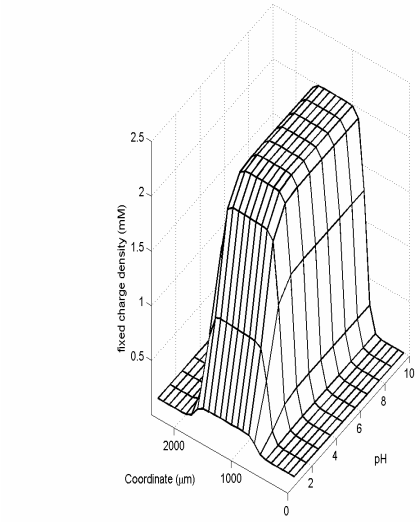

(c) $I = 8.0\text{mM}$

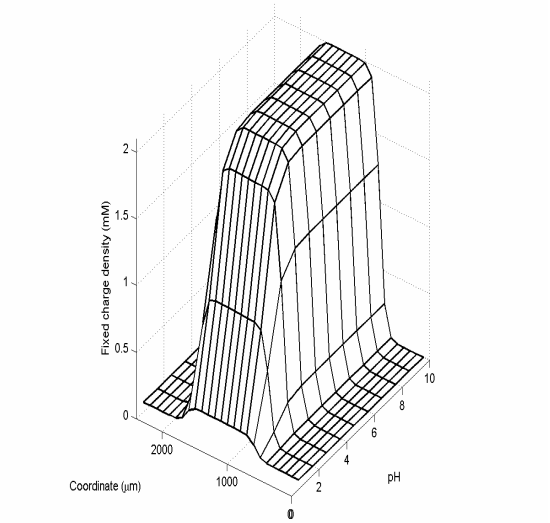

(d) $I = 16.0\text{mM}$

Figure 3.24 Distributive profiles of fixed charge density c_f with coupled influences of solution pH and external electric voltage V_e as well as ionic strength I (V_e=0.16V).

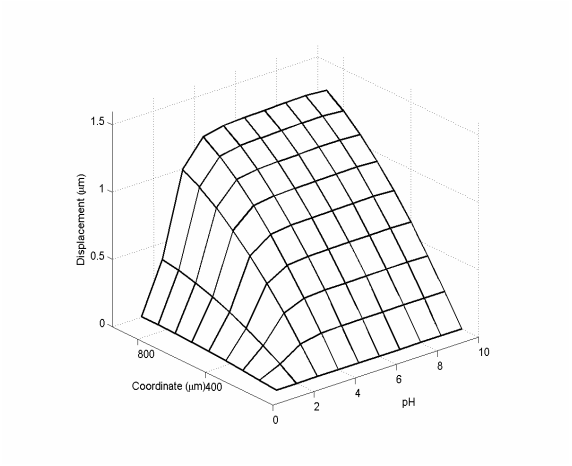

(a) $I = 2.0\text{mM}$

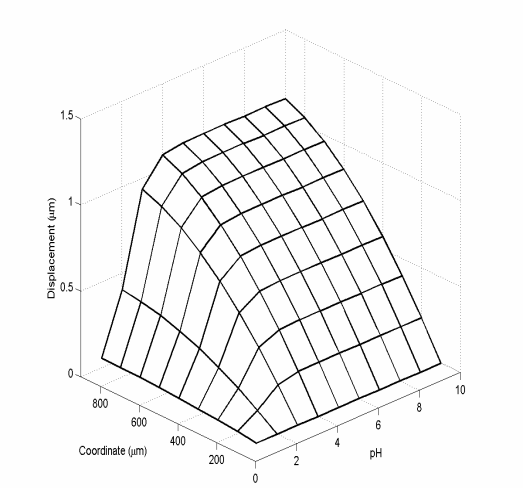

(b) $I = 4.0\text{mM}$

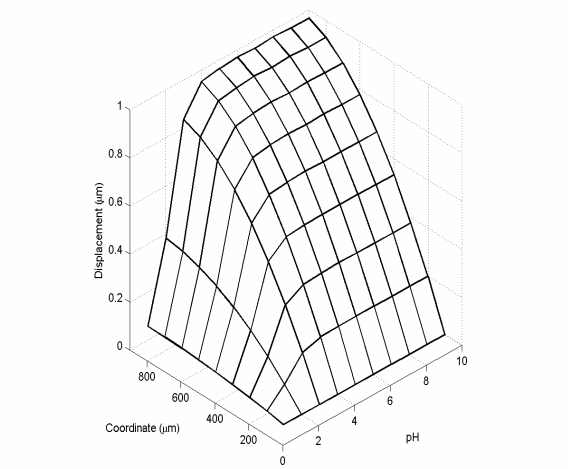

(c) $I = 8.0\text{mM}$

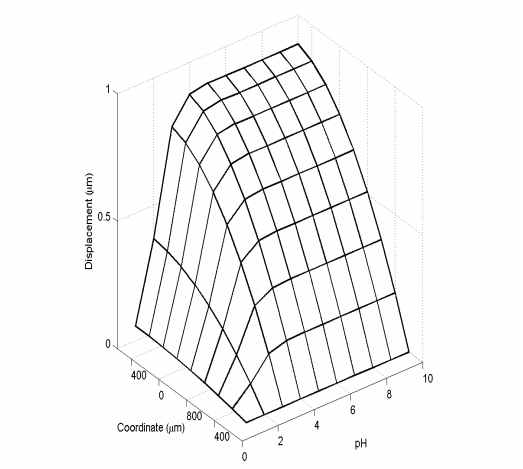

(d) $I = 16.0\text{mM}$

Figure 3.25 Distributive profiles of displacement u with coupled influences of solution pH and external electric voltage V_e as well as ionic strength I (V_e=0.16V).

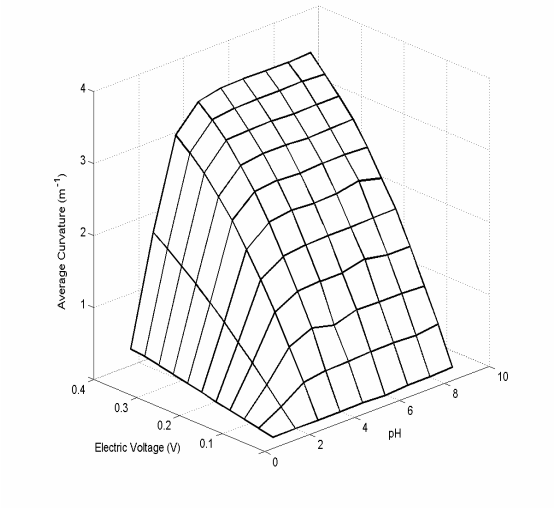

(a) $I = 2.0\text{mM}$

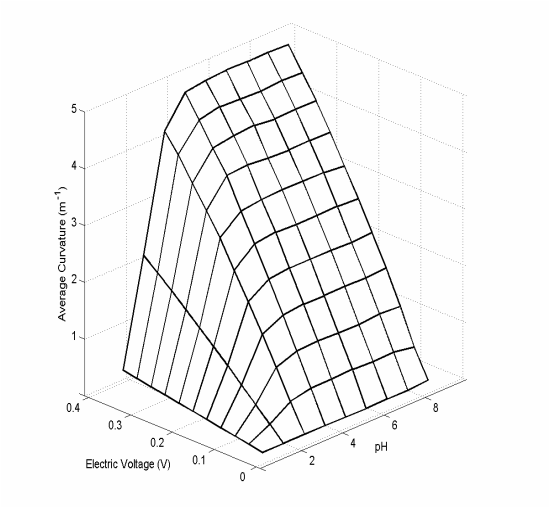

(b) $I = 4.0\text{mM}$

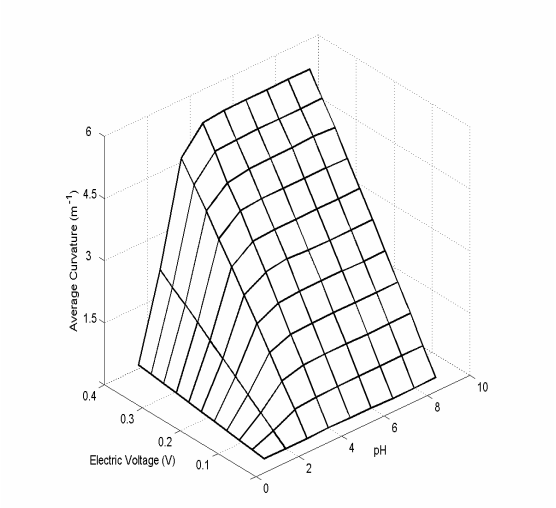

(c) $I = 8.0\text{mM}$

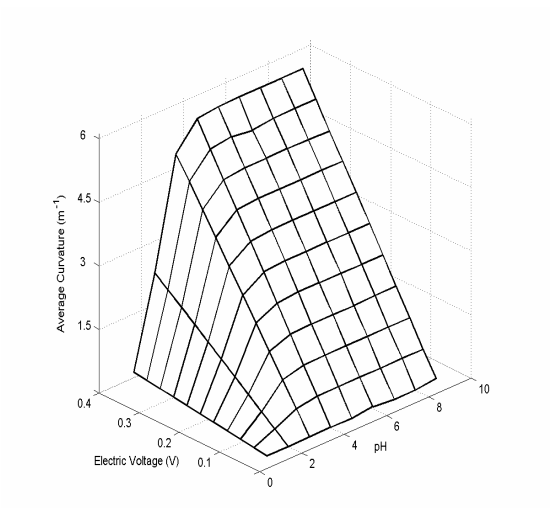

(d) $I = 16.0\text{mM}$

Figure 3.26 Coupling effect of ionic strength I and electric voltage V_e as well as solution pH on variation of average curvature K_a.

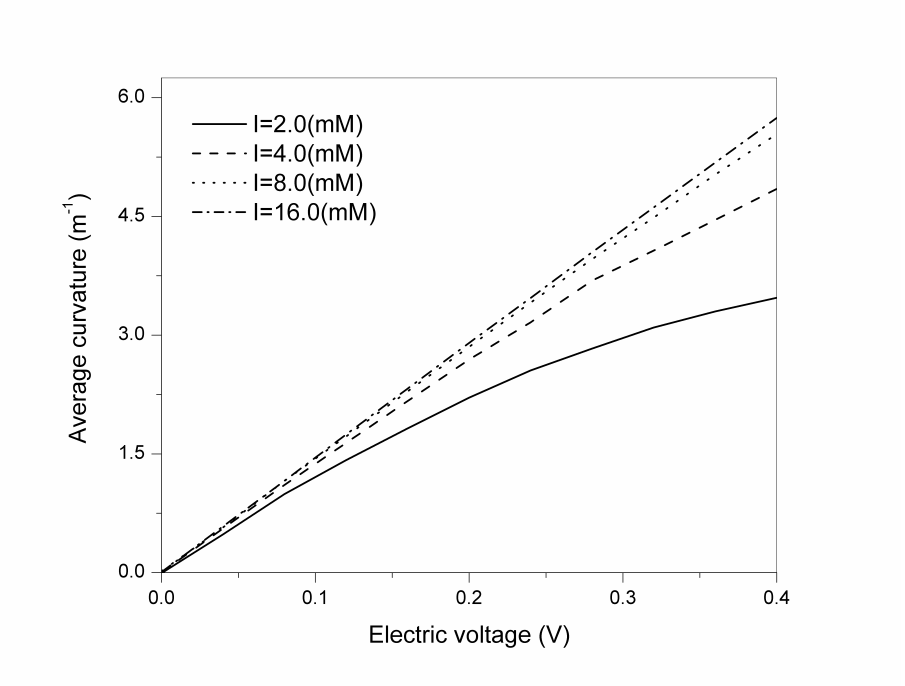

Figure 3.27 Coupled effect of ionic strength I and electric voltage V_e as well as solution pH on variation of average curvature K_a (pH=4.0).

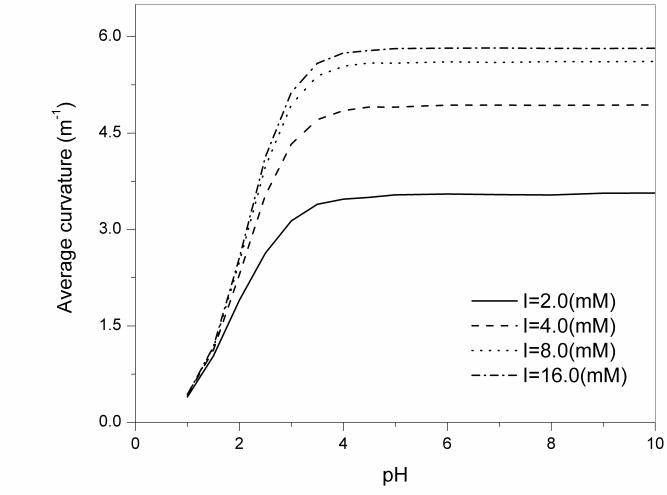

Figure 3.28 Coupled effect of ionic strength I and electric voltage V_e as well as solution pH on variation of curvature K_a (V_e=0.4V).

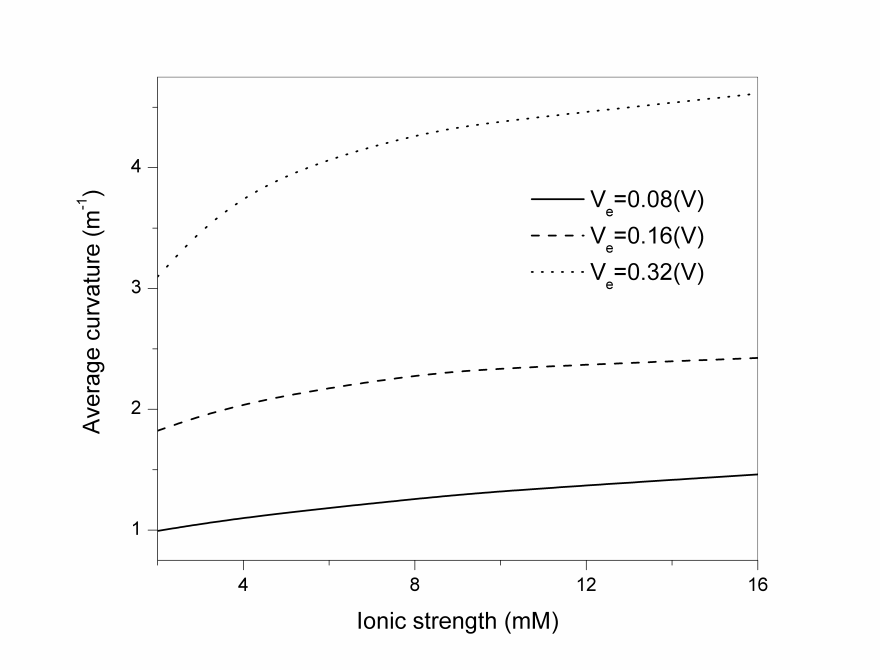

Figure 3.29 Profile of average curvature K_a with Coupling influences of ionic strength I and electric voltage V_e as well as solution pH (pH=4.0).

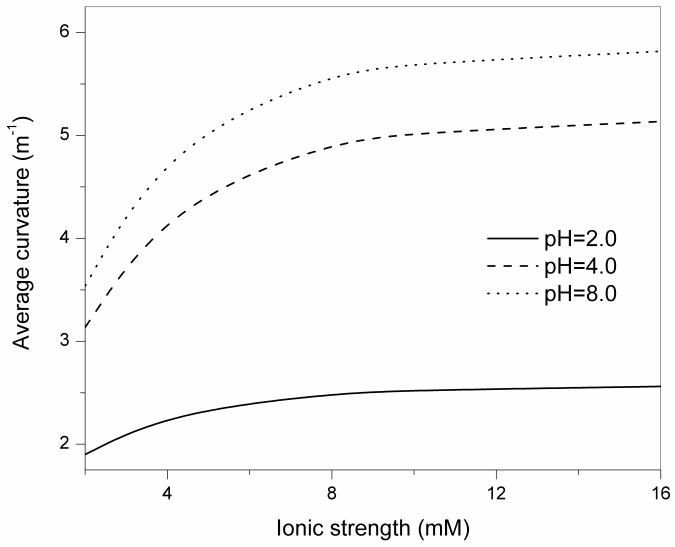

Figure 3.30 Coupled effect of ionic strength I and electric voltage V_e as well as solution pH on variation of swelling ratio R_s ($V_e = 0.4$ V).

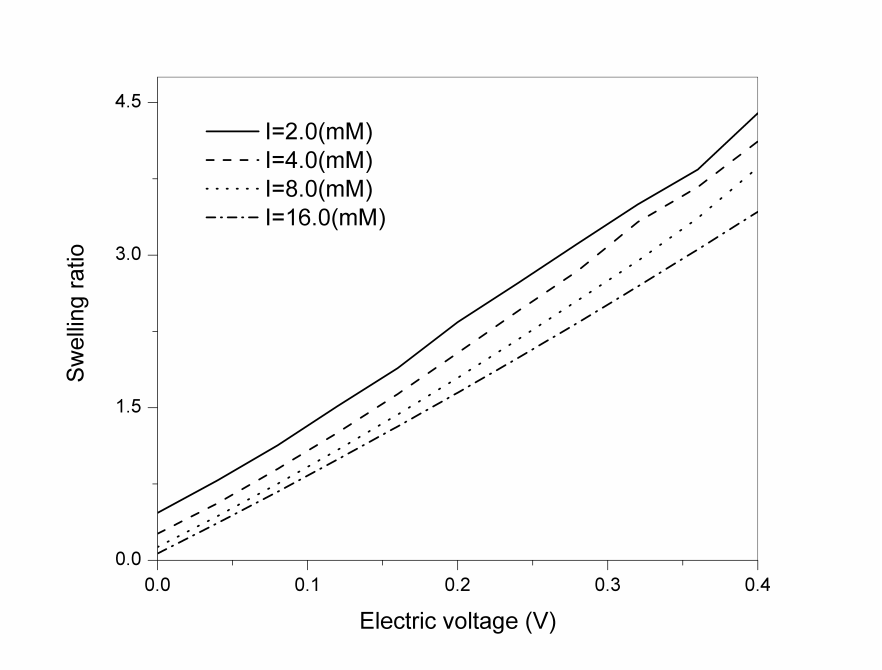

Figure 3.31 Coupled effect of ionic strength I and electric voltage V_e as well as solution pH on variation of swelling ratio R_s (pH=4.0).

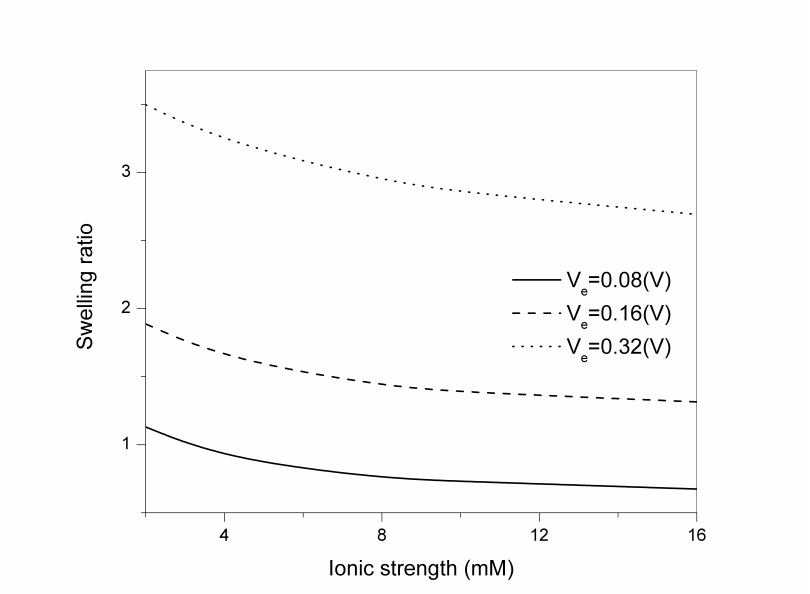

Figure 3.32 Profile of average curvature K_a with Coupling influences of ionic strength I and electric voltage V_e as well as solution pH (pH=4.0).

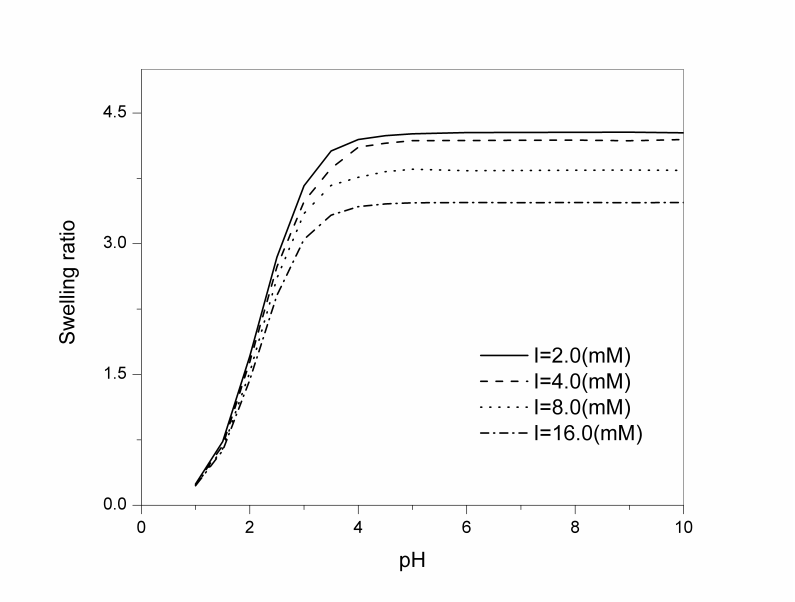

Figure 3.33 Coupled effect of ionic strength I and electric voltage V_e as well as solution pH on variation of swelling ratio R_s (V_e=0.4V).

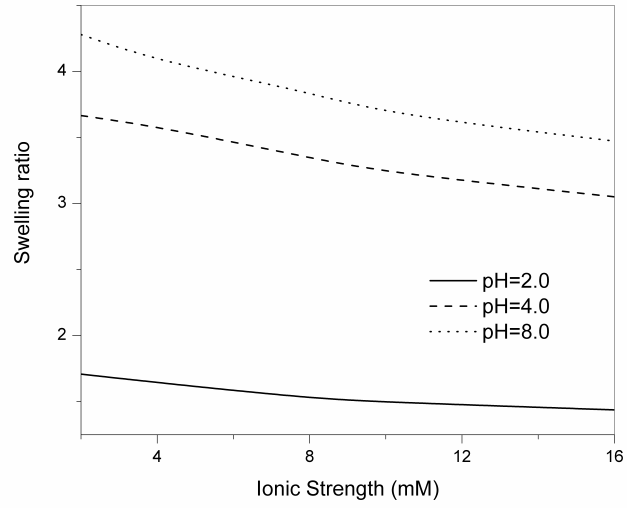

Figure 3.34 Profile of swelling ratio R_s with coupled effect of ionic strength I and electric voltage V_e as well as solution pH on variation of ($V_e = 0.4$ V).

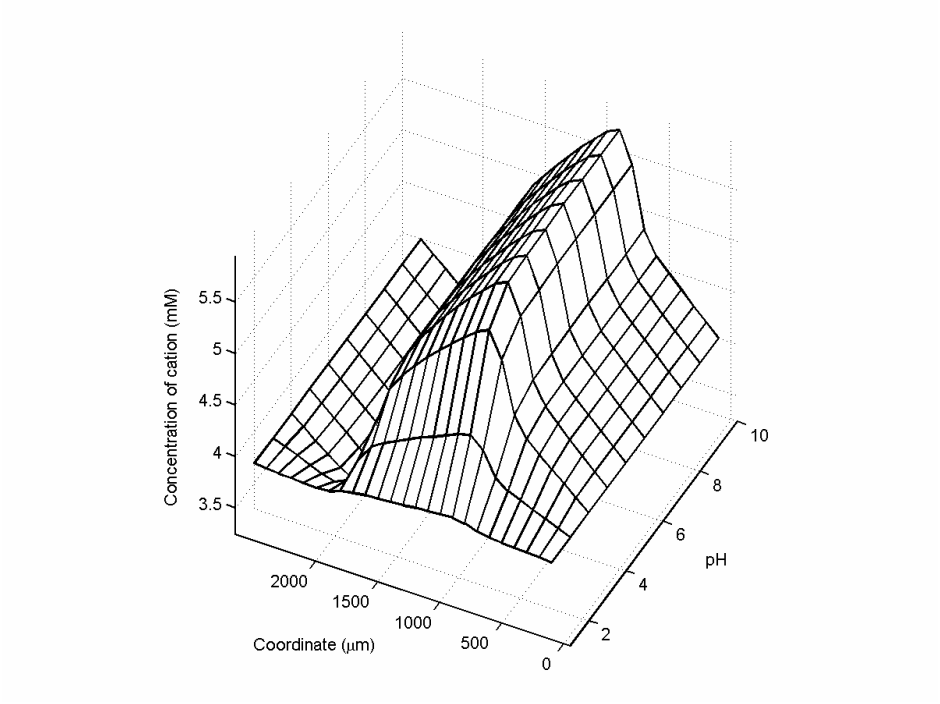

(a) $|z_k|=1$

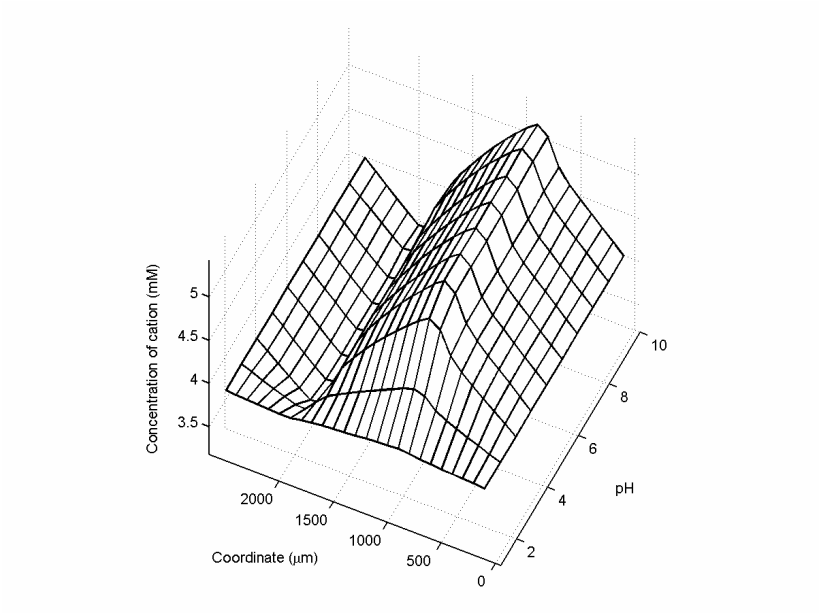

(b) $|z_k|=2$

Figure 3.35 Distributive profiles of cation with coupled influences of solution pH and external electric voltage V_e as well as ionic valence (V_e=0.16V).

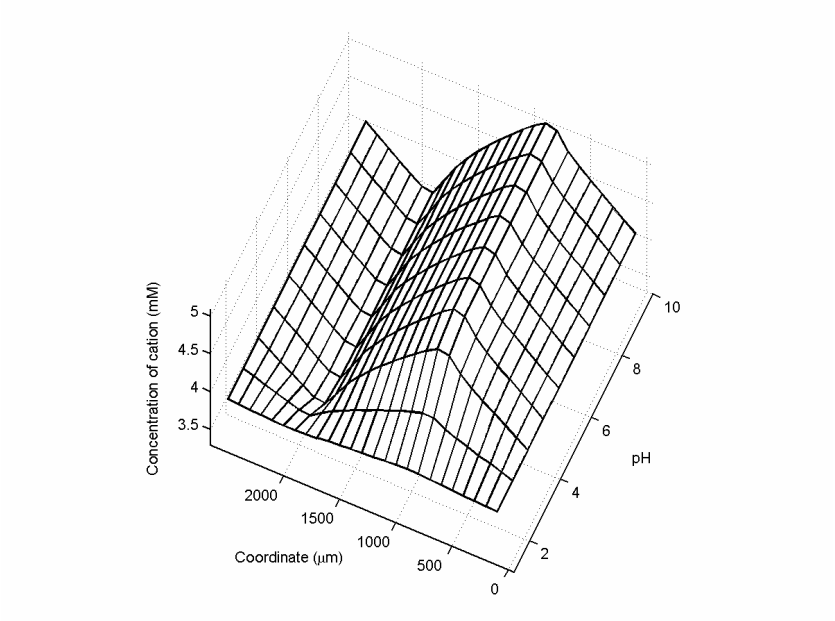

(c) $|z_k|=3$

Figure 3.35 Distributive profiles of cation with coupled influences of solution pH and external electric voltage V_e as well as ionic valence (V_e=0.16V).

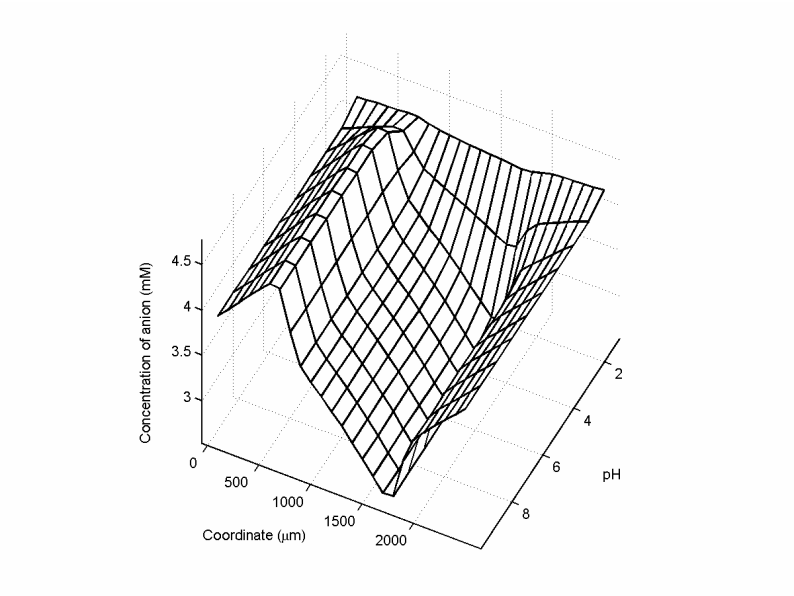

(a) $|z_k|=1$

Figure 3.36 Distributive profiles of anion with coupled influences of solution pH and external electric voltage V_e as well as ionic valence (V_e=0.16V).

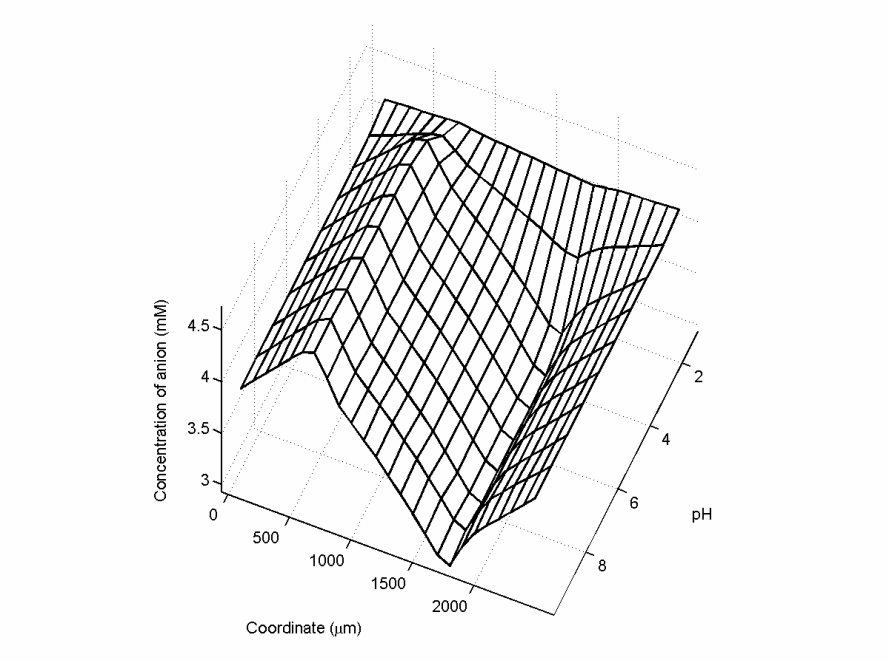

(b) $|z_k|=2$

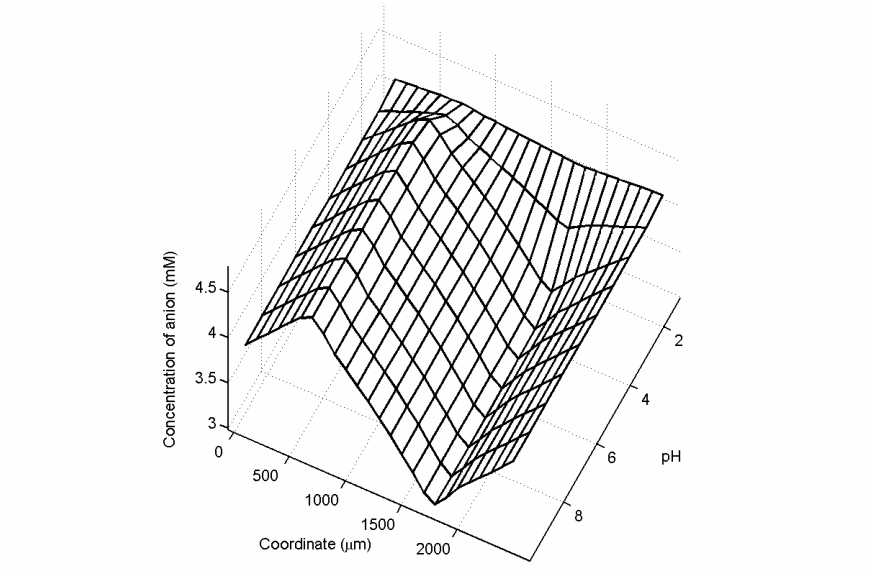

(c) $|z_k|=3$

Figure 3.36 Distributive profiles of anion with coupled influences of solution pH and external electric voltage V_e as well as ionic valence (V_e=0.16V).

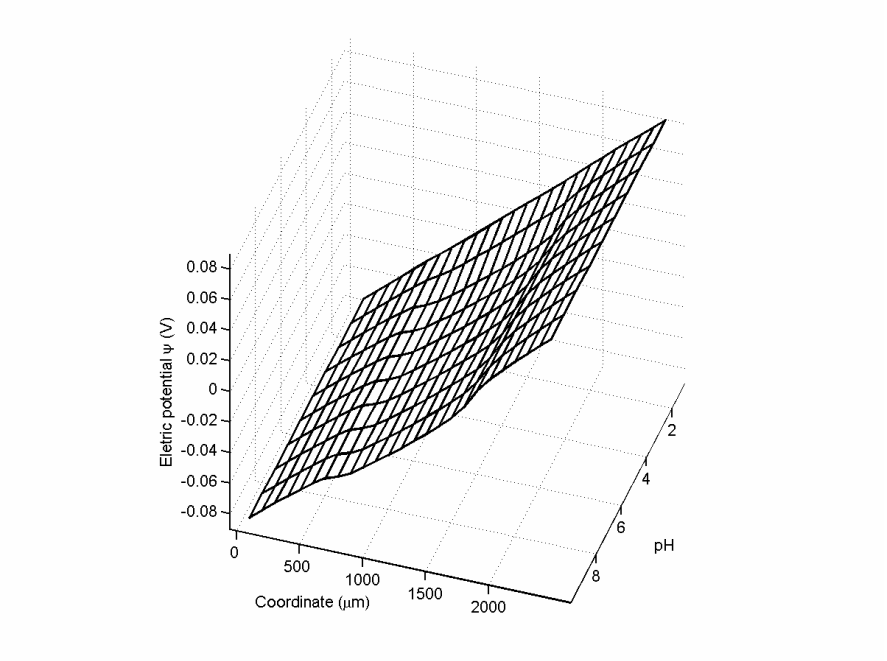

(a) $|z_k|=1$

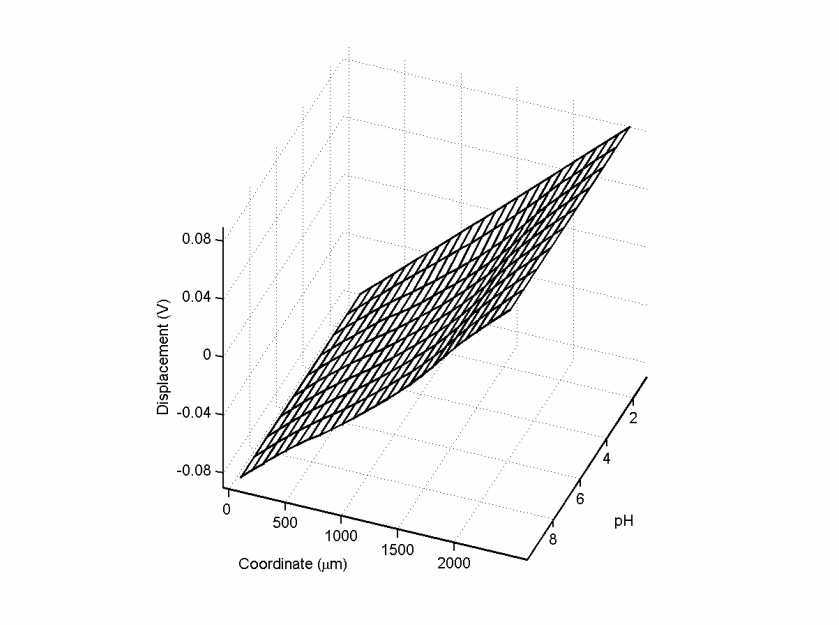

(b) $|z_k|=2$

Figure 3.37 Distributive profiles of electric potential ψ with coupled influences of solution pH and external electric voltage V_e as well as ionic valence (V_e=0.16V).

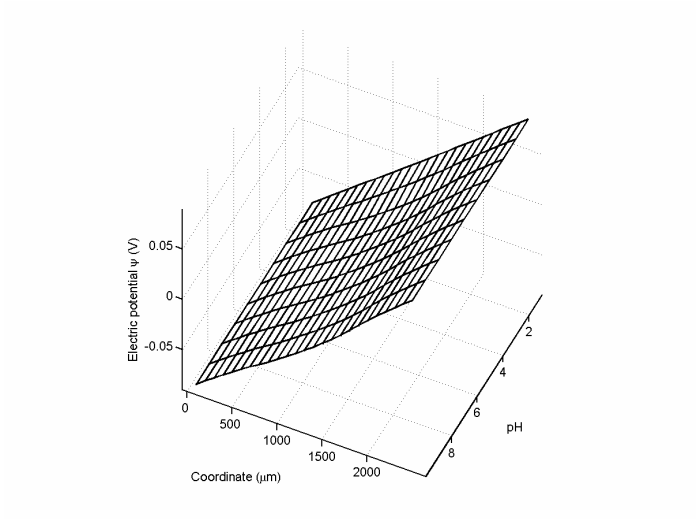

(c) $|z_k|=3$

Figure 3.37 Distributive profiles of electric potential ψ with coupled influences of solution pH and external electric voltage V_e as well as ionic valence (V_e=0.16V).

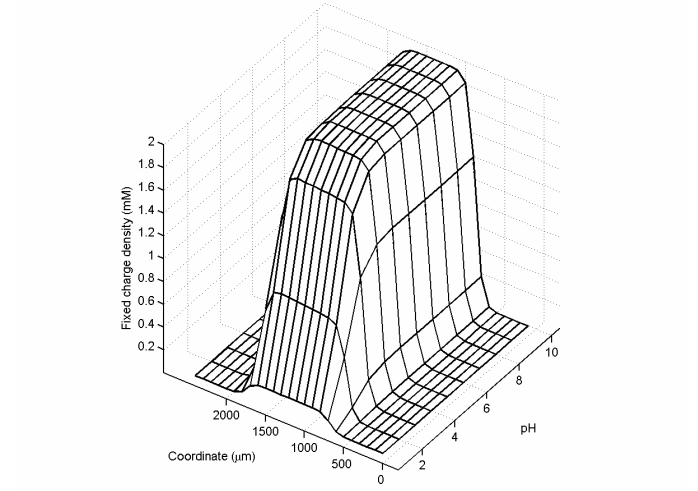

(a) $|z_k|=1$

Figure 3.38 Distributive profiles of fixed charge density c_f with coupled influences of solution pH and external electric voltage V_e as well as ionic valence (V_e=0.16V).

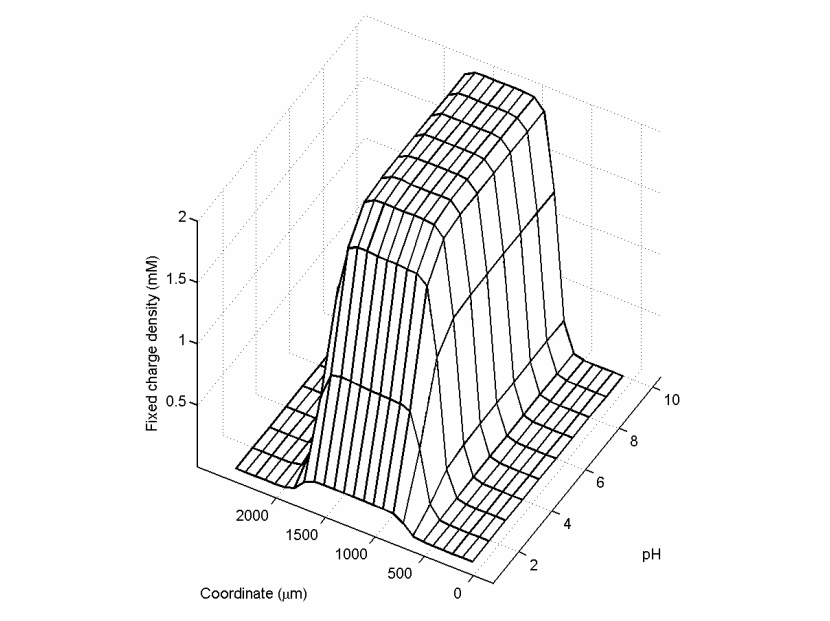

(b) $|z_k|=2$

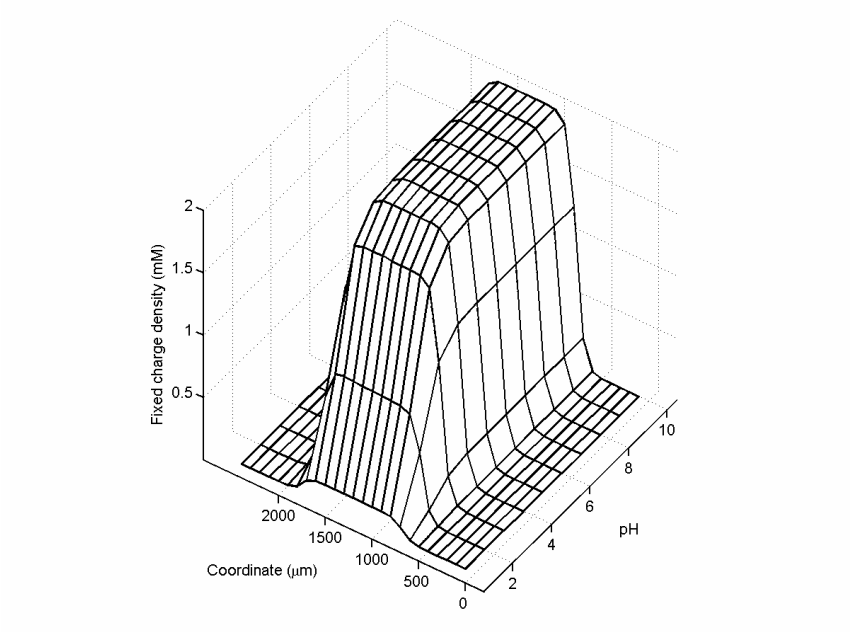

(c) $|z_k|=3$

Figure 3.38 Distributive profiles of electric potential ψ with coupled influences of solution pH and external electric voltage V_e as well as ionic valence (V_e=0.16V).

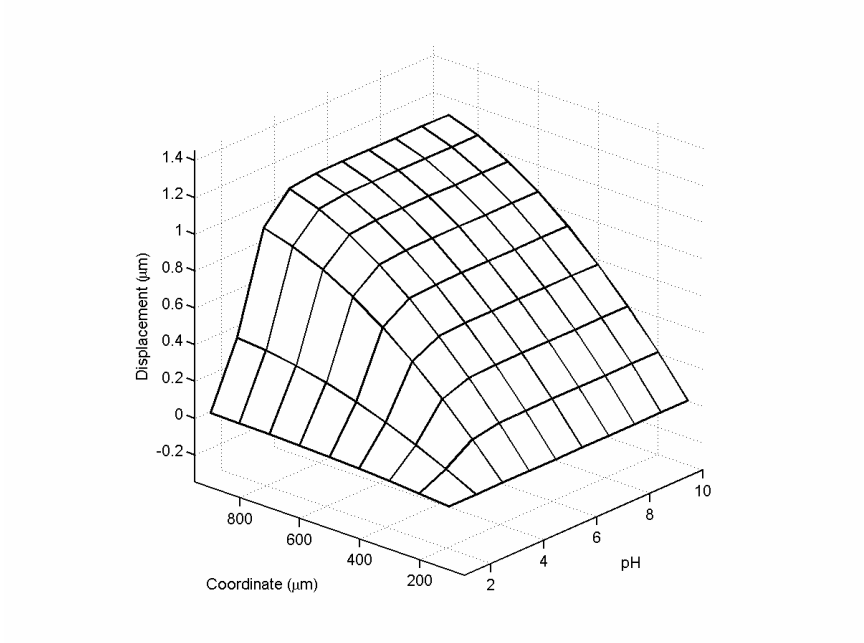

(a) $|z_k|=1$

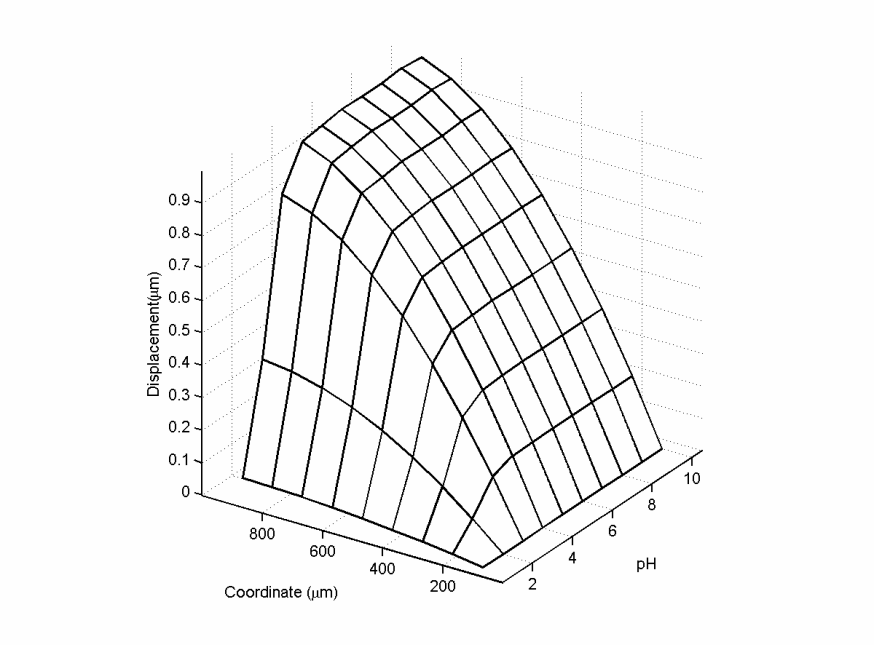

(b) $|z_k|=2$

Figure 3.39 Distributive profiles of displacement u with coupled influences of solution pH and external electric voltage V_e as well as ionic valence (V_e=0.16V).

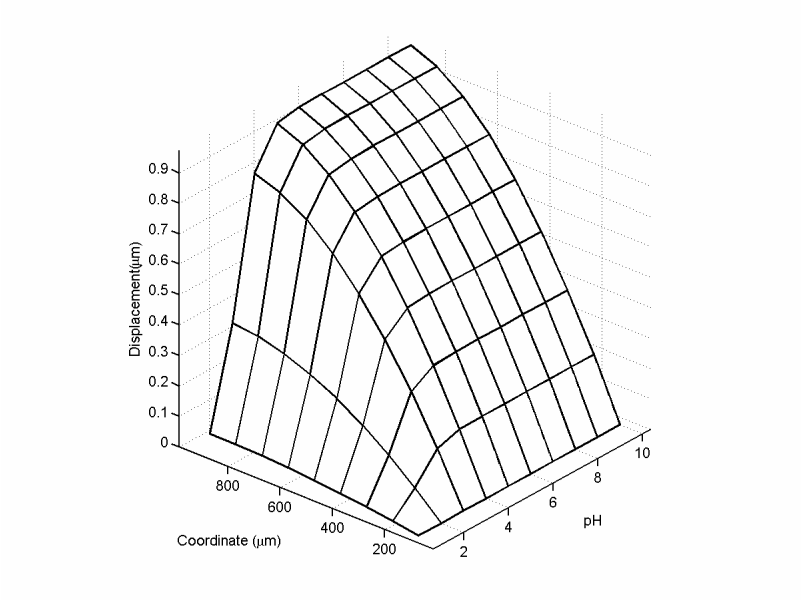

(c) $|z_k|=3$

Figure 3.39 Distributive profiles of displacement u with coupled influences of solution pH and external electric voltage V_e as well as ionic valence (V_e=0.16V).

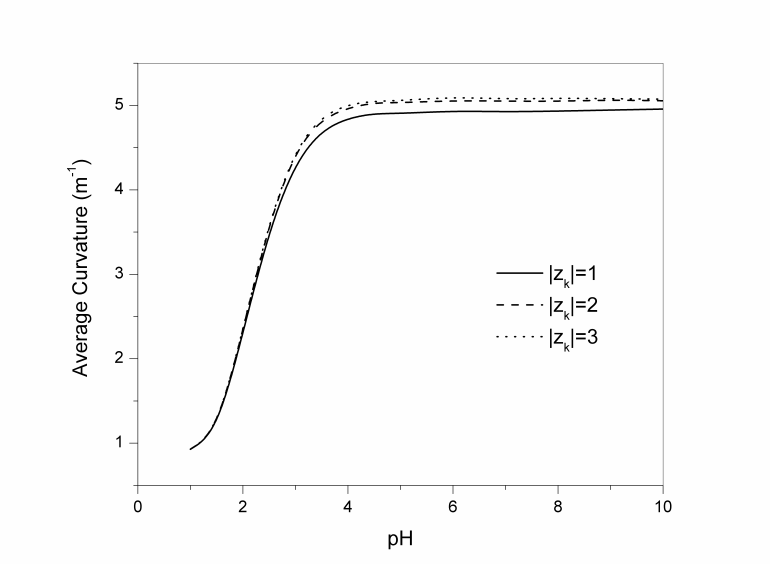

Figure 3.40 Coupled effect of ionic valence and electric voltage V_e as well as solution pH on variation of average curvature K_a ($V_e = 0.4$ V).

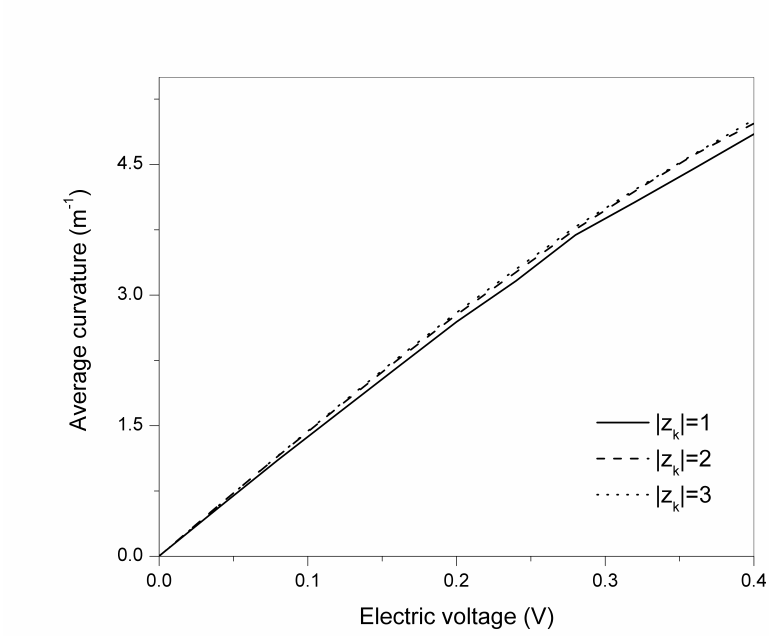

Figure 3.41 Coupled effect of ionic valence and electric voltage V_e as well as solution pH on variation of average curvature K_a (pH=4.0).

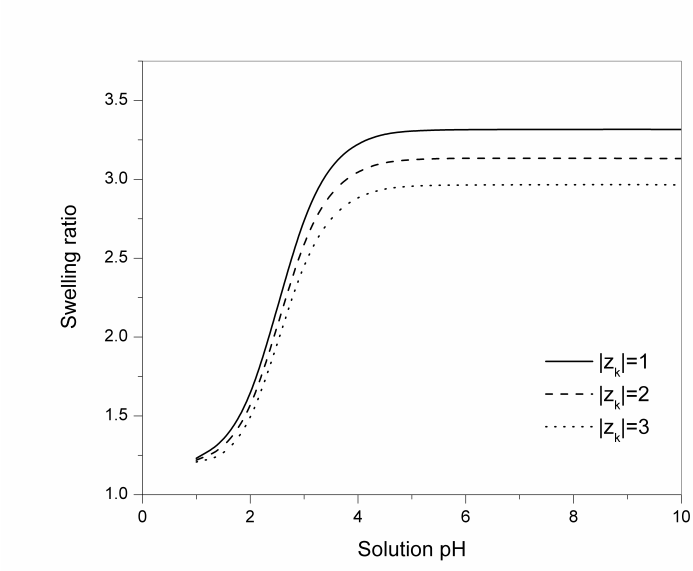

Figure 3.42 Coupled effect of ionic valence and electric voltage V_e as well as solution pH on variation of swelling ratio R_s ($V_e = 0.4$ V).

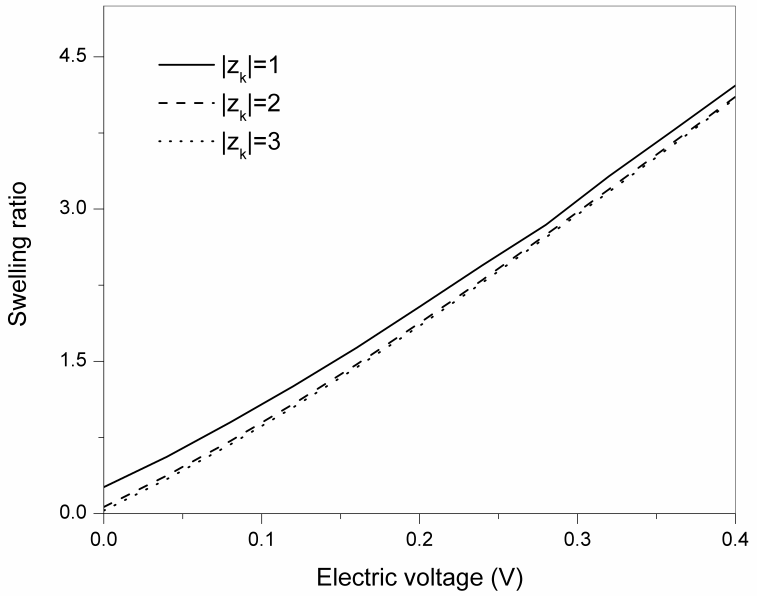

Figure 3.43 Coupled effect of ionic valence and electric voltage V_e as well as solution pH on variation of swelling ratio R_s (pH=4.0).

Chapter 4

A Refined Multi-Effect-Coupling Electric-Stimulus (rMECe) Model for Electric-Sensitive Hydrogels

4.1 Introduction

From the theoretical point of view, the responsive mechanism of the electric-sensitive hydrogels is similar to that of the pH-sensitive hydrogels (Tanaka, 1981). When an electric field is applied to the bath solution in which a hydrogel is immersed, mobile ions will redistribute in both the hydrogel and the surrounding solution. Due to the fixed charge groups bound to the crosslinked macromolecular chains, the diffusion gives rise to the ionic concentration differences between the interior hydrogel and exterior solution. Accordingly, an osmotic pressure is generated because of the concentration differences, which drives the swelling or shrinking of the hydrogel. The deformation of the hydrogel results in redistribution of the diffusive ions and fixed charge groups, which causes new ionic concentration differences and the hydrogel deforms again. This process will repeat until the increase of mechanical energy balances the decrease of the free energy of the system. This also explains the process how the chemical energy converts to the mechanical energy.

Despite that many research efforts have been put into the experiment-based work over the past several decades, few of them involve the development of the

mathematical models for simulations of the responsive behaviors of environmental-sensitive hydrogels. Based on the previous work (Mow et al., 1980; Myers et al., 1984; Lanir, 1987; Eisenberg and Grodzinsky, 1987), Lai et al. (1991) proposed a triphasic mechano-electro-chemical theory for the responsive behaviors of hydrogel-like tissues. Although the theory explained explicitly the fixed charge density and diffusive ionic concentrations, it only partially accounts for the mechanical properties of the tissues and is not successful in simulating the physiochemical and electrochemical phenomena in the hydrogels, such as the ionic diffusion, mechanical expansion of solid matrix and the effect of the fixed charge groups on distribution of ionic concentrations. Later, Wallmersperger et al. (2001) used the finite element method to simulate the deformation of the electric-sensitive hydrogels subject to the externally applied electric field. However, the method by Wallmersopereger et al. assumed that the hydrogels undergo a small deformation under high electric voltage. In fact, the hydrogel could have large deformation when subjected to a high voltage and thus the model will become inadequate to account for the large deformation. Zhou et al. (2002) developed a model to simulate the equilibrium behaviors of the electric-sensitive hydrogels, including the distribution of the diffusive ionic concentrations and electric potential. It partially considers the steady-state behaviors of the hydrogel and the computational domain covers the hydrogel only in Zhou's model, which limits its application. Therefore, more efforts are required to elucidate the response mechanism of the electric-sensitive hydrogels and attempt to expand the scope of their applications.

The purpose of the work presented in this chapter on modeling for the electric-sensitive hydrogels is threefold:

1. to examine multiphysically how the equilibrium response of electric-sensitive hydrogels is triggered by externally applied DC electric voltage;
2. to show the distributions of ionic concentrations and the electric potential as well as the fixed charge density across the domain of both hydrogel and surrounding solution;
3. to evaluate the effects of several important conditions on the equilibrium behaviors of the electric-sensitive hydrogels.

This chapter is organized as follows. By modifying the two previously developed models, the multi-effect-coupling pH-stimulus (MECpH) and multi-effect-coupling electric-stimulus (MECe) models, Section 4.2 presents a refined multi-effect-coupling electric-stimulus (rMECe) model, in which the governing equations are formulated and the boundary conditions are proposed. Section 4.3 discritizes the rMECe model. Section 4.4 validates the model by comparison the simulation results with published experiments. Section 4.5 carried out several parameters studies of the important physical conditions. Finally, the concluded remarks on the model are drawn in Section 4.6.

4.2 Development of The rMECe Model — Refinements of MECe Model

4.2.1 Review of MECpH and MECe Models

For simulations of the behaviors of the hydrogels responsive to the stimulus of solution pH or externally applied electric field, two mathematical models were developed, and termed the multi-effect-coupling pH-stimulus (MECpH) and multi-effect-coupling electric-stimulus (MECe) models, respectively. (Li et al., 2004 and 2005) They are reviewed firstly and then used as a platform for the further refinement of a mathematical model.

4.2.1.1 Review of Multi-Effect-Coupling pH-stimulus (MECpH) model

The MECpH model is developed for simulation of the behavior of the responsive hydrogels stimulated by solution pH (Li et al., 2005). In this model, the convection-diffusion equations, Poisson equation and mechanical equation are coupled together to describe the chemical and electric fields as well as mechanical field, respectively.

Based on the law of mass conservation, the change in the amount of the species k contained in the volume with respect to time t is given by the difference between the fluxes entering and leaving the reference volume. For simplicity of describing the flux of ionic species k in solution, the convective transport of the ionic species is neglected here. Thus, the Nernst-Planck type of the mass conservation is derived as

$$\frac{\partial c_k}{\partial t} + div(\mathbf{J}_k) = 0 \qquad (k = 1, 2, \ldots, N) \qquad (4.1)$$

$$\mathbf{J}_k = -[D_k]\left(\mathbf{grad}(c_k) + \frac{z_k F}{RT} c_k \mathbf{grad}(\psi) + c_k \mathbf{grad}(\ln \gamma_k) \right) \tag{4.2}$$

where $\mathbf{J}_k$, $[D_k]$, c_k and z_k are the flux (mM/s), the diffusivity tensor, the concentration (mM) and the valence number of the k^{th} diffusive ionic species, ψ is the electrostatic potential (V) and γ_k is the chemical activity coefficient, *F*, *R* and *T* are the Faraday's constant (9.6487×10^4 C/mol), universal gas constant ($8.314\ \text{J/mol} \cdot \text{K}$) and absolute temperature (K) , respectively.

The three terms on the right hand side of the equation (4.2) represent the diffusive flux due to the concentration gradient, the migration flux due to the gradient of the electrical potential and chemical flux related to several semi-empirical equations developed to calculate the chemical activity coefficient.

The diffusion coefficient D_k is determined by the Einstein relationship

$$D_k = \upsilon_k RT \tag{4.3}$$

where υ_k is defined as the mobility of the ionic species *k*.

The Poisson equation can be used to describe the spatial distribution of the electric potential in the domain and it is given as

$$\nabla^2 \psi = -\frac{F}{\varepsilon \varepsilon_0} \left(\sum_k z_k c_k + z_f c_f \right) \tag{4.4}$$

where ε is the relative dielectric constant of the surrounding medium, ε_0 is the vacuum permittivity or dielectric constant ($8.85418 \times 10^{-12}\ \text{C}^2/\text{Nm}^2$) and c_f is the density of the fixed charged group in the hydrogel. It is observed that the electroneutrality and constant field hypotheses are in fact special cases of the Poisson equation. The electroneutrality assumption is applicable only when the concentrations

are high while the constant field hypotheses are valid for low concentrations.

Based on the assumptions of electroneutrality conserved at any point in the solution and the global flow of all ions across the boundary yielding a null current, the Poisson equation is simplified,

Null current: $$\sum_k z_k \mathbf{J}_k = 0 \tag{4.5}$$

Electroneutrality in interior hydrogel: $$\sum_k z_k c_k + z_f c_f = 0 \tag{4.6}$$

Electroneutrality in exterior bathing solution: $$\sum_k z_k c_k = 0 \tag{4.7}$$

As a relation between the concentrations of the ion species of interior and exterior hydrogels, the Donnan equilibrium condition can be used for computation of ionic concentrations within hydrogels according to the ionic concentrations of the dilute surrounding solution. The Donnan equilibrium condition for the dilute solution is given as

$$\beta = \left(\frac{c_{i+}}{\bar{c}_{i+}} \right)^{\left| \frac{1}{z_{i+}} \right|} = \left(\frac{\bar{c}_{i-}}{c_{i-}} \right)^{\left| \frac{1}{z_{i-}} \right|} \tag{4.8}$$

where β is the Donnan partitioning ratio relating the ionic concentration $\bar{c}_i$ within the hydrogels to the external ionic concentration c_i.

The hydrogen ion is bound by the fixed charge attached on the network chains of hydrogels stimulated by solution pH. This process is similar to monolayer-absorbing of the identical surface which has a specific number of binding sites. The each binding site is assumed to absorb one molecule only,

$$MS \xrightarrow{K} M + S \tag{4.9}$$

$$M + S \xrightarrow{Ka} MS \tag{4.10}$$

where *MS* is the occupied fixed charge/site such as c_H^b being the concentration of occupied fixed charge, *M* is mobile hydrogen ions such as c_H being the concentration of mobile molecules including hydrogen ions, *S* is the unoccupied fixed charge/site such as $c_{m0} - c_H^b$ being the concentration of unoccupied sites, c_f is the current concentration of membrane fixed charge group, c_{m0} is the total concentration of ionizable groups in the hydrogel, *K* is dissociation constant and *Ka* is absorption constant.

According to the Langmuir monolayer absorption isotherm, the dissociation constant *K* can be expressed as

$$K = \frac{[M][S]}{[MS]} = \frac{c_H(c_{m0} - c_H^b)}{c_H^b} \tag{4.11}$$

Concentration of the occupied fixed charge/site, c_H^b, is thus obtained as

$$c_H^b = \frac{c_{m0} \cdot c_H}{K + c_H} \tag{4.12}$$

Then the current concentration of fixed charge group, c_f, is expressed as follows,

$$c_f = c_{m0} - c_H^b = c_{m0} - \frac{c_{m0} \cdot c_H}{K + c_H} = \frac{c_{m0} \cdot K}{K + c_H} \tag{4.13}$$

Based on the definition of concentration, the total concentration of the ionizable groups in the hydrogel in the relaxed state, c_{m0}^s, and the current concentration of ionizable groups in the hydrogel, c_{m0}, can be written as follows

$$c_{m0}^s = \frac{n}{V^s} \tag{4.14}$$

$$c_{m0} = \frac{n}{V^w} = \frac{n}{V^s}\frac{V^s}{V^w} = \frac{c_{m0}^s}{H} \tag{4.15}$$

where n is the moles of fixed-charge group, V^s and V^w are the volumes of dry gel and intramembrane fluid respectively, V is current total volume ($V = V^s + V^w$) and H is local hydration of the hydrogel ($H = \frac{V^w}{V^s}$).

Therefore a relation between the fixed charge and diffusive hydrogen ion can be developed, whereby the concentration of the fix charged group is calculated as a function of c_{m0}^s and c_H by

$$c_f = \frac{1}{H}\frac{c_{m0}^s K}{K + c_H} \tag{4.16}$$

where c_f and z_f are the concentration and the valence of the fixed charge groups on the polymer chains, for example, $z_f = -1$ if the carboxylic acid groups are used as the fixed charges on the polymer chains. K is the dissociation constant of the carboxylic acid groups, c_{m0}^s is the total concentration of the ionizable groups within the hydrogel in the relaxed state, c_H is the concentration of hydrogen ions H^+ within the hydrogel and H is the local hydration of the hydrogel.

For simulation of the mechanical deformation of the hydrogels stimulated by the pH of surrounding solution, the coupled mechanical governing equation is

$$\rho\left.\frac{\partial^2 u}{\partial t^2}\right|_i + f\left.\frac{\partial u}{\partial t}\right|_i = \sigma_{ij,j} + \rho b_i \tag{4.17}$$

where ρ is the mass density, t is the time variable and u is the displacement of the solid phase, f represents the viscous damping coefficient between the solvent and solid-phase network, σ_{ij} is the total stress tensor of the interior hydrogel, and b_i is the body force that is not of interest in present work. Further, it can be shown that the stress contributions in the hydrogels arisen from two main sources, namely the

mechanical elastic restoring stress tensor exerted by the solid-phase network $F_{elastic-restoring_{ij}}$ (Pa), and the osmotic pressure $P_{osmotic}$ (Pa), hence the equation (4.17) can be rewritten as

$$\rho\frac{\partial^2 u}{\partial t^2}\bigg|_i + f\frac{\partial u}{\partial t}\bigg|_i = \sigma_{ij,j} = (F_{elasticrestoring} - P_{osmotic}\delta_{ij})_{,j} \tag{4.18}$$

where $P_{osmotic}$ is the osmotic pressure and is calculated according to the concentration difference between the stress-free and swelling states,

$$P_{osmotic} = RT\sum_k (c_k - c_k^0) \tag{4.19}$$

where c_k^0 is the concentration of the k^{th} ion species in the stress-free state and c_k the concentration of k^{th} ion species within the hydrogel at the swelling state.

For a one-dimensional steady-state case, by substituting the equation (4.19) into the equation (4.18), the linear-elastic equilibrium equation which describes the mechanical deformation is written in final form as

$$\frac{\partial\sigma}{\partial x} = \frac{\partial}{\partial x}\left((2\mu+\lambda)\frac{\partial u}{\partial x} - P_{osmotic}\right) = \frac{\partial}{\partial x}\left((2\mu+\lambda)\frac{\partial u}{\partial x} - RT\sum_{k=1}^{N}(c_k - c_k^0)\right) = 0 \tag{4.20}$$

where λ and μ are the Lamé coefficient of the solid matrix.

4.2.1.2 Review of Multi-Effect-Coupling electric-stimulus (MECe) model

The MECe model is developed to simulate the chemo-electro-mechanical coupled behaviors of responsive hydrogels immersed in a bath solution subject to an externally applied electric field (Li et al., 2004).

The MECe model is based on the triphase mixture theory (Lai et al., 1991). The hydrogel is assumed to consist of the solid phase, interstitial water phase and ion phase.

When an electric field is applied to the solution, ions flow, diffuse and redistribute within the hydrogels and surrounding solution, which is charactered by convection-diffusion equations and the Poisson equation,

$$(D_k c_{k,i})_{,i} + \frac{Fz_k}{RT}(D_k c_k \psi_{,i})_{,i} = \frac{\partial c_k}{\partial t} + (c_k v_k)_{,i} \qquad (k = 1, 2, \cdots, N) \tag{4.21}$$

$$\nabla^2 \psi = -\frac{F}{\varepsilon_0 \varepsilon}(\sum_k z_k c_k + z_f c_f) \tag{4.22}$$

where the fixed charge density c_f is expressed as follows

$$c_f = \frac{\phi_0^w c_f^0}{\phi^w[1 + \mathrm{tr}(E)]} = \frac{c_f^0}{[1 + \mathrm{tr}(E)/\phi_0^w]} \tag{4.23}$$

where c_f^0 is the fixed charge density at reference configuration and ϕ_0^w is the volume fraction of the water phase at reference configuration (Lai et al., 1991).

Because of the effect of fixed charge groups attached to the polymer chains of the hydrogels, the differences in ionic concentrations occur at the interface between the hydrogels and surrounding solution. It gives rise to osmotic pressure, which drives the deforming of hydrogels. The mechanical displacement of hydrogel is governed simultaneously by momentum and continuity equations

$$\nabla \cdot \sigma = 0 \tag{4.24}$$

$$\sigma = -p\mathbf{I} + \lambda_s \,\mathrm{tr}(\mathbf{E})\mathbf{I} + 2\mu_s E \tag{4.25}$$

$$\nabla \frac{\partial u^s}{\partial t} = \nabla[\frac{(\phi^w)^2}{f_{ws}}(\nabla p + RT\nabla \sum_k (1 - \phi^k)c^k + F\sum_k z^k c^k \nabla \psi + B_w \nabla \,\mathrm{tr}(\mathbf{E}))] \tag{4.26}$$

where *s*, *w* and *k* denote the solid matrix, interstitial water and ion phase, ϕ is the volume fraction, $\mathbf{E}$ is the elastic strain vector of the solid phase, *p* is osmotic pressure, and B_w coupling coefficient.

4.2.2 Refinements of MECe Model

Compared with the mathematical models mentioned in the literature survey, the MECpH model described above has several advantages. Firstly, the computational domain covers both the hydrogel and exterior bathing solution, and the model is able to demonstrate the distributions of concentrations of all diffusive ionic species, electric potential in both the hydrogels and surrounding solution simultaneously. Secondly, it takes account for the electrical coupling of various ionic fluxes into the Poisson equation and easily incorporates multiple species of ions. Finally, the model is in more concise form and readily applicable for numerical implementation as compared with other models and also achieves good agreement between the experimental data and simulation results.

Despite the progress gained in the MECpH model, it still has some limitations. Firstly, it is assumed in the MECpH model that the fixed charge density is constant within the hydrogel. The effect of externally applied electric field on fixed charge can not be incorporated into the MECpH model. However, the fixed charge density is in fact affected by the externally applied electric field and it should have a gradient distribution as the free mobile ions do. Secondly, the mechanical equation of the MECpH model can be used only for analysis of small deformation. Experiments show that a high electric voltage may drive the hydrogel to swell drastically or to deform very large (Kim et al., 2003). Due to the hydrogel undergoing large deformation, the difference between the initial configuration and the deformed configuration can not be

neglected as is done in the MECpH model.

In order to overcome the limits mentioned above, the MECpH model is refined in this chapter by the two revisions. The first is to reformulate the fixed charge density for including the effect of externally applied electric field on the distribution of fixed charge density. The second is to approach better to the true situation for the hydrogel undergoing large deformation.

4.2.2.1 Reformulating the fixed charge density

The first revision is based on the triphasic theory referred in the MECe model, the formulation of fixed charge density is expressed as follows

$$c_f = \frac{\phi_0^w \cdot c_f^0}{\phi^w[1+\mathrm{tr}(\boldsymbol{E})]} \tag{4.27}$$

ϕ^α (α=s, w, or k) represents the volume fraction of phase α, and the saturation equation is

$$\sum_{\alpha=s,w,k} \phi^\alpha = 1 \tag{4.28}$$

The infinitesimal deformation of mixture is

$$\phi^w = 1 - \frac{\phi_0^s}{1+\mathrm{tr}(\boldsymbol{E})} \tag{4.29}$$

where ϕ_0^s is the volume fraction of the solid phase at reference configuration and $\boldsymbol{E}$ is the elastic strain vector of solid phase.

Compared with ϕ^s and ϕ^w, ϕ^k is infinitesimal, then the saturation equation can be rewritten as follows,

$$\phi^s + \phi^w \approx 1 \tag{4.30}$$

The volume fraction of the current water phase is thus expressed as

$$\phi^w = \frac{\mathrm{tr}(\boldsymbol{E}) + \phi_0^w}{1 + \mathrm{tr}(\boldsymbol{E})} \tag{4.31}$$

Substituting the equation (4.31) into the equation (4.27), the formulation of fixed charge density is obtained as

$$c_f = \frac{c_f^0}{1 + \mathrm{tr}(\boldsymbol{E}) / \phi_0^w} \tag{4.32}$$

4.2.2.2 Approach of finite deformation theory

The second revision is to account for the large deformation that the hydrogel undergoes when immersed into the solution subject to externally applied electric field. As mentioned above, the previous MECpH model assumes that the hydrogels undergo small mechanical deformation and then is solved by the linear theory of elasticity. The momentum equation for the MECpH model are thus given as

$$\nabla \cdot \sigma + \boldsymbol{b} = 0 \qquad \text{in } \Omega \tag{4.33}$$

$$\sigma = -p_{osmotic}\boldsymbol{I} + \lambda_s \,\mathrm{tr}(\boldsymbol{E})\boldsymbol{I} + 2\mu_s \boldsymbol{E} \tag{4.34}$$

$$\boldsymbol{u} = \boldsymbol{g} \qquad \text{in } \Gamma_g \tag{4.35}$$

$$\sigma \cdot \boldsymbol{n} = \boldsymbol{h} \qquad \text{in } \Gamma_h \tag{4.36}$$

where σ is the Cauthy stress tensor, $\boldsymbol{b}$ is the body force vector, $p_{osmotic}$ is the osmotic pressure, λ_s and μ_s are the Lame coefficient of solid matrix, $\boldsymbol{u}$ is the displacement vector, $\boldsymbol{g}$ is the specified displacement vector on the boundary portion Γ_g, $\boldsymbol{h}$ is the surface traction vector on the boundary Γ_h, $\boldsymbol{n}$ is the unit outward normal vector and $\boldsymbol{I}$ is the identity tensor. In present studies, the body force is neglected, and

the equation (4.33) is reduced to,

$$\nabla \cdot \sigma = 0 \qquad \text{in } \Omega \tag{4.37}$$

In the coupled chemo-electro-mechanical analysis of the electric-stimulus responsive hydrogels, when the applied electric voltage is high, the hydrogels will undergo large deformation, in which the linear theory may produce inaccurate results, the difference between the initial (reference) and deformed configurations can not be neglected as it is done for analysis of linear elasticity in the MECpH model.

For geometrically nonlinear analysis, the governing equations for large deformation using a total Lagrangian description are given as follows,

$$\nabla \cdot \mathbf{P} = 0 \qquad \text{in } \Omega \tag{4.38}$$

$$\mathbf{u} = \mathbf{G} \qquad \text{in } \Gamma_g \tag{4.39}$$

$$\mathbf{P} \cdot \mathbf{N} = \mathbf{H} \qquad \text{in } \Gamma_h \tag{4.40}$$

where ***P*** is the first Piola-Kirchhoff stress tensor, ***u*** is the displacement vector from the initial configuration ***X*** to the deformed configuration ***x***, ***G*** is the specified displacement vector on the boundary portion Γ_g, ***H*** is the surface traction vector on the boundary Γ_h, ***N*** is the unit outward normal vector. These variables are described in initial configuration ***X***.

The first Piola-Kirchhoff stress tensor ***P*** is a kind of expatriate, living partially in the deformed (current) configuration ***x*** and partially in the reference configuration ***X*** (where $\mathbf{x} = \mathbf{X} + \mathbf{u}$), and is unable to measure. For this reason and because of the absence of symmetry in the first Piola-Kirchhoff stress tensor ***P***, it is seldom used in constitutive equations. However, the second Piola-Kirchhoff stress tensor ***S*** is

symmetric and is often used as the stress measure, and then the second Piola-Kirchhoff stress tensor ***S*** is chosen to analyze the large deformation. The relationship between the first Piola-Kirchhoff stress tensor ***P*** and the second Piola-Kirchhoff stress tensor ***S*** is given as follows,

$$\mathbf{P} = \mathbf{S}\mathbf{F}^{\mathrm{T}} \tag{4.41}$$

where $\mathbf{F}$ is the deformation gradient tensor and defined as,

$$\mathbf{F} = \mathbf{I} + \nabla \mathbf{u} \tag{4.42}$$

The second Piola-Kirchhoff stress tensor ***S*** is given by,

$$\mathbf{S} = \mathbf{C}\mathbf{E} - p_{osmotic}\mathbf{I} \tag{4.43}$$

Where $\mathbf{C}$ the material tensor and $\mathbf{E}$ is is the Green-Lagrangian strain tensor that is used as the strain measure,

$$\mathbf{E} = \frac{1}{2}(\mathbf{F}^{\mathrm{T}}\mathbf{F} - \mathbf{I}) \tag{4.44}$$

Substituting the equations (4.41) and (4.43) into the equation (4.38), the governing equation for large deformation can be written as follows

$$\nabla \cdot [(\mathbf{C}\mathbf{E} - p_{osmotic}\mathbf{I})\mathbf{F}^{\mathrm{T}}] = 0 \tag{4.45}$$

So far the full governing equations of the refined model are completed. For the one-dimensional special case, the rMECe model consists of the Nernst-Planck convection-diffusion equation for ion concentration, Poisson equation for the electric potential, and nonlinear mechanical equation for the large displacement of hydrogels, namely

$$div\left\{-\left[D_k\right]\left(\operatorname{grad}(c_k) + \frac{z_k F}{RT} c_k \operatorname{grad}(\psi)\right)\right\} = 0 \tag{4.2}$$

$$\nabla^2\psi = -\frac{F}{\varepsilon\varepsilon_0}\left(\sum_k z_k c_k + z_f c_f\right) \tag{4.4}$$

$$c_f = \frac{c_f^0}{1+\mathrm{tr}(\boldsymbol{E})/\phi_0^w} \tag{4.32}$$

$$(\lambda+2\mu)[\frac{d^2u}{dX^2}+3\frac{du}{dX}\frac{d^2u}{dX^2}+\frac{3}{2}(\frac{du}{dX})^2\frac{d^2u}{dX^2}]-\frac{dp_{osmotic}}{dX}=0 \tag{4.45}$$

In this study, only one-dimensional simulations are conducted. Two kinds of boundary conditions are required at the solution ends (electrodes) and the hydrogel-solution interfaces, respectively, as shown in Figure 4.2. The first is the Dirichlet boundary conditions for the ionic concentrations and electric potential applied at two ends of the solution as,

$$c\big|_{Anode} = c\big|_{Cathode} = c^* \tag{4.46}$$

$$\psi\big|_{Anode} = 0.5V_e \quad \text{and} \quad \psi\big|_{Cathode} = -0.5V_e \tag{4.47}$$

where c^* is the initial ionic concentration of the bath solution and V_e is the externally applied electric voltage.

Another boundary conditions is to assign the values of the fluid pressure and hydrogel displacement at the hydrogel-solution interfaces. Based on the assumption that, in equilibrium state, the chemical potentials of water and ion phase within the hydrogels must be equal to those outside the hydrogels, the boundary conditions of the fluid pressure at the hydrogel-solution interfaces are thus given as

$$p_{interface} = RT\sum_k (c_k^{in-interface} - c_k^{out-interface}) - p_0 \tag{4.48}$$

where $c_k^{in-interface}$ are the ion concentrations within the hydrogels near the interfaces, $c_k^{out-interface}$ are the ion concentrations within exterior solution near the interfaces, and p_0 denotes the fluid pressure at reference configuration.

In addition, the two boundary conditions of mechanical deformation of the hydrogel are imposed on both the ends *a* and *b* of the hydrogel, as shown in Figure 4.2, respectively. In order to eliminate rigid body motion,

$$u\big|_{X_{hydrogel}=0} = 0 \qquad \text{(at the left end } a \text{ of the hydrogel strip)} \tag{4.49}$$

where $X_{hydrogel}$ is defined as the coordinate within the hydrogel domain only. Because of the zero stress on the surface of the hydrogel,

$$\left.\frac{du}{dx}\right|_{X_{hydrogel}=L_{gel}} = \frac{p_{\text{interface}}}{(3\lambda_s + 2\mu_s)} \qquad \text{(at the right end } b \text{ of the hydrogel strip)} \tag{4.50}$$

in which L_{gel} denotes the length of the hydrogel.

Solving the rMECe model will face several mathematical challenges such as the mixed energy domains expressed by the coupled nonlinear partial differential equations, the moving boundaries and the localized high gradients over the hydrogel-solution interfaces. To solve the coupled equations, the Hermite-cloud method mentioned in Chapter 1 is employed here for simulation of the responses of the electric-stimulus-responsive hydrogel. By the computational flowchart of numerical technique, illustrated in Figure 4.1, the Nernst-Planck equations (4.2) and Poisson equation (4.4) are discretized first into a set of nonlinear algebraic equations, which are subsequently solved by the Newton's iterative technique to obtain the converged ionic concentrations c_k and electric potential ψ. Substituting the converged ionic concentrations into the mechanical equilibrium equation (4.45), the corresponding hydrogel displacement *u* is computed. As the hydrogel deforms, the fixed charge density c_f is redistributed within the hydrogel and computed by the equations (4.32). The redistributed c_f is used as input for next iterative computation for solution of the

Poisson-Nernst-Planck equations again. In this way, the iterations are carried out continuously until the convergence of the hydrogel displacement u is achieved.

4.3 Discritization of rMECe Model

For computational convenience, a set of non-dimensional variables is defined as,

$$\begin{aligned} &\bar{x} = \frac{x}{L_{ref}}, \qquad \bar{u} = \frac{u}{L_{ref}}, \qquad \bar{c}_k = \frac{c_k}{c_{ref}}, \quad \bar{c}_f = \frac{c_f}{c_{ref}}, \\ &\bar{\psi} = \frac{\psi}{\psi_{ref}} = \frac{F\psi}{\eta RT}, \qquad \bar{p}_{osmotic} = \frac{p_{osmotic}}{\xi c_{ref} RT} \end{aligned} \tag{4.51}$$

The non-dimensional form of partial differential governing equations of the rMECe model are then written as

$$\frac{d^2\bar{c}_k}{d\bar{x}^2} + \eta z_k \frac{d\bar{c}_k}{d\bar{x}}\frac{d\bar{\psi}}{d\bar{x}} + \eta z_k \bar{c}_k \frac{d^2\bar{\psi}}{d\bar{x}^2} = 0 \qquad (k = 1,2,\cdots,N) \tag{4.52}$$

$$\frac{d^2\bar{\psi}}{d\bar{x}^2} = -\frac{F^2}{\varepsilon\varepsilon_0 RT}\frac{L_{ref}^2 c_{ref}}{\eta}(z_f \bar{c}_f + \sum_{k=1}^{N} z_k \bar{c}_k) \tag{4.53}$$

$$[\frac{d^2\bar{u}}{d\bar{x}^2} + 3\frac{d\bar{u}}{d\bar{x}}\frac{d^2\bar{u}}{d\bar{x}^2} + \frac{3}{2}(\frac{d\bar{u}}{d\bar{x}})^2 \frac{d^2\bar{u}}{d\bar{x}^2}] - \frac{\xi c_{ref} RT}{f_1}\frac{d\bar{p}_{osmotic}}{d\bar{x}} = 0 \tag{4.54}$$

The non-dimensional osmotic pressure equation is given as

$$\bar{p}_{osmotic} = \frac{1}{\xi}\sum_k (\bar{c}_k - \bar{c}_k^0) \tag{4.55}$$

Based on the Hermite-cloud method, the unknown variables are discretized as

$$\bar{c}_k(\bar{x}_i) = \sum_{j=1}^{np} N_j(\bar{x}_i)\bar{c}_{kj} + \sum_{m=1}^{np}(\bar{x}_i - \sum_{j=1}^{np} N_j(\bar{x}_i)\bar{x}_j) M_m(\bar{x}_i)\bar{c}_{km,x} \tag{4.56}$$

$$\bar{\psi}(\bar{x}_i) = \sum_{j=1}^{np} N_j(\bar{x}_i)\bar{\psi}_j + \sum_{m=1}^{np}(\bar{x}_i - \sum_{j=1}^{np} N_j(\bar{x}_i)\bar{x}_j) M_m(\bar{x}_i)\bar{\psi}_{m,x} \tag{4.57}$$

$$\bar{u}(\bar{x}_i) = \sum_{j=1}^{npGel} N_j(\bar{x}_i)\bar{u}_j + \sum_{m=1}^{npGel}(\bar{x}_i - \sum_{j=1}^{npGel} N_j(\bar{x}_i)\bar{x}_j)M_m(\bar{x}_i)\bar{u}_{m,x} \tag{4.58}$$

Finally, the discrete form of the non-dimensional 1-D steady-state partial differential governing equations of the rMECe model and auxiliary conditions are obtained as

$$\begin{aligned}&\sum_{j=1}^{np} N_{j,xx}(\bar{x}_i)\bar{c}_{kj} + \eta z_k[\sum_{m=1}^{np} M_m(\bar{x}_i)\bar{c}_{km,x}][\sum_{m=1}^{np} M_m(\bar{x}_i)\bar{\psi}_{m,x}] + \\ &+\eta z_k[\sum_{j=1}^{np} N_j(\bar{x}_i)\bar{c}_{kj} - \sum_{m=1}^{np}(\bar{x}_i - \sum_{j=1}^{np} N_j(\bar{x}_i)\bar{x}_j)M_m(\bar{x}_i)\bar{c}_{km,x}] \\ &\times[\sum_{j=1}^{np} N_{j,xx}(\bar{x}_i)\bar{\psi}_j] = 0\end{aligned} \tag{4.59}$$

$$\begin{aligned}&\sum_{j=1}^{np} N_{j,xx}(\bar{x}_i)\bar{\psi}_j + \frac{F^2}{\varepsilon\varepsilon_0 RT}\frac{L_{ref}^2 c_{ref}}{\eta}\{z_f c_f + \sum_{k=1}^{N} z_k[\sum_{j=1}^{np} N_j(\bar{x}_i)\bar{c}_{kj} - \\ &\sum_{m=1}^{np}(\bar{x}_i - \sum_{j=1}^{np} N_j(\bar{x}_i)\bar{x}_j)M_m(\bar{x}_i)\bar{c}_{km,x}]\} = 0\end{aligned} \tag{4.60}$$

$$\begin{aligned}&f_1\{\sum_{j=1}^{npGel} N_{j,xx}(\bar{x}_i)\bar{u}_j + 3[\sum_{m=1}^{npGel} M_m(\bar{x}_i)\bar{u}_{m,x}][\sum_{j=1}^{npGel} N_{j,xx}(\bar{x}_i)\bar{u}_j] \\ &+\frac{3}{2}[\sum_{m=1}^{npGel} M_m(\bar{x}_i)\bar{u}_{m,x}][\sum_{m=1}^{npGel} M_m(\bar{x}_i)\bar{u}_{m,x}][\sum_{j=1}^{npGel} N_{j,xx}(\bar{x}_i)\bar{u}_j]\} \\ &-\frac{1}{\xi}\sum_k[\sum_{m=1}^{npGel} M_m(\bar{x}_i)\bar{c}_{km,x}] = 0 \qquad (k = 1,2,\cdots)\end{aligned} \tag{4.61}$$

$$\sum_{j=1}^{np} N_{xj}(\bar{x}_i)\bar{c}_k - [\sum_{j=1}^{np} N_{xj}(\bar{x}_i)\bar{x}_j]\sum_{m=1}^{np} M_m(\bar{x}_i)\bar{c}_{km,x} = 0 \tag{4.62}$$

$$\sum_{j=1}^{np} N_{xj}(\bar{x}_i)\bar{\psi} - [\sum_{j=1}^{np} N_{xj}(\bar{x}_i)\bar{x}_j]\sum_{m=1}^{np} M_m(\bar{x}_i)\bar{\psi}_{m,x} = 0 \tag{4.63}$$

$$\sum_{j=1}^{npGel} N_{xj}(\bar{x}_i)\bar{u} - [\sum_{j=1}^{npGel} N_{xj}(\bar{x}_i)\bar{x}_j]\sum_{m=1}^{npGel} M_m(\bar{x}_i)\bar{u}_{m,x} = 0 \tag{4.64}$$

where *np* is the number of the scattered points in the whole domain covering the hydrogel and surrounding solution, and *npGel* is that within the hydrogel domain only.

4.4 Comparison with Experiment

For examination of the rMECe model, a comparison of simulating results is conducted numerically with the experimental data (Zhou et al., 2002) for a given hydrogel strip with positive fixed charge groups. The experimental parameters used as input data in simulation include $R = 8.3145$ J/mol·K, $F = 9.648 \times 10^4$ C/mol, T=278K, $\varepsilon_0 = 8.854 \times 10^{-12}$ C^2/Nm^2, $\varepsilon = 80$, $c^* = 5.5$ mM, $c_f^0 = 20$ mM, $z_f = +1$, $3\lambda_s + 2\mu_s = 0.12$ MPa, $\phi_0^w = 0.8$, the hydrogel strip thickness $h = 1$ mm, and the one-dimensional computational domain $L = 20$ mm. In general, freely mobile ions diffuse between the porous hydrogel and surrounding solution, if the polyelectrolyte hydrogel is immersed in a bath solution. When an electric field is applied to the bath solution, the diffusive ions will redistribute in the hydrogels and surrounding solution. Due to presence of the fixed charge groups, the diffusion gives rise to the difference in ionic concentrations between the interior hydrogel and exterior solution, which results in the osmotic pressure that drives the swelling or shrinking of the hydrogel. The deformation of the hydrogel leads again to the redistributions of the diffusive ions and fixed charge groups, which causes subsequently the ionic concentration difference and the hydrogel deformation again. Finally, the recurrent kinetics stops until the system reaches an equilibrium state.

The comparison is presented in Figure 4.3, where an average curvature K_a for measurement of the hydrogel deformation is defined as $K_a = 2(e_1 - e_2)/[h(2 + e_1 + e_2)]$ (e_1 and e_2 are the strains of the hydrogel strip at the two ends of the computational

hydrogel domain) at the middle point of hydrogel thickness. It is observed from the figure that the average curvature K_a increases linearly when the applied voltage V_e is small. If V_e is below 2V, the average curvatures K_a computed by both the linear and nonlinear elastic theories agree well with the experimental data. However, with increasing the applied voltage V_e, the average curvatures K_a obtained by the nonlinear elastic theory is much better than that by the linear one. One of the reasons may be that the deformation of the electric-sensitive hydrogels is characterized by many effects, such as the applied electric voltage, fixed charge group, electrolyte composition, ionic diffusion and convection, chemical reactions, temperature and heat conduction. However, the effects of chemical reactions, temperature and heat conduction are neglected here to simplify the present rMECe model with several assumptions: (a) the hydrogel is isotropic and macroscopically homogeneous, (b) all the three phases are incompressible, including the polymeric solid matrix, interstitial water and mobile ions, (c) effect of electro-osmosis is neglected, (d) bath solution is ideal so that the variation of the activity coefficients with ionic strength can be negligible, i.e., its effect on the concentration profiles is negligible, (e) the smart hydrogel is immersed in an unstirred solution in vibration-free experimental device. The bulk flow of fluid or hydrodynamic velocity can thus be eliminated and subsequently the convective flux is neglected, and (f) the pore of the present hydrogel is narrow enough so that the diffusion dominates the transmission of flux. When the applied electric voltage V_e is low such as below V_e=2V, the computational accuracy of the rMECe model is sufficient even if the linear elastic deformation theory is used in

the mechanical equilibrium governing equation. However, with increasing the electric voltage V_e such as above V_e=2V, the coupled nonlinear effects of the physical parameters mentioned before become more and more significant, and then the nonlinear elastic deformation theory has to be employed. Anyway, Figure 4.3 shows a very good agreement in the comparison between the computation and experiment, which validates the rMECe model suitable for simulation of the electric-sensitive hydrogels.

4.5 Simulations and Discussions

4.5.1 Effect of Electric Voltage

In order to further understand the influences of several key physical parameters on the responsive distribution of electric potential and fixed-charge density for the hydrogels subject to electric stimulus, the simulations are carried out with the input parameters as $R = 8.3145\text{J/mol}\cdot\text{K}$, $F = 9.648\times10^4\text{C/mol}$, $T = 298\text{K}$, $z_f = -1$, $\varepsilon = 80$, $\varepsilon_0 = 8.854\times10^{-12}\text{C}^2/\text{Nm}^2$, $3\lambda_s + 2\mu_s = 0.12\text{MPa}$, $\phi_0^w = 0.8$. In the present discussion, the influences of the externally applied electric voltage V_e, are studied in details on the distribution of ionic concentrations, electric potential ψ, fixed-charge density c_f, displacement u and curvature K_a of the hydrogel strip.

It is known that the electroneutrality exists in the bath solution and the hydrogel strip with the fixed charge groups. When the initially fixed charge density

$c_f^0 = 2.0$ mM, the concentration of the bath solution $c^* = 1.0$ mM at pH=7.0, $L = 10$ mm, and $h = 2$ mm, the distributions of the diffusive ionic concentrations are simulated and shown in Figure 4.4, where no external electric field is applied, i.e. $V_e = 0$. It is observed from the figure that the electroneutrality condition is obeyed in the bath solution and the hydrogel strip with the fixed charge groups. The concentrations of the diffusive ionic species are distributed uniformly and symmetrically in the system. This results in a uniform swelling of hydrogel strip without bending deformation. However, once an electric field is applied, the concentration of diffusive ionic species is no longer uniform in the hydrogels and bath solution. Figure 4.5 demonstrates the distributions of the diffusive Na^+ and Cl^- concentrations when the electric voltage is applied at V_e = 0.04V. Due to the voltage applied, the distributions of the diffusive ion concentrations are no longer symmetrical, resulting in the nonzero gradient of the concentration distributions. It is also seen from Figure 4.5 that the difference of ionic concentrations at the hydrogel-solution interfaces between the interior hydrogel and exterior bath solution near the anode is larger than that near the cathode. Actually the boundary layers of ionic concentration over the hydrogel-solution interfaces should be in the Debye-length scale. There is a large boundary layers of ionic concentration obtained in the present simulations, which is an imperfection of the rMECe model developed in this study. They result from the limitation of the computational capability of the rMECe model as a macroscopic continuum model. However, the computational approximation caused by the imperfection is acceptable, especially in the domain far away from the

hydrogel-solution interfaces (Doi et al., 1992). Furthermore, a potential approach to overcome the limitation is a high performance computational technique called the multi-scale algorithm, in which the authors will move in the future work. It is also noted that the present hydrogel is assumed to be charged negatively. When the electric field is applied, the mobile cations transport from anode region to cathode one until the equilibrium state is achieved (Doi et al., 1992). Therefore, the Na^+ concentration increases at the hydrogel edge near the cathode, and decreases at the hydrogel edge near the anode. When the electric current is constant in equilibrium state, one can assume that the electroneutrality conserves at every local point in the solution and the global flow of all ions across the boundary yields a null current. As a result, the Cl^- concentration also increases at the hydrogel edge near the cathode and decreases near the anode. With increasing the distance from the cathode, the concentrations of the diffusive ionic species decrease within the hydrogels. The simulated results shown in the Figure 4.5 agree well with the experimental phenomena (Doi et al., 1992). In brief, the externally applied electric voltage has effect directly on the distributions of ion concentrations. If no electric voltage is applied, the diffusive ion concentrations are distributed uniformly in the hydrogels and surrounding solution. However, the gradients of ion concentration distributions will be nonzero once an electric voltage is applied. The gradients are relatively small or shallow when the applied voltage is low, and they increase responsively with the voltage. The simulations are consistent with experimental observation (Kim and Shin, 1999).

For the following discussions, the simulations are conducted to investigate the

influences of the externally applied electric voltage (V_e=0, 0.1, 0.2 and 0.3V) on the ionic concentrations of the diffusive species, the electric potential, the fixed-charge density and the hydrogel displacement, with the input parameters as, T=298K, c_f^0=4.0mM, $z_f = -1$, $|z_k| = 1$, c^*=2.0mM, L=10mm, and h=2mm.

Figures 4.6 and 4.7 are plotted to discuss the influence of the externally applied electric voltage V_e on the distributions of diffusive ionic concentrations. It is observed that the concentrations of the two mobile ionic species, Na^+ and Cl^-, distribute symmetrically in whole domain, if no electric field is imposed V_e=0. After applying the electric voltage V_e and then increasing V_e, the concentrations of the two mobile ionic species over the hydrogel-solution interface near the cathode increase, and the concentrations decrease near the anode. The gradients of the ionic concentrations increase within the hydrogels. It is also found that the distance between the two hydrogel-solution interfaces enlarges with increasing V_e, meaning the swelling of the hydrogel strip. The simulating results illustrated in Figures 4.6 and 4.7 also agree well with the theoretical analysis mentioned above. The present simulations of the hydrogel swelling qualitatively agree well with the published experiments (Homma et al., 2000; Fei et al., 2002).

Figures 4.8 and 4.9 are plotted for analysis of the influence of the externally applied electric voltage V_e on the distributions of electric potential ψ and fixed-charge density c_f for the hydrogel. It is seen from Figure 4.8 that the gradient of electric potential ψ increases with the externally applied voltage V_e, and the gradient variation of electric potential ψ distributed within the hydrogels is smaller

than that in the surrounding solution because of the higher conductivity of the mobile ions within the hydrogels. It is also seen from Figure 4.9 that the fixed-charge density c_f decreases when the electric voltage V_e increases, and there is an increasing gradient in the asymmetrically distributive profile of the fixed-charge density c_f. It is known that the effect of an electric field on the polyelectrolyte hydrogels is related to the dissociation of the acidic or basic moiety, motion and the redistribution of mobile charged species (Tanaka et al., 1982). There are generally three competing forces acting on the ionic polymeric network. They are the rubber elasticity, the polymer-polymer affinity and the ion pressure. The charged groups on the hydrogel polymeric chains and the mobile ions both inside and outside the hydrogel may be the main contributors to the change in the swelling and/or bending of the hydrogels (Shahinpoor, 1995). When an electric field is applied to the negatively charged hydrogel in the bath solution, the counterions (sodium ions) in the gel move toward the cathode. In the presence of higher electrolyte concentration in solution, more counterions enter the hydrogel than those migrate from the hydrogel to the cathode. With increment of the applied voltage V_e, the diffusive ionic concentrations over the hydrogel-solution interface decrease near the anode, but increase near the cathode. This amplifies the concentration difference of the diffusive ions between the hydrogel-solution interfaces. The osmotic pressure increases at the side near anode, but decreases at the side near cathode. The swelling is more significant at the hydrogel side near the anode. Consequently, the difference of the osmotic pressure occurred in the hydrogel makes the hydrogel strip bent toward the cathode and swelling (Shiga et al.,

1992; Kim et al., 2003b). Thus the fixed charge group redistributes in the hydrogel and the corresponding density c_f decreases. The discussions based on the simulation are qualitatively consistent with experimental phenomena (Homma et al., 2000; Fei et al., 2002).

Figure 4.10 is presented for analysis of the influence of the externally applied electric voltage V_e on the distribution of the displacement *u* of the hydrogel. It is known from the figure that the displacement *u* of the hydrogel increases with the applied voltage V_e, especially the displacement *u* of the hydrogel increases nonlinearly when the applied voltage V_e becomes higher. Therefore, the electric-sensitive hydrogel under externally applied electric voltage can gain great axial deformation and enhance the mechanical strength. It is also seen that the distribution of the displacement *u* is linear at low voltage V_e, and becomes nonlinear at high V_e. The present simulating results are good consistent with the experimental phenomenon reported by Shiga and Kurauchi (1990) for study of deformation of ionic polymer gels under electric field. The numerical results demonstrate that the hydrogel is a suitable candidate for powerful actuator and artificial muscles for BioMEMS application.

Figure 4.11 is plotted for analysis of the influence of the externally applied electric voltage V_e on the curvature K_a of the hydrogel strip. It is observed that the hydrogel displacement increases with the applied voltage, and the increment becomes increasingly nonlinear as the voltage is correspondingly increased. It is also seen that the distribution of the hydrogel displacement is linear at the low voltage, and gradually

becomes nonlinear at the higher level.

4.5.2 Effect of Initially Fixed Charge Group Density

In order to further understand the influences of various physical parameters on the responsive deformation of the hydrogels subject to electric stimulus, several simulations are carried out with the input parameters as $R = 8.3145$ J/mol·K, $F = 9.648 \times 10^4$ C/mol, $T = 298$ K, $\varepsilon_0 = 8.854 \times 10^{-12}$ C^2/Nm^2, $\varepsilon = 80$, $3\lambda_s + 2\mu_s = 0.12$ MPa, $z_f = -1$. In this section, the influences of the initially fixed charge density c_f^0 and the externally applied electric field V_e are discussed on the distribution of diffusive ionic concentrations, the electric potential ψ, fixed-charge density c_f and the displacement u of the electric-sensitive hydrogel. The coupled influences of the electric voltage V_e, initially fixed charge density c_f^0 and hydrogel strip thickness h are also studied in detail on the hydrogel curvature K_a.

Figures 4.12 and 4.13 demonstrate the influence of the initially fixed charge density c_f^0 on the distribution of diffusive ionic concentrations, when V_e=0.12V, $c^* = 1.0$ mM, $|z_k|$=1, $L = 10$ mm, $h = 2$ mm, $c_f^0 = 2.0$, 3.0, 4.0, 5.0 and 6.0mM, respectively. It is shown from Figure 4.12 that, as the initially fixed charge density c_f^0 increases linearly, the concentrations distributions of the cation Na^+ increase rapidly within the hydrogels, and the increase of the distance between the two hydrogel-solution interfaces reveals the hydrogel strip swelling. It is found from Figure 4.13 that the influence of the initially fixed charge density c_f^0 on the distribution of

Cl^- concentration is relatively smaller than those on the cation Na^+ concentrations. Probably the reason is that the negative fixed-charge groups ($z_f = -1$) attached onto the polymeric network chains attract the mobile cation Na^+ to compensate the electric potential for electroneutrality within the hydrogel. The concentrations of the cation within the hydrogels increase obviously with increase of the initially fixed-charge density c_f^0, which makes main contribution into the increment of the ionic concentration differences between the hydrogel-solution interfaces. Similarly, this leads to the increase of osmotic pressure and then causes the swelling of the hydrogel. The simulated results are confirmed by the experimental phenomena (Fei et al., 2002).

Figures 4.14 and 4.15 demonstrate the influence of the initially fixed charge density c_f^0 on the distributions of the electric potential ψ and fixed-charge density c_f for the electric-sensitive hydrogel, when V_e =0.12V, $c^* = 1.0$ mM, $|z_k| = 1$, $L = 10$ mm, $h = 2$ mm, $c_f^0 = 2.0$, 3.0, 4.0, 5.0 and 6.0mM, respectively. It is shown from Figure 4.14 that, as the initially fixed charge density c_f^0 increases linearly, the gradient of electric potential ψ distributed within the hydrogels becomes smaller, compared with that in the surrounding solution. It is also found from Figure 4.15 that the fixed charge density c_f increases almost linearly. It is known that the cations H^+ and Na^+ concentrations within the hydrogels increase obviously with the increase of the initially fixed-charge density c_f^0, which is one of main contributions into the increase of the ionic concentration differences between the hydrogel-solution interfaces. The more mobile ions diffuse into the hydrogel and then the higher

conductivity is achieved, which results in the smaller gradient of electric potential ψ. This enlarges alike the osmotic pressure and the hydrogel swells. At equilibrium state, the redistributed fixed charge density c_f is smaller than the initially fixed charge density c_f^0. Similar experimental phenomenon has been reported (Kim et al., 2003), in which the HA-PVA IPN hydrogel with higher HA content as fixed charge groups exhibits deswelling much more. The reason may be that the initially fixed charge density on the crosslinking networks affects the mechanical properties of a polymer, such as the Young's modulus and ultimate tensile strength of the hydrogel.

Figure 4.16 demonstrates the influence of the initially fixed charge density c_f^0 on the hydrogel displacement *u*, when V_e=0.12V, $c^* = 1.0$ mM, $|z_k|$=1, $L = 10$ mm, $h = 2$ mm, $c_f^0 = 2.0$, 3.0, 4.0, 5.0 and 6.0mM, respectively. It is shown from the figure that, as the initially fixed charge density c_f^0 increases linearly, the hydrogel displacement *u* increases rapidly, and the displacement distributions remain linear.

In order to investigate the influences of the electric voltage V_e coupled with initially fixed charge density c_f^0 on the hydrogel curvature K_a, Figure 4.17 is illustrated for different electric voltages V_e = 0.08, 0.16 and 0.32V, and Figure 4.18 for different initially fixed charge densities c_f^0 =2.0, 4.0, 8.0 and 16.0mM, when $c^* = 2.0$ mM, $|z_k| = 1$, $h = 5$ mm, $L = 15$ mm. For a given initially fixed charge density c_f^0, as the externally applied electric voltage V_e increases, the differences of the ionic concentrations and electric potential increase between the hydrogel strip and bathing solution. This will enlarge then the bending deformation and the corresponding average curvature K_a increases drastically. The relation between the average

curvature K_a and initially fixed charge density c_f^0 becomes more and more nonlinear with increase of electric voltage V_e. For a given applied voltage V_e, the average curvature K_a increases with the initially fixed charge density c_f^0. Figure 4.19 shows the coupled influence of externally applied electric voltage V_e and hydrogel strip thickness *h* on the average curvature K_a for V_e=0.04, 0.20, 0.40 and 0.80V, respectively, where $c_f^0 = 10$ mM, $c^* = 1.0$ mM, $|z_k| = 1$, $L = 15$ mm. As expected, the average curvature K_a of the hydrogel strip decreases rapidly with increasing thickness *h*, especially when electric voltage V_e is higher. The present simulations are in good agreement with the experimental phenomena (Homma et al. 2000, 2001, Sun and Mak 2001, Fei et al. 2002).

4.5.3 Effect of Ionic Strength

For further understanding of the influences of various physical parameters on the ionic transport and responsive distribution of diffusive ionic concentrations when the hydrogel is subjected to electric stimulus, several simulations are made with the input parameters as $R = 8.3145$ J/mol·K, $F = 9.648 \times 10^4$ C/mol, $T = 298$ K, $\varepsilon_0 = 8.854 \times 10^{-12}$ C^2/Nm^2, $\varepsilon = 80$, $3\lambda_s + 2\mu_s = 0.12$ MPa, $z_f = -1$. In this subsection, the influences of the solution ionic strength *I* ($I = \frac{1}{2}\sum_k c_k z_k^2$) is discussed on the equilibrium response of the electric-sensitive hydrogel.

To study the influence of ionic strength *I* of the surrounding solution on the distribution of diffusive ionic concentrations, the simulations are conducted and shown

in Figures 4.20-22, with V_e =0.10V, $c_f^0 = 10.0$ mM, $L = 10$ mm, $h = 2$ mm and $I = 1.0$, 2.0, 4.0, 6.0 and 8.0mM, respectively. It is found from Figure 4.20 that, with increasing the ionic strength *I*, the distribution of H^+ concentration decreases rapidly within the hydrogels, and the distance reduces between the two hydrogel-solution interfaces. This means the shrinking of the hydrogel strip. On the other hand, Figures 4.21 and 4.22 reveal that the distributions of the concentrations of the diffusive ions, Na^+ and Cl^-, within the hydrogels increase rapidly with increasing ionic strength *I*. Actually the increase of ionic strength *I* makes more contribution into the increase of concentration of the surrounding solution, relatively compared with the contribution into that in the hydrogels. This reduces the concentration differences of diffusive ionic species between the hydrogel-solution interfaces, resulting in the decrease of the osmotic pressure. Therefore, the hydrogels shrink. The similar phenomena are observed in the experiments (Sannino et al., 2005; Caykara and Aycicek, 2005).

For study of the influence of ionic strength *I* of the surrounding solution on the distributions of electric potential ψ and fixed-charge density c_f of the hydrogel, the simulations are conducted and shown in Figures 4.23 and 4.24, with V_e =0.10V, $c_f^0 = 10.0$ mM, $L = 10$ mm, $h = 2$ mm and I = 1.0, 2.0, 4.0, 6.0 and 8.0mM, respectively. It is observed from Figure 4.23 that, with increasing the ionic strength *I*, the gradient of electric potential ψ within the hydrogel increases, and the distribution of electric potential ψ looks linear in the whole domain covering the hydrogel and bathing solution, especially at high ionic strength *I*. Probably, the higher ionic strength makes the mobile ions diffuse more into the hydrogel, then the conductivity of

hydrogels is almost equal to that of surrounding solutions, which results in the electric potential ψ quasi-linearly distribute in the whole domain. From Figure 4.24, it is known that the fixed charge density c_f and the corresponding gradient in the hydrogel increase with the ionic strength *I*. It is noted that the dissociation of carboxylic groups in the polymeric matrix imparts ionic character to the hydrogels and affects the ion osmotic swelling pressure (Bajpai, 2001). In fact, as the ionic strength *I* increases, more contribution into the increase of the concentration in the surrounding solution, relatively compared with the contribution to that in the hydrogels. This reduces the concentration differences of diffusive ions between the hydrogel-solution interfaces. The reducing concentration differences decrease the osmotic pressure. It is also observed from the experimental swelling phenomena of polyelectrolyte gels that the osmotic pressure reduces ultimately the equilibrium swelling capacity of the hydrogels. Then the hydrogels shrink. This makes the fixed charge density and the corresponding gradient increase (Khare and Peppas, 1995).

For study of the influence of ionic strength *I* of the surrounding solution on the variation of hydrogel displacement *u*, the simulations are conducted and shown in Figure 4.25, with V_e=0.10V, $c_f^0 = 10.0\,\text{mM}$, $L = 10\,\text{mm}$, $h = 2\,\text{mm}$ and $I = 1.0$, 2.0, 4.0, 6.0 and 8.0mM, respectively. It is found that, with increasing the ionic strength *I*, the hydrogel displacement *u* decreases and the displacement distribution changes to nonlinear profile from linear one.

Figure 4.26 illustrates the influence of the ionic strength *I* on the variation of average curvature K_a with $c_f^0 = 10.0\,\text{mM}$, V_e=0.08, 0.2 and 0.4(V), respectively. It

is shown that an optimal *I* value of the surrounding solution triggers the hydrogel strip to reach the largest bending deformation. When the ionic strength *I* is bigger than the optimal value, the bending deformation of hydrogel strip decreases. The simulation results are consistent with the experimental phenomena (Sun et al., 2001; Fei et al., 2002).

4.5.4 Effect of Ionic Valence

To further understand the influences of various physical parameters on the deformation of the hydrogels in response to electric stimulus, several simulations are carried out with the following input parameters, $R = 8.3145$ J/mol·K, $F = 9.648 \times 10^4$ C/mol, $T = 298$ K, $\varepsilon_0 = 8.854 \times 10^{-12}$ C^2/Nm^2, $\varepsilon = 80$, $3\lambda_s + 2\mu_s = 0.12$ MPa, $z_f = -1$. In this subsection, the influences of the externally applied electric field V_e and ionic valence $|z_k|$ are examined on the equilibrium behavior of the electric-sensitive hydrogel.

Figures 4.27 and 4.28 illustrate the influence of the ionic valence $|z_k|$ of the surrounding solution on the distributions of diffusive ionic concentrations, where V_e=0.10V, $c_f^0 = 2.0$ mM, $c^* = 1.0$ mM, $L = 10$ mm, $h = 2$ mm and $|z_k|$=1, 2, and 3, respectively. It is noted that the changes of the concentrations distribution of diffusive ionic species when $|z_k|$ varies from 1 to 2 is much more than those when $|z_k|$ varies from 2 to 3. In fact, if the surrounding solution is changed from univalent electrolyte to bivalent or trivalent one, the concentration difference of diffusive cations decreases significantly between the hydrogel and solution, the variation of the

concentration distributions is relatively small for the diffusive anions. This gives rise to the smaller osmotic pressure and then the hydrogels shrink. Anyway, the presently computed results agree well with the experimental phenomena (Homma et al., 2000, 2001).

Figures 4.29 and 4.30 are plotted for discussion of the influence of the ionic valence $|z_k|$ of the surrounding solution on the distribution of electric potential ψ and fixed-charge density c_f of the hydrogel, where V_e =0.10V, $c_f^0 = 2.0$ mM, $c^* = 1.0$ mM, $L = 10$ mm, $h = 2$ mm and $|z_k|$= 1, 2 and 3, respectively. It is noted that, when $|z_k|$ varies from 1 to 2, the changes of the distributions of electric potential ψ and fixed-charge density c_f are much larger than those when $|z_k|$ varies from 2 to 3. If the surrounding solution is changed from univalent electrolyte to bivalent or trivalent one, the concentration difference of diffusive cations decreases obviously between the hydrogel and solution, the variation of the concentration distributions of the diffusive anions is relatively small. The presence of the negative charge groups fixed onto the hydrogel networks may be the reason for the observed results. To maintain the electroneutrality condition in the hydrogel, the amount of single-valent ions (such as sodium ions Na^+) required to bind to the carboxylate ions will be almost the double of the amount of bivalent ions (such as calcium ions Ca^{2+}) for the same degree of ionization inside the polymer network. As such, when the ion valence increases, the ion osmotic pressure decreases significantly, because fewer amount of counterions diffuse into the hydrogel to neutralize the fixed charge groups. This reduces the osmotic pressure and then causes the hydrogels to shrink, which agrees

well with the experimental phenomena (Siegel and Firestone, 1988; Siegel, 1990b; Homma et al., 2000, 2001; Bajpai, 2001).

Figure 4.31 indicates the influence of the ionic valence $|z_k|$ of the surrounding solution on the hydrogel displacement u, where $V_e = 0.1\text{V}$, $c_f^0 = 2.0$ mM, $c^* = 1.0$ mM, $L = 10$ mm, $h = 2$ mm and $|z_k| = 1$, 2, and 3, respectively. It is noted that the changes of the hydrogel displacement u when $|z_k|$ varies from 1 to 2 is much more than those when $|z_k|$ varies from 2 to 3. It is also seen that the hydrogel displacements u distribute nonlinearly at $|z_k| = 2$ and 3. The presently computed results agree well with the experimental phenomena (Homma et al. 2000, 2001).

Figure 4.32 examines the influence of the ionic valence on the bending deformation of the electric-sensitive hydrogel. It is shown that the average curvature K_a increases linearly at the beginning stage of the applied electric voltage, while the K_a increases gradually as the applied voltage is intensified. It is also found that the magnitude of K_a increases with the increment of ionic valence, especially when $|z_k|$ increases from 1 to 2. Figure 4.33 shows the impact of the ionic valence on the swelling ratio of the hydrogel. The hydrogel shows the essential behavior whereby the swelling ratio increases linearly with increasing applied electric voltage.

4.6 Remarks

This chapter has modeled and simulated the equilibrium responsive behaviors of stimulus-sensitive hydrogels subject to the externally applied electric field. The

refined model can be used to explain and predict theoretically the experimental phenomena of the distributions of ionic concentration, electric potential and network deformation. By direct comparison with experimental data, the rMECe model for the electric-sensitive hydrogels presented in this chapter has been verified and can be reasonably used to examine how the equilibrium response of electric-sensitive hydrogels is triggered by externally applied DC electric voltage, to show the distributions of ionic concentrations and the electric potential as well as the fixed charge density across the domain of both hydrogel and surrounding solution, and to evaluate the effects of various conditions on the behaviors of the electric-sensitive hydrogels.

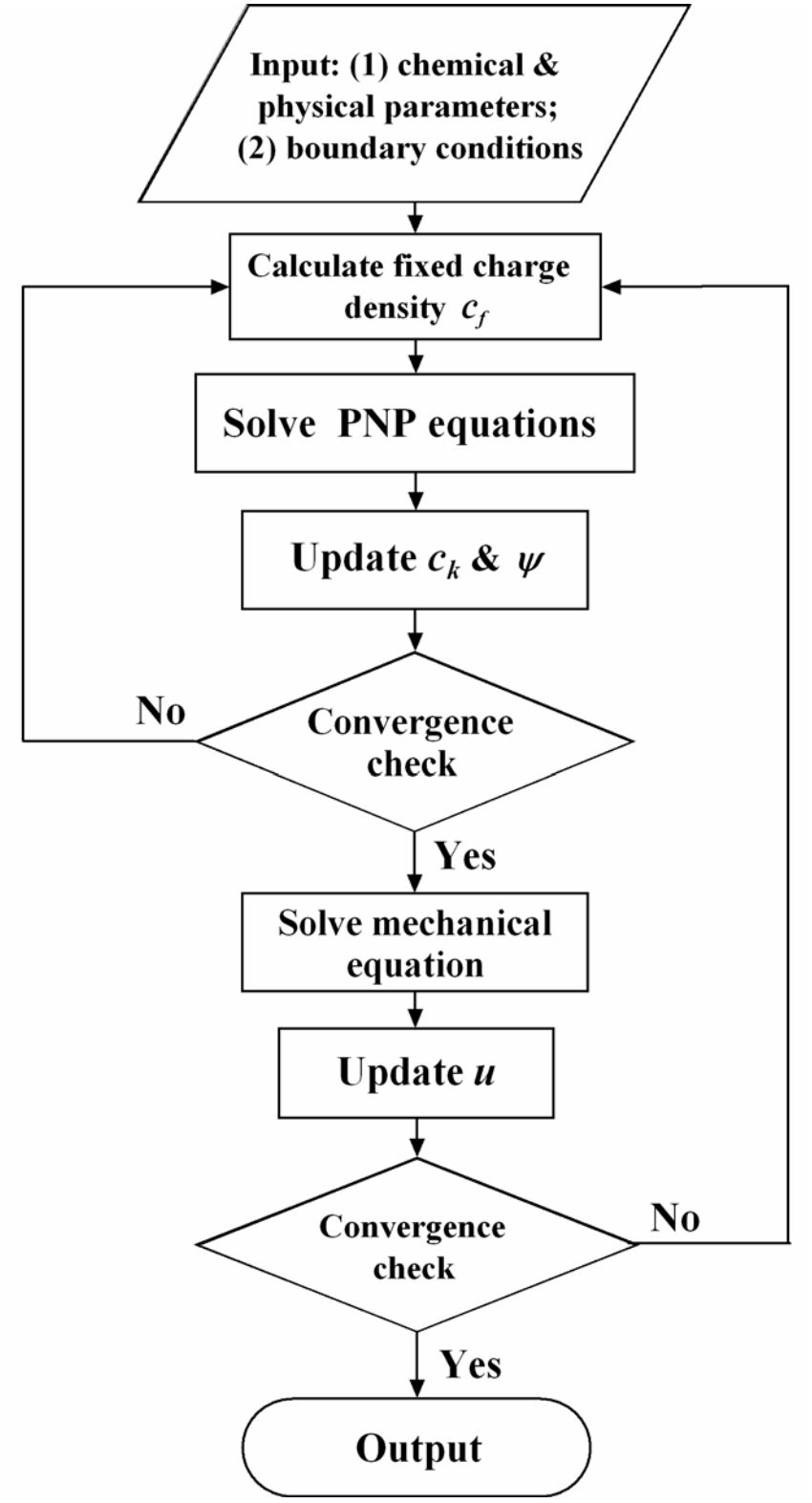

Figure 4.1 Computational flowchart of rMECe model.

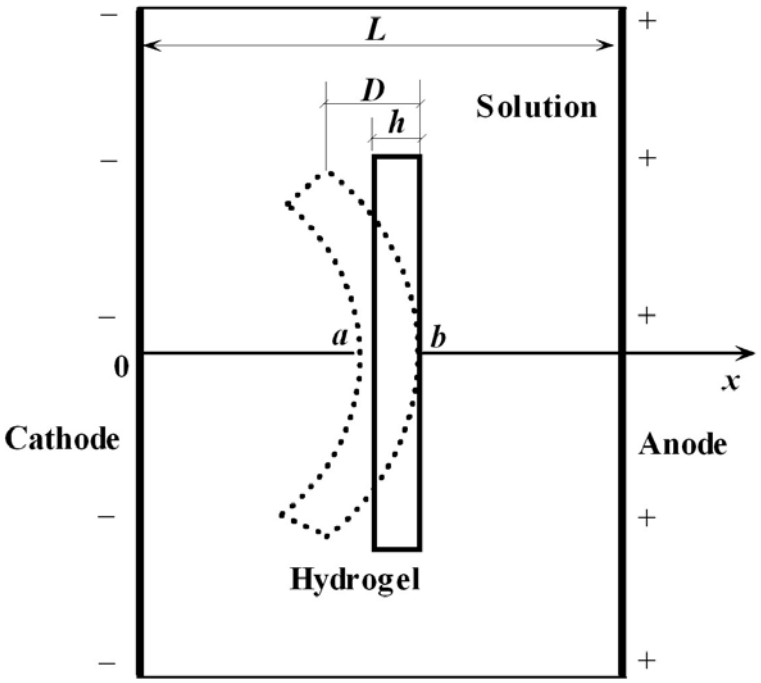

Figure 4.2 Schematic diagram of a hydrogel strip immersed in bath solution under externally applied electric field.

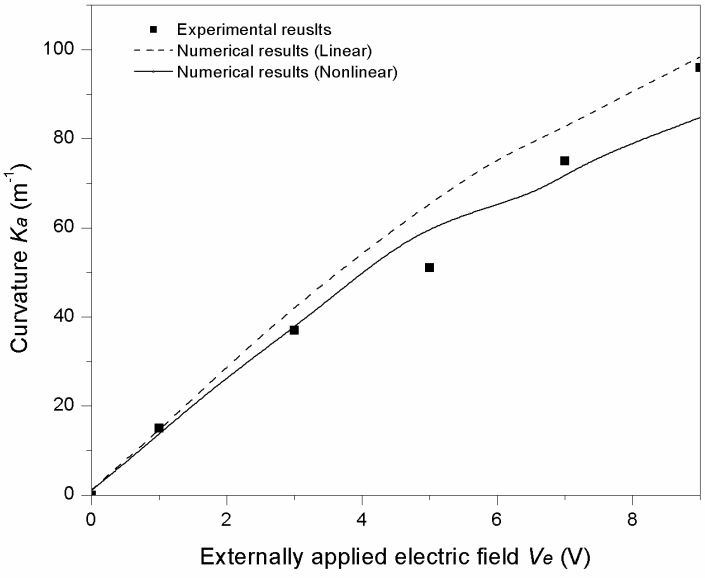

Figure 4.3 Comparison of numerically computed results with experimental data (Zhou et al., 2002).

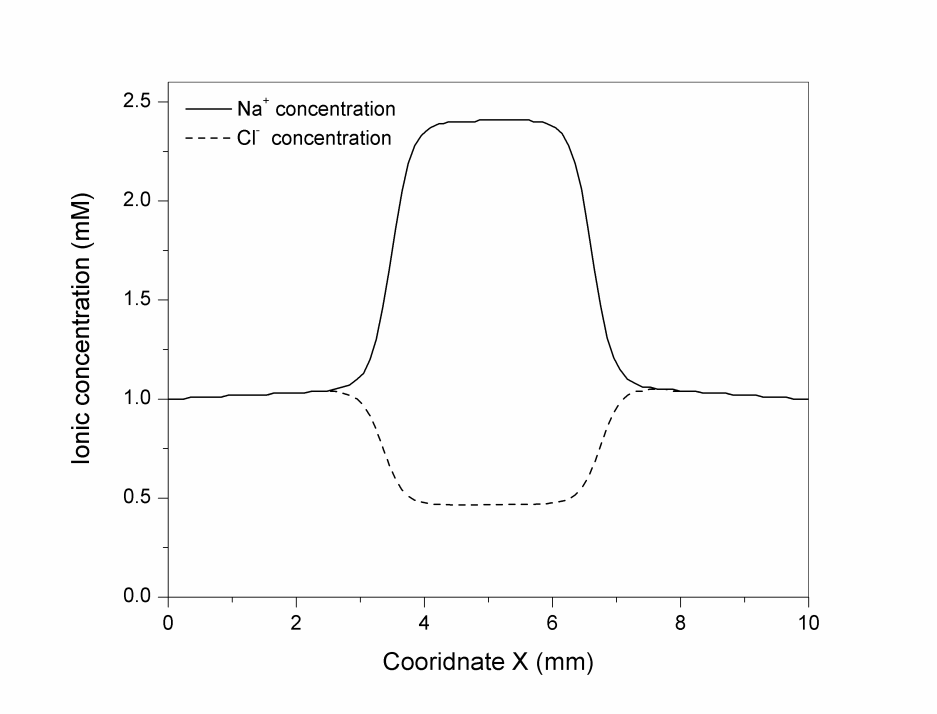

Figure 4.4 Distribution of diffusive ionic concentrations without external electric field ($V_e = 0$).

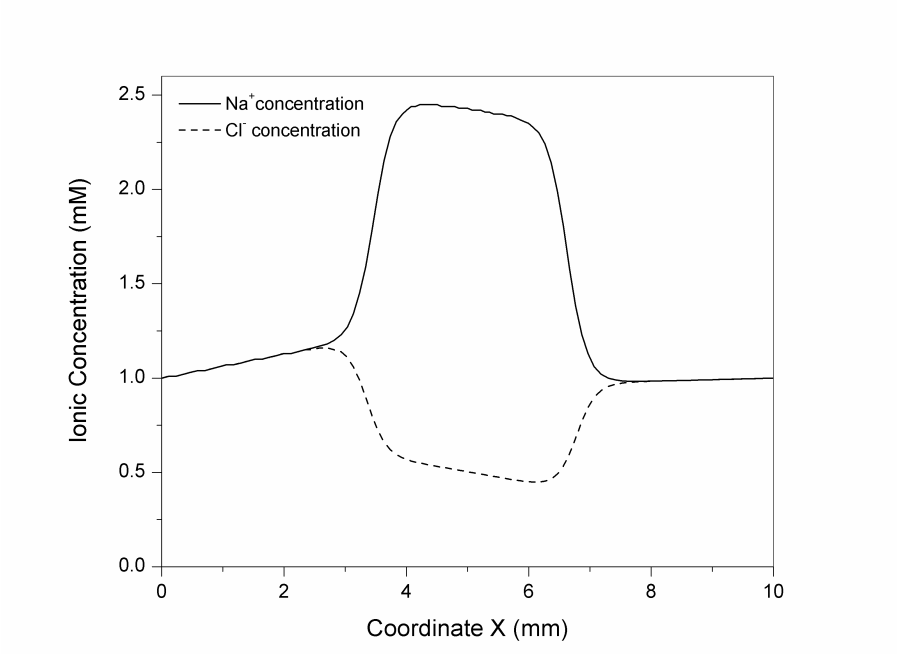

Figure 4.5 Distribution of the diffusive ionic concentrations with external electric field ($V_e = 0.04$ V).

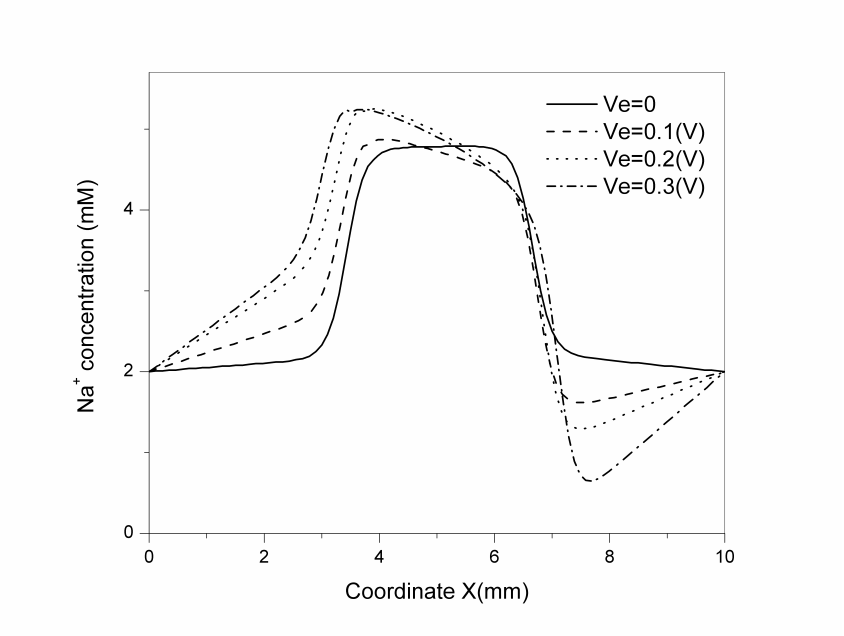

Figure 4.6 Influence of the externally applied electric voltage V_e on the distribution of the diffusive Na^+ concentration ($c_f^0 = 4.0$ mM, $c^* = 2.0\,\text{mM}$, $|z_k|=1$).

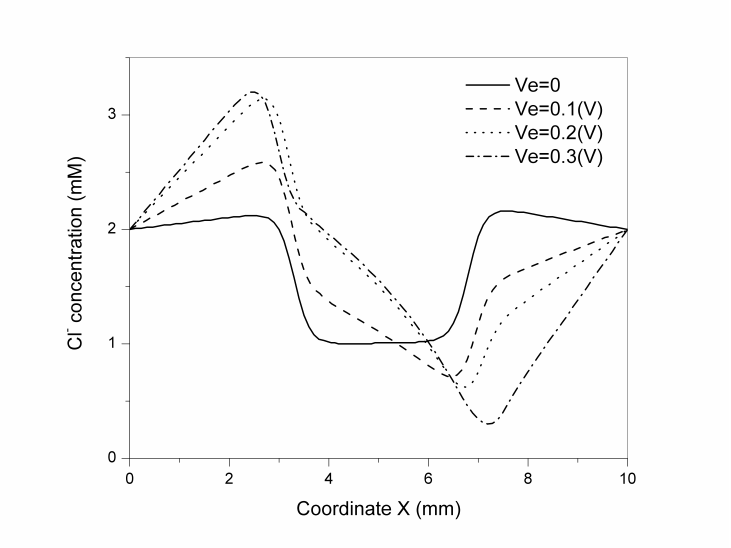

Figure 4.7 Influence of the externally applied electric voltage V_e on the distribution of the diffusive Cl^- concentration ($c_f^0 = 4.0$ mM, $c^* = 2.0\,\text{mM}$, $|z_k|=1$).

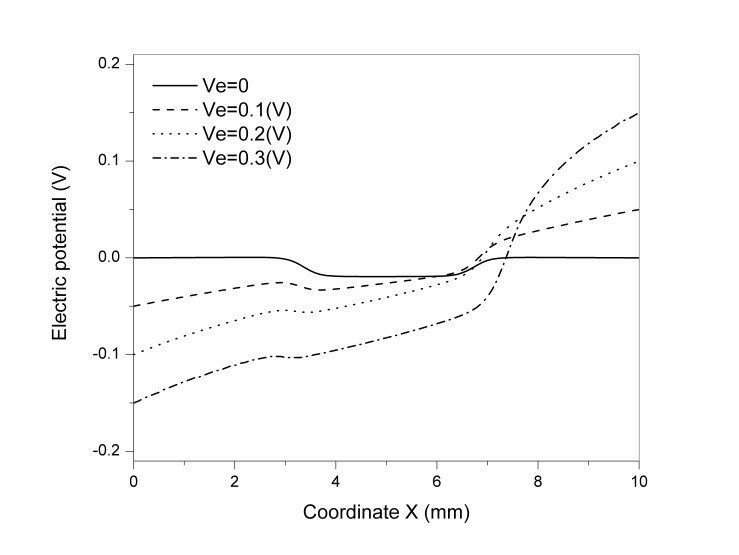

Figure 4.8 Influence of the externally applied electric voltage V_e on the distribution of the electric potential ψ ($c_f^0 = 4.0$ mM, $c^* = 2.0$ mM, $|z_k|=1$).

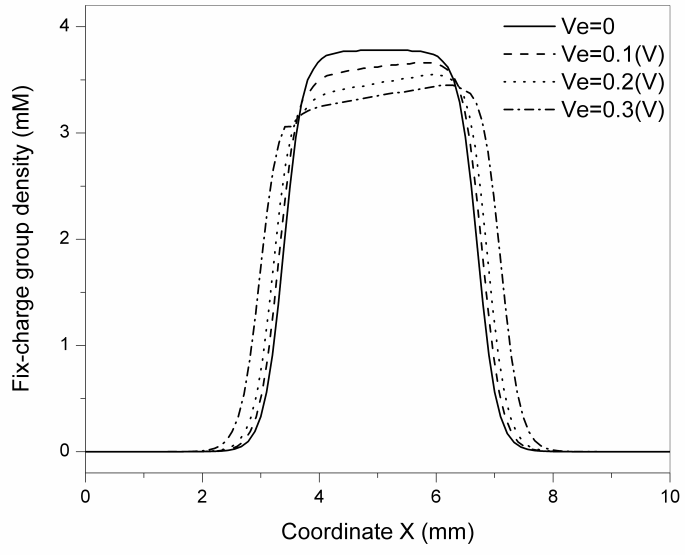

Figure 4.9 Influence of the externally applied electric voltage V_e on the distribution of the fixed charge density c_f ($c_f^0 = 4.0$ mM, $c^* = 2.0$ mM, $|z_k|=1$).

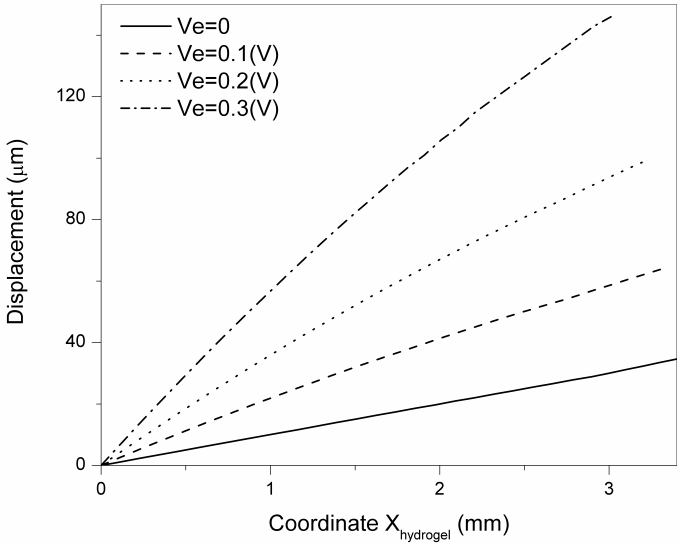

Figure 4.10 Influence of the externally applied electric voltage V_e on the displacement u of the hydrogel strip ($c_f^0 = 4.0\,\text{mM}$, $c^* = 2.0\,\text{mM}$, $|z_k|=1$).

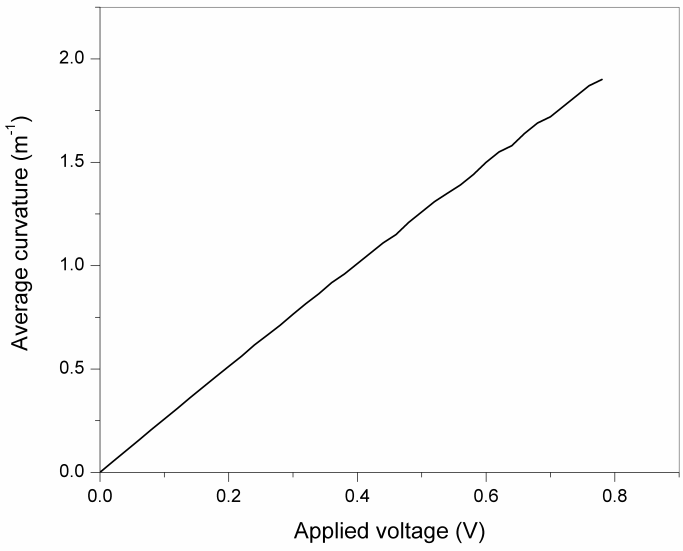

Figure 4.11 Influence of the externally applied electric voltage V_e on the curvature K_a of the hydrogel strip ($c_f^0 = 4.0\,\text{mM}$, $c^* = 2.0\,\text{mM}$, $|z_k|=1$).

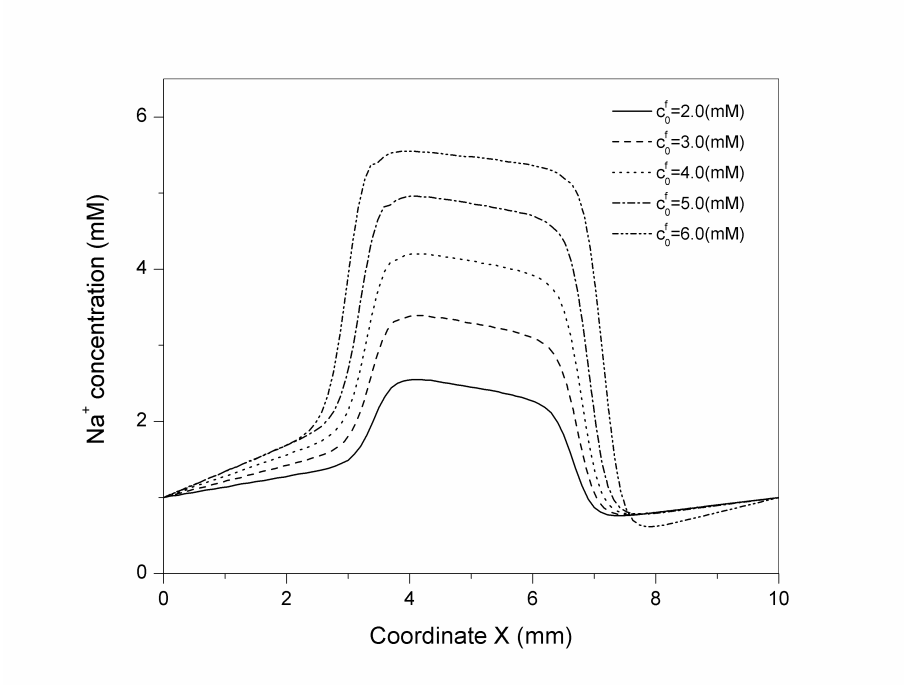

Figure 4.12 Influence of the initially fixed charge density c_f^0 on the distributions of the diffusive Na^+ concentration (V_e=0.12V, $c^* = 1.0\,\text{mM}$, $|z_k|$=1).

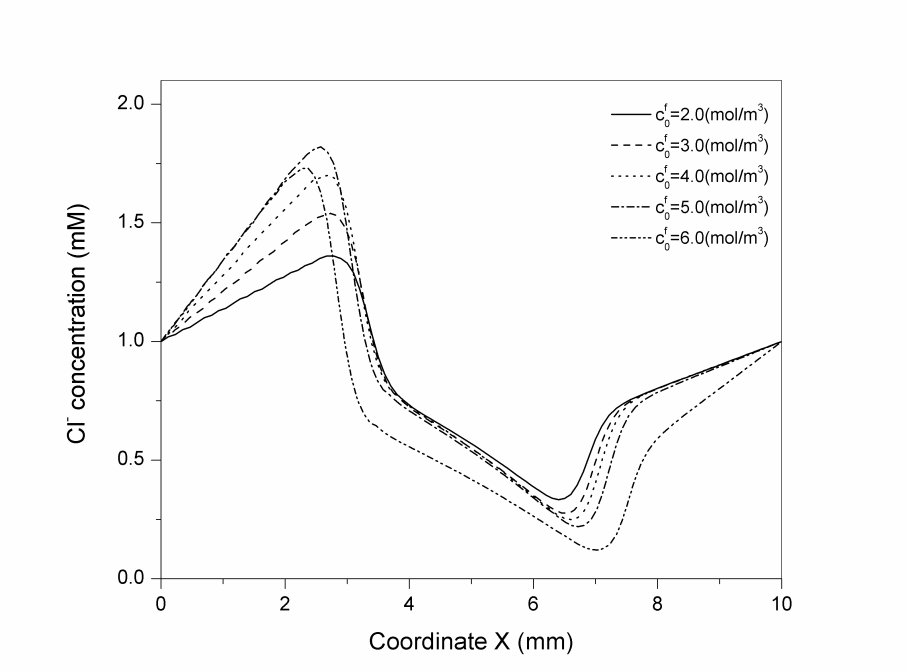

Figure 4.13 Influence of the initially fixed charge density c_f^0 on the distributions of the diffusive Cl concentration (V_e=0.12V, $c^* = 1.0\,\text{mM}$, $|z_k|$=1).

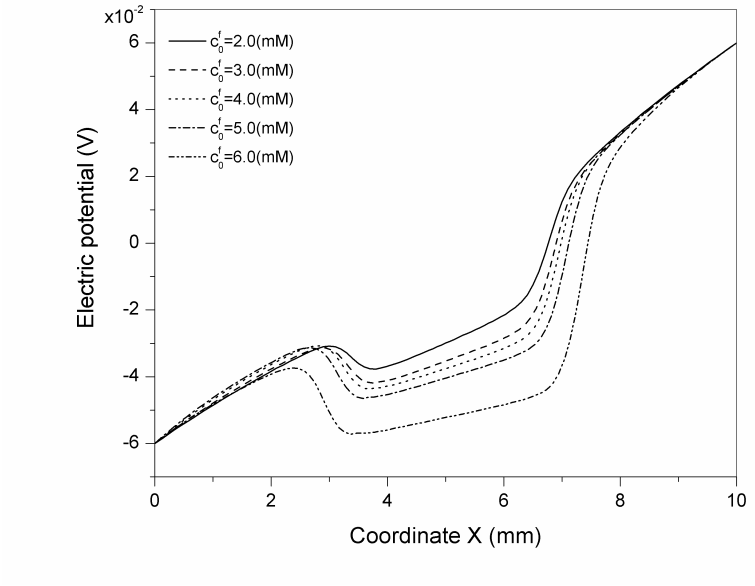

Figure 4.14 Influence of initially fixed charge density c_f^0 on the distribution of electric potential ψ (V_e=0.12V, $c^* = 1.0\,\text{mM}$, $|z_k|$=1).

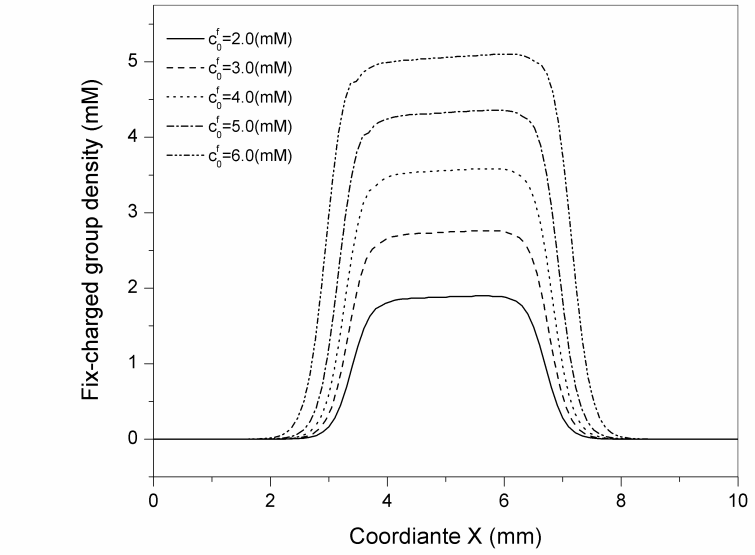

Figure 4.15 Influence of initially fixed charge density c_f^0 on the distribution of fixed charge density c_f (V_e=0.12V, $c^* = 1.0\,\text{mM}$, $|z_k|$=1).

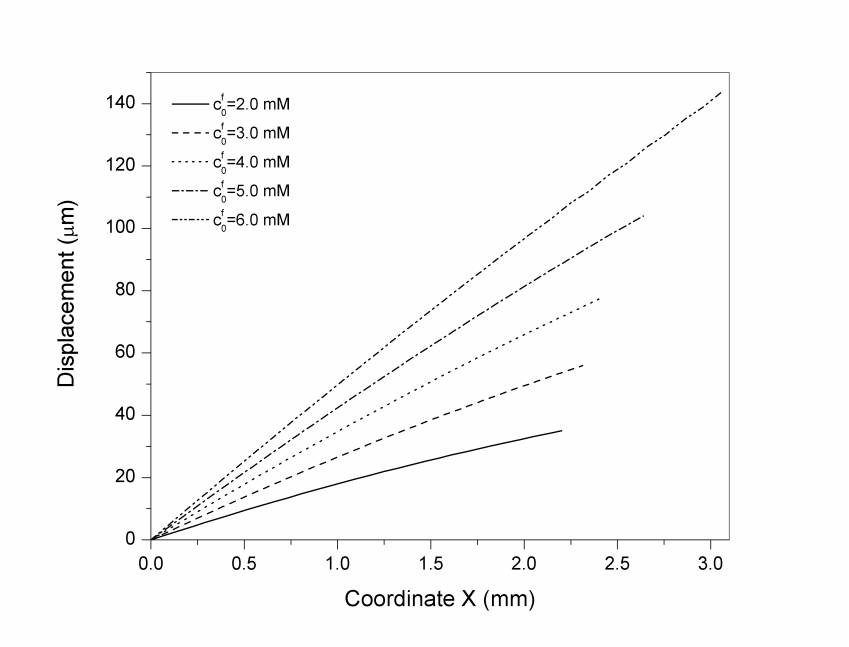

Figure 4.16 Influence of initially fixed charge density c_f^0 on the variation of displacement u (V_e=0.12V, $c^* = 1.0\,\text{mM}$, $|z_k|$=1).

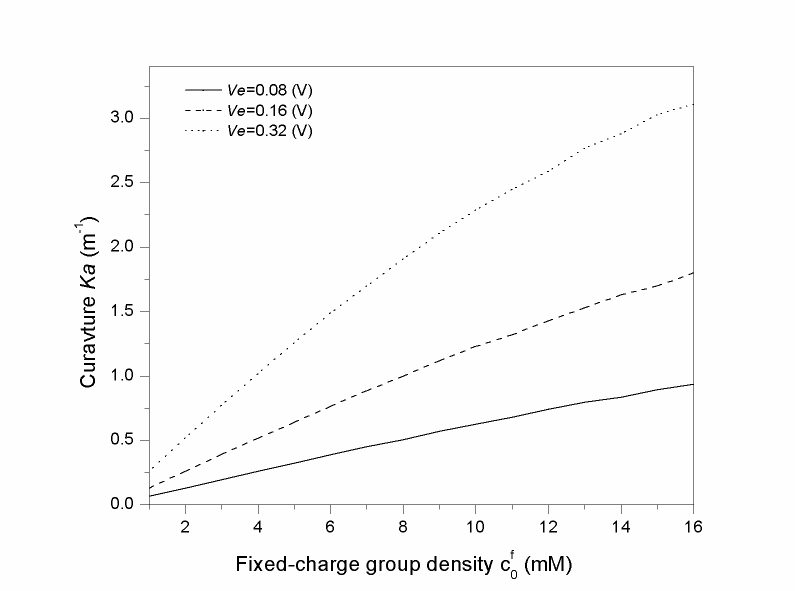

Figure 4.17 Coupling influence of externally applied voltage V_e and the initially fixed charge density c_f^0 on the average curvature K_a ($c^* = 2.0\,\text{mM}$, $|z_k|$=1).

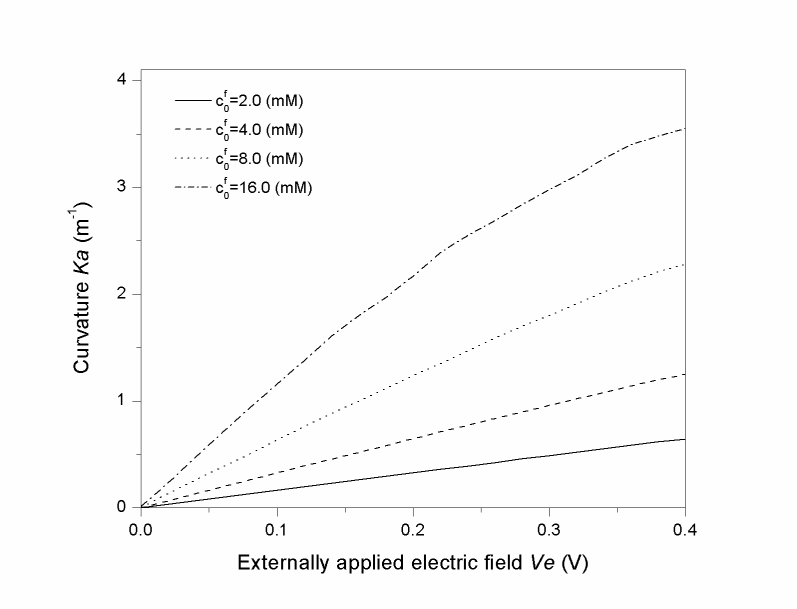

Figure 4.18 Coupling influence of the initially fixed charge density c_f^0 and externally applied electric voltage V_e on the average curvature K_a ($c^* = 2.0\,\text{mM},\ |z_k|=1$).

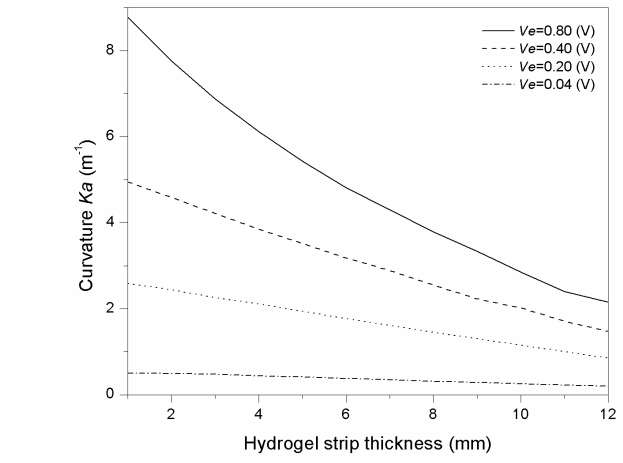

Figure 4.19 Coupling influence of externally applied voltage V_e and the hydrogel strip thickness h on the average curvature K_a ($c_f^0 = 10.0$ mM, $c^* = 1.0\,\text{mM},\ |z_k|=1$).

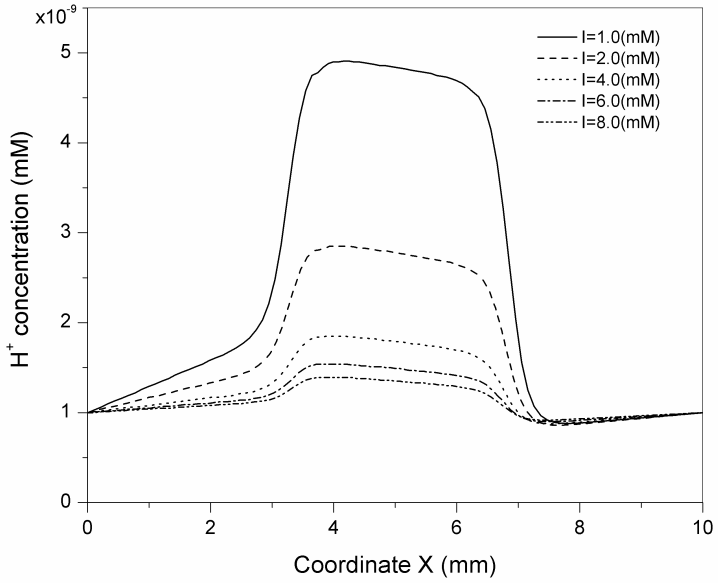

Figure 4.20 Influence of the ionic strength *I* of bath solution on the distributions of the diffusive H^+ concentration (V_e=0.10V, $c_f^0 = 10.0$ mM).

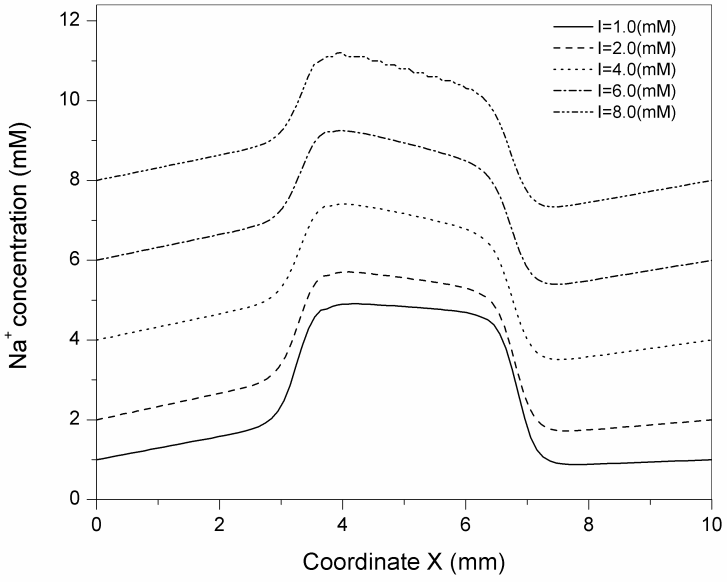

Figure 4.21 Influence of the ionic strength *I* of the bath solution on the distributions of the diffusive Na^+ concentration (V_e=0.10V, $c_f^0 = 10.0$ mM).

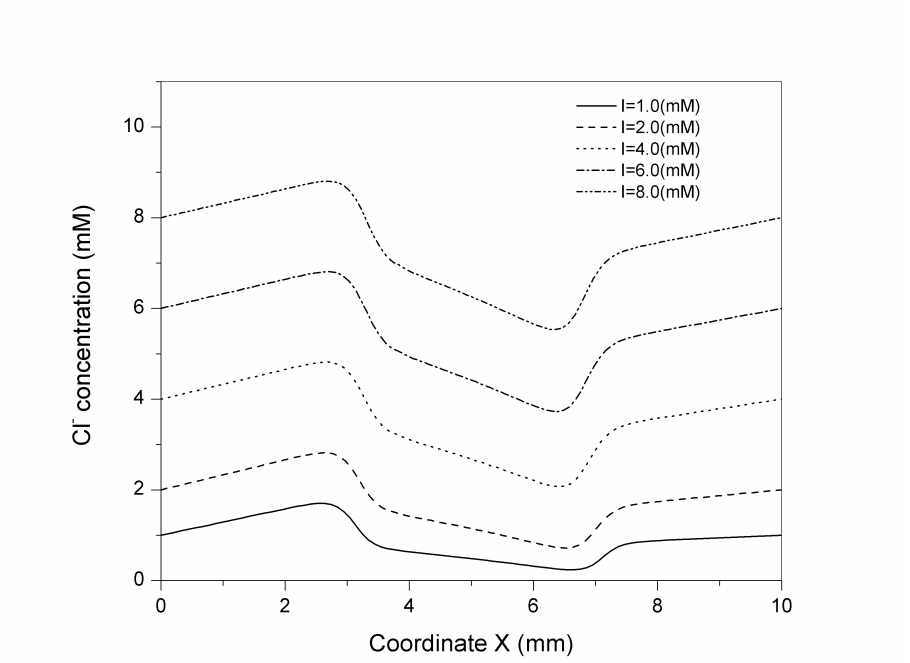

Figure 4.22 Influence of the ionic strength I of the bath solution on the distributions of the diffusive Cl concentration (V_e=0.10V, $c_f^0 = 10.0\,\text{mM}$).

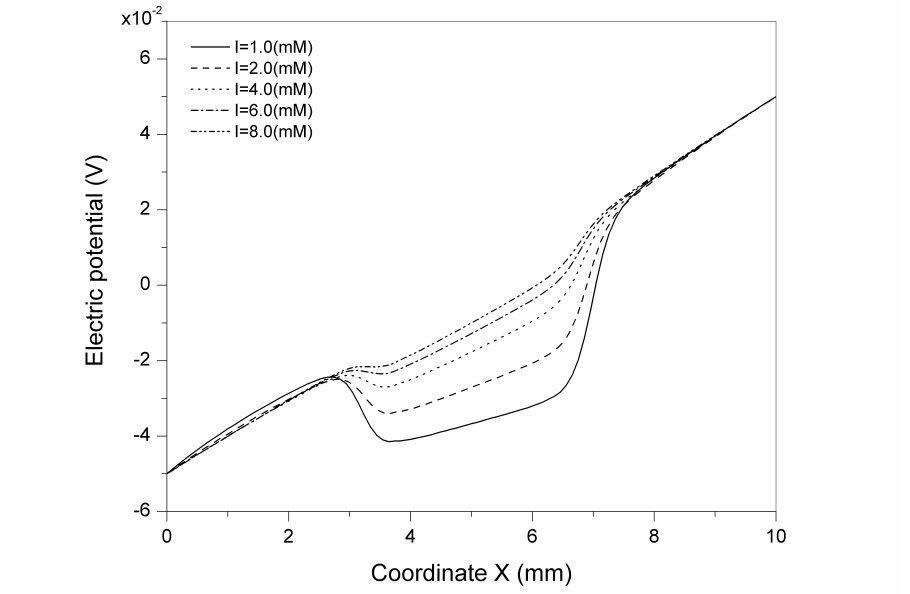

Figure 4.23 Influence of ionic strength I of bath solution on the distribution of electric potential ψ (V_e=0.10V, $c_f^0 = 10.0\,\text{mM}$).

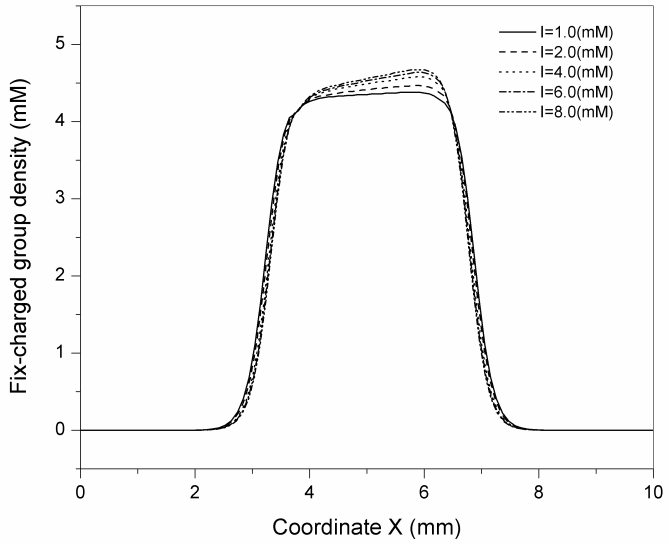

Figure 4.24 Influence of ionic strength I of bath solution on the distribution of fixed charge density c_f (V_e=0.10V, $c_f^0 = 10.0\,\text{mM}$).

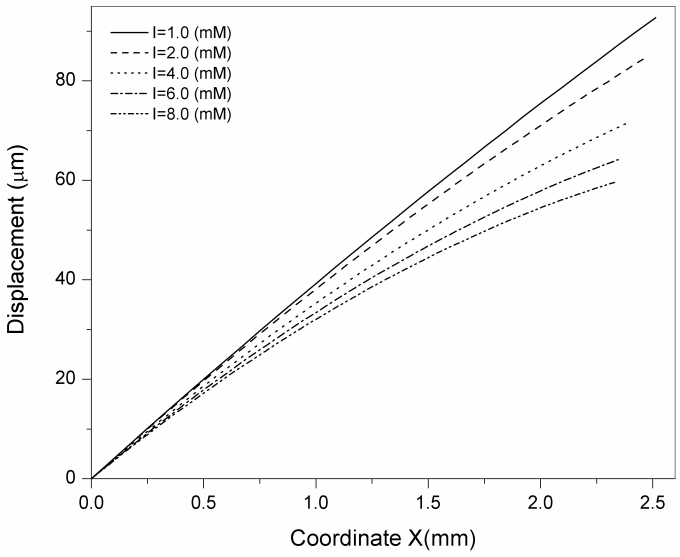

Figure 4.25 Influence of ionic strength I on the variation of displacement u (V_e=0.10V, $c_f^0 = 10.0\,\text{mM}$).

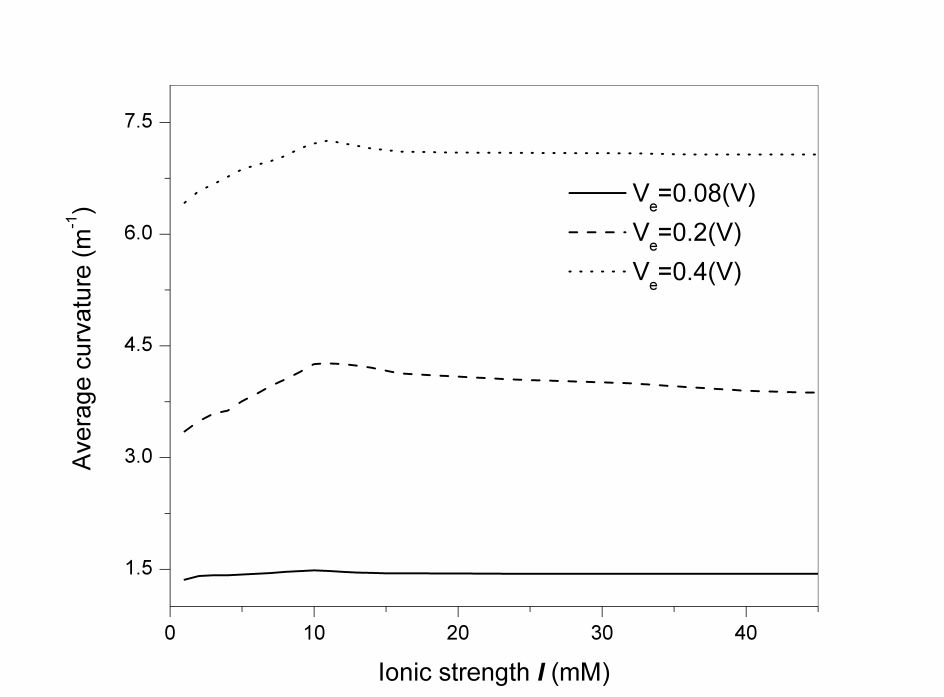

Figure 4.26 Influence of ionic strength I on the average curvature K_a of the hydrogel strip ($c_f^0 = 10.0\,\text{mM}$).

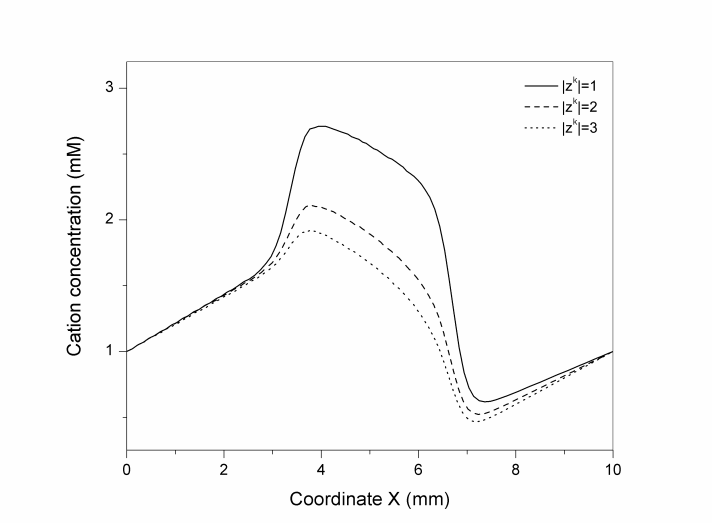

Figure 4.27 Influence of the ionic valence $|z_k|$ of the bath solution on the distributions of the diffusive cation concentration (V_e =0.10V, $c_f^0 = 2.0\,\text{mM},\ c^* = 1.0\,\text{mM}$).

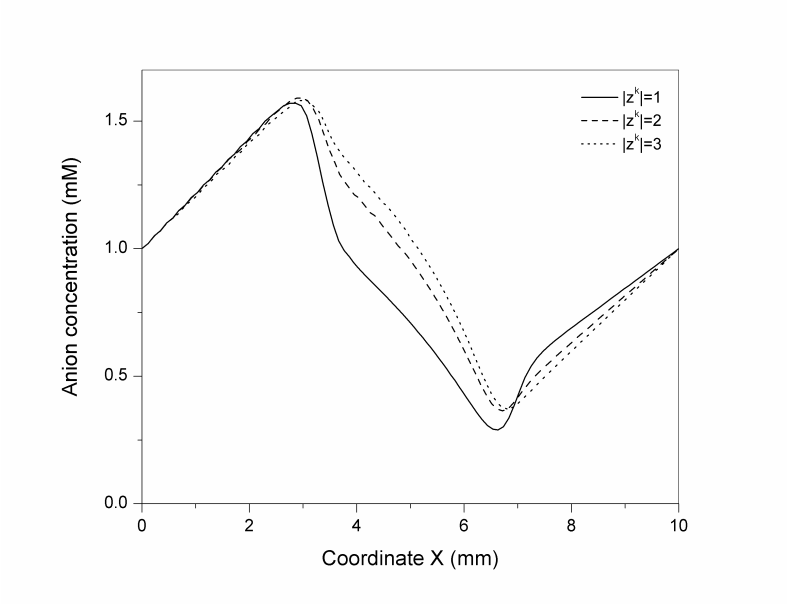

Figure 4.28 Influence of the ionic valence $|z_k|$ of the bath solution on the distributions of the diffusive anion concentration (V_e =0.10V, $c_f^0 = 2.0\,\text{mM}$, $c^* = 1.0\,\text{mM}$).

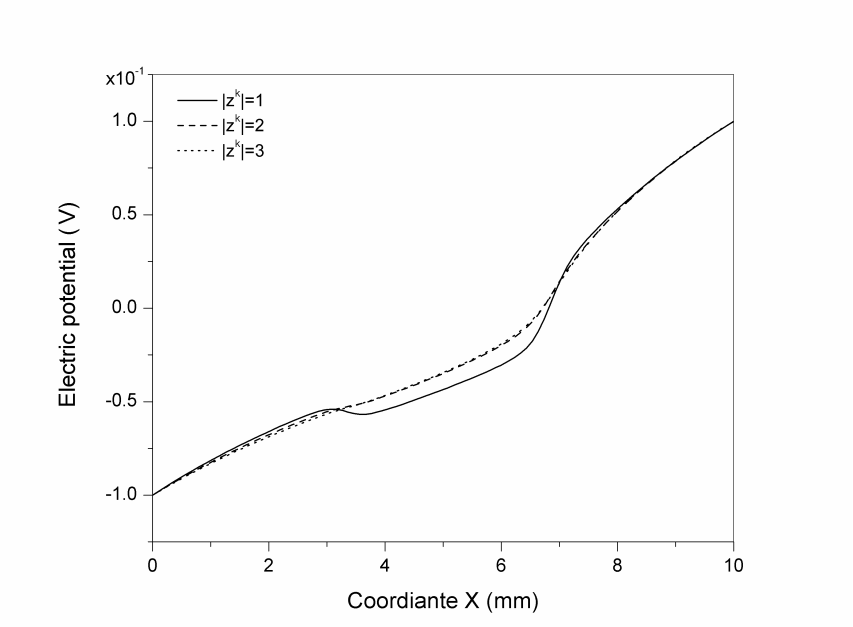

Figure 4.29 Influence of ionic valence $|z_k|$ of bath solution on the distribution of electric potential ψ (V_e=0.10V, $c_f^0 = 2.0\,\text{mM}$, $c^* = 1.0\,\text{mM}$).

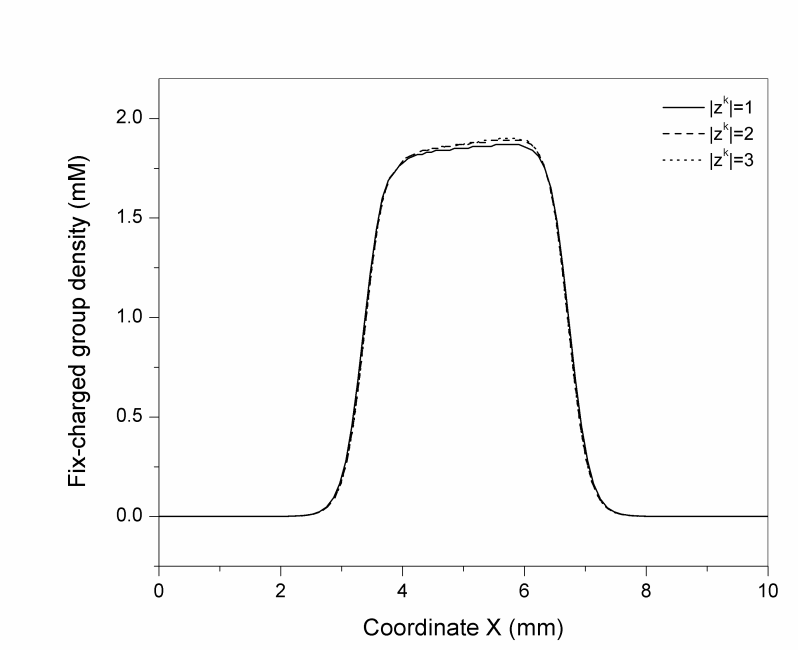

Figure 4.30 Influence of ionic valence $|z_k|$ of bath solution on the distribution of fixed charge density c_f (V_e=0.10V, $c_f^0 = 2.0\,\text{mM}$, $c^* = 1.0\,\text{mM}$).

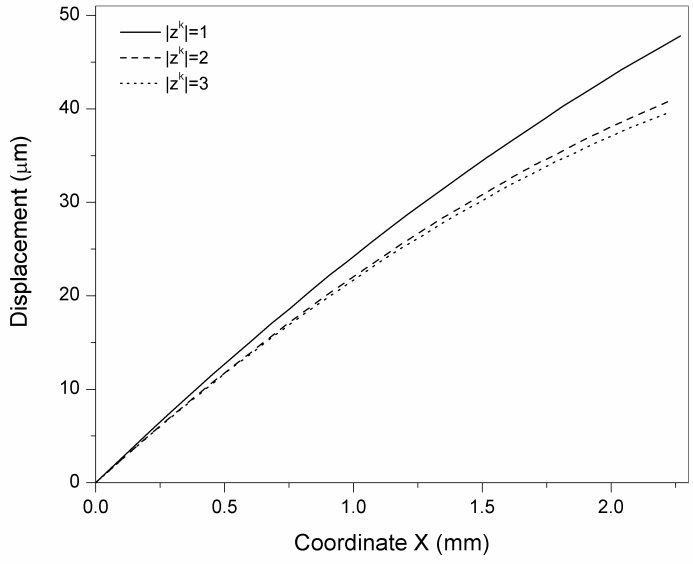

Figure 4.31 Influence of ionic valence $|z_k|$ on the variation of displacement u (V_e=0.10V, $c_f^0 = 2.0\,\text{mM}$, $c^* = 1.0\,\text{mM}$).

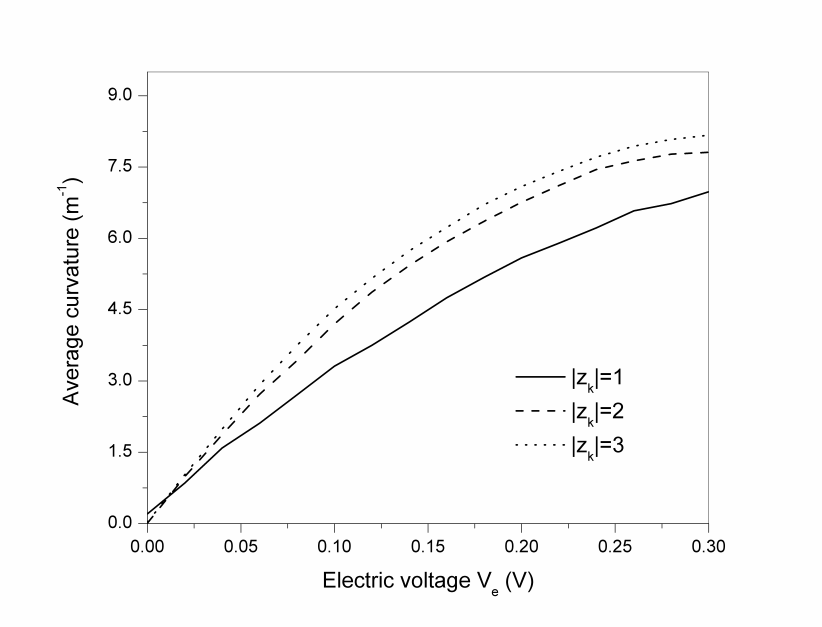

Figure 4.32 Influence of ionic valence $|z_k|$ on the variation of curvature K_a (V_e=0.10V, $c_f^0 = 2.0\,\text{mM}$, $c^* = 1.0\,\text{mM}$).

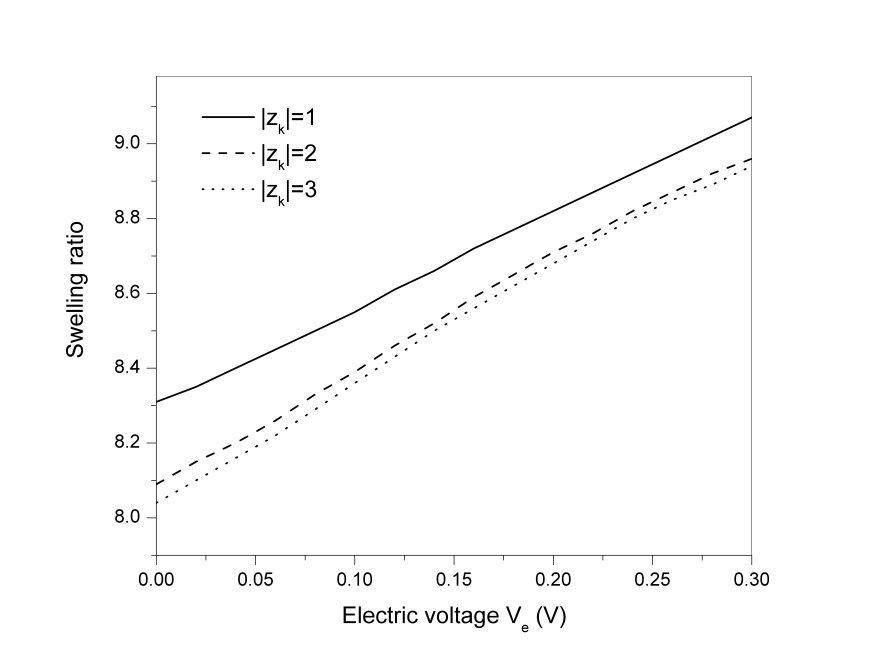

Figure 4.33 Influence of ionic valence $|z_k|$ on the swelling ratio of the hydrogel (V_e=0.10V, $c_f^0 = 2.0\,\text{mM}$, $c^* = 1.0\,\text{mM}$).

Chapter 5
Conclusions and Future Work

This thesis has conducted a series of studies aimed at obtaining a better understanding of responsive behaviors of the environmentally sensitive hydrogels. This is accomplished by establishing a set of mathematical models for studying environmentally sensitive hydrogels systems. The objectives of this chapter are to summarize all the studies completed in this thesis, to discuss some remaining controversies, and to suggest the several future studies.

5.1 Conclusions

In this thesis, a theoretical consideration related to the equilibrium behaviors of the environmental-sensitive hydrogels has been presented. Furthermore, it has dealt with the chemo-electro-mechanical coupled effect on the environmental-sensitive hydrogels responsive to the stimuli of the electric field, pH-electric coupled environment and blood glucose concentration, respectively. The corresponding mathematical models have been developed and termed the refined Multi-Effect-Coupling electric-stimulus (rMECe) model, the Multi-Effect-Coupling pH-electric coupled stimuli (MECpHe) model, and the Multi-Effect-Coupling glucose-stimulus (MECglu) model. These studies are based on the hypothesis that, when the environmental stimulus, such as the electric field, solution pH and blood

glucose concentration, is imposed to the hydrogels composed of elastic solid matrix, interstitial fluid and ionic species, the free energy of hydrogel system will decrease and the chemical energy will be converted into mechanical energy, which can cause the hydrogels to swell and/or bend until the increase of mechanical energy of the elastic solid matrix balances the decrease of the free energy of the system (Peppas and Merrill, 1977). These models consist of Poisson-Nernst-Planck equations for the ion transport within both the surrounding solution and the hydrogel, and the governing equations for the mechanical finite deformation of the environmental-sensitive hydrogels. They can predict the distributions of the ionic species concentrations, the electric potential and the fixed charge density, and the profiles of the displacement, swelling ratio and bending curvature of the hydrogels.

In the three models, the MECglu model has been used successfully for analysis of the responsive behaviors of equilibrium glucose-sensitive hydrogels responding to the change of the blood glucose concentration. The model can explain well the experimental phenomena of the distribution of ionic concentration, electric potential and network deformation. Many physical parameters can affect the responsive behaviors of equilibrium glucose-sensitive hydrogels. The enzymes, consisting of glucose oxidase (GOD) and catalase, will convert the glucose into gluconic acid and lower the pH in the hydrogel. The concentration of the enzymes is one of the major factors in an enzyme-mediated reaction. Compared with the glucose concentration of human being blood and owning to its low solubility in aqueous solution, the sparse availability of oxygen is known to be a fundamental limitation of all implanted glucose

oxidase-based sensitive devices. The physiological pH will change from 6.7 to 7.8, and in this rang of pH, the SDM-PDMMa hydrogel shows dramatical pH-dependent volume transition (Kang and Bae, 2003). The density of fixed charge groups on the crosslinking chains regulates efficiently the volume phase transition of hydrogels. The increase of the ionic strength of environmental solution inherently and spontaneously decreases the swelling of anionic and cationic hydrogels. The suitable geometry can endow the hydrogel system fast response to the external stimuli, high mechanical strength, better physical integrity and storage capacity (Suzuki and Kumagai, 2003; Ziaie et al., 2004). The mechanical properties of polymeric network directly affect the deformation of the hydrogel system, which result from the chain structure of the materials (Arridge, 1975). Despite the complexity of the swelling mechanism, the developed model in Chapter 2 has studied systematically the effects of various parameters on the distributions of diffusive ionic concentration and electric potential in both the hydrogel and the surrounding solution, and distributions of the degree of equilibrium swelling and the displacement as well as swelling ratio of the glucose-sensitive hydrogels.

The multi-effect-coupling pH-electric-stimuli (MECpHe) model has been presented for polyelectrolyte hydrogels subjected to simultaneous changes in the solution pH and an external electric field. It is a chemo-electro-mechanical coupled model that incorporates the fixed charge density, the finite deformation of the hydrogel, the electric field and mobile ionic species inside the hydrogel as well as in the surrounding solvent. The model, comprising nonlinear coupled governing equations,

moving boundaries and steep gradients at the solvent/hydrogel interface, has been solved by a hierarchical iteration technique and the meshless Hermite-cloud method. The model has then been validated with experimentally measured bending angles of a hydrogel strip at various pH values in an electric field, and good agreement is found. Furthermore, the model is applied to investigate the steady-state bending deformation of a hydrogel strip. The influences of the externally applied electric voltage and pH are discussed in detail for the distributions of mobile ionic species, the electric potential, the fixed charge density and the displacement of the hydrogel.

As the key external stimulus, the externally applied electric field is found to play a critically important role in the responses of the electric-sensitive hydrogels. Due to the drag force of electric field, the mobile ions in the bath solution diffuse into the hydrogels and cause the ionic concentration difference over the both hydrogel-solution interfaces. Different concentrations result in the different osmotic pressure at both interfaces, which gives rise to the hydrogel bending deformation. A comparison of simulating results by the rMECe model is conducted numerically with the experimental data (Zhou et al. 2002) for a given hydrogel strip with positive fixed charge groups. A substantial agreement in the comparison between the computation and experiment is achieved, which validates the rMECe model suitable for simulation of the electric-sensitive hydrogels.

The purpose of this thesis is to model and simulate the equilibrium behaviors of the environmental-sensitive hydrogels. To this end, the three models have been developed and this thesis has made the following contributions in this area:

- the responsive mechanism is described for the equilibrium behavior of environmentally sensitive hydrogel based on chemo-electro-mechanical theories;
- the diffusion-reaction relation is investigated for the glucose-sensitive hydrogel;
- the density of fixed charge groups is reformulated and incorporated into the Poisson-Nernst-Planck systems to describe the diffusion of mobile ions. The finite deformation theory is employed for the equilibrium mechanical deformation;
- the profiles are plotted and discussed for the distribution of diffusive ionic concentration and electric potential in both the hydrogel and the surrounding solution, the fixed charge density, the displacement, the curvature and swelling ratio of the environmentally sensitive hydrogels;
- the influences of several important physical and chemical conditions are investigated on the equilibrium behaviors of the environmental-sensitive.

In addition, the agreements between the simulated results and the experimental phenomena have been achieved for the three models, which indicate that the mathematical models based on the multiphasic theory provide a possible tool for simulation of the complicated nonlinear responses. The numerical predictions of the models don't agree exactly with the really measured data. However, they are closely

coherent with the qualitative observations of the experimental data, and do provide a benchmark to the behavior of the stimulus-sensitive hydrogels under the wide range of environmental conditions, which have been analyzed and illustrated in the parametric studies.

5.2 Future Work

Mathematical modeling of the environmentally sensitive hydrogels still has a long way to go. Even though the present three models have been validated by comparison of the simulated results with the published experimental data, the models are not meant to reproduce exactly the data from experimental measurements for several important physical parameters, but rather to provide a platform for observation of the fundamental effects of these parameters on the equilibrium behaviors of the environmentally sensitive hydrogels. Future work remains to be done in these models to quantitatively accounts for more experimental data to examine the generality of the proposed models.

Due to the complexity of the chemo-electro-mechanical coupled effects, some assumptions and approximations have been made in the mathematical models, which should be further improved. The fluid velocity has been assumed to be a negligible effect in developed models. In fact, the convection item should not be neglected in the Nernst-Planck equation for determining the swelling/deswelling of the smaller hydrogels when the environment has obviously fluidic flow (De and Aluru, 2004). The

insight gained from this effort would likely help developing comprehensive models for the complex material behavior.

All the numerical simulations conducted are for the equilibrium and steady-state case studies, which is merely a foundation stone for the solution to a much more general problem. A thorough knowledge of the response of the environmentally sensitive hydrogels relies on fully understanding of the relationships between transient behavior and stimuli. Future work is suggested to focus on developing and understanding these relationships, and then incorporating them with the present equilibrium studies into a more usefully predictive and robust constitutive model.

In this thesis, the hydrogels are assumed to be homogenous. Therefore, the possible effect from irregular geometry is neglected. Extension of the present one-dimensional formulations to two- or three-dimensional model may help to understand the possible influences of the key parameters.

Further study is also recommended to investigate the effect of the electrolysis near the electrodes, which could change the environmental conditions. When an electric field is applied to the bath solution where the hydrogel is immersed into, the electrochemical reactions occur near the electrodes. It is recommended that future work could focus on the bending deformation of the hydrogel which may be affected by the local ionic concentration gradient attributed to water electrolysis.

The diffusion causes the hydrogel swelling and its surface erosion, which strongly affects the release profile of drug contemporarily (Nam et al., 2004). In the enzyme-loaded hydrogels, the oxygen concentration plays a role of bottleneck for the

reaction of conversion glucose into gluconic acid. It is desired to develop more physical-based diffusion-reaction relations and to overcome the limitation due to the oxygen depletion for the glucose-sensitive hydrogels, which is meaningful to feasibly design a “closed loop” insulin delivery system in terms of the oxygen delivery, the glucose responsiveness and the fast response time.

Appendix Discretization of Formulations of MECglu Model

In order to efficiently develop the computational source codes for the MECglu model in Chapter 2, a set of dimensionless parameters is defined as following,

$$\bar{x}=\frac{x}{L_{ref}}\ ,\quad \bar{u}=\frac{u}{L_{ref}}\ ,\quad \bar{c}_k=\frac{c_k}{c_{ref}}\ ,\quad \bar{c}_f=\frac{c_f}{c_{ref}}\ ,\quad \bar{\psi}=\frac{\psi}{\psi_{ref}}=\frac{F\psi}{\eta RT}\ ,$$

$$\bar{D}_k=D_k\frac{\tau}{L_{ref}^2}\ ,\quad \bar{K}_g=\frac{K_g}{c_{g\_ref}}\ ,\quad \bar{K}_{ox}=\frac{K_{ox}}{c_{ox\_ref}}\ ,\quad \bar{V}_{\max}=\frac{V_{\max}\tau}{c_{ref}}\ ,\quad \bar{V}=\frac{\tau}{L_{ref}}V\ , \tag{A.1}$$

$$\bar{K}_1=K_1\frac{c_{ref}}{RT},\quad \bar{K}_2=K_2\frac{c_{ref}^2}{RT}$$

where $\bar{x}$, $\bar{u}$, $\bar{c}_k$, $\bar{c}_f$, $\bar{\psi}$ are the dimensionless variables of coordinates, displacement, diffusive species concentration, fixed charge density and electric potential, respectively. L_{ref} , c_{ref} , ψ_{ref} , τ and η are the referenced dimensionless configurations of characteristic length, concentration, electric potential, time and weighted coefficient, respectively.

So far, the development of the MECglu model has been completed and the model is summarized as,

Nernst-Planck Equations

$$\left[\frac{\partial^2 c_k}{\partial x^2}+\frac{z_kF}{RT}\frac{\partial c_k}{\partial x}\frac{d\psi}{dx}+\frac{z_kFc_k}{RT}\frac{\partial^2\psi}{\partial x^2}\right]+\frac{v_k}{D_k}r$$
$$-\frac{\partial}{D_k\partial x}(c_kV)+\left[\frac{(-K_1+4K_2c_k)}{RT}(\frac{\partial c_k}{\partial x})^2+\frac{(-K_1+2K_2c_k)c_k}{RT}\frac{\partial^2 c_k}{\partial x^2}\right]=0 \tag{A.2}$$

Based on the assumptions mentioned in Section 2.2, only first two terms will be considered in the present studies for the Nernst-Planck equation (A.2).

$$\left[\frac{\partial^2 c_k}{\partial x^2}+\frac{z_kF}{RT}\frac{\partial c_k}{\partial x}\frac{\partial\psi}{\partial x}+\frac{z_kFc_k}{RT}\frac{\partial^2\psi}{\partial x^2}\right]+\frac{v_k}{D_k}\frac{V_{\max}c_gc_{ox}}{c_{ox}(c_g+K_g)+K_{ox}c_g}=0$$

$$\left[\frac{\partial^2 c_k}{\partial x^2}+\frac{z_k F}{RT}\frac{\partial c_k}{\partial x}\frac{\partial \psi}{\partial x}+\frac{z_k F c_k}{RT}\frac{\partial^2 \psi}{\partial x^2}\right]\left[c_{ox}(c_g+K_g)+K_{ox}c_g\right]+\frac{v_k}{D_k}V_{\max}c_g c_{ox}=0 \quad \text{(A.3)}$$

The chemical reaction, $\text{Glucose}+\frac{1}{2}\text{O}_2 \xrightarrow{\text{GOD/Catalase}} \text{Gluconate}+\text{H}^+$, is in the hydrogel, then the stoichiometric coefficient for the four chemical substances is $v_g=-1$, $v_{ox}=-1/2$, $v_a=1$ and $v_{H^+}=1$, respectively. And the chemical reaction ratio r is expressed as the full Ping-Pong mechanism,

$$r(c_g,c_{ox})=\frac{V_{\max}c_g c_{ox}}{c_{ox}(c_g+K_g)+K_{ox}c_g} \quad \text{(A.4)}$$

Poisson Equation

$$\frac{\partial^2 \psi}{\partial x^2}=-\frac{F}{\varepsilon\varepsilon_0}\left(\sum_{k=1}^{N}z_k c_k+z_f c_f\right) \quad \text{(A.5)}$$

Density of the fixed charge groups

$$c_f=\frac{1}{H}\frac{c_{f,s}^0 K}{K+c_{\text{H}^+}} \qquad \text{for anionic hydrogel } (z_f=-1) \quad \text{(A.6)}$$

$$c_f=\frac{1}{H}\frac{c_{f,s}^0 c_{\text{H}^+}}{K+c_{\text{H}^+}} \qquad \text{for cationic hydrogel } (z_f=+1) \quad \text{(A.7)}$$

Mechanical Governing Equation

$$(\lambda+2\mu)\left[\frac{\partial^2 u}{\partial X^2}+3\frac{\partial u}{\partial X}\frac{\partial^2 u}{\partial X^2}+\frac{3}{2}\left(\frac{\partial u}{\partial X}\right)^2\frac{\partial^2 u}{\partial X^2}\right]-\frac{\partial p_{osmotic}}{\partial X}=0 \quad \text{(A.8)}$$

Osmotic Pressure

$$p_{osmotic}=RT\sum_{k=1}^{N}c_k=RT\sum_{k=1}^{N}(c_k^{in}-c_k^{out}) \quad \text{(A.9)}$$

Nondimensional implementation

Nondimensional Nernst-Planck Equations

$$\left[\frac{\partial^2 c_k}{\partial x^2}+\frac{z_k F}{RT}\frac{\partial c_k}{\partial x}\frac{\partial \psi}{\partial x}+\frac{z_k F c_k}{RT}\frac{\partial^2 \psi}{\partial x^2}\right]\left[c_{ox}(c_g+K_g)+K_{ox}c_g\right]+\frac{v_k}{D_k}V_{\max}c_g c_{ox}=0$$

$$\Rightarrow\ \frac{c_{k\_ref}}{L_{ref}^2}\left[\frac{\partial^2 \overline{c}_k}{\partial \overline{x}^2}+\eta z_k\frac{\partial \overline{c}_k}{\partial \overline{x}}\frac{\partial \overline{\psi}}{\partial \overline{x}}+\eta z_k \overline{c}_k\frac{\partial^2 \overline{\psi}}{\partial \overline{x}^2}\right]\left[c_{ox\_ref}\overline{c}_{ox}(c_{g\_ref}\overline{c}_g+K_g)+K_{ox}c_{g\_ref}\overline{c}_g\right]$$

$$+c_{g\_ref}c_{ox\_ref}\frac{v_k}{D_k}V_{\max}\overline{c}_g\overline{c}_{ox}=0 \qquad \text{(A.10)}$$

Divided $\frac{c_{k\_ref}}{L_{ref}^2}c_{g\_ref}c_{ox\_ref}$ at both sides of the Nernst-Planck equation (A.10),

$$\left[\frac{\partial^2 \overline{c}_k}{\partial \overline{x}^2}+\eta z_k\frac{\partial \overline{c}_k}{\partial \overline{x}}\frac{\partial \overline{\psi}}{\partial \overline{x}}+\eta z_k \overline{c}_k\frac{\partial^2 \overline{\psi}}{\partial \overline{x}^2}\right]\left[\overline{c}_{ox}(\overline{c}_g+\frac{K_g}{c_{g\_ref}})+\frac{K_{ox}}{c_{ox\_ref}}\overline{c}_g\right]$$

$$+\frac{L_{ref}^2}{c_{k\_ref}}\frac{v_k}{D_k}V_{\max}\overline{c}_g\overline{c}_{ox}=0 \qquad \text{(A.11)}$$

Expanding the Nernst-Planck equation (A.11), one can have

$$\frac{\partial^2 \overline{c}_k}{\partial \overline{x}^2}\overline{c}_{ox}\overline{c}_g+\frac{\partial^2 \overline{c}_k}{\partial \overline{x}^2}\frac{K_g}{c_{g\_ref}}\overline{c}_{ox}+\frac{\partial^2 \overline{c}_k}{\partial \overline{x}^2}\frac{K_{ox}}{c_{ox\_ref}}\overline{c}_g$$

$$+\eta z_k\frac{\partial \overline{c}_k}{\partial \overline{x}}\frac{\partial \overline{\psi}}{\partial \overline{x}}\overline{c}_{ox}\overline{c}_g+\eta z_k\frac{\partial \overline{c}_k}{\partial \overline{x}}\frac{\partial \overline{\psi}}{\partial \overline{x}}\frac{K_g}{c_{g\_ref}}\overline{c}_{ox}+\eta z_k\frac{\partial \overline{c}_k}{\partial \overline{x}}\frac{\partial \overline{\psi}}{\partial \overline{x}}\frac{K_{ox}}{c_{ox\_ref}}\overline{c}_g$$

$$+\eta z_k\overline{c}_k\frac{\partial^2 \overline{\psi}}{\partial \overline{x}^2}\overline{c}_{ox}\overline{c}_g+\eta z_k\overline{c}_k\frac{\partial^2 \overline{\psi}}{\partial \overline{x}^2}\frac{K_g}{c_{g\_ref}}\overline{c}_{ox}+\eta z_k\overline{c}_k\frac{\partial^2 \overline{\psi}}{\partial \overline{x}^2}\frac{K_{ox}}{c_{ox\_ref}}\overline{c}_g$$

$$+\frac{L_{ref}^2}{c_{k\_ref}}\frac{v_k}{D_k}V_{\max}\overline{c}_g\overline{c}_{ox}=0 \qquad (k=1,2,...,N) \qquad \text{(A.12)}$$

In the equation (A.12), *k* represents the *k*th species. In the present studies, totally there are six species, H^+, $C_6H_{12}O_6$, O_2, gluconate acid, Na^+ and Cl^-, to be considered.

(1) For hydrogen H^+, $c_{k\_ref}=c_{H\_ref}$, $v_k=v_H$, $D_k=D_H$

$$\left[\frac{\partial^2 \overline{c}_H}{\partial \overline{x}^2}+\eta z_H\frac{\partial \overline{c}_H}{\partial \overline{x}}\frac{\partial \overline{\psi}}{\partial \overline{x}}+\eta z_H\overline{c}_H\frac{\partial^2 \overline{\psi}}{\partial \overline{x}^2}\right]\left[\overline{c}_{ox}(\overline{c}_g+\frac{K_g}{c_{g\_ref}})+\frac{K_{ox}}{c_{ox\_ref}}\overline{c}_g\right]$$

$$+\frac{L_{ref}^2}{c_{H\_ref}}\frac{v_H}{D_H}V_{\max}\overline{c}_g\overline{c}_{ox}=0$$

$\Rightarrow$

$$\frac{\partial^2 \overline{c}_H}{\partial \overline{x}^2}\overline{c}_{ox}\overline{c}_g + \frac{\partial^2 \overline{c}_H}{\partial \overline{x}^2}\frac{K_g}{c_{g\_ref}}\overline{c}_{ox} + \frac{\partial^2 \overline{c}_H}{\partial \overline{x}^2}\frac{K_{ox}}{c_{ox\_ref}}\overline{c}_g$$

$$+\eta z_H \frac{\partial \overline{c}_H}{\partial \overline{x}}\frac{\partial \overline{\psi}}{\partial \overline{x}}\overline{c}_{ox}\overline{c}_g + \eta z_H \frac{\partial \overline{c}_H}{\partial \overline{x}}\frac{\partial \overline{\psi}}{\partial \overline{x}}\frac{K_g}{c_{g\_ref}}\overline{c}_{ox} + \eta z_H \frac{\partial \overline{c}_H}{\partial \overline{x}}\frac{\partial \overline{\psi}}{\partial \overline{x}}\frac{K_{ox}}{c_{ox\_ref}}\overline{c}_g$$

$$+\eta z_H \overline{c}_H \frac{\partial^2 \overline{\psi}}{\partial \overline{x}^2}\overline{c}_{ox}\overline{c}_g + \eta z_H \overline{c}_H \frac{\partial^2 \overline{\psi}}{\partial \overline{x}^2}\frac{K_g}{c_{g\_ref}}\overline{c}_{ox} + \eta z_H \overline{c}_H \frac{\partial^2 \overline{\psi}}{\partial \overline{x}^2}\frac{K_{ox}}{c_{ox\_ref}}\overline{c}_g$$

$$+\frac{L_{ref}^2}{c_{H\_ref}}\frac{v_H}{D_H}V_{\max}\overline{c}_g\overline{c}_{ox} = 0 \tag{A.13}$$

(2) For glucose ($C_6H_{12}O_6$), $c_{k\_ref} = c_{g\_ref}$, $v_k = v_g$, $D_k = D_g$, $z_g = 0$

$$\left[\frac{\partial^2 \overline{c}_g}{\partial \overline{x}^2}\right]\left[\overline{c}_{ox}(\overline{c}_g + \frac{K_g}{c_{g\_ref}}) + \frac{K_{ox}}{c_{ox\_ref}}\overline{c}_g\right] + \frac{L_{ref}^2}{c_{g\_ref}}\frac{v_g}{D_g}V_{\max}\overline{c}_g\overline{c}_{ox} = 0$$

$\Rightarrow$

$$\frac{\partial^2 \overline{c}_g}{\partial \overline{x}^2}\overline{c}_{ox}\overline{c}_g + \frac{\partial^2 \overline{c}_g}{\partial \overline{x}^2}\frac{K_g}{c_{g\_ref}}\overline{c}_{ox} + \frac{\partial^2 \overline{c}_g}{\partial \overline{x}^2}\frac{K_{ox}}{c_{ox\_ref}}\overline{c}_g + \frac{L_{ref}^2}{c_{g\_ref}}\frac{v_g}{D_g}V_{\max}\overline{c}_g\overline{c}_{ox} = 0 \tag{A.14}$$

(3) For Oxygen (O_2), $c_{k\_ref} = c_{ox\_ref}$, $v_k = v_{ox}$, $D_k = D_{ox}$, $z_{ox} = 0$

$$\left[\frac{\partial^2 \overline{c}_{ox}}{\partial \overline{x}^2}\right]\left[\overline{c}_{ox}(\overline{c}_g + \frac{K_g}{c_{g\_ref}}) + \frac{K_{ox}}{c_{ox\_ref}}\overline{c}_g\right] + \frac{L_{ref}^2}{c_{ox\_ref}}\frac{v_g}{D_g}V_{\max}\overline{c}_g\overline{c}_{ox} = 0$$

$\Rightarrow$

$$\frac{\partial^2 \overline{c}_{ox}}{\partial \overline{x}^2}\overline{c}_{ox}\overline{c}_g + \frac{\partial^2 \overline{c}_{ox}}{\partial \overline{x}^2}\frac{K_g}{c_{g\_ref}}\overline{c}_{ox} + \frac{\partial^2 \overline{c}_{ox}}{\partial \overline{x}^2}\frac{K_{ox}}{c_{ox\_ref}}\overline{c}_g + \frac{L_{ref}^2}{c_{ox\_ref}}\frac{v_{ox}}{D_{ox}}V_{\max}\overline{c}_g\overline{c}_{ox} = 0 \tag{A.15}$$

(4) For gluconate acid, $c_{k\_ref} = c_{a\_ref}$, $v_k = v_a$, $D_k = D_a$, $z_a = -1$

$$\left[\frac{\partial^2 \overline{c}_a}{\partial \overline{x}^2} + \eta z_a \frac{\partial \overline{c}_a}{\partial \overline{x}}\frac{\partial \overline{\psi}}{\partial \overline{x}} + \eta z_a \overline{c}_a \frac{\partial^2 \overline{\psi}}{\partial \overline{x}^2}\right]\left[\overline{c}_{ox}(\overline{c}_g + \frac{K_g}{c_{g\_ref}}) + \frac{K_{ox}}{c_{ox\_ref}}\overline{c}_g\right]$$

$$+\frac{L_{ref}^2}{c_{a\_ref}}\frac{v_a}{D_a}V_{\max}\overline{c}_g\overline{c}_{ox} = 0$$

$$\Rightarrow \quad \frac{\partial^2 \overline{c}_a}{\partial \overline{x}^2}\overline{c}_{ox}\overline{c}_g + \frac{\partial^2 \overline{c}_a}{\partial \overline{x}^2}\frac{K_g}{c_{g\_ref}}\overline{c}_{ox} + \frac{\partial^2 \overline{c}_a}{\partial \overline{x}^2}\frac{K_{ox}}{c_{ox\_ref}}\overline{c}_g$$

$$+\eta z_a \frac{\partial \overline{c}_a}{\partial \overline{x}} \frac{\partial \overline{\psi}}{\partial \overline{x}} \overline{c}_{ox} \overline{c}_g + \eta z_a \frac{\partial \overline{c}_a}{\partial \overline{x}} \frac{\partial \overline{\psi}}{\partial \overline{x}} \frac{K_g}{c_{g\_ref}} \overline{c}_{ox} + \eta z_a \frac{\partial \overline{c}_a}{\partial \overline{x}} \frac{\partial \overline{\psi}}{\partial \overline{x}} \frac{K_{ox}}{c_{ox\_ref}} \overline{c}_g$$

$$+\eta z_a \overline{c}_a \frac{\partial^2 \overline{\psi}}{\partial \overline{x}^2} \overline{c}_{ox} \overline{c}_g + \eta z_a \overline{c}_a \frac{\partial^2 \overline{\psi}}{\partial \overline{x}^2} \frac{K_g}{c_{g\_ref}} \overline{c}_{ox} + \eta z_a \overline{c}_a \frac{\partial^2 \overline{\psi}}{\partial \overline{x}^2} \frac{K_{ox}}{c_{ox\_ref}} \overline{c}_g$$

$$+\frac{L_{ref}^2}{c_{a\_ref}} \frac{v_a}{D_a} V_{\max} \overline{c}_g \overline{c}_{ox} = 0 \tag{A.16}$$

(5) For Sodium ion (Na^+), which doesn't take part in the chemical reaction,

$$\left[\frac{\partial^2 \overline{c}_{Na}}{\partial \overline{x}^2} + \eta z_{Na} \frac{\partial \overline{c}_{Na}}{\partial \overline{x}} \frac{\partial \overline{\psi}}{\partial \overline{x}} + \eta z_{Na} \overline{c}_{Na} \frac{\partial^2 \overline{\psi}}{\partial \overline{x}^2} \right] = 0 \tag{A.17}$$

(6) For Cl^-, which doesn't take part in the chemical reaction yet,

$$\left[\frac{\partial^2 \overline{c}_{Cl}}{\partial \overline{x}^2} + \eta z_{Cl} \frac{\partial \overline{c}_{Cl}}{\partial \overline{x}} \frac{\partial \overline{\psi}}{\partial \overline{x}} + \eta z_{Cl} \overline{c}_{Cl} \frac{\partial^2 \overline{\psi}}{\partial \overline{x}^2} \right] = 0 \tag{A.18}$$

Nondimensional Poisson Equation

$$\frac{\psi_{ref} \partial^2 \overline{\psi}}{L_{ref}^2 \partial \overline{x}^2} = -\frac{F}{\varepsilon \varepsilon_0} \left(\sum_{k=1}^{N} z_k \overline{c}_k c_{k\_ref} + z_f \overline{c}_f \right)$$

$$\Rightarrow \quad \frac{\partial^2 \overline{\psi}}{\partial \overline{x}^2} = -\frac{F^2}{\varepsilon \varepsilon_0 RT} \frac{L_{ref}^2}{\eta} \left(z_H \overline{c}_H c_{H\_ref} + z_a \overline{c}_a c_{a\_ref} + z_{Na} \overline{c}_{Na} c_{Na\_ref} + z_f \overline{c}_f \right) \tag{A.19}$$

Nondimensional Fixed Charge Density

$$c_f = \frac{1}{H} \frac{c_{f,s}^0 K}{K + c_{H^+}}$$

$$\Rightarrow c_{ref} \overline{c}_f = \frac{1}{H} \frac{c_{ref} \overline{c}_{f,s}^0 c_{ref} \overline{K}}{c_{ref} \overline{K} + c_{ref} \overline{c}_{H^+}}$$

$$\Rightarrow \overline{c}_f = \frac{1}{H} \frac{\overline{c}_{f,s}^0 \overline{K}}{\overline{K} + \overline{c}_{H^+}} \qquad \text{for anionic hydrogel} \tag{A.20}$$

$$c_f = \frac{1}{H} \frac{c_{f,s}^0 c_{H^+}}{K + c_{H^+}}$$

$$\Rightarrow c_{ref} \overline{c}_f = \frac{1}{H} \frac{c_{ref} \overline{c}_{f,s}^0 c_{ref} \overline{c}_{H^+}}{c_{ref} \overline{K} + c_{ref} \overline{c}_{H^+}}$$

$$\Rightarrow \bar{c}_f = \frac{1}{H}\frac{\bar{c}_{f,s}^0 \bar{c}_{\mathrm{H}^+}}{\bar{K} + \bar{c}_{\mathrm{H}^+}} \qquad \text{for cationic hydrogel} \tag{A.21}$$

Nondimensional Mechanical Equilibrium Equation

$$(\lambda + 2\mu)[\frac{\partial^2 u}{\partial X^2} + 3\frac{\partial u}{\partial X}\frac{\partial^2 u}{\partial X^2} + \frac{3}{2}(\frac{\partial u}{\partial X})^2 \frac{\partial^2 u}{\partial X^2}] - \frac{\partial p_{osmotic}}{\partial X} = 0$$

$$\Rightarrow (\lambda + 2\mu)[\frac{L_{ref}\partial^2 \bar{u}}{L_{ref}^2 \partial \bar{X}^2} + 3\frac{L_{ref}\partial \bar{u}}{L_{ref}\partial \bar{X}}\frac{L_{ref}\partial^2 \bar{u}}{L_{ref}^2 \partial \bar{X}^2} + \frac{3}{2}(\frac{L_{ref}\partial \bar{u}}{L_{ref}\partial \bar{X}})^2 \frac{L_{ref}\partial^2 \bar{u}}{L_{ref}^2 \partial \bar{X}^2}]$$

$$-\frac{c_{ref}RT\partial}{L_{ref}\partial \bar{X}}(\sum_{k=1}^{N}(\bar{c}_k^{in} - \bar{c}_k^{out})) = 0$$

$$\Rightarrow (\lambda + 2\mu)[\frac{\partial^2 \bar{u}}{L_{ref}\partial \bar{X}^2} + 3\frac{\partial \bar{u}}{\partial \bar{X}}\frac{\partial^2 \bar{u}}{L_{ref}\partial \bar{X}^2} + \frac{3}{2}(\frac{d\bar{u}}{d\bar{X}})^2 \frac{\partial^2 \bar{u}}{L_{ref}\partial \bar{X}^2}] - \frac{c_{ref}RT\partial}{L_{ref}\partial \bar{X}}(\sum_{k=1}^{N}(\bar{c}_k^{in} - \bar{c}_k^{out})) = 0$$

$$\Rightarrow (\lambda + 2\mu)[\frac{\partial^2 \bar{u}}{\partial \bar{X}^2} + 3\frac{\partial \bar{u}}{\partial \bar{X}}\frac{\partial^2 \bar{u}}{\partial \bar{X}^2} + \frac{3}{2}(\frac{\partial \bar{u}}{\partial \bar{X}})^2 \frac{\partial^2 \bar{u}}{\partial \bar{X}^2}] - \frac{c_{ref}RT\partial}{\partial \bar{X}}(\sum_{k=1}^{N}(\bar{c}_k^{in} - \bar{c}_k^{out})) = 0 \tag{A.22}$$

Finally, the non-dimensional nonlinear MECglu model consisting of governing equations are briefly summarized as

$$\left[\frac{\partial^2 \bar{c}_k}{\partial \bar{x}^2} + \eta z_k \frac{\partial \bar{c}_k}{\partial \bar{x}}\frac{\partial \bar{\psi}}{\partial \bar{x}} + \eta z_k \bar{c}_k \frac{\partial^2 \bar{\psi}}{\partial \bar{x}^2}\right]\left[\bar{c}_{ox}(\bar{c}_g + \bar{K}_g) + \bar{K}_{ox}\bar{c}_g\right] + \frac{v_k}{\bar{D}_k}\bar{V}_{\max}\bar{c}_g\bar{c}_{ox}$$

$$+\left\{-\frac{1}{\bar{D}_k}\frac{\partial}{\partial \bar{x}}(\bar{c}_k\bar{V}) + \left[(-\bar{K}_1 + 4\bar{K}_2\bar{c}_k)(\frac{\partial \bar{c}_k}{\partial \bar{x}})^2 + (-\bar{K}_1 + 2\bar{K}_2\bar{c}_k)\bar{c}_k\frac{\partial^2 \bar{c}_k}{\partial \bar{x}^2}\right]\right\}$$

$$\times\left[\bar{c}_{ox}(\bar{c}_g + \bar{K}_g) + \bar{K}_{ox}\bar{c}_g\right] = 0 \quad (k = 1,...,N) \tag{A.23}$$

$$\frac{\partial^2 \bar{\psi}}{\partial \bar{x}^2} = -\frac{F^2}{\varepsilon\varepsilon_0 RT}\frac{L_{ref}^2 c_{ref}}{\eta}\left(\sum_{k=1}^{N} z_k \bar{c}_k + z_f \bar{c}_f\right) \tag{A.24}$$

$$\bar{c}_f = \frac{1}{H}\frac{\bar{c}_{f,s}^0 \bar{K}}{\bar{K} + \bar{c}_{\mathrm{H}^+}} \quad \text{for anionic hydrogel} \tag{A.25}$$

$$\bar{c}_f = \frac{1}{H}\frac{\bar{c}_{f,s}^0 \bar{c}_{\mathrm{H}^+}}{\bar{K} + \bar{c}_{\mathrm{H}^+}} \quad \text{for cationic hydrogel} \tag{A.26}$$

$$(\lambda + 2\mu)[\frac{\partial^2 \bar{u}}{\partial \bar{X}^2} + 3\frac{\partial \bar{u}}{\partial \bar{X}}\frac{\partial^2 \bar{u}}{\partial \bar{X}^2} + \frac{3}{2}(\frac{\partial \bar{u}}{\partial \bar{X}})^2 \frac{\partial^2 \bar{u}}{\partial \bar{X}^2}] - \frac{c_{ref}RT\partial}{\partial \bar{X}}(\sum_{k=1}^{N}(\bar{c}_k^{in} - \bar{c}_k^{out})) = 0 \tag{A.27}$$

Discretization implementation

In order to solve the MECglu system by the Hermite-cloud technique (Li et al., 2003), the governing equations mentioned above should be discretized.

Spatial discretization for the primary variables

$$\overline{c}_k(\overline{x}_i) = \sum_{n=1}^{np} N_n(\overline{x}_i)\overline{c}_{kn} + \sum_{m=1}^{np}(\overline{x} - \sum_{n=1}^{np} N_n(\overline{x}_i)\overline{x}_n)M_m(\overline{x}_i)\overline{c}_{km,x} \tag{A.28}$$

$$\overline{\psi}(\overline{x}_i) = \sum_{n=1}^{np} N_n(\overline{x}_i)\overline{\psi}_n + \sum_{m=1}^{np}(\overline{x} - \sum_{n=1}^{np} N_n(\overline{x}_i)\overline{x}_n)M_m(\overline{x}_i)\overline{\psi}_{m,x} \tag{A.29}$$

$$\overline{u}(\overline{x}_i) = \sum_{n=1}^{np} N_n(\overline{x}_i)\overline{u}_n + \sum_{m=1}^{np}(\overline{x} - \sum_{n=1}^{np} N_n(\overline{x}_i)\overline{x}_n)M_m(\overline{x}_i)\overline{u}_{m,x} \tag{A.30}$$

where *np* is the number of points scattered in the computational domain, *N* and *M* are the appropriate Hermite-cloud shape functions depending on the highest order of the governing equations. The subscripts after the comma denote the derivatives with respect to the variable. The first order derivatives of the primary variable, i.e., $\overline{c}_{kx}, \overline{\psi}_x$, $\overline{u}_x$ will be considered as independent variables and given according to Hermite-cloud formulas as

$$\overline{c}_{kx}(\overline{x}_i) = \sum_{m=1}^{np} M_m(\overline{x}_i)\overline{c}_{km,x} \tag{A.31}$$

$$\overline{\psi}_x(\overline{x}_i) = \sum_{m=1}^{np} M_m(\overline{x}_i)\overline{\psi}_{m,x} \tag{A.32}$$

$$\overline{u}_x(\overline{x}_i) = \sum_{m=1}^{np} M_m(\overline{x}_i)\overline{u}_{m,x} \tag{A.33}$$

After complicated formulation, the nondimensional discrete form of the steady-state partial differential governing equations of the MECglu model and auxiliary equations is finally obtained as

Nernst-Planck Equations

$$\left\{\left[\sum_{n=1}^{np} N_n(\bar{x}_i)\bar{c}_{gn} + \sum_{m=1}^{np}(\bar{x} - \sum_{n=1}^{np} N_n(\bar{x}_i)\bar{x}_n) M_m(\bar{x}_i)\bar{c}_{gm,x}\right]\right.$$

$$\times\left[\sum_{n=1}^{np} N_n(\bar{x}_i)\bar{c}_{oxn} + \sum_{m=1}^{np}(\bar{x} - \sum_{n=1}^{np} N_n(\bar{x}_i)\bar{x}_n) M_m(\bar{x}_i)\bar{c}_{oxm,x}\right]\left[\sum_{n=1}^{np} N_{n,xx}(\bar{x}_i)\bar{c}_{kn}\right]$$

$$+\bar{K}_g\left[\sum_{n=1}^{np} N_n(\bar{x}_i)\bar{c}_{oxn} + \sum_{m=1}^{np}(\bar{x} - \sum_{n=1}^{np} N_n(\bar{x}_i)\bar{x}_n) M_m(\bar{x}_i)\bar{c}_{oxm,x}\right]\left[\sum_{n=1}^{np} N_{n,xx}(\bar{x}_i)\bar{c}_{kn}\right]$$

$$\left.+\bar{K}_{ox}\left[\sum_{n=1}^{np} N_n(\bar{x}_i)\bar{c}_{gn} + \sum_{m=1}^{np}(\bar{x} - \sum_{n=1}^{np} N_n(\bar{x}_i)\bar{x}_n) M_m(\bar{x}_i)\bar{c}_{gm,x}\right]\left[\sum_{n=1}^{np} N_{n,xx}(\bar{x}_i)\bar{c}_{kn}\right]\right\}$$

$$+\left\{\eta z_k\left[\sum_{n=1}^{np} N_n(\bar{x}_i)\bar{c}_{gn} + \sum_{m=1}^{np}(\bar{x} - \sum_{n=1}^{np} N_n(\bar{x}_i)\bar{x}_n) M_m(\bar{x}_i)\bar{c}_{gm,x}\right]\right.$$

$$\times\left[\sum_{n=1}^{np} N_n(\bar{x}_i)\bar{c}_{oxn} + \sum_{m=1}^{np}(\bar{x} - \sum_{n=1}^{np} N_n(\bar{x}_i)\bar{x}_n) M_m(\bar{x}_i)\bar{c}_{oxm,x}\right]$$

$$\times\left[\sum_{m=1}^{np} M_m(\bar{x}_i)\bar{c}_{km,x}\right]\left[\sum_{m=1}^{np} M_m(\bar{x}_i)\bar{\psi}_{m,x}\right]$$

$$+\eta z_k\bar{K}_g\left[\sum_{n=1}^{np} N_n(\bar{x}_i)\bar{c}_{oxn} + \sum_{m=1}^{np}(\bar{x} - \sum_{n=1}^{np} N_n(\bar{x}_i)\bar{x}_n) M_m(\bar{x}_i)\bar{c}_{oxm,x}\right]$$

$$\times\left[\sum_{m=1}^{np} M_m(\bar{x}_i)\bar{c}_{km,x}\right]\left[\sum_{m=1}^{np} M_m(\bar{x}_i)\bar{\psi}_{m,x}\right]$$

$$+\eta z_k\bar{K}_{ox}\left[\sum_{n=1}^{np} N_n(\bar{x}_i)\bar{c}_{gn} + \sum_{m=1}^{np}(\bar{x} - \sum_{n=1}^{np} N_n(\bar{x}_i)\bar{x}_n) M_m(\bar{x}_i)\bar{c}_{gm,x}\right]$$

$$\left.\times\left[\sum_{m=1}^{np} M_m(\bar{x}_i)\bar{c}_{km,x}\right]\left[\sum_{m=1}^{np} M_m(\bar{x}_i)\bar{\psi}_{m,x}\right]\right\}$$

$$+\left\{\eta z_k\left[\sum_{n=1}^{np} N_n(\bar{x}_i)\bar{c}_{gn} + \sum_{m=1}^{np}(\bar{x} - \sum_{n=1}^{np} N_n(\bar{x}_i)\bar{x}_n) M_m(\bar{x}_i)\bar{c}_{gm,x}\right]\right.$$

$$\times\left[\sum_{n=1}^{np} N_n(\bar{x}_i)\bar{c}_{oxn} + \sum_{m=1}^{np}(\bar{x} - \sum_{n=1}^{np} N_n(\bar{x}_i)\bar{x}_n) M_m(\bar{x}_i)\bar{c}_{oxm,x}\right]$$

$$\left.\times\left[\sum_{n=1}^{np} N_n(\bar{x}_i)\bar{c}_{kn} + \sum_{m=1}^{np}(\bar{x} - \sum_{n=1}^{np} N_n(\bar{x}_i)\bar{x}_n) M_m(\bar{x}_i)\bar{c}_{km,x}\right]\left[\sum_{n=1}^{np} N_{n,xx}(\bar{x}_i)\bar{\psi}_n\right]\right.$$

$$+\eta z_k \bar{K}_g \left[\sum_{n=1}^{np} N_n(\bar{x}_i)\bar{c}_{oxn} + \sum_{m=1}^{np}(\bar{x} - \sum_{n=1}^{np} N_n(\bar{x}_i)\bar{x}_n) M_m(\bar{x}_i)\bar{c}_{oxm,x}\right]$$

$$\times\left[\sum_{n=1}^{np} N_n(\bar{x}_i)\bar{c}_{kn} + \sum_{m=1}^{np}(\bar{x} - \sum_{n=1}^{np} N_n(\bar{x}_i)\bar{x}_n) M_m(\bar{x}_i)\bar{c}_{km,x}\right]\left[\sum_{n=1}^{np} N_{n,xx}(\bar{x}_i)\bar{\psi}_n\right]$$

$$+\eta z_k \bar{K}_{ox} \left[\sum_{n=1}^{np} N_n(\bar{x}_i)\bar{c}_{gn} + \sum_{m=1}^{np}(\bar{x} - \sum_{n=1}^{np} N_n(\bar{x}_i)\bar{x}_n) M_m(\bar{x}_i)\bar{c}_{gm,x}\right]$$

$$\times\left[\sum_{n=1}^{np} N_n(\bar{x}_i)\bar{c}_{kn} + \sum_{m=1}^{np}(\bar{x} - \sum_{n=1}^{np} N_n(\bar{x}_i)\bar{x}_n) M_m(\bar{x}_i)\bar{c}_{km,x}\right]\left[\sum_{n=1}^{np} N_{n,xx}(\bar{x}_i)\bar{\psi}_n\right]\Bigg\}$$

$$+\frac{v_k}{\bar{D}_k}\bar{V}_{\max}\left[\sum_{n=1}^{np} N_n(\bar{x}_i)\bar{c}_{gn} + \sum_{m=1}^{np}(\bar{x} - \sum_{n=1}^{np} N_n(\bar{x}_i)\bar{x}_n) M_m(\bar{x}_i)\bar{c}_{gm,x}\right]$$

$$\times\left[\sum_{n=1}^{np} N_n(\bar{x}_i)\bar{c}_{oxn} + \sum_{m=1}^{np}(\bar{x} - \sum_{n=1}^{np} N_n(\bar{x}_i)\bar{x}_n) M_m(\bar{x}_i)\bar{c}_{oxm,x}\right]$$

$$=\left[\sum_{n=1}^{np} N_n(\bar{x}_i)\bar{c}_{gn}\right]\left[\sum_{n=1}^{np} N_n(\bar{x}_i)\bar{c}_{oxn}\right]\left[\sum_{n=1}^{np} N_{n,xx}(\bar{x}_i)\bar{c}_{kn}\right]$$

$$+\left[\sum_{n=1}^{np} N_n(\bar{x}_i)\bar{c}_{gn}\right]\left[\sum_{m=1}^{np}(\bar{x} - \sum_{n=1}^{np} N_n(\bar{x}_i)\bar{x}_n) M_m(\bar{x}_i)\bar{c}_{oxm,x}\right]\left[\sum_{n=1}^{np} N_{n,xx}(\bar{x}_i)\bar{c}_{kn}\right]$$

$$+\left[\sum_{m=1}^{np}(\bar{x} - \sum_{n=1}^{np} N_n(\bar{x}_i)\bar{x}_n) M_m(\bar{x}_i)\bar{c}_{gm,x}\right]\left[\sum_{n=1}^{np} N_n(\bar{x}_i)\bar{c}_{oxn}\right]\left[\sum_{n=1}^{np} N_{n,xx}(\bar{x}_i)\bar{c}_{kn}\right]$$

$$+\left[\sum_{m=1}^{np}(\bar{x} - \sum_{n=1}^{np} N_n(\bar{x}_i)\bar{x}_n) M_m(\bar{x}_i)\bar{c}_{gm,x}\right]\left[\sum_{m=1}^{np}(\bar{x} - \sum_{n=1}^{np} N_n(\bar{x}_i)\bar{x}_n) M_m(\bar{x}_i)\bar{c}_{oxm,x}\right]$$

$$\times\left[\sum_{n=1}^{np} N_{n,xx}(\bar{x}_i)\bar{c}_{kn}\right]$$

$$+\bar{K}_g\left[\sum_{n=1}^{np} N_n(\bar{x}_i)\bar{c}_{oxn}\right]\left[\sum_{n=1}^{np} N_{n,xx}(\bar{x}_i)\bar{c}_{kn}\right]$$

$$+\bar{K}_g\left[\sum_{n=1}^{np}(\bar{x} - \sum_{n=1}^{np} N_n(\bar{x}_i)\bar{x}_n) M_m(\bar{x}_i)\bar{c}_{oxm,x}\right]\left[\sum_{n=1}^{np} N_{n,xx}(\bar{x}_i)\bar{c}_{kn}\right]$$

$$+\bar{K}_{ox}\left[\sum_{n=1}^{np} N_n(\bar{x}_i)\bar{c}_{gn}\right]\left[\sum_{n=1}^{np} N_{n,xx}(\bar{x}_i)\bar{c}_{kn}\right]$$

$$+\bar{K}_{ox}\left[\sum_{m=1}^{np}(\bar{x} - \sum_{n=1}^{np} N_n(\bar{x}_i)\bar{x}_n) M_m(\bar{x}_i)\bar{c}_{gm,x}\right]\left[\sum_{n=1}^{np} N_{n,xx}(\bar{x}_i)\bar{c}_{kn}\right]$$

$$+\eta z_k\left[\sum_{n=1}^{np}N_n(\overline{x}_i)\overline{c}_{gn}\right]\left[\sum_{n=1}^{np}N_n(\overline{x}_i)\overline{c}_{oxn}\right]\left[\sum_{m=1}^{np}M_m(\overline{x}_i)\overline{c}_{km,x}\right]\left[\sum_{m=1}^{np}M_m(\overline{x}_i)\overline{\psi}_{m,x}\right]$$

$$+\eta z_k\left[\sum_{n=1}^{np}N_n(\overline{x}_i)\overline{c}_{gn}\right]\left[\sum_{m=1}^{np}(\overline{x}-\sum_{n=1}^{np}N_n(\overline{x}_i)\overline{x}_n)M_m(\overline{x}_i)\overline{c}_{oxm,x}\right]$$

$$\times\left[\sum_{m=1}^{np}M_m(\overline{x}_i)\overline{c}_{km,x}\right]\left[\sum_{m=1}^{np}M_m(\overline{x}_i)\overline{\psi}_{m,x}\right]$$

$$+\eta z_k\left[\sum_{n=1}^{np}(\overline{x}-\sum_{n=1}^{np}N_n(\overline{x}_i)\overline{x}_n)M_m(\overline{x}_i)\overline{c}_{gm,x}\right]\left[\sum_{n=1}^{np}N_n(\overline{x}_i)\overline{c}_{oxn}\right]$$

$$\times\left[\sum_{m=1}^{np}M_m(\overline{x}_i)\overline{c}_{km,x}\right]\left[\sum_{m=1}^{np}M_m(\overline{x}_i)\overline{\psi}_{m,x}\right]$$

$$+\eta z_k\left[\sum_{n=1}^{np}(\overline{x}-\sum_{n=1}^{np}N_n(\overline{x}_i)\overline{x}_n)M_m(\overline{x}_i)\overline{c}_{gm,x}\right]\left[\sum_{m=1}^{np}(\overline{x}-\sum_{n=1}^{np}N_n(\overline{x}_i)\overline{x}_n)M_m(\overline{x}_i)\overline{c}_{oxm,x}\right]$$

$$\times\left[\sum_{m=1}^{np}M_m(\overline{x}_i)\overline{c}_{km,x}\right]\left[\sum_{m=1}^{np}M_m(\overline{x}_i)\overline{\psi}_{m,x}\right]$$

$$+\eta z_k\overline{K}_g\left[\sum_{n=1}^{np}N_n(\overline{x}_i)\overline{c}_{oxn}\right]\left[\sum_{m=1}^{np}M_m(\overline{x}_i)\overline{c}_{km,x}\right]\left[\sum_{m=1}^{np}M_m(\overline{x}_i)\overline{\psi}_{m,x}\right]$$

$$+\eta z_k\overline{K}_g\left[\sum_{m=1}^{np}(\overline{x}-\sum_{n=1}^{np}N_n(\overline{x}_i)\overline{x}_n)M_m(\overline{x}_i)\overline{c}_{oxm,x}\right]\left[\sum_{m=1}^{np}M_m(\overline{x}_i)\overline{c}_{km,x}\right]\left[\sum_{m=1}^{np}M_m(\overline{x}_i)\overline{\psi}_{m,x}\right]$$

$$+\eta z_k\overline{K}_{ox}\left[\sum_{n=1}^{np}N_n(\overline{x}_i)\overline{c}_{gn}\right]\left[\sum_{m=1}^{np}M_m(\overline{x}_i)\overline{c}_{km,x}\right]\left[\sum_{m=1}^{np}M_m(\overline{x}_i)\overline{\psi}_{m,x}\right]$$

$$+\eta z_k\overline{K}_{ox}\left[\sum_{m=1}^{np}(\overline{x}-\sum_{n=1}^{np}N_n(\overline{x}_i)\overline{x}_n)M_m(\overline{x}_i)\overline{c}_{gm,x}\right]\left[\sum_{m=1}^{np}M_m(\overline{x}_i)\overline{c}_{km,x}\right]\left[\sum_{m=1}^{np}M_m(\overline{x}_i)\overline{\psi}_{m,x}\right]$$

$$+\eta z_k\left[\sum_{n=1}^{np}N_n(\overline{x}_i)\overline{c}_{gn}\right]\left[\sum_{n=1}^{np}N_n(\overline{x}_i)\overline{c}_{oxn}\right]\left[\sum_{n=1}^{np}N_n(\overline{x}_i)\overline{c}_{kn}\right]\left[\sum_{n=1}^{np}N_{n,xx}(\overline{x}_i)\overline{\psi}_n\right]$$

$$+\eta z_k\left[\sum_{n=1}^{np}N_n(\overline{x}_i)\overline{c}_{gn}\right]\left[\sum_{n=1}^{np}N_n(\overline{x}_i)\overline{c}_{oxn}\right]$$

$$\times\left[\sum_{m=1}^{np}(\overline{x}-\sum_{n=1}^{np}N_n(\overline{x}_i)\overline{x}_n)M_m(\overline{x}_i)\overline{c}_{km,x}\right]\left[\sum_{n=1}^{np}N_{n,xx}(\overline{x}_i)\overline{\psi}_n\right]$$

$$+\eta z_k\left[\sum_{n=1}^{np}N_n(\overline{x}_i)\overline{c}_{gn}\right]\left[\sum_{m=1}^{np}(\overline{x}-\sum_{n=1}^{np}N_n(\overline{x}_i)\overline{x}_n)M_m(\overline{x}_i)\overline{c}_{ox,x}\right]$$

$$\times\left[\sum_{n=1}^{np}N_n(\overline{x}_i)\overline{c}_{kn}\right]\left[\sum_{n=1}^{np}N_{n,xx}(\overline{x}_i)\overline{\psi}_n\right]$$

$$+\eta z_k\left[\sum_{n=1}^{np}N_n(\overline{x}_i)\overline{c}_{gn}\right]\left[\sum_{m=1}^{np}(\overline{x}-\sum_{n=1}^{np}N_n(\overline{x}_i)\overline{x}_n)M_m(\overline{x}_i)\overline{c}_{ox,x}\right]$$

$$\times\left[\sum_{m=1}^{np}(\overline{x}-\sum_{n=1}^{np}N_n(\overline{x}_i)\overline{x}_n)M_m(\overline{x}_i)\overline{c}_{km,x}\right]\left[\sum_{n=1}^{np}N_{n,xx}(\overline{x}_i)\overline{\psi}_n\right]$$

$$+\eta z_k\left[\sum_{m=1}^{np}(\overline{x}-\sum_{n=1}^{np}N_n(\overline{x}_i)\overline{x}_n)M_m(\overline{x}_i)\overline{c}_{g,x}\right]\left[\sum_{n=1}^{np}N_n(\overline{x}_i)\overline{c}_{oxn}\right]$$

$$\times\left[\sum_{n=1}^{np}N_n(\overline{x}_i)\overline{c}_{kn}\right]\left[\sum_{n=1}^{np}N_{n,xx}(\overline{x}_i)\overline{\psi}_n\right]$$

$$+\eta z_k\left[\sum_{m=1}^{np}(\overline{x}-\sum_{n=1}^{np}N_n(\overline{x}_i)\overline{x}_n)M_m(\overline{x}_i)\overline{c}_{gm,x}\right]\left[\sum_{n=1}^{np}N_n(\overline{x}_i)\overline{c}_{oxn}\right]$$

$$\times\left[\sum_{m=1}^{np}(\overline{x}-\sum_{n=1}^{np}N_n(\overline{x}_i)\overline{x}_n)M_m(\overline{x}_i)\overline{c}_{km,x}\right]\left[\sum_{n=1}^{np}N_{n,xx}(\overline{x}_i)\overline{\psi}_n\right]$$

$$+\eta z_k\left[\sum_{m=1}^{np}(\overline{x}-\sum_{n=1}^{np}N_n(\overline{x}_i)\overline{x}_n)M_m(\overline{x}_i)\overline{c}_{g,x}\right]\left[\sum_{m=1}^{np}(\overline{x}-\sum_{n=1}^{np}N_n(\overline{x}_i)\overline{x}_n)M_m(\overline{x}_i)\overline{c}_{ox,x}\right]$$

$$\times\left[\sum_{n=1}^{np}N_n(\overline{x}_i)\overline{c}_{kn}\right]\left[\sum_{n=1}^{np}N_{n,xx}(\overline{x}_i)\overline{\psi}_n\right]$$

$$+\eta z_k\left[\sum_{m=1}^{np}(\overline{x}-\sum_{n=1}^{np}N_n(\overline{x}_i)\overline{x}_n)M_m(\overline{x}_i)\overline{c}_{gm,x}\right]\left[\sum_{m=1}^{np}(\overline{x}-\sum_{n=1}^{np}N_n(\overline{x}_i)\overline{x}_n)M_m(\overline{x}_i)\overline{c}_{oxm,x}\right]$$

$$\times\left[\sum_{m=1}^{np}(\overline{x}-\sum_{n=1}^{np}N_n(\overline{x}_i)\overline{x}_n)M_m(\overline{x}_i)\overline{c}_{km,x}\right]\left[\sum_{n=1}^{np}N_{n,xx}(\overline{x}_i)\overline{\psi}_n\right]$$

$$+\eta z_k\overline{K}_g\left[\sum_{n=1}^{np}N_n(\overline{x}_i)\overline{c}_{oxn}\right]\left[\sum_{n=1}^{np}N_n(\overline{x}_i)\overline{c}_{kn}\right]\left[\sum_{n=1}^{np}N_{n,xx}(\overline{x}_i)\overline{\psi}_n\right]$$

$$+\eta z_k\overline{K}_g\left[\sum_{n=1}^{np}N_n(\overline{x}_i)\overline{c}_{oxn}\right]\left[\sum_{m=1}^{np}(\overline{x}-\sum_{n=1}^{np}N_n(\overline{x}_i)\overline{x}_n)M_m(\overline{x}_i)\overline{c}_{km,x}\right]\left[\sum_{n=1}^{np}N_{n,xx}(\overline{x}_i)\overline{\psi}_n\right]$$

$$+\eta z_k\overline{K}_g\left[\sum_{m=1}^{np}(\overline{x}-\sum_{n=1}^{np}N_n(\overline{x}_i)\overline{x}_n)M_m(\overline{x}_i)\overline{c}_{oxm,x}\right]$$

$$\times\left[\sum_{n=1}^{np}N_n(\overline{x}_i)\overline{c}_{kn}\right]\left[\sum_{n=1}^{np}N_{n,xx}(\overline{x}_i)\overline{\psi}_n\right]$$

$$+\eta z_k \bar{K}_g \left[\sum_{m=1}^{np}(\bar{x}-\sum_{n=1}^{np}N_n(\bar{x}_i)\bar{x}_n)M_m(\bar{x}_i)\bar{c}_{oxm,x}\right]$$

$$\times\left[\sum_{m=1}^{np}(\bar{x}-\sum_{n=1}^{np}N_n(\bar{x}_i)\bar{x}_n)M_m(\bar{x}_i)\bar{c}_{km,x}\right]\left[\sum_{n=1}^{np}N_{n,xx}(\bar{x}_i)\bar{\psi}_n\right]$$

$$+\eta z_k \bar{K}_{ox}\left[\sum_{n=1}^{np}N_n(\bar{x}_i)\bar{c}_{gn}\right]\left[\sum_{n=1}^{np}N_n(\bar{x}_i)\bar{c}_{kn}\right]\left[\sum_{n=1}^{np}N_{n,xx}(\bar{x}_i)\bar{\psi}_n\right]$$

$$+\eta z_k \bar{K}_{ox}\left[\sum_{n=1}^{np}N_n(\bar{x}_i)\bar{c}_{gn}\right]\left[\sum_{m=1}^{np}(\bar{x}-\sum_{n=1}^{np}N_n(\bar{x}_i)\bar{x}_n)M_m(\bar{x}_i)\bar{c}_{km,x}\right]\left[\sum_{n=1}^{np}N_{n,xx}(\bar{x}_i)\bar{\psi}_n\right]$$

$$+\eta z_k \bar{K}_{ox}\left[\sum_{m=1}^{np}(\bar{x}-\sum_{n=1}^{np}N_n(\bar{x}_i)\bar{x}_n)M_m(\bar{x}_i)\bar{c}_{gm,x}\right]$$

$$\times\left[\sum_{n=1}^{np}N_n(\bar{x}_i)\bar{c}_{kn}\right]\left[\sum_{n=1}^{np}N_{n,xx}(\bar{x}_i)\bar{\psi}_n\right]$$

$$+\eta z_k \bar{K}_{ox}\left[\sum_{m=1}^{np}(\bar{x}-\sum_{n=1}^{np}N_n(\bar{x}_i)\bar{x}_n)M_m(\bar{x}_i)\bar{c}_{gm,x}\right]$$

$$\times\left[\sum_{m=1}^{np}(\bar{x}-\sum_{n=1}^{np}N_n(\bar{x}_i)\bar{x}_n)M_m(\bar{x}_i)\bar{c}_{km,x}\right]\left[\sum_{n=1}^{np}N_{n,xx}(\bar{x}_i)\bar{\psi}_n\right]$$

$$+\frac{v_k}{\bar{D}_k}\bar{V}_{\max}\left[\sum_{n=1}^{np}N_n(\bar{x}_i)\bar{c}_{gn}\right]\left[\sum_{n=1}^{np}N_n(\bar{x}_i)\bar{c}_{oxn}\right]$$

$$+\frac{v_k}{\bar{D}_k}\bar{V}_{\max}\left[\sum_{n=1}^{np}N_n(\bar{x}_i)\bar{c}_{gn}\right]\left[\sum_{m=1}^{np}(\bar{x}-\sum_{n=1}^{np}N_n(\bar{x}_i)\bar{x}_n)M_m(\bar{x}_i)\bar{c}_{oxm,x}\right]$$

$$+\frac{v_k}{\bar{D}_k}\bar{V}_{\max}\left[\sum_{m=1}^{np}(\bar{x}-\sum_{n=1}^{np}N_n(\bar{x}_i)\bar{x}_n)M_m(\bar{x}_i)\bar{c}_{gm,x}\right]\left[\sum_{n=1}^{np}N_n(\bar{x}_i)\bar{c}_{oxn}\right]$$

$$+\frac{v_k}{\bar{D}_k}\bar{V}_{\max}\left[\sum_{m=1}^{np}(\bar{x}-\sum_{n=1}^{np}N_n(\bar{x}_i)\bar{x}_n)M_m(\bar{x}_i)\bar{c}_{gm,x}\right]\left[\sum_{m=1}^{np}(\bar{x}-\sum_{n=1}^{np}N_n(\bar{x}_i)\bar{x}_n)M_m(\bar{x}_i)\bar{c}_{oxm,x}\right] \tag{A.34}$$

Poisson Equation

$$\sum_{n=1}^{np}N_{n,xx}(\bar{x}_i)\bar{\psi}_n+\frac{F^2}{\varepsilon\varepsilon_0 RT}\frac{L_{ref}^2 c_{ref}}{\eta}\{z_f\bar{c}_f+\sum_{k=1}^{N}z_k[\sum_{n=1}^{np}N_n(\bar{x}_i)\bar{c}_{kn}$$

$$+\sum_{m=1}^{np}(\bar{x}_i-\sum_{n=1}^{np}N_n(\bar{x}_i)\bar{x}_n)M_m(\bar{x}_i)\bar{c}_{km,x}]\}=0 \tag{A.35}$$

Mechanical Governing Equation

$$(\lambda+2\mu)\{\sum_{n=1}^{npGel} N_{n,xx}(\bar{x}_i)\bar{u}_n + 3[\sum_{m=1}^{npGel} M_m(\bar{x}_i)\bar{u}_{m,x}][\sum_{n=1}^{npGel} N_{n,xx}(\bar{x}_i)\bar{u}_n]$$

$$+\frac{3}{2}[\sum_{m=1}^{npGel} M_m(\bar{x}_i)\bar{u}_{m,x}][\sum_{m=1}^{npGel} M_m(\bar{x}_i)\bar{u}_{m,x}][\sum_{n=1}^{npGel} N_{n,xx}(\bar{x}_i)\bar{u}_n]\}$$

$$-c_{ref}RT\sum_k[\sum_{m=1}^{npGel} M_m(\bar{x}_i)\bar{c}_{km,x}] = 0 \qquad (k=1,2,\cdots,N) \tag{A.36}$$

Auxiliary Equations

$$\sum_{n=1}^{np} N_{xn}(\bar{x}_i)\bar{c}_{kn} - [\sum_{n=1}^{np} N_{xn}(\bar{x}_i)\bar{x}_n]\sum_{m=1}^{np} M_m(\bar{x}_i)\bar{c}_{km,x} = 0 \tag{A.37}$$

$$\sum_{n=1}^{np} N_{xn}(\bar{x}_i)\bar{\psi}_n - [\sum_{n=1}^{np} N_{xn}(\bar{x}_i)\bar{x}_n]\sum_{m=1}^{np} M_m(\bar{x}_i)\bar{\psi}_{m,x} = 0 \tag{A.38}$$

$$\sum_{n=1}^{npGel} N_{xn}(\bar{x}_i)\bar{u}_n - [\sum_{n=1}^{npGel} N_{xn}(\bar{x}_i)\bar{x}_n]\sum_{m=1}^{npGel} M_m(\bar{x}_i)\bar{u}_{m,x} = 0 \tag{A.39}$$

where *np* is the number of the scattered points in all the domains covering the both hydrogel and surrounding solution, and *npGel* is that within the hydrogel domain only.

According to the Newton-Raphson method, the residuals R are defined as

$$R^k_{N-P}(\bar{x}_i) = \left\{\left[\sum_{n=1}^{np} N_n(\bar{x}_i)\bar{c}_{gn} + \sum_{m=1}^{np}(\bar{x} - \sum_{n=1}^{np} N_n(\bar{x}_i)\bar{x}_n)M_m(\bar{x}_i)\bar{c}_{gm,x}\right]\right.$$

$$\times\left[\sum_{n=1}^{np} N_n(\bar{x}_i)\bar{c}_{oxn} + \sum_{m=1}^{np}(\bar{x} - \sum_{n=1}^{np} N_n(\bar{x}_i)\bar{x}_n)M_m(\bar{x}_i)\bar{c}_{oxm,x}\right]\left[\sum_{n=1}^{np} N_{n,xx}(\bar{x}_i)\bar{c}_{kn}\right]$$

$$+\bar{K}_g\left[\sum_{n=1}^{np} N_n(\bar{x}_i)\bar{c}_{oxn} + \sum_{m=1}^{np}(\bar{x} - \sum_{n=1}^{np} N_n(\bar{x}_i)\bar{x}_n)M_m(\bar{x}_i)\bar{c}_{oxm,x}\right]\left[\sum_{n=1}^{np} N_{n,xx}(\bar{x}_i)\bar{c}_{kn}\right]$$

$$\left.+\bar{K}_{ox}\left[\sum_{n=1}^{np} N_n(\bar{x}_i)\bar{c}_{gn} + \sum_{m=1}^{np}(\bar{x} - \sum_{n=1}^{np} N_n(\bar{x}_i)\bar{x}_n)M_m(\bar{x}_i)\bar{c}_{gm,x}\right]\left[\sum_{n=1}^{np} N_{n,xx}(\bar{x}_i)\bar{c}_{kn}\right]\right\}$$

$$+\left\{\eta z_k\left[\sum_{n=1}^{np} N_n(\bar{x}_i)\bar{c}_{gn} + \sum_{m=1}^{np}(\bar{x} - \sum_{n=1}^{np} N_n(\bar{x}_i)\bar{x}_n)M_m(\bar{x}_i)\bar{c}_{gm,x}\right]\right.$$

$$\times\left[\sum_{n=1}^{np}N_n(\overline{x}_i)\overline{c}_{oxn}+\sum_{m=1}^{np}(\overline{x}-\sum_{n=1}^{np}N_n(\overline{x}_i)\overline{x}_n)M_m(\overline{x}_i)\overline{c}_{oxm,x}\right]$$

$$\times\left[\sum_{m=1}^{np}M_m(\overline{x}_i)\overline{c}_{km,x}\right]\left[\sum_{m=1}^{np}M_m(\overline{x}_i)\overline{\psi}_{m,x}\right]$$

$$+\eta z_k\overline{K}_g\left[\sum_{n=1}^{np}N_n(\overline{x}_i)\overline{c}_{oxn}+\sum_{m=1}^{np}(\overline{x}-\sum_{n=1}^{np}N_n(\overline{x}_i)\overline{x}_n)M_m(\overline{x}_i)\overline{c}_{oxm,x}\right]$$

$$\times\left[\sum_{m=1}^{np}M_m(\overline{x}_i)\overline{c}_{km,x}\right]\left[\sum_{m=1}^{np}M_m(\overline{x}_i)\overline{\psi}_{m,x}\right]$$

$$+\eta z_k\overline{K}_{ox}\left[\sum_{n=1}^{np}N_n(\overline{x}_i)\overline{c}_{gn}+\sum_{m=1}^{np}(\overline{x}-\sum_{n=1}^{np}N_n(\overline{x}_i)\overline{x}_n)M_m(\overline{x}_i)\overline{c}_{gm,x}\right]$$

$$\times\left[\sum_{m=1}^{np}M_m(\overline{x}_i)\overline{c}_{km,x}\right]\left[\sum_{m=1}^{np}M_m(\overline{x}_i)\overline{\psi}_{m,x}\right]$$

$$+\left\{\eta z_k\left[\sum_{n=1}^{np}N_n(\overline{x}_i)\overline{c}_{gn}+\sum_{m=1}^{np}(\overline{x}-\sum_{n=1}^{np}N_n(\overline{x}_i)\overline{x}_n)M_m(\overline{x}_i)\overline{c}_{gm,x}\right]\right.$$

$$\times\left[\sum_{n=1}^{np}N_n(\overline{x}_i)\overline{c}_{oxn}+\sum_{m=1}^{np}(\overline{x}-\sum_{n=1}^{np}N_n(\overline{x}_i)\overline{x}_n)M_m(\overline{x}_i)\overline{c}_{oxm,x}\right]$$

$$\times\left[\sum_{n=1}^{np}N_n(\overline{x}_i)\overline{c}_{kn}+\sum_{m=1}^{np}(\overline{x}-\sum_{n=1}^{np}N_n(\overline{x}_i)\overline{x}_n)M_m(\overline{x}_i)\overline{c}_{km,x}\right]\left[\sum_{n=1}^{np}N_{n,xx}(\overline{x}_i)\overline{\psi}_n\right]$$

$$+\eta z_k\overline{K}_g\left[\sum_{n=1}^{np}N_n(\overline{x}_i)\overline{c}_{oxn}+\sum_{m=1}^{np}(\overline{x}-\sum_{n=1}^{np}N_n(\overline{x}_i)\overline{x}_n)M_m(\overline{x}_i)\overline{c}_{oxm,x}\right]$$

$$\times\left[\sum_{n=1}^{np}N_n(\overline{x}_i)\overline{c}_{kn}+\sum_{m=1}^{np}(\overline{x}-\sum_{n=1}^{np}N_n(\overline{x}_i)\overline{x}_n)M_m(\overline{x}_i)\overline{c}_{km,x}\right]\left[\sum_{n=1}^{np}N_{n,xx}(\overline{x}_i)\overline{\psi}_n\right]$$

$$+\eta z_k\overline{K}_{ox}\left[\sum_{n=1}^{np}N_n(\overline{x}_i)\overline{c}_{gn}+\sum_{m=1}^{np}(\overline{x}-\sum_{n=1}^{np}N_n(\overline{x}_i)\overline{x}_n)M_m(\overline{x}_i)\overline{c}_{gm,x}\right]$$

$$\left.\times\left[\sum_{n=1}^{np}N_n(\overline{x}_i)\overline{c}_{kn}+\sum_{m=1}^{np}(\overline{x}-\sum_{n=1}^{np}N_n(\overline{x}_i)\overline{x}_n)M_m(\overline{x}_i)\overline{c}_{km,x}\right]\left[\sum_{n=1}^{np}N_{n,xx}(\overline{x}_i)\overline{\psi}_n\right]\right\}$$

$$+\frac{v_k}{\overline{D}_k}\overline{V}_{\max}\left[\sum_{n=1}^{np}N_n(\overline{x}_i)\overline{c}_{gn}+\sum_{m=1}^{np}(\overline{x}-\sum_{n=1}^{np}N_n(\overline{x}_i)\overline{x}_n)M_m(\overline{x}_i)\overline{c}_{gm,x}\right]$$

$$\times\left[\sum_{n=1}^{np}N_n(\overline{x}_i)\overline{c}_{oxn}+\sum_{m=1}^{np}(\overline{x}-\sum_{n=1}^{np}N_n(\overline{x}_i)\overline{x}_n)M_m(\overline{x}_i)\overline{c}_{oxm,x}\right] \tag{A.40}$$

$$R_p\left(\overline{x}_i\right)=\sum_{n=1}^{np}N_{n,xx}(\overline{x}_i)\overline{\psi}_n+\frac{F^2}{\varepsilon\varepsilon_0 RT}\frac{L_{ref}^2 c_{ref}}{\eta}\{z_f c_f+\sum_{k=1}^{N}z_k[\sum_{n=1}^{np}N_n(\overline{x}_i)\overline{c}_{kn}$$

$$+\sum_{m=1}^{np}(\overline{x}_i-\sum_{n=1}^{np}N_n(\overline{x}_i)\overline{x}_n)M_m(\overline{x}_i)\overline{c}_{km,x}]\} \tag{A.41}$$

$$R_M\left(\overline{x}_i\right)=(\lambda+2\mu)\{\sum_{n=1}^{npGel}N_{n,xx}(\overline{x}_i)\overline{u}_n+3[\sum_{m=1}^{npGel}M_m(\overline{x}_i)\overline{u}_{m,x}][\sum_{n=1}^{npGel}N_{n,xx}(\overline{x}_i)\overline{u}_n]$$

$$+\frac{3}{2}[\sum_{m=1}^{npGel}M_m(\overline{x}_i)\overline{u}_{m,x}][\sum_{m=1}^{npGel}M_m(\overline{x}_i)\overline{u}_{m,x}][\sum_{n=1}^{npGel}N_{n,xx}(\overline{x}_i)\overline{u}_n]\}-c_{ref}RT\sum_{k}[\sum_{m=1}^{npGel}M_m(\overline{x}_i)\overline{c}_{km,x}]$$

$$(k=1,2,\cdots,N) \tag{A.42}$$

$$R_{cx}(\overline{x}_i)=\sum_{n=1}^{np}N_{xn}(\overline{x}_i)\overline{c}_{kn}-[\sum_{n=1}^{np}N_{xn}(\overline{x}_i)\overline{x}_n]\sum_{m=1}^{np}M_m(\overline{x}_i)\overline{c}_{km,x}=0 \tag{A.43}$$

$$R_{\psi x}(\overline{x}_i)=\sum_{n=1}^{np}N_{xn}(\overline{x}_i)\overline{\psi}_n-[\sum_{n=1}^{np}N_{xn}(\overline{x}_i)\overline{x}_n]\sum_{m=1}^{np}M_m(\overline{x}_i)\overline{\psi}_{m,x} \tag{A.44}$$

$$R_{ux}(\overline{x}_i)=\sum_{n=1}^{npGel}N_{xn}(\overline{x}_i)\overline{u}_n-[\sum_{n=1}^{npGel}N_{xn}(\overline{x}_i)\overline{x}_n]\sum_{m=1}^{npGel}M_m(\overline{x}_i)\overline{u}_{m,x} \tag{A.45}$$

The incremental vector $\{\delta u\}$:

$$\{\delta u\}=\delta\begin{bmatrix}\overline{c}_k\\ \overline{\psi}\\ \overline{u}\\ \overline{c}_{kx}\\ \overline{\psi}_x\\ \overline{u}_x\end{bmatrix} \tag{A.46}$$

According to the Newton-Raphson method, the nonlinear system can be linearized and solved in the form of

$$[\boldsymbol{J}]\{\delta u\}=-\{R\} \tag{A.47}$$

The $[\boldsymbol{J}]$ is the Jacobian matrix and defined as

$$[\boldsymbol{J}]=\begin{bmatrix}
\frac{\partial R_{N-P}^{k}}{\partial \overline{c}_{k}} & \frac{\partial R_{N-P}^{k}}{\partial \overline{\psi}} & \frac{\partial R_{N-P}^{k}}{\partial \overline{u}} & \frac{\partial R_{N-P}^{k}}{\partial \overline{c}_{kx}} & \frac{\partial R_{N-P}^{k}}{\partial \overline{\psi}_{x}} & \frac{\partial R_{N-P}^{k}}{\partial \overline{u}_{x}} \\
\frac{\partial R_{P}}{\partial \overline{c}_{k}} & \frac{\partial R_{P}}{\partial \overline{\psi}} & \frac{\partial R_{P}}{\partial \overline{u}} & \frac{\partial R_{P}}{\partial \overline{c}_{kx}} & \frac{\partial R_{P}}{\partial \overline{\psi}_{x}} & \frac{\partial R_{P}}{\partial \overline{u}_{x}} \\
\frac{\partial R_{M}}{\partial \overline{c}_{k}} & \frac{\partial R_{M}}{\partial \overline{\psi}} & \frac{\partial R_{M}}{\partial \overline{u}} & \frac{\partial R_{M}}{\partial \overline{c}_{kx}} & \frac{\partial R_{M}}{\partial \overline{\psi}_{x}} & \frac{\partial R_{M}}{\partial \overline{u}_{x}} \\
\frac{\partial R_{cx}^{k}}{\partial \overline{c}_{k}} & \frac{\partial R_{cx}^{k}}{\partial \overline{\psi}} & \frac{\partial R_{cx}^{k}}{\partial \overline{u}} & \frac{\partial R_{cx}^{k}}{\partial \overline{c}_{kx}} & \frac{\partial R_{cx}^{k}}{\partial \overline{\psi}_{x}} & \frac{\partial R_{cx}^{k}}{\partial \overline{u}_{x}} \\
\frac{\partial R_{\psi x}}{\partial \overline{c}_{k}} & \frac{\partial R_{\psi x}}{\partial \overline{\psi}} & \frac{\partial R_{\psi x}}{\partial \overline{u}} & \frac{\partial R_{\psi x}}{\partial \overline{c}_{kx}} & \frac{\partial R_{\psi x}}{\partial \overline{\psi}_{x}} & \frac{\partial R_{\psi x}}{\partial \overline{u}_{x}} \\
\frac{\partial R_{ux}}{\partial \overline{c}_{k}} & \frac{\partial R_{ux}}{\partial \overline{\psi}} & \frac{\partial R_{ux}}{\partial \overline{u}} & \frac{\partial R_{ux}}{\partial \overline{c}_{kx}} & \frac{\partial R_{ux}}{\partial \overline{\psi}_{x}} & \frac{\partial R_{ux}}{\partial \overline{u}_{x}}
\end{bmatrix} \tag{A.48}$$

References

Abdekhodaie, M.J. and X.Y. Wu. Modeling of a cationic glucose-sensitive membrane with consideration of oxygen limitation, *Journal of Membrane Science*, 254 119-127, **2005**.

Alberty, R.A. and R. J. Silbey. *Physical chemistry*, John Wiley & Sons, Inc, Singapore, pp127, pp183, and pp845-846, **1997**.

Albin, G., Horbett, T.A. and B. Ratner. Glucose sensitive membranes for controlled delivery of insulin: insulin transport studies, *J. controlled release*, 2, 153-164, **1985**.

Albin, G., Horbett, T.A., Miller, S.R. and N.L. Ricker. Theoretical and experimental studies of glucose sensitive membranes, *J. controlled release*, 6, 267-191, **1987**.

Ali, A. and E.A. Hegazy. Radiation synthesis of poly(ethylene glycol)/acrylic acid hydrogel as carrier for site specific drug delivery, *Journal of Biomedical Materials Research Part B-Applied Biomaterials*, 81B (1), 168-174, **2007**.

Aluru, N.R. and G. Li. Finite cloud method: a true meshless technique based on a fixed reproducing kernel approximation, *International Journal for Numerical Methods in Engineering*, 50, 2373-2410, **2001**.

Amsden, B. Solute diffusion within hydrogels: Mechanisms and models, *Macromolecues*, 31, 8382-8395, **1998**.

Arridge, R.G.C. *Mechanics of Polymers*, Clarendon Press, Oxford, **1975**.

Asher, S.A., Alexeev, V.L., Goponenko, A.V., Sharma, A.C., Lednev, I.K., Wilcox, C.S. and D.N. Finegold. Photoic crystal carbohydrate sensors: Low ionic strength sugar sensing, *J.Am.Chem.Soc*., 125, 3322-3329, **2003**.

Bajpai S.K. Swelling-deswelling behavior of poly(acrylamide-co-maleic acid) hydrogels, *Journal of Applied Polymer Science*, 80, 2782-2789, **2001**.

Bajpai, S.K. and A. Giri. Swelling dynamics of a macromolecular hydrophilic network and evaluation of its potential for controlled release of agrochemicals, *Reactive & Functional Polymers*, 53, 125-141, **2002**.

Bajpai, S.K. and S. Dubey. In vitro dissolution studies for release of vitamin B12 from

poly(N-vinyl-2-pyrrolidone-co-acrylic acid) hydrogels, *Reactive & Functional Polymers*, 62, 93-104, **2005**.

Bajpai, A.K. and S. Kankane. Preparation and characterization of macroporous poly(2-hydroxyethyl methacrylate)-based biomaterials: water sorption property and in vitro blood compatibility, *Journal of Applied Polymer Science*, 104(3), 1559-1571, **2007**.

Bashir, R., Hilt, J.Z., Elibol, O., Gupta, A. and N.A. Peppas. Micromechanical cantilever as an ultrasensitive pH microsensor, *Applied Physics Letters*, 81, 3091-3093, **2002**.

Beebe, D.J., Moore, J., Bauer, J., Yu, Q., Liu, R.H., Devadoss, C. and B.H. Jo. Functional hydrogel structures for autonomous flow control inside microfluidic channels, *Nature*, 404, 588-590, **2000**.

Belytschko, T., Lu, Y.Y. and L. Gu. Element free Galerkin methods, *International Journal for Numerical Methods in Engineering*, 37, 229-256, **1994**.

Bird, B.R., Stewart, W.E. and E.N. Lightfoot. *Transport phenomena*, John Wiley & Sons, Inc, New York, **1960**.

Blandino, A., Macias, M. and D. Cantero. Modelling and simulation of a bienzymatic reaction system co-immoilised within hydrogel-membrane liquid-core capsules, *Enzyme and Microbial Technology*, 31, 556-565, **2002**.

Brahim, S., Narinesingh, D. and A. Guiseppi-Elie. Bio-smart hydrogels: co-joined molecular recognition and signal transduction in biosensor fabrication and drug delivery, *Biosensors and Bioelectronics*, 17, 973-981, **2002**.

Brannon-Peppas, L. and N.A. Peppas. Equilibrium swelling behavior of pH-sensitive hydrogels, *Chem Eng. Sci*, 46, 715-722, **1991**.

Brazel, C.S. and N.A. Peppas. Pulsatile local delivery of thrombolytic and antithrombotic agents using poly(*N*-iso-propylacrylamide-*co*-methacrylic acid) hydrogels, *Journal of Controlled Release*, 39, 57-64, **1996**.

Briggs, G.E. and J.B.S. Haldane. A note on the kinetics of enzyme action, *Biochem. J.*, 19, 339-339, **1925**.

Bromberg, L.E. and E.S. Ron. Temperature-responsive gels and thermogelling polymer

matrices for protein and peptide delivery, *Advanced Drug Delivery Reviews*, 31, 197-221, **1998**.

Cao, X., Lai, S. and L.J. Lee. Design of a self-regulated drug delivery device, *Biomed. Microdevices*, 3, 109-118, **2001**.

Carlson, K.T., Setton, L.A. and A. Chilkoti. Swelling and mechanical behaviors of chemically cross-linked hydrogels of elastin-like polypeptides, *Biomacromolecules*, 4, 572-580, **2003**.

Caykara, T. and I. Aycicek. External stimuli-responsive characteristics of ionic poly[(*N*,*N*-diethylaminoethyl methacrylate)-*co*-(*N*-vinyl-2-pyrrolidone)] hydrogels, *Macromolecular Materials and Engineering*, 290, 468-474, **2005**.

Caykara, T. and I. Akcakaya. Synthesis and network structure of ionic poly(N,N-dimethylacrylamide-co-acrylamide) hydrogels: comparison of swelling degree with theory, *European Polymer Journal*, 42, 1437-1445, **2006**.

Caykara, T., Bozkaya, U. and O. Kantoglu. Network structure and swelling behavior of poly(acrylamide/crotonic acid) hydrogels in aqueous salt solutions, *J Polym Sci Part B: Polym Phys*, 41, 1656-1664, **2003**.

Chang, R. *Chemistry*, McGraw-Hill, New York, **2002**.

Chen, G. and A.S. Hoffman. Graft copolymers that exhibit temperature-induced phase transitions over a wide range of pH, *Nature*, 373, 49-52, **1995**.

Chen, L.Y., Tian, Z.G. and Y.M. Du. Synthesis and pH sensitivity of carboxymethyl chitosan-based polyampholyte hydrogels for protein carrier matrices, *Biomaterials*, 25, 3725-3732, **2004**.

Chiarellim, P and D. De Rossi. Determination of mechanical parameters related to the kinetics of swelling in an activated contractile gel, *Prog. Colloid Polym. Sci*. 78, 4-8, **1988**.

Chiarellim, P. and D. De Rossi. Bi-phasic elastodynamics of electron conducting polymers, *Polymer Gels and Network*. 4, 499-508, **1996**.

Choy, B. and D. D. Reible. *Diffusion models of environmental transport*, Lewis Publishers, New York, **2000**.

Clark, L.C., Spokane, R.B., Sudan, R. and T. L. Stroup. Long-lived implanted silastic

drum glucose sensors. *Trans. Am. Soc. Artif. Intern. Organs*, 33, 323-328, **1987**.

Cukier, R.I. Diffusion of Brownian spheres in semidilute polymer solutions, *Macromolecules*, *17*, 252-255, **1984**.

De, S.K. and N.R. Aluru. A chemo-electro-mechanical mathematical model for simulation of pH sensitive hydrogels, *Mechanics of Materials*, 36, 395-410, **2004**.

Dhanarajan, A.P. and R.A. Siegel. Time-dependent permeabilities of hydrophobic, pH-sensitive hydrogels exposed to pH gradients, *Macromol. Symp.*, 227, 105-114, **2005**.

Dinarvand, R.D. and A. Emanuele. Use of thermoresponsive hydrogels for on-off release of molecyles, *Jounal of Controlled Release*, 36, 221-227, **1995**.

Doi, M., Matsumoto, M. and Y. Hirose. Deformation of ionic polymer gels by electric fields, *Macromolecules*, 25, 5504-5511, **1992**.

Dolbow, J., Fried, E. and H.D. Ji. Chemically induced swelling of hydrogels, *Journal of the Mechanics and Physics of Solids*. In press, **2007**.

Dong, L.C. and A.S. Hoffman. Synthesis and application of thermally reversible heterogels for drug delivery, *Journal of Controlled Release*, 13, 21-31, **1990**.

Dong, L.C. and A.S. Hoffman. A novel approach for preparation of pH-sensitive hydrogels for enteric drug delivery, *Journal of Controlled Release*, 15, 141-152, **1991**.

El-Hag Ali, A., Abd El-Rehim, H.A., Hegazy, E.A. and M.M. Ghobashy. Synthesis and electrical response of acrylic acid/vinyl sulfonic acid hydrogels prepared by γ-irradiation, *Radiation Physics and Chemistry*, 75(9), 1041-1046, **2006**.

Emileh, A. Vasheghani-Farahani, E. and M. Imani. Swelling behavior, mechanical properties and network parameters of pH- and temperature-sensitive hydrogels of poly((2-dimethyl amino) ethyl methacrylate-co-butyl methacrylate), *European Polymer Journal*, 43, 1986-1995, **2007**.

English, A., Tanaka, T. and E. R. Edelman. Equilibrium and non-equilibrium phase transitions in copolymer polyelectrolyte hydrogels, *Journal of Chemical Physics*, 107, 1645-1654, **1997**.

Erman, B. and P.J. Flory. Critical phenomena and transitions in swollen polymer networks and in linear macromolecules, *Macromolecules*, 19, 2342-2353, **1986**.

Flory, P.J. Thermodynamics of high polymer solutions, *Journal of Chemical Physics*, 9(8), 660-661, **1941**.

Flory, P.J. *Principles of Polymer Chemistry*, Cornell University Press, Ithaca, NY, **1953**.

Flory, P.J. and J. Rehner. Statistical mechanics of cross-linked polymer networks. II. Swelling, *Journal of Chemical Physics*, 11, 521-526, **1943**.

Fei, J.Q., Zhang, Z.P. and L.X. Gu. Bending behavior of electroresponsive poly(vinyl alcohol) /poly(acrylic acid) semi-interpenetrating network hydrogel fibers under an electric stimulus, *Polymer International*, 51, 502-509, **2002**.

Gehrke, S.H. Synthesis and properties of hydrogels used for drug delivery. In Transport Proseses. In *Pharmaceutical Systems*, Amidon, G.L., Lee, P.I. and E.M. Topp, Eds.; Marcel Dekker, New York, vol 102, pp 473, **2000**.

Glodrich, M. and J. Kost. Glucose sensitive polymeric matrices for controlled drug delivery, *Clin. Mater.* 13, 135-142, **1993**.

Gonzalez, B.M., Christie, G., Davidson, C., Blyth, J. and C.R. Lowe. Divalent metal ion-sensitive holographic sensors, *Analytical Chimica Acta*, 528(2), 219-228, **2005**.

Gough, D.A, Lusisano, J. Y. and P.H.S. Tse. Two dimensional enzyme electrode sensor for glucose, *Anal. Chem.*, 57, 2351-2357, **1985**.

Grimshaw, P.E., Nussbaum, J.H., Grodzinsky, A.J. and M.L. Yarmush. Kinetics of electrically and chemically induced swelling in polyelectrolyte gels. Journal of Chemical Physics, **93,** 4462-4472, **1990**.

Gupta, S., Kuckling, D., Kretschmer, K., Choudhary, V. and H.J. Adler. Synthesis and characterization of stimuli-sensitive micro- and nano-hydrogels based on photocrosslinkable poly(dimethylaminoethyl methacrylate), *Journal of Polymer Science Part A-Polymer Chemistry*, 45(4), 669-679, **2007**.

Gutoswka, A., Bae, Y.H., Feijen, J. and S.W. Kim. Heparin release from thermosensitive hydrogels, *Journal of Controlled Release*, 22, 95-104, **1992**.

Guyyon, A.C. *Textbook of Medical Physiology*, 8th ed. Philadelphia, W.B. Saunders

Company, pp 433-443, **1991**.

Hassan, C.M., Doyle III, F.J. and N.A. Peppas. Dynamic behavior of glucose-repsonsive poly(methacrylic acid-g-ethylene glycol) hydrogel, *Macrolecules*, 30, 6166-6173, **1997**.

Heller, J. Modulated release from drug delivery devices, *Crit. Rev. Therap. Drug Carrier Syst.* 10, 253-305, **1993**.

Herber, S., Bomer, J., Olthuis, W., Bergveld, P. and A. van den Berg. A miniaturized carbon dioxide gas sensor based on sensing of pH-sensitive hydrogel swelling with a pressure sensor, *Biomedical Microdevices*, 7(3), 197-204, **2005**.

Hickey, A.S. and N.A. Peppas. Meshsize and diffusive characteristics of semicrystalline poly(vinyl alcohol) membranes prepared by freezing/thawing techniques, *Journal of Membrane Science*, 107, 229-237, **1995**.

Hino, T. and J.M. Prausnitz. Molecular thermodynamic for volume-change transitions in temperature-sensitive polymer gels, *Polymer*, 39, 3279-3283, **1998**.

Hoffman, W.S. *The Biochemistry of Clinical Medicine* (Chapter 6), Year Book Medical Publishers, Chicago, **1970**.

Homma, M., Seida, Y. and Y. Nakano. Evaluation of optimum condition for designing high performance electro-driven polymer hydrogel systems, *Journal of Applied Polymer Science*, 75, 111-118, **2000**.

Homma, M., Seida, Y. and Y. Nakano. Effect of ions on the dynamic behavior of an electrodriven ionic polymer hydrogel membrane, *Journal of Applied Polymer Science*, 82, 76-80, **2001**.

Hon, Y. C., Lu, M.W., Xue, W. M. and X. Zhou. A new formulation and computation of the triphasic model for mechano-electrochemical mixtures, *Computational Mechanics*, 24(3), 155-165, **1999**.

Horkay, F., Tasaki, I. and P.J. Basser. Effect of monovalent-divalent cation exchange on the swelling of polyacrylate hydrogels in physiological salt solutions, *Biomacromolecules*, 2, 195-199, **2001**.

Huggins, M.L. Solutions of long chain compounds, *Journal of Chemical Physics*, 9(5), 440, **1941**.

Irie, M. Stimuli-responsive poly(N-isopropylacrylamide) photo- and chemical- induced phase transition, *Advenced Polymer Science*, 110, 49-65, **1993**.

Isayeva, I.S., Yankovshi, S.A. and J. P. Kennedy. Novel amphiphilic membranes of poly(N,N-dimethyl acrylamide) crosslinked with octa-methacrylate-telechelic polyisobutylene stars, *Polymer Bulletin*, 48, 475-482, **2002**.

Ishihara, K., Kobayashi, M., Ishimaru, N. and I. Shinohara. Glucose induced permeation control of insulin through a complex membrane consisting of immobilized glucose oxidase and a poly(amine), *Polym. J.* 16, 625-631, **1984**.

Ishihara, K. and K. Matsui. Glucose-responsive insulin release from polymer capsule, *J. Polym. Sci. Polym. Lett. Ed.* 24, 413-417, **1986**.

Jennedy, F.P. Recent developments in insulin delivery techniques: current status and future potential, *Drugs*, 42, 213-227, **1991**.

Jin, X. and Y.L. Hsieh. pH-responsive swelling behavior of poly(vinyl alcohol)/poly(acrylic acid) bi-component fibrous hydrogel membranes, *Polymer*, 46, 5149-5160, **2005**.

Johnson, B., Niedermaier, D.J., Crone, W.C., Moorthy, J. and D.J. Beebe. Mechanical properties of a pH sensitive hydrogel. *Society for Experiemtnal Mechanics, SEM Annual Conference Proceedings*, Milwaukee, WI. USA, **2002**.

Kang, S.I. and Y.H. Bae. pH-induced volume-phase transition of hydrogels containing sulfonamide side group by reversible crystal formation, *Macromolecules*. 34, 8173-8178, **2001**.

Kang, S.I. and Y.H. Bae. pH-induced solubility transition of sulfonamide-based polymers, *Journal of Controlled Release*, 80, 145-155, **2002**.

Kang, S.I. and Y.H. Bae. A sulfonamide based glucose-responsive hydrogel with covalently immobilized glucose oxidase and catalase, *Journal of Controlled Release*, 86, 115-121, **2003**.

Kataoka, K., Miyazaki, H., Bunya, M., Okano, T. and Y. Sakurai. Totally synthetic polymer gels responding to external glucose concentration: their preparation and application to on-off regulation of insulin release, *Journal of American Chemical Society*, 120, 12694-12695, **1998**.

Katayama, S., Myoga, A. and Y. Akahori. Swelling behavior of amphoteric gel and the volume phase transition, *J. Phys. Chem.*, 96, 4698-4701, **1992**.

Katchalsky, A. and I. Michaeli. Polyelectrolyte gels in salt solution, *Journal of Polymer Science*, 15, 69-86. **1955**.

Kato, E. Pressure-induced volume phase transition of polyacrylamide gels in acetone–water mixtures, *Journal of Chemical Physics*, 113, 1310-1314, **2000**.

Kato, N., Takahashi, F. and S. Yamanobe. Property of magneto-driven poly(N-isopropylacrylamide) gel containingiron oxide in NaCl solution as a chemomechanical device, *Materials of Science Engineering*, 5, 141-147, **1997**.

Khare, A.R. and N.A. Peppas. Swelling/deswelling of anionic copolymer gels, *Biomaterials*, 16,559-567, **1995**.

Kidoaki, S., Nakayama, Y. and T. Matsuda. Measurement of the interaction forces between proteins and iniferter-based graft-polymerized surfaces with an atomic force microscope in aqueous media, *Langmuir*, 17, 1080-1087, **2001**.

Kikuchi, A., Suzuki, K., Okabayashi, O., Hoshino, H., Kataoka, K., Sakurai, Y. and T. Okano. Glucose-sensing electrode coated with polymer complex gel containing phenylboronic acid, *Anal. Chem.*, 68(5), 823-828, **1996**.

Kim, S.J., Lee, C.K., Lee, Y.M., Kim, I.Y. and S.I. Kim. Electrical/pH-sensitive swelling behavior of polyelectrolyte hydrogels prepared with hyaluronic acid-poly(vinyl alcohol) interpenetrating polymer networks, *Reactive and Functional Polymers*, 55,291-298, **2003a**.

Kim, S.J., Lee, C.K. and S.I. Kim. Electrical/pH responsive properties of poly(2-acrylamido-2-methylpropane sulfonic acid)/hyaluronic acid hdyrogels, *Journal of Applied Polymer Science*. 92, 1731-1736, **2004a**.

Kim, S.J., Lee, K.J., Kim, S.I., Lee, Y.M., Chung, T.D. and S.H. Lee. Electrochemical behavior of an interpenetrating polymer network hydrogel composed of poly(propylene glycol) and poly(acrylic acid), *Journal of Applied polymer Science* 89, 2301-2305, **2003b**.

Kim, S.J., Yoon, S.G., Lee, S.M., Lee, S.H. and S.I. Kim. Electrical sensitivity behavior of a hydrogel composed of polymethacrylic acid/poly(Vinyl alcohol),

Journal of Applied Polymer Science, 91, 3613-3617, **2004b**.

Kim, S.Y. and H.S. Shin. Properties of electro-responsive poly(vinglalcohol) /poly(acrylic acid) IPN hydrogels under an electric stimulus, *Journal of Applied Polymer Science*, 73, 1675-1683, **1999**.

Kizilay, M.Y. and O. Okey. Effect of hydrolysis on spatial inhomogeneity in poly(acrylamide) gels of various crosslink densities, *Polymer*, 44, 5239-5250, **2003**.

Klumb, L.A. and T.A. Horbett. Design of insulin delivery device based on glucose-sensitive membrane, *J. Controlled Release*, 18, 59-80, **1992**.

Klumb, L.A. and T.A. Horbett. The effect of hydronium ion transport on the transient behavior of glucose sensitive membranes, *J. Controlled Release*, 27, 95-114, **1993**.

Kodzwa, M.G., Staben, M.E. and D.G. Rethwisch. Photoresponsive control of ion-exchange in leucohodroxide containing hydrogel membranes, *Journal of Membrane Science*, 158, 85-92, **1999**.

Kokufuta, E., Zhang, Y.Q. and T. Tanaka. Saccharide-sensitive phase transition of a lectin-loaded gel, *Nature*, 351, 302-304, **1991**.

Kost, J., Horbett, T.A. and B.D. Ratner. Glucose-sensitive membranes containing glucose oxidase: activity, swelling, and permeability studies, *J. Biomed. Mater. Res.*, 19, 1117-1133, **1984**.

Krall, L.P. and R.S. Beaser. *Joslin Diabtetes Manual*, 12th Ed., Lea and Febiger, Philadelphia, PA, **1989**.

Kratz, K., Hellweg, T. and W. Hirata. Influence of charge density on the swelling of colloidal poly(*N*-isopropylacrylamide-*co*-acrylic acid) microgels, *Colloids Surf. A.,* 170, 137-149, **2000**.

Kurnik, R.T., Berner, B., Tamada, J. and R.O. Potts. Design and simulation of a reverse lontophoretic glucose monitoring device, *Journal of electrochemistry Society*, 145(12), 4119-4125, **1998**.

Lai, W.M., Hou, J.S. and V.C. Mow. A triphasic theory for the swelling and deformation behaviors of articular cartilage, *ASME Journal of Biomechanical Engineering*, 113, 245-258, **1991**.

Lai, W.M., Rubin, D. and E. Krempl. *Introduction to Continuum Mechanics*, Pergamon Press, Inc., **1974**.

Lam, K.Y., Li, H., Ng, T.Y. and R.M. Luo. Modeling and simulation of the deformation of multi-state hydrogels subjected to electrical stimuli, *Engineering Analysis with Boundary Elements* 30, 1011-1017, **2006**.

Lee, K.K., Cussler, E.L., Marchetti, M. and M.A. McHugh. Pressure-dependent phase transitions in hydrogels, *Chemical Engineering Science*, 45, 766-767, **1990**.

Lele, A.K., Badiger, M.V., Hirve, M.M. and R.A. Mashelkar. Thermodynamics of hydrogen-bonded polymer gel-solvent systems, *Chem. Eng. Sci.*, 50, 3535-3542, **1995**.

Leypoldt, J.K., and D.A. Gough. Model of a two-substrate enzyme electrode for glucose, *Anal. Chem.*, 56, 2896-2904, **1984**.

Li, H., Chen, J. and K.Y. Lam. Multiphysical modeling and meshless simulation of electric-sensitive hydrogel, *Journal of polymer Science: Part B: Polymer Physics*, 42, 1514-1531, **2004**.

Li, H., Luo, R.M. and K.Y. Lam. Modeling and simulation of deformation of hydrogels responding to electric stimulus, *Journal of Biomechanics*, 40, 1091-1098, **2007**.

Li, H., Ng, T.Y., Yew, Y.K. and K.Y. Lam. Modeling and simulation of the swelling behavior of pH-stimulus-responsive hydrogels, *Biomacromolecules*, 6, 109-120, **2005a**.

Li, H., Wang, X.G., Wang, Z.J. and K.Y. Lam. Multiphysics modelling of volume phase transition of ionic hydrogels responsive to thermal stimulus, *Macromolecular Bioscience*, 5(9), 904-914, **2005b**.

Li, H., Wang, Z.J., Wang, X.G. and K.Y. Lam. Simulation of the influences of bathing solution and crosslink density on the swelling equilibrium of ionic thermo-sensitive hydrogels, *Biophysical Chemistry*, 118(2-3), 57-68, **2005c**.

Li, Y. and T. Tanaka. Phase transitions of gels, *Annu. Rev. Mater. Sci.*, 22, 243-276, **1992**.

Liu, G.R. *Mesh Free Methods: Moveing Beyond the Finite Element Method*, Florida: CRC Press, **2003**.

Liu, G.R. and Y.T. Gu. A point interpolation method for two-dimension solids, *International Journal for Numerical Methods in Engineering*, 50, 937-951, **2001a**.

Liu, G.R. and Y.T. Gu. A local radial point interpolation method for stress analysis of two-dimension solids, *Structural Engineering and Mechanics*, 11(2), 221-236, **2001b**.

Liu, G.R. and Y.T. Gu. Application of meshless local Petrov-Galerkin (MLPG) approach to fluid flow problem, *First Asian-Pacific Congress on Computational Mechanics*, Sydney, Australia, pp20-23, **2001c**.

Lu, Z.R., Kopeckova, P. and J. Kopecek. Antigen responsive hydrogels based on polymerizable antibody Fab fragment, *Macromolecular Bioscience*, 3(6), 296-300, **2003**.

Lucy, L. A numerical approach to testing the fission hypothesis, *Astronomical Journal*, 82, 1013-1024, **1977**.

Lusisano, J.Y. and D.A. Gough. Transient response of the two dimensional glucose sensor, *Anal. Chem.*, 60, 1272-1281, **1988**.

Lustig, S.R. and N.A. Peppas. Solute diffusion in swollen membranes. IX. Scaling laws for solute diffusion in gels. *J. Appl. Polym. Sci.* 36 (4), 735-745, **1988**.

Mackie, J. S. *Meares*, P. Proc. R. Soc. London, A232, pp498, **1955**.

Malikkides, C.O. and R.H. Weiland. On the mechanism of immobilezed glucose oxidase deactivation by hydrogen peroxide, *Biotechnology and Bioengineering*, 24(11), 2419-2439, **1982**.

Malvern, L.E. *Introduction to the mechanics of a continuous medium*, Prentice-Hall, Inc., Eaglewood Cliffs, New Jersey, **1969**.

Mamada, A., Tanaka, T., Kungwatchakun, D. and M. Irie. Photo induced phasetransition of gels, *Macromolecules*, 23, 1517-1519, **1990**.

Mano, N., Mao, F. and A. Heller. On the parameters affecting the characteristics of "wired" glucose oxidase anode, *Journal of electroanalytical chemistry*, 574, 347-357, **2005**.

Mao, J.S. and M.J. McShane. Transduction of volume change in pH-sensitive hydrogels with resonance energy transfer, *Advanced Materials*, 18, 2289-2293,

2006.

McMahon, C.P., Rocchitta, G., Serra, P.A., Kirwan, S.M., Lowry, J.P. and R.D. O'Neill. Control of the Oxygen Dependence of an Implantable Polymer/Enzyme Composite Biosensor for Glutamate, *Anal. Chem.* 78, 2352-2359, **2006**.

Michaelis, L. and M. Menten. Die Kinetik der Invertinwirkung, *Biochem. Z.*, 49, 333-369, **1913**.

Misra, G.P. and R.A. Siegel. New mode of drug delivery: long term autonomous rthymic hormone release across a hydrogel membrane, *Journal of Controlled Release*, 81, 1-6, **2002**.

Miyata, T., Asami, N. and T. Uragami. A reversibly antigen-responsive hydrogel, *Nature*, 399, 766-769, **1999**.

Miyata, T., Uragami, T. and K. Nakamae. Biomolecule-sensitive hydrogels, *Advanced drug delivery reviews*, 54, 79-98, **2002**.

Moelwyn-Hughes, E.A. *Physical Chemistry*, second revised edition, Pergamon Press, New York, pp 831-835, **1978**.

Mortimer, R.G. and H. Eyring. Elementary transition state theory of the Soret and Dufour effects, *Proc Natl Acad Sci U S A*. 77(4), 1728–1731, **1980**.

Nam, K.W., Watanabe, J. and K. Ishihara. Modeling of swelling and drug release behavior of spontaneously forming hydrogels composed of phospholipids polymers, *International Journal of Pharmaceutics*, 275, 259-269, **2004**.

Narasimhan, B. and N.A. Peppas. The role of modeling studies in the development of future controlled release devices, In *Controlled Drug Delivery: Challenges and Strategies*, Park, K. Ed., American Chemical Society, Washington, DC, pp. 529-557, **1997**.

Nayroles, B., Touzot, G. and P. Villion. Generalizing the finite element method: diffuse approximation and diffuse elements, *Computational Mechanics*, 10, 307-318, **1992**.

Ni, H.M., Kawaguchi, H. and T. Endo. Preparation of pH-sensitive hydrogel microspheres of poly(acrylamide-co-methacrylic acid) with sharp pH-volume transition, *Colloid Polymer Science*, 295, 819-826, **2007**.

Nikonenko, V., Lebedev, K., Manzanares J.A. and G. Pourcelly. Modelling the transport of carbonic acid anions through anion-exchange membranes, *Electrochimica Acta* 48, 3639-3650, **2003**.

Ogston, A.G., Preston. B.N. and J.D. Wells. *Proc. R. Soc*. London Ser. A 333, 297-316, **1973**.

Okano, T., Bae, Y.H., Jacobs, H. and S.W. Kim. Thermally on-off switching polymers for drug permeation and release, *Journal of Controlled Release*, 11, 255-265, **1990**.

Okay, O. and S.B. Sarusil. Swelling behavior of poly(acrylamide-co-sodium acrylate) hydrogels in aqueous salt solutions: theory versus experiments, *Eur. Polym J*., 36, 393-399, **2000**.

Okuyama, Y., Yoshida, R., Sakai, K., Okano, T. and Y. Sakurai. Swelling controlled zero order and sigmoidal drug release from thermo-responsive poly(N-isopropylacrylamide-cobutyl methacrylate) hydrogel, *Journal of Biomaterials Science, Polymers Edition*, 4, 545-556, **1993**.

Onate, E., Idelsohn, S., Zienkiewicz, O.C. and R.L. Taylor. A finite point method in computational mechanics. Applications to convective transport and fluid flow, *International Journal for Numerical Methods in Engineering*, 39, 3839-3866, **1996**.

Oppermann, W. In *polyelectrolyte Gels: Properties, Preparation and Applications*, ACS Symposium Series, Vol. 480, Harland, R.S., Pridhomme, R.K. Eds, American Chemical Society: Washington, DC, **1992**.

Orakdogen, N. and O. Okay. Effect of initial monomer concentration on the equilibrium swelling and elasticity of hydrogels, *European Polymer Journal*, 42, 955-960, **2006**.

Otake, K., Inomata, H., Konno, M. and S. Saito. A new model for the thermally induced volume phase transition of gels, *J. Chem. Phys*. 91, 1345-1350, **1989**.

Otake, M., Kayami, Y., Inaba, M. and H. Inoue. Motion design of a starfish-shaped gel robot made of electro-active polymer gel. *Robotics Autonomous Systems*, 40, 185-191, **2002**.

Park, T.G. and A.S. Hoffman. Sodium chloride-induced phase transition in nonionic

poly(N-isopropylacrylamide) gel, *Macromolecules*, 26, 5045-5048, **1993**.

Parker, J.W. and C.S. Schwartz. Modeling the kinetics of immobilized glucose oxidase, *Biotechnology and Bioengineering*, 30, 724-735, **1987**.

Parker, R.S., Doyle III, F.J. and N.A. Peppas. A model-based algorithm for blood glucose control in type I diabetic patients, *IEEE Trans. Biomed. Eng.*, 46, 148-157, **1999**.

Peppas, N.A. and E.W. Merrill. Crosslinked PVA hydrogels as swollen elastic networks, *J. Appl. Polym. Sci.*, 21, 1763-1770, **1977**.

Peppas, N.A., Bures, P., Leobandung, W. and H. Ichikawa. Hydrogels in pharmaceutical formulations, *European Journal of Pharmaceutics and Biopharmaceutics*, 50, 27-46, **2000**.

Peppas, N.A. and N.K. Mongia. Ultrapure poly(vinyl alcohol) hydrogels with mucoadhesive drug delivery characteristics, *European Journal of Pharmaceutics and Biopharmaceutics*, 43, 51-58, **1997**.

Petrova, S., Kostov, Y., Jeffris, K. and G. Rao. Optical ratiometric sensor for alcohol measurements, *Analytical Letters*, 40(4), 715-717, **2007**.

Pickup, J., McCartney, L., Rolinski, O. and D. Birch. In vivo glucose sensingfor diabetes management: progress towards non-invasive monitoring, *British Medical Journal*, 319, 1289-1293, **1999**.

Plawsky, J.L. *Transport Phenomena Fundamentals*, Marcel Dekker, Inc., New York, **2001**.

Podual, K. and N.A. Peppas. Relaxational behavior and swelling-pH master curves of poly[(diethylaminoethyl methacrylate)-graft-(ethylene glycol)] hydrogels, *Polymer International*, 54, 581-593, **2005**.

Podual, K., Doyle III, F.J. and N.A. Peppas. Preparation and dynamic response of cationic copolymer hydrogels containing glucose oxidase, *Polymer*, 41, 3975-3983, **2000**.

Qiu, Y. and K.N. Park. Environment-sensitive hydrogels for drug delivery, *Advanced Drug Delivery Reviews*, 53, 321-339, **2001**.

Rasmussen, K., Willemsen, P.R. and K. Ostgaard. Barbacle settlement on hydrogels,

Biofouling, 18(3), 177-191, **2002**.

Rehor, A., Botterhuis, N.E., Hubbell, J.A., Sommerdijk, N.A. and N. Tirelli. Glucose sensitivity through oxidation responsiveness. An example of cascade-responsive nano-sensors, *Journal of Materials Chemistry*. 15, 4006-4009, **2005**.

Rong, W.Z., Pelling, A.E., Ryan, A., Gizewski, J.K. and S.K. Friedlander. Complementary TEM and AFM force spectroscopy to characterize the nanomechanical properties of nanoparticle chain aggregates, *Nano letters*, 4, 2287-2292, **2004**.

Sannino, A., Pappada, S., Madaghiele, M., Maffezzoli, A., Ambrosio, L. and L. Nicolais. Crosslinking of cellulose derivatives and hyaluronic acid with water-soluable carbodiimide, *Polymer*, 46, 11206-11212, **2005**.

Sarkyt, E.K. and B.S. Vladimir. Swelling, shrinking, deformation, and oscillation of polyampholyte gels based on vinyl 2-aminoethyl ether and sodium acrylate. *Langmuir*, 15, 4230-4235, **1999**.

Sata, T. *Ion Exchange Membranes: Preparation, Characterization, Modification and Application*, Royal Society of Chemistry (RSC), printed by Athenaeum Press Ltd, Gateshead, Tyne and Wear, UK, **2004**.

Schild, H.G. Poly(N-isopropylacrylamide): experiment, theory and application, *Progress in Polymer Science*, 17, 163-249, **1992**.

Schreyer, H.B., Gebhart, N., Kim, W.J. and M. Shahinpoor. Electrical activation of artificial muscles containing polyacrylonitrile gel fibers, *Biomacromolecules*, 1 642-647, **2000**.

Schroder, C.R., Polerecky, L. and I. Klimant. Time-resolved pH/pO_2 mapping with luminescent hybrid sensors, *Anal. Chem.*, 79, 60-70, **2007**.

Shahinpoor, M. Micro-electro-mechanics of ionic polymeric gels as electrically-controllable artificial muscles, *Journal of Intelligent Material Systems and Structures*, 6(3), 307-314, **1995**.

Shihinpoor, M. Ionic polymer-conductor composites as biomimetic sensors, robotic actuators and artificial muscles-a review, *Electrochimica Acta*, 48, 2343-2353, **2003**.

Shiga, T., Hirose, Y., Okada, A. and T. Kurauchi. Electric field-associated deformation of polyelectrolyte gel near a phase transition point, *Journal of Applied Polymer Science*, 46, 635-640, **1992**.

Shiga, T. and T. Kurauchi. Deformation of polyelectrolyte gels under the influence of electric field, *Journal of Applied Polymer Science*, 39, 2305-2320, **1990**.

Shin, B.C., Kim, S.S., Ko, J.K., Jegal, J. and B.M. Lee. Gradual phase transition of poly(*N*-iso-propylacrylamide-*co*-acrylic acid) gel induced by electric current, *European Polymer Journal*, 39, 579-584, **2003**.

Siegel, R.A. (ed) *Pulsed and self-regulated drug delivery*, CRC Press, Boca Raton, FL, pp129, **1990a**.

Siegel, R.A. pH sensitive gels: swelling equilibria, kinetics and applications for drug delivery. In *Pulse and Self-Regulated Drug Delivery*, Kost J, ed. CRC Press: Boca Raton; pp129-155, **1990b**.

Siegel, R.A. Hydrophobic weak polyelectrolyte gels: Studies of swelling equilibria and kinetics. In *Advanced in polymer science/responsive gel*s: Volume I, New York, Springer-Verlag Press, pp 233-267, **1993**.

Siegel, R.A. and B.A. Firestone. pH-dependent equilibrium swelling properties of hydrophobic polyelectrolyte copolymer gels, *Macromolecules*, 21,3254-3259, **1988**.

Siegel, R.A., Gu, Y.D., Baldi, A. and B. Ziaie. Novel swelling/shrinking behaviors of glucose-binding hydrogels and their potential use in a microfluidic insulin delivery system, *Macromol. Symp.*, 207, 249-256, **2004**.

Spiegel, M.R. and J. Liu, *Mathematical handbook of formulas and tables*, 2nd edition, McGRAW-HILL, Singapore, **1999**.

Stauffer, S.R. and N.A. Peppas. Poly(vinyl alcohol) hydrogels prepared by freezing-thawing cyclic processing, *Polymer*, 33, 3932-3936, **1992**.

Stauthamer, W., Engbersen, J.F., Verboom, W. and D.N. Reinhoudt. Influence of plasticizer on the selectivity of nitrate-sensitive chemfets, *Sensors and Actuators B-Chemical*, 17(3), 197-201, **1994**.

Sudipto, K.D., Aluru, N.R., Johnson, B., Crone, W.C., Beebe, D.J. and J. Moore.

Equilibrium swelling and kinetics of pH-responsive hydrogels: Models, experiments, and simulations, *Journal of Microelelctromechanical Systems*, 11(5), 544-555, **2002**.

Sun, S. and A.F.T. Mak. The dynamical response of a hydrogel fiber to electrochemical stimulation, *Journal of Polymer Science B: Polymer Physics*, 39, 236-246, **2001**.

Sun, S., Wong, Y.W., Yao, K. and A.F.T. Mak. A study on mechano-electro-chemical behavior of chitosan/poly(propylene glycol) composite fibers, *Journal of Applied Polymer Science*, 76, 542-551, **2000**.

Suzuki, A. and T. Tanaka. Phase transition in polymer gels induced by visible light, *Nature*, 346, 345-347, **1990**.

Suzuki, H. and A. Kumagai. A disposable biosensor employing a glucose-sensitive biochemomechanical gel, *Biosensor and Bioelectrionics*, 18, 1289-1297, **2003**.

Suzuki, Y., Tanihara, M, Nishimura, Y., Suzuki, K., Kakimaru, Y. and Y. Z. Shimizu. A new drug delivery system with controlled release of antibiotic only in the presence of infection, *Journal of Biomedical Materials Reseach*, 42, 112-116, **1998**.

Sawahata, K., Hara, M., Yasunaga, H. and Y. Osada. Electrically controlled drug delivery system using polyelectrolyte gels, *Journal of Controlled Release*, 14, 253-262, **1990**.

Tanaka, T., Ishiwata, S and C. Ishimoto. Critical behavior of density fluctuations in gels. *Phys Rev Lett*, 38, 771-774, **1977**.

Tanaka, T., Nishio, I., Sun, S.T. and N.S. Ueno. Collapse of gels in an electric field. *Science*, 218, 467-469, **1982**.

Tanihara, M., Suzuki, Y., Nishimura, Y., Suzuki, K., Kakimaru, Y. and Y. Fukunishi. A novel microbial infection-responsive drug release system, *Journal of Pharm. Science*, 88, 510-514, **1999**.

Temtem, M., Casimiro, T., Mano, J.F. and A. Aguiar-Ricardo. Green synthesis of a temperature sensitive hydrogel, *Green Chemistry*, 9(1), 75-79, **2007**.

Ten, B.G. and F.E. Karasz. Lower critical solution temperature behavior in polymer blends: compressibility and directional-specific interactions, *Macromolecules*, 17, 815-820, **1984**.

Tozeren, A. and S.W. Byers. *New Biology for Engineers and Computer Scientists*, Pearson Prentice Hall, Upper Saddle River, New Jersey, pp26-27, **2004**.

Trinh, Q.T., Gerlach, G., Sorber, J. and K.F. Arndt. Hydrogel-based piezoresistive pH sensors: Design, simulation and output characteristicvs, *Sensors and Actuators* B, 117, 17-26, **2006**.

Traitel, T., Cohen, Y. and J. Kost. Characterization of glucose-sensitive insulin release systems in simulated in vivo conditions, *Biomaterials*, 21, 1679-1687, **2000**.

Traitel, T., Kost, J. and S.A. Lapidot. Modeling ionic hydrogles swelling: Characterization of the Non-steady state, *Biotechnology and Bioengineering*, 84 20-28, **2003**.

Tse, P.H.S and D.A. Gough. Time-dependent inactivation of immobilized glucose oxidase and catalase, *Biotechnology and Bioengineering*, 29, 705-713, **1987**.

Valencia, J. and I.F. Pierola. Interpretation of the polyelectrolyte and antipolyelectrolyte effects of poly(N-vinylimidazole-co-sodium styrenesulfonate) hydrogels, *Journal of Polymer Science Part B: Polymer Physics*, 45(13), 1683-1893, **2007**.

Varley, H., Gowenlock, A.H. and M. Bell. *Practical Clinical Biochemistry*, vol.1 (Chapter 24). William Heinemann Medical Books, London, **1980**.

Wallmersperger, T. and B. Kroeplin. Modeling and analysis of the chemistry and electromechanics. In *Electroactive Polymer Actuators as artificial muscles*, Bar-Cohen, Y. (Ed.), SPIE Press, pp285-307, **2001**.

Wang, J.Q. and W.H. Wu. Swelling behaviors, tensile properties and thermodynamic studies of water sorption of 2-hydroxyethyl methacrylate/epoxy methacrylate copolymeric hydrogels, *European Polymer Journal*, 41, 1143-1151, **2005**.

Wang, Y.X., Zhong, X. and S.H. Wang. Pressure cycling to enhance an immobilized enzymic reaction by enzyme entrapment in a pressure-sensitive gel, *Journal of Chemical Technology and Biotechnology*, 67(3), 243-247, **1996**.

Weiss, A.M., Grodzinsky, A.J. and M.L. Yarmush. Chemically and electrically controlled membranes: size specific transport of fluorescent solutes through PMAA membranes, *AICHE Sump.Ser.*, 250, 85-98, **1986**.

Whitaker, J.R.. *Principle of enzymology for the food science* (2nd), Marcel Dekker, Inc, New York, **1994**.

Yang, Y.J. and J. Engberts. Stimuli response of polysoap hydrogels in aqueous solution and DC electric fields, *Colloids and Surfaces A: Physicochmeical and Engineering Aspects*, 169, 85-94, **2000**.

Yin, W.S., Li, J., Gu, T.R. and J.P. Wu. Design and synthesis of conducting secondary crosslinked interpenetrating polymer network, *Journal of applied polymer science*, 63, 13-16, **1997**.

Yoshida, M., Asano, M., Kumakura, M., Kataki, R., Mashimo, T., Yuasa, H. and H. Yamanaka. Thermo-responsive hydrogels based on acryloyl-L-proline methyl ester and their use as long acting testosterone delivery systems, *Drug Design Delivery*, 7, 159-174, **1991**.

Yoshida, R., Uchida, K., Kaneko, Y., Sakai, K., Kikuchi, A., Sakurai, Y. and T. Okano. Comb-type grafted hydrogels with rapid de-swelling response to temperature changes, *Nature*, 374, 240-242, **1995**.

Zhang, K. and X.Y. Wu. Modulated insulin permeation across a glucose sensitive polymeric composite membrane, *Journal of controlled release*, 80 169-181, **2002**.

Zhang, L. and W.R. Seitz. A pH sensor based on force generated by pH-dependent polymer swelling, *Analytical and Bioanalytical Chemistry*, 373(7), 555-559, **2002**.

Zhang, T.Z. and E.V. Anslyn. Using an indicator displacement assay to monitor glcuoe oxidase activity in blood serum, *Organic Letters*, 9(9), 1627-1629, **2007**.

Zhou, X, Hon, Y.C., Sun, S. and A. Mak. Numerical simulation of the steady-state deformation of a smart hydrogel under an external electric field, *Smart Materials and Structures,* 11,459-467, **2002**.

Zhong, X., Wang, Y.X. and S.C. Wang. Pressure dependence of the volume phase-transition of temperature-sensitive gels, *Chemical Engineering Science*, 51, 3235-3239, **1996**.

Ziaie, B., Baldi, A., Lei, M., Gu, Y.D. and R.A. Siegel. Hard and soft micromachining for BioMEME: review of techniques andexamples of applications in microfluidics and drug delivery, *Advanced Drug Delivery Reviews*, 56, 145-172, **2004**.

Zrinyi, M., Szabo, D. and H.G. Kilian. Kinetics of the shape change of magnetic field sensitive polymer gels, *Polymer Gels Networks*, 6, 441-454, **1998**.

Publications Arising from This Thesis

Book Chapter

1. Hua Li, **Rongmo Luo**, and K.Y. Lam, Modelling of environmentally sensitive hydrogels for drug delivery: an overview and recent developments. In: *Frontiers in Drug Design and Discovery* Volume 2, G. W. Caldwell et al. (edited). Bentham Science. 2006, pp. 295-331.

Journal Papers

2. K. Y. Lam, Hua Li, T. Y. Ng and **Rongmo Luo**, Modeling and simulation of the deformation of multi-state hydrogels subjected to electrical stimuli, *Engineering Analysis with Boundary Conditions*, 30(11), 1011-1017, 2006.
3. Hua Li, **Rongmo Luo**, and K. Y. Lam. Modeling and simulation of deformation of hydrogels responding to electric stimulus, *Journal of Biomechanics*, 40(5), 1091-1098, 2007.
4. Hua Li, **Rongmo Luo**, and K. Y. Lam, Modeling of ionic transport in electric-stimulus-responsive hydrogels, *Journal of Membrane Science*, 289, 284-296, 2007.
5. Hua Li, **Rongmo Luo**, Erik Birgersson, and K. Y. Lam, Multiphysics Modeling of Multiphase Smart Hydrogels Responding to pH and Electric Voltage Coupled Stimuli, *Journal of Applied Physics*, 101, 114905_1-7, 2007.
6. **Rongmo Luo**, Hua Li, and Khin Yong Lam. Coupled chemo-electro-mechanical

simulation for smart hydrogels responsive to external electric field, *Smart Materials and Structures*, 16(4), 1185-1191, 2007.

7. **Rongmo Luo**, Hua Li, and K. Y. Lam, Modeling and Simulation of Chemo-Electro-Mechanical Behavior of pH-Electric-Sensitive Hydrogel, *Analytical and Bioanalytical Chemistry*, 389(3), 863-873, 2007.
8. **Rongmo Luo**, Hua Li, Erik Birgersson, and Khin Yong Lam, Modeling of electric-stimulus responsive hydrogels immersed in different bathing solutions, *Journal of Biomedical Materials Research A*, 85, 248-257, 2008.
9. **Rongmo Luo**, Hua Li, and K. Y. Lam, Modeling and analysis of pH-electric-stimuli responsive hydrogels, *Journal of Biomaterials Science: Polymer Edition*, (Accepted on 01 November 2007).
10. Hua Li, **Rongmo Luo**, and K. Y. Lam. Modeling and Behavior Simulation of Electrochemomechanically Functioning Hydrogels Responsive to pH-Electric Coupled Stimuli, *Journal of Micromechanics and Microengineering* (submitted).

Proceedings of International Conferences

11. **Rongmo Luo**, Hua Li, and K. Y. Lam, Simulation of smart hydrogels to pH-electric coupled stimuli, *International Conference on Computational methods 2007* , Hiroshima, Japan, April 4-6, 2007.
12. **Rongmo Luo**, K.Y. Lam, Hua Li and T.Y. Ng, Model development and behavior simulation of pH-electric-stimuli responsive hydrogels, *International Conference on Materials for Advanced Technologies* (ICMAT), Singapore, July 4-7, 2007.